STATIC AND DYNAMIC STATE ESTIMATION OF POWER SYSTEMS

A Thesis submitted to The University of Manchester for the degree of

Doctor of Philosophy

In the Faculty of Science & Engineering

2017

by

Zhaoyang Jin

School of Electrical and Electronic Engineering

List of Content

Final count: 55739 words.

List of Figures

List of Tables

List of Abbreviations

CF	Constrained formulation (type)
CKF	Cubature Kalman Filter
CNlog10	Condition number in log 10 scale
CSE	Conventional state estimator
DB	Direct branch
DI	Direct island
DSE	Dynamic state estimator
EMS	Energy measurement system
EKF	Extended Kalman filter
IEKF	Iterated extended Kalman filter
ILP	Integer linear programming
HSE	Hybrid state estimator
LSE	Linear state estimator
NI	Normalised innovation
OPI	Overall performance index
PF	Pseudo flow (type)
PMU	Phasor measurement unit
PP	Post-processing (type)
PV	Pseudo voltage (type)
RTU	Remote terminal unit
RC	Rectangular current (type)
SCADA	Supervisory control and data acquisition
SKF	Second-order Kalman filter
SMT	Synchronised measurement technology
SSE	Static state estimator
UKF	Unscented Kalman Filter
WAMPAC	Wide area monitoring, protection and control
WAMS	Wide area monitoring system

WLS	Weighted least square

Abstract

The University of Manchester
Faculty of Engineering and Physical Sciences

PhD Thesis
Static and Dynamic State Estimation of Power Systems

Zhaoyang Jin
December, 2017.

Power system state estimation has been playing a core part in the energy management system (EMS) utilised by power system operators since its establishment in the 1970s. The state estimator is responsible for providing accurate information (e.g. voltage magnitudes and angles of all buses in the network) for the EMS so that its security assessment functions can be deployed reliably. Recently, the power system is experiencing unprecedented evolution of complexity due to the increasing injection of renewable energy, increasing usage of power electronic devices and the increasing number of HVDC links in the network. One of the solutions to such challenges is to deploy Wide Area Monitoring System (WAMS) supported by the Synchronised Measurement Technology (SMT).

Prior to state estimation, an observability analysis must be performed to make sure the measurements (e.g. power injection and flow measurements) received can support the normal functioning of the state estimator. If the measurements cannot provide full observability of the network, the observability analysis function identifies the observable islands where state estimation can still be performed within the observable islands. In this thesis it is shown that the existing method may not correctly identify the observable islands in the so called pathological cases; the thesis proposes a new method for observability analysis that overcomes this problem. Furthermore the execution time of the proposed method is shorter than existing methods. To support the deployment of the SMT in state estimation, the thesis also proposes a new method for including the synchronised measurements in the observability analysis function.

The synchronised measurements provided by phasor measurement units (PMUs) have significantly higher accuracy and sampling rate than conventional measurements. However, the widespread installation of PMUs is limited by its high costs. A more feasible method that takes advantage of SMT is to use a hybrid state estimator (HSE). It uses a combination of PMU measurements and the existing conventional methods. To support the observability of the HSE, the thesis first proposes a new method for optimal PMU placement in the presence of conventional measurements. Then, the thesis performs simulations in the IEEE 14 and 118 Bus Test Systems comparing the performance of five different HSEs. It is found that even a small number of PMUs in a large network can significantly improve the estimation accuracy of the HSE compared to the conventional state estimator. Furthermore, the rectangular current type HSE has the best performance in terms of estimation accuracy, execution time and convergence. These conclusions are rigorously validated by mathematical analysis.

The final work presented in this thesis is the development of a new algorithm for a dynamic state estimator (DSE) supported by SMT. The new method applies the Cubature Kalman Filter which is demonstrated to be more efficient but more sensitive to the anomalies compared to the DSEs using other nonlinear filters. Thus, the new algorithm also involves new methods that can accurately detect and identify three different types of anomaly, including bad data, sudden change of load, and sudden change of topology due to fault, to mitigate the impact of this sensitivity.

Declaration

No portion of the work referred to in the thesis has been submitted in support of an application for another degree or qualification of this or any other university or other institute of learning.

Copyright Statement

To my parents

Acknowledgements

I would like to take this good opportunity to express my sincere gratitude to Prof Vladimir Terzija for securing the funding for my PhD research, for the supervision of my PhD, and for all the encouragement and support he has given to me during the past four years. I would also like to thank Dr James Yu and Scottish Power for providing this funding.

I would also like to thank Dr Peter Wall and Miss Papiya Dattaray for the generous help they have offered to me since we started working together as a team on the VISOR project, and all my colleagues for their help in all aspects of my life during my stay at the University of Manchester. It has been my honour to work in a team of such kind and brilliant members.

Finally, although it is impossible to put into words, I would like to take this opportunity to express my gratitude and love to my family. Without their love and care since I was born, it would have been impossible for me to carry out this PhD research and finish this thesis. I will always keep them in my thoughts wherever I am in the future.

Chapter 1 Introduction

Before the employment of energy management systems (EMS), the power system operator was in charge of conducting many real-time control centre functions, including, scheduling generation and interchange, scheduling frequency and time corrections, monitoring outages, coordinating bias settings, and emergency restoration of the system [1]-[4]. All of these real-time functions were conducted using the estimations from a large number of load flows that were performed at the planning stage. However, such a monitoring and control scheme can only cover a limited number of scenarios for any operation condition, and thus the system could be vulnerable to unexpected events. In addition, it was recognized that the planning load flows did not meet the exact needs of the operator because of the random variation nature of the loads. These problems were first recognized and subsequently addressed by Fred Schweppe, who first proposed the idea of power system state estimation formulated in 1969 [6]-[8]. The first state estimator which was proposed in [6]-[8] was formulated as a weighted least square problem. The state estimator provides estimations of all parameters in the power system based on real-time measurements collected from the network, which is reliable enough to guarantee the normal operation of all control centre functions. The state estimator, therefore, forms the main part of EMS and the key component in power system.

The state estimator, supported by the conventional techniques, has been proved effective in monitoring the power network. However, the evolving complexity of the power network and thus the emerging development of smart grids are the main drivers of deeper and more extensive research into state estimation [9]. The challenges include:

- Growing penetration of renewable energy such as wind plant and solar panels, which are characterized by their intermittent generation and decentralized distribution [10].
- The need to monitor and control power system over wide area as a result of increased size of power networks and interconnections between the power networks, and thus the challenge of the central operator to manage large amount of data from different areas [11].
- The challenge to integrate Synchronised Measurement Technology (SMT) into the power

system, which is technically more reliable, but limited by the high cost of infrastructure investment [12].

- The need for further development of the dynamic state estimator (DSE) and its applications because the high sampling rate provided by SMT have made it possible for DSE to reveal electromechanical responses [13].

In order to deal with the abovementioned challenges, it is necessary to develop new methods and algorithms in state estimation and its related functions to minimise the impact of the increasing complexity of the power system and maximize the benefits brought by the new measurement technology.

1.1 Research background

1.1.1 Static State Estimation

Static state estimation is deemed as the procedure for determining the voltage magnitudes and angles of all buses in the power system at a given moment in time [1]. It is a basic module and the enabler of the EMS: the advanced applications of EMS cannot work using the raw data collected from the network without being processed by the state estimator [4]. The reason for this is that such an approach would be vulnerable to missing data, bad data and errors in measurements, parameters and network topology [5]-[8]. The state estimation procedure is responsible for filtering out these errors and finding an optimal estimate using a redundant set of measurements. It is assumed that the measurements of the quantities are taken at the same time. However, this is practically impossible due to data transmission delays and a lack of common measurement time tag. Therefore, a certain amount of time skew will also exist between the measurements. Nevertheless, this assumption is valid since in normal conditions the power system operates in a quasi-steady state, i.e. the change in the operation conditions of the power system is very slow in comparison to the time skews between the measurements. It is also assumed that the topology and the network parameters including line impedance, shunt impedance and circuit breaker positions are already known prior to state estimation, and that the number of measurements is adequate to guarantee a unique estimate of the states. These

assumptions are also valid since the state estimator is supported by a series of auxiliary functions that work in sequence with the state estimator, as shown in Figure 1.1:

Information about any change in the network topology and the estimate of the states will be sent to the topology-processor [14], an internal functional block of the state estimator, to update the network topology. Based on the topology of the network and the measurements received, the observability analysis function determines if the number of measurements is enough for the estimation of the full network. After the topology and observability of the network are determined, the main function of the state estimator can then calculate the optimal estimates from the measurements and the network model. However, this estimate, usually based on the measurements only, is vulnerable to gross errors and network parameter errors. Hence, it must be further processed by functions of bad data detection and parameter and structural error detection.

Figure 1-1: Flow Chart of the State Estimation Functions

With the advent of synchronised measurement technology (SMT), the conventional measurements obtained from the remote terminal units (RTUs), including the measurements of voltage magnitudes, active and reactive power injections and flows, are challenged by the synchronised measurements obtained from the phasor measurement units (PMUs) that provide direct measurement of voltage and current phasors. According to the different types of measurement inputs, state estimators can be classified into three categories:

- Conventional State Estimator (CSE) [6]-[8], [15]-[17]
- Linear State Estimator (LSE) [1], [18]-[20]
- Hybrid State Estimator (HSE) [21]-[25]

As suggested by their names, the CSE uses only the conventional measurements for state estimation; the LSE uses only the PMU measurements, and the HSE uses both types of the

measurements. Since the measurements for the LSE consist of only voltage and current phasors, the estimate of the states can be calculated directly. In comparison, the CSE and HSE require recursive estimation techniques, such as weighted least squares (WLS), to ensure the minimum-variance unbiased estimate of the states.

The state estimators can also be designed in various formulations that serves different purposes, such as incorporating synchronised measurements with conventional measurements in HSEs, addressing some problems discovered in the real power system such as the angle bias errors of the PMUs, estimation of the states of generators, HVDC components, or any other states except for the voltage phasors of the network buses.

1.1.2 Network Observability

Prior to the state estimation, observability analysis determines whether or not a unique solution can be found with the given network topology and measurements available [26]. Observability analysis may be carried out off-line, to determine the adequacy of the measurements at the initial stage of state estimator installation [4]. If the measurements are insufficient to support state estimation in the network, additional measurements would have to be placed at particular locations. Observability analysis is also required online, to check the observability of the network, i.e. to make sure that any changes in measurements due to telecommunication or meter failures do not affect the unique estimation of the states. When the network is unobservable, the system will contain several observable islands. Each observable island contains one or several connected substations sharing a common reference angle that is independent to that of other islands. In such cases, observability analysis identifies all observable islands so that the following state estimation can still be performed with multiple reference angles.

There are two categories of different methods for network observability analysis. The first category includes different types of topological method [27]-[32]. It is based on the graph theory where observability is determined through logical operations according to the topology

of the network and the type and location of the measurements. The second category includes different types of numerical methods [26], [32]-[42]. The numerical methods allow faster and more flexible identification of network observability based on the decoupled DC state estimation model and the measurement Jacobian matrix. However, the current numerical methods are vulnerable to some special network topology and measurements that are known as pathological cases, and are limited to the analysis of conventional measurements. The thesis presents a thorough study into these pathological cases and proposes two new methods for observability analysis that enable the pathological cases to be avoided, and a new strategy for including the PMU measurements into observability analysis.

1.1.3 Synchronised Measurement Technology

Synchronised Measurement Technology (SMT) [12] [43]-[46] is the base line and enabler of Wide-Area Monitoring Systems (WAMS). The history and functionality of SMT and how it could control and monitor modern power system are discussed in this sub-section.

The idea of phasor measurement unit (PMU) was first proposed in early 1980s [47], and the first PMU was invented in 1988 by Prof A. Phadke and Prof J. Thorp at Virginia Tech, USA [48]. Until then, the power system has used the conventional measurements from the Supervisory Control and Data Acquisition (SCADA) system. Limited by a lack of a common reference, the SCADA system cannot directly measure the angle of the voltage. Thus, the voltage magnitude, power flow and injection measurements are used to indirectly monitor the system states (voltage magnitudes and angles). What is more, its slow reporting rate of 0.2 to 0.5 Hz further limits the capability of the system operator to monitor the network in real-time. The invention of the PMU has completely changed the system operator's practice in power system monitoring, and started a new trend of control centre applications [12]. Synchronised by a common time tag provided by the Global Positioning System (GPS), the PMU is able to directly measure the voltage and current phasors, creating the potential of a linear solution of power system state estimation. The PMU is also featured by its fast reporting rate from 50 to 100 Hz [12], which is about 100 times faster than that provided by the SCADA system. This

enables the real-time monitoring of the power system and even the monitoring of the transients of the system. In addition, the PMUs also provide the measurements of frequency and rate of change of frequency (ROCOF) [49]. Although they might not be used in state estimation, these measurements are key information for power system security assessment. With the abovementioned advantages, the SMT technology and PMUs are expected to bring the following evolutionary changes to power systems [12]:

- Significantly improving the reliability of the power system by reducing the number of system blackouts;
- Enabling the cost-efficient operation of the power system;
- Allowing a considerable increase in the penetration of renewable energy in the power network

To maximally exploit the benefits of the PMUs, three major investments are required [12]. First, the old instrument transformers should be replaced with high accuracy instrument transformers so that the errors of the PMU measurements can be minimised. Second, the communication infrastructure and the related communication technology should be improved to satisfy the real-time reporting rate of the PMUs. Lastly, to manage and process the huge amount of data from a large network with high reporting rates, big data technology, such as distributed file stores and data integration, and possibly a cloud super computer should be applied. Hence, the overall cost of installing a PMU that is fully functioning may be very expensive. So, further studies should concentrate on how to exploit the benefits of the PMUs while minimising the costs. The related focus topics in literature include optimal PMU placement, hybrid state estimation and dynamic state estimation. The background and related research into these three topics will be discussed in detail in later chapters in this thesis.

1.1.4 Hybrid State Estimation

The advent of the SMT sheds light on real-time monitoring of the power system with significantly increased reliability. The accurate measurement of the phases / angles of the

voltages and currents not only remarkably reduces the skew errors caused by the asynchrony of the measurements, but also makes it possible to linearly solve the state estimation problem. However, as it requires all buses to be observed by PMUs, the deployment of a linear state estimator (LSE) in a large network is still far from being realised due to the very high costs. A more viable and economically sound method to exploit the benefits brought by the PMUs is to use a hybrid state estimator (HSE) that combines both the conventional measurements from the SCADA and the synchronised measurements from the PMUs.

The first of the three topics involves the idea of integrating the synchronised measurements into the hybrid state estimation problem and was first proposed in [21]. In this paper, a post-processing (PP) HSE is proposed: a preliminary result is produced using the conventional measurements in a Classical State Estimator (CSE), and the preliminary result is then corrected using the PMU measurements in a LSE. The advantage of this type of HSE is that the existing CSE is preserved while the LSE can be applied in advance, making it a smoother transition from CSE to LSE. However, separating the state estimation process into separate stages would result in a reduction in measurement redundancy. Particularly on the CSE side, the estimator is required to be fully observable with only the conventional measurements.

To overcome the observability problem and potential loss of accuracy of the PP HSE, the integrated HSE was proposed in [21], in which the PMU measurements and conventional measurements are processed in a single state estimator. The challenge of implementing an integrated HSE is that the derivatives of the current measurements in polar form might be singular, which would eventually lead to non-convergence. In [22], the rectangular current (RC) integrated HSE is proposed, where current phasor measurements are separated into real and imaginary parts, whose derivatives are free of singular points. Several other formulations of the integrated HSE are also identified in literature. They overcome the convergence problem by transforming the current phasor measurements into alternative forms, including pseudo flow (PF) [23], pseudo voltage (PV) [24] and constrained formulation (CF) [25].

Apart from the first topic of finding methods for combining the PMU measurements and conventional measurements into a HSE, the research topics of HSE have now been extended to

alternative methods for (hybrid) state estimation itself (i.e. not a weighted least squares procedure) and the applications of HSE. Examples of the alternative state estimation methods include HSE using the multi-agent system combined with cubature Kalman filter [50], HSE in distributed system using hybrid particle swarm optimisation [51]，decentralised HSE [52]-[58] and HSE using Taguchi differential evolution algorithm [59].

The third topic is the applications of HSE.: the HSE has been found to be beneficial for dynamic state estimation [61]-[63], HSE for tracking the transients states of the system [64], distributed state estimation [65], and state estimation and control in the presence of HVDC links [66]-[68].

In this thesis, the focus of the HSE research is on the first topic, and a comprehensive simulation study is conducted to assess the performance of the five abovementioned HSEs in both IEEE 14 and 118 Bus Test Systems. Furthermore, underlying reasons for results from the simulations are explained using mathematical derivations.

1.1.5 Dynamic State Estimation

The static state estimator (SSE), which has been widely used in power networks around the world since it was introduced in 1970, uses a redundant set of measurements to produce the estimate of the states. As an improved algorithm that might be used in the future, dynamic state estimator (DSE) performs state estimation using not only the measurements received at the current time instant but also the predictions of the states, based on the dynamic model and the estimate at the previous time instant. This allows the system operator more time to make decisions such as economic dispatch, security assessment, or other related functions [70].

The idea of dynamic state estimation was proposed in the same year that the concepts of SSE were established [71]-[75]. However, limited by computation capabilities of the control centre and a lack of accurate dynamic models, the DSE was not developed as the SSE. Recently, with the development of the information and communication technology the deployment of the DSE

has become possible in large networks. In addition, the predictions of the load and hence the states have become much more accurate since nowadays open access to the operation of the transmission network is allowed. Hence, the potential of the DSE is becoming increasingly attractive in modern power systems. Especially under the panorama of the WAMS, the real-time monitoring of the power system provided by the SMT technology is giving the DSE more edge over the SSE.

One aspect of in the field of dynamic state estimation is the use of the DSE to detect anomalies. By comparing the residuals of the measurements, the SSE is able to detect and identify bad data. With the additional prediction data the DSE is capable of detecting other types of anomaly, such as bad data and sudden load change. In [69] varying weighting factors are assigned to the predictions and measurements so that the specific predictions of states and the specific measurements that have large errors are given less weights and the magnitude of errors can be reduced. However, using this method to reduce the risk of bad data and wrong predictions might not be as effective compared to the direct rejection of bad data, and the effect of reduced weights takes effect at the next time step making it unable to detect the anomalies in a timely manner. It is pointed out in [76]-[77] that these anomalies can be detected using the normalised innovations of the measurements. However, the methods for identifying the anomalies are not given, and there is no specific scheme about how to set the thresholds and discriminate different types of anomalies under different scenarios.

Another popular aspect of dynamic state estimation concerns the applications of the DSE: In [50], [78]-[79], the DSE is used to improve the performance of the hybrid state estimation problem; in [80]-[82], the DSE is applied to distribution system state estimation to improve the estimator's tracking ability during disturbance. With its unique state tracking ability and the real-time measurements provided by the PMUs, the DSEs are also applied to the estimation of the generator parameters [83]-[87], and the estimation of the unknown inputs (the mechanical power and the field electromotive force) to the generator [88]-[89]. Other topics related to dynamic state estimation include observability analysis of the DSEs [90], optimal PMU placement for DSE [91], distributed DSE [92], the applications of DSEs [93] etc.

1.2 Objectives

- To improve the reliability of state estimation, making sure enough measurements are placed at the right locations so that state estimation and its related functions such as bad data detection and parameter estimation can operate normally.
- To propose a convenient and effective method for finding the optimal location of the PMUs to guarantee the observability of state estimation.
- To comprehensively investigate the methods to include the synchronised measurements in state estimation, and propose philosophies for designing the new methods that can maximise the estimation accuracy and minimise the convergence time.
- To propose a new algorithm for dynamic state estimation so that it can achieve higher estimation accuracy, and more precisely and effectively deal with the different types of anomaly.

1.3 Thesis Structure

Chapter 2 – Review of Static State Estimation Methods

This chapter provides a review of the fundamental theories of state estimation including the formulation of the weighted least square estimator, network observability analysis and bad data detection. The basic network model, as well as the formulations of the power flows and power injections in the network, are discussed. The basic concepts introduced in this chapter will be used as the basis for the development of new theories, methods and algorithms which will be discussed in later chapters.

Chapter 3 – Numerical Observability Analysis

In this chapter, the existing methods for numerical observability analysis are re-examined. The theory which supports the existing method is revised following the identification of its flaw. This leads to the proposition of a new fully iterative method for observability analysis. To improve the efficiency of observability analysis, an iteration screening law and a direct method

for observability analysis are proposed. The chapter also presents a new method that integrates the PMU measurements into observability analysis, explores the possibility of improving the execution speed of observability analysis in other aspects, and discusses the feasibility of using alternative methods that can ensure the correctness of the result without using the methods proposed in this thesis.

Chapter 4 – Optimal PMU Placement

This chapter proposes a new method for optimal PMU placement in the presence of conventional methods. The new method ensures the correctness of the PMU placement, and reduces the occurrence of sub-optimal solutions compared to the existing methods based on new network observability criteria and a new network transformation scheme as given in this chapter.

Chapter 5 – Hybrid State Estimation

This chapter compares the performance of five different formulations of hybrid state estimators (HSEs) in three aspects of estimation accuracy, execution time and convergence. The comparison was initially made in a small network of the IEEE 14 Bus Test System considering all possible PMU placements. The conclusions are then validated in the IEEE 118 Bus Test System testing a number of optimally selected sets of PMU placements. After this, the underlying reasons for these results are explained by mathematical analysis. Apart from the cases where the HSEs are only affected by the Gaussian measurement errors, this chapter also presents the research results regarding the performance of the HSEs in the cases where the HSEs are also affected by gross measurement errors and parameter errors.

Chapter 6 – Dynamic State Estimation

In this chapter, a new algorithm for dynamic state estimation is presented based on the Cubature Kalman Filter (CKF). It is demonstrated through simulations that the CKF based dynamic state estimator (DSE) is significantly more accurate but also more affected by the anomalies in comparison to the DSEs that use other nonlinear filters. Thus, a set of new methods is proposed that can precisely detect, discriminate different types of anomaly

according to the normalised innovations and the skewness of the measurements. In addition, two new methods are proposed for identifying two types of anomaly, i.e. sudden change of load and sudden change of topology due to fault.

Chapter 7 – Thesis Summary

This chapter summarises the research results and contributions presented in the thesis. It also provides discussions on the limits of the presented research, and thus proposes some possible opportunities and ideas for further development of the presented research.

1.4 Contribution of this Research

The research presented in this thesis focuses on proposing new algorithms to improve the performance of power system state estimation. The contributions of this thesis can be divided into four parts:

1. Observability Analysis (Paper [A.1])
2. Optimal PMU Placement (Papers [A.2], [A.3], [A.7])
3. Hybrid State Estimation (Papers [A.2], [A.4], [A.7])
4. Dynamic State Estimation (Paper [A.5])

Details of these parts are given as follows.

1. New algorithms and theories for numerical observability analysis.
    a. Proposition of a fully-iterative method for numerical observability analysis, which can guarantee the correct identification of observable islands, after identifying and revising the flaw in the theory of the existing numerical method for observability analysis.
    b. Proposition of the convergence theorem for numerical observability analysis which proves the definite convergence of observability analysis.
    c. Proposition of the pathological case identification rule (*PCIR*) which can precisely distinguish normal cases and pathological cases.

   d. Proposition of the direct observable island identification method that identifies the observable islands in only one step.
   e. Proposition of a new algorithm for numerical observability analysis based on the *PCIR* and the direct observable island identification method.
   f. Proposition of a new method for integrating the PMU measurements into the algorithm of numerical observability analysis.

2. A new algorithm for optimal PMU placement in the presence of conventional measurements.
   a. Proposition of a new global network observability criterion.
   b. Proposition of a new network transformation scheme.
   c. Proposition of a new algorithm for optimal PMU placement in the presence of conventional measurements, which can ensure correct PMU placement with less sub-optimal problems compared to the existing methods, based on the new global network observability criterion and the new network transformation scheme.

3. A comprehensive analysis of the impact of estimator formulations on the performance of the hybrid state estimator (HSEs) taking the Gaussian measurement errors, gross measurement errors and parameter errors into account.
   a. Identification of the accuracy curves of five different formulations characterized by the knee point, which clearly indicates the benefits of using HSE compared to the conventional state estimator (CSE); that is to say, even with a small number of PMUs the state estimation accuracy can be significantly improved compared to the CSE.
   b. Identification of the relative estimation accuracy of the five different HSEs in the IEEE 14 Bus Test System. Before the knee point: Rectangular Current (RC) > Pseudo Flow (PF) ≈ Constrained Formulation (CF) ≈ Pseudo Voltage (PV) > Post-processing (PP); after the knee point: RC > PF ≈ CF > PP > PV.
   c. Validation of the knee point characteristic of the HSE accuracy curves and the relative estimation accuracy of the HSEs using simulations in the IEEE 118 Bus Test System and mathematical analysis.

   d. Setting out the reasons why the RC HSE is the most accurate while the PP HSE and PV HSE are the least accurate using mathematical analysis.
   e. Comparison of the execution time and convergence of the five HSE, and establishing that the CF HSE and PV HSE have poor performance in these two aspects.
   f. Recommendation of the RC HSE as the HSE to be implemented in the power system based on the comparison of the HSEs in terms of estimation accuracy, execution time and convergence.
   g. Discovering that the PMU placement can significantly affect the performance of the HSEs in the presence of gross measurement errors and parameter errors.
4. New algorithms for dynamic state estimation.
   a. Proposition of a new algorithm for detecting different types of anomaly.
   b. Proposition of the pseudo injection method for identifying the anomaly of sudden change of load.
   c. Proposition of the branch power flow variation ratio method for identifying the anomaly of a sudden change of topology due to fault.
   d. Proposition of a new algorithm for dynamic state estimation based on the Cubature Kalman Filter and the proposed anomaly detection and identification methods.

A list of publications (Papers [A.1]-[A.7]) produced during the PhD is presented in Appendix E.

Chapter 2 Review of Static State Estimation Methods

State estimation is responsible for constantly monitoring the power system to help guarantee that it operates in a normal and secure state. It uses a redundant set of measurements to produce the optimal estimate of the system's current operating state. The state estimator plays a key role in the Energy Management Systems (EMS), which are equipped with various other applications. Figure 2-1 shows an example of how the state estimator functions with various applications involved in the online static security assessment procedure. As detailed in the introduction, the function of the state estimator is supported by functions that include topology processor, observability analysis and bad data detection. Based on the estimate of the voltage angle and magnitudes of all the buses in the network, one of the three states is determined: emergency, restorative and normal. If the system is determined to be operating in emergency state or restorative state, the corresponding emergency control or restorative control will be activated. If the system is found to be in a normal state, it is assessed using a contingency analysis application to further check the security of the system. In the case of insecurity state, while the system is at risk of some contingencies, the preventive actions need to be planned after running the security constrained optimal power flow.

Although the DSEs have shown their advantages with the advent of SMT, the static state estimator (SSE) has formed the heart of nearly all modern network control systems since its establishment in the early 1970s. The SSE obtains the voltage phasors at a given point in time using the Weighted Least Square (WLS) method. The WLS method is derived under the Gaussian error assumption and the maximum likelihood estimation (MLE) theory. It guarantees that the estimate is the most likely state of the system based on the measurements received. Although it is suggested that some robust estimators, such as weighted least absolute value (WLAV) estimators and M-estimators, are less vulnerable to outliers (the measurements whose errors have large influence on the estimate of states) than the WLS method, they have not been adopted by the control centres because of their heavy computational burden.

In the following sections, the algorithm of the WLS method for static state estimation, and the existing methods for observability analysis and bad data detection are presented. In the later chapters, new methods are proposed based on the basic theory presented here.

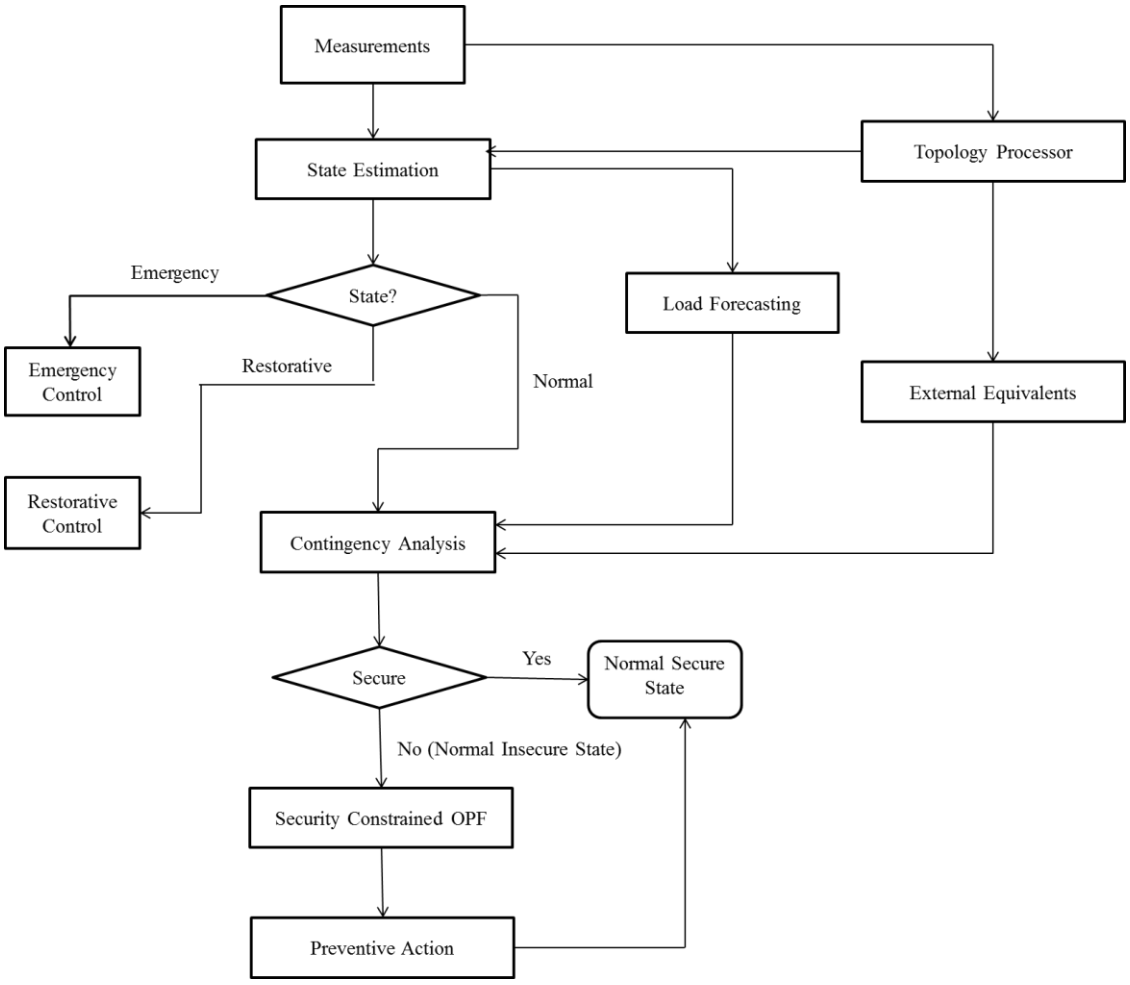

Figure 2-1: Online Static Security Assessment: Functional Diagram

2.1 Weighted Least Square Estimator

In this subsection, a general introduction about stochastic process and random variables and detailed discussion about the weighted least square (WLS) state estimator, including the measurement functions, the WLS objective function and its optimal solution, the measurement Jacobian matrix and the WLS state estimation algorithm, are presented.

2.1.1 Stochastic Process and Random Variables

In probability theory and related fields, a stochastic or random process is a mathematical object usually defined as a collection of random variables [94], and a random variable is defined as a variable whose possible values are numerical outcomes of a random phenomenon [95]. In power systems, the measurements received from the measurement devices installed across the network are affected by a series of random errors including device measurement errors, telecommunication errors, skew errors, loss of data. Thus, the process of measurement collection, transmission and reception is a stochastic process, and the measurements are random variables, which are commonly accepted in literature to follow the Gaussian distribution. The probability density function (p.d.f.) of the standard Gaussian distributed variable is illustrated in Figure 2-2.

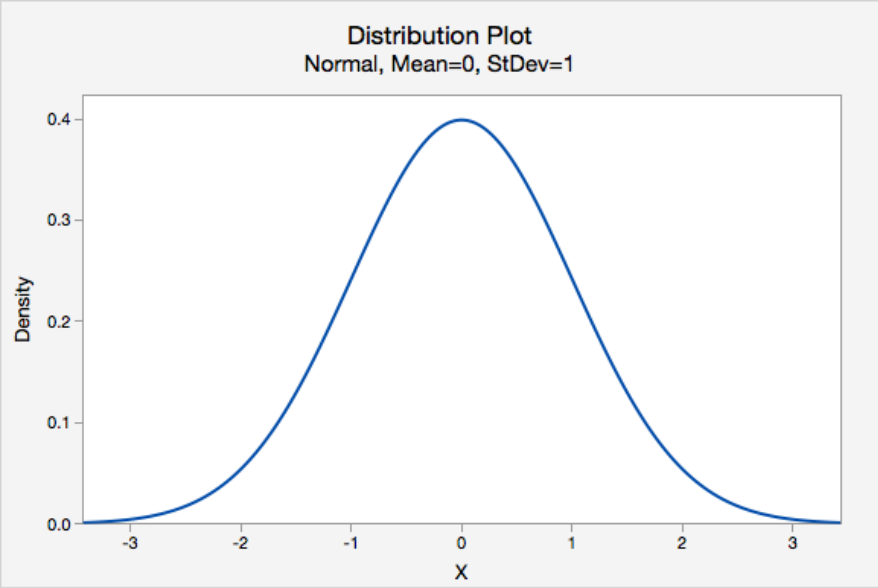

Figure 2-2: Probability Density Function of the Standard Gaussian Distribution

Since the measurements contain a certain amount of errors, a redundant set of measurements are used to monitor the states of the system. For example, the air temperature in the room is 27 °C, and is simultaneously monitored by five thermometers. The readings of the five thermometers are 27.3 °C, 26.5 °C, 27.2 °C, 26.9 °C and 27.2 °C, respectively. Since all of the five thermometers are affected by random errors, the most likely temperature is the average of the five numbers, 27.02 °C, which is very close to the true temperature in the room. Here, the

room is the *system*, the room temperature is the *state* of system, the average value of the readings of the five thermometers is the *estimate* of states, and the average function is the *estimator*. In general, an estimator can be defined as the function or application that provide the most likely estimate of the states based on observations / measurements that are affected by random errors. There are various types of estimators created for different purposes, such as weighted least square (WLS) estimator [1], least absolute value (LAV) estimator [1], M-estimator [1], Kalman filters [164]-[167] and so on. In static state estimation for power systems, the most widely used estimator is the WLS estimator. In the following subsections, a detailed discussion of the WLS estimator will be given, as well as the measurement functions (Section 2.1.2), the objective function and the optimal solution (Section 2.1.3), the expressions of the elements of its measurement Jacobian matrix (Section 2.1.4), and the algorithm of the WLS estimator (Section 2.1.5).

2.1.2 The Measurement Functions

A generalized formulation of the static state estimator using the WLS method utilizes five different types of conventional measurements for estimating the state of the system. The structure of the measurement vector, **z**, is given below:

$$\mathbf{z} = \begin{bmatrix} \mathbf{P}_{inj} \\ \mathbf{Q}_{inj} \\ \mathbf{P}_{flow} \\ \mathbf{Q}_{flow} \\ \mathbf{V}_{mag} \end{bmatrix} \tag{2.1}$$

where $\mathbf{P}_{inj}$, $\mathbf{Q}_{inj}$, $\mathbf{P}_{flow}$, $\mathbf{Q}_{flow}$ are the vectors of active and reactive injection measurements and flow measurements, and **V** is the vector of voltage magnitude measurements. The conventional measurements are related to the states using a set of nonlinear functions as given in (2.2):

$$\mathbf{z} = \mathbf{h}(\mathbf{x}) + \mathbf{e} \tag{2.2}$$

where **x** is the state vector that consists of voltage angles and magnitudes of all buses in the network, **h** is the vector of nonlinear functions relating the measurements and the states, and **e** is the vector of Gaussian errors. Note that since the conventional measurements are not synchronised like the PMU measurements, the slack bus is set usually as the reference bus. The angle of the reference bus is set at 0, and it is excluded from the state vector. Assuming the network parameters are known, the measurement equations for the five types of conventional measurement are based on the network structure in Figure 2-3 and are expressed as follows:

- Real and reactive power injection measurements

$$P_i = V_i \sum_{j=1}^{N} V_j (G_{ij} \cos\theta_{ij} + B_{ij} \sin\theta_{ij}) \tag{2.3}$$

$$Q_i = V_i \sum_{j=1}^{N} V_j (G_{ij} \sin\theta_{ij} - B_{ij} \cos\theta_{ij}) \tag{2.4}$$

- Real and reactive power flow measurements

$$P_{ij} = \frac{V_i^2}{a_{ij}^2}(g_{si} + g_{ij}) - \frac{V_i V_j}{a_{ij}}(g_{ij} \cos\theta_{ij} + b_{ij} \sin\theta_{ij}) \tag{2.5}$$

$$Q_{ij} = -\frac{V_i^2}{a_{ij}^2}(b_{si} + b_{ij}) - \frac{V_i V_j}{a_{ij}}(g_{ij} \sin\theta_{ij} - b_{ij} \cos\theta_{ij}) \tag{2.6}$$

$$P_{ji} = V_j^2(g_{sj} + g_{ij}) - \frac{V_j V_i}{a_{ij}}(g_{ij} \cos\theta_{ji} + b_{ij} \sin\theta_{ji}) \tag{2.7}$$

$$Q_{ji} = -V_j^2(b_{sj} + b_{ij}) - \frac{V_j V_i}{a_{ij}}(g_{ij} \sin\theta_{ji} - b_{ij} \cos\theta_{ji}) \tag{2.8}$$

- Voltage magnitude measurements

$$V_i = V_i \tag{2.9}$$

where G_{ij} and B_{ij} are the real and imaginary parts of the ij^{th} element of the network admittance matrix, respectively, g_{ij} and b_{ij} are the conductance and susceptance of the transmission line,

respectively, g_{si} and b_{si} are the shunt conductance and shunt susceptance of the shunt branch, respectively, and a_{ij} is the tap ratio of the transformer connecting Bus *i* and Bus *j*.

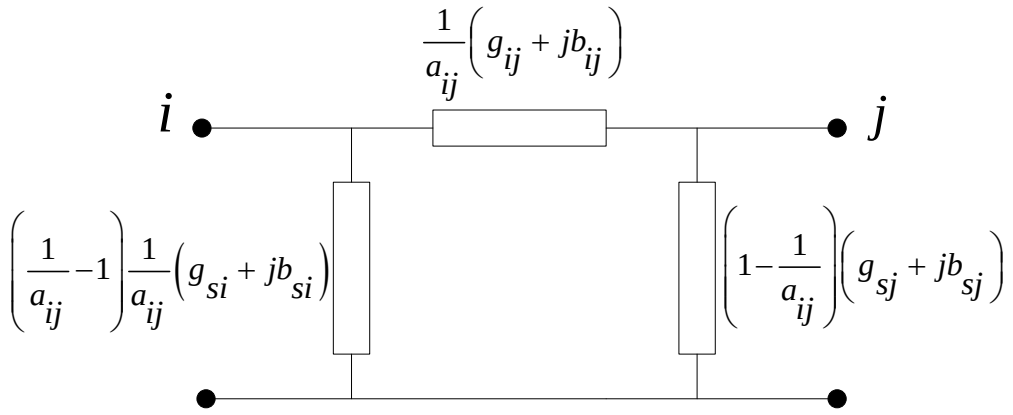

Figure 2-3: Transmission Line Represented in Pi Equivalent Model

2.1.3 The WLS Objective Function and Its Optimal Solution

According to the MLE theory, the optimal estimate of the state from the measurement equation (2.2) is achieved when the following WLS objective function is minimised:

$$J(\mathbf{x}) = \left[\mathbf{z} - \mathbf{h}(\mathbf{x})\right]^T \cdot \mathbf{R}^{-1} \cdot \left[\mathbf{z} - \mathbf{h}(\mathbf{x})\right] \tag{2.10}$$

where **R** is the covariance matrix of the error vector, **e**. The minimum of the objective function is found when its first derivative is zero:

$$\begin{aligned} &\frac{\partial J^T(\mathbf{x})}{\partial \mathbf{x}} = -2\mathbf{H}^T\mathbf{R}^{-1} \cdot \left[\mathbf{z} - \mathbf{h}(\mathbf{x})\right] = \mathbf{0} \\ &\Rightarrow \mathbf{m}(\mathbf{x}) = \mathbf{H}^T\mathbf{R}^{-1}\left[\mathbf{z} - \mathbf{h}(\mathbf{x})\right] = \mathbf{0} \end{aligned} \tag{2.11}$$

where **H** is the Jacobian matrix of the measurement to state function, **h**. Since the derived objective function, **m**(**x**), is still nonlinear, it has to be iteratively solved using the Newton-Raphson method. The iteration steps are derived as given in (2.12) and (2.13).

$$\mathbf{M} = \frac{\partial \mathbf{m}^T(\mathbf{x})}{\partial \mathbf{x}} = -\mathbf{H}^T\mathbf{R}^{-1}\mathbf{H} \tag{2.12}$$

$$\begin{aligned}\Delta\mathbf{x}^k &= -\mathbf{M}^{-1}\mathbf{g}\left(\mathbf{x}^k\right) = \left(\mathbf{H}^T\mathbf{R}^{-1}\mathbf{H}\right)^{-1}\mathbf{H}^T\mathbf{R}^{-1}\left[\mathbf{z}-\mathbf{h}(\mathbf{x})\right] \\ &= \left[\mathbf{G}\left(\mathbf{x}^k\right)\right]^{-1}\mathbf{t}^k\end{aligned} \tag{2.13}$$

$$\mathbf{G}\left(\mathbf{x}^k\right) = \mathbf{H}\left(\mathbf{x}^k\right)^T\mathbf{R}^{-1}\mathbf{H}\left(\mathbf{x}^k\right) \tag{2.14}$$

$$\mathbf{t}^k = \mathbf{H}^T\mathbf{R}^{-1}\left[\mathbf{z}^k - \mathbf{h}\left(\mathbf{x}^k\right)\right] \tag{2.15}$$

$$\mathbf{G}\left(\mathbf{x}^k\right)\Delta\mathbf{x}^k = \mathbf{t}^k \tag{2.16}$$

where $\mathbf{G}(\mathbf{x}^k)$ is the *Gain Matrix*, $\Delta\mathbf{x}^k = \mathbf{x}^{k+1} - \mathbf{x}^k$ is the difference of the state estimate between iterations, and (2.16) is referred to as the *Normal Equations*. The iteration terminates when $\Delta\mathbf{x}^{k+1}$ is below a pre-defined threshold.

The gain matrix can be used for observability analysis of the network, and it is crucial for static state estimation as its inversion is the most computational demanding part. According to [4], the gain matrix has the following properties:

- It is structurally and numerically symmetric.
- It is sparse, yet less sparse compared to **H**.
- In general it is a non-negative definite matrix, i.e. all of its eigenvalues are non-negative. It is positive definite for fully observable networks.

The sparsity of the gain matrix can be exploited to improve the computational efficiency and reduce the memory requirement. Details of the technique are given in [4].

2.1.4 The Measurement Jacobian Matrix

The measurement Jacobian matrix, **H**, as defined after (2.11) has the following structure:

$$\mathbf{z} = \begin{bmatrix} \dfrac{\partial \mathbf{P}_{inj}}{\partial \boldsymbol{\theta}} & \dfrac{\partial \mathbf{P}_{inj}}{\partial \mathbf{V}} \\ \dfrac{\partial \mathbf{Q}_{inj}}{\partial \boldsymbol{\theta}} & \dfrac{\partial \mathbf{Q}_{inj}}{\partial \mathbf{V}} \\ \dfrac{\partial \mathbf{P}_{flow}}{\partial \boldsymbol{\theta}} & \dfrac{\partial \mathbf{P}_{flow}}{\partial \mathbf{V}} \\ \dfrac{\partial \mathbf{Q}_{flow}}{\partial \boldsymbol{\theta}} & \dfrac{\partial \mathbf{Q}_{flow}}{\partial \mathbf{V}} \\ \mathbf{0} & \dfrac{\partial \mathbf{V}_{mag}}{\partial \mathbf{V}} \end{bmatrix} \tag{2.17}$$

Based on the transmission line model shown in Figure 2-3, the expressions for each partition are given below:

1. Jacobian elements of the real power injection measurements:

$$\frac{\partial P_i}{\partial \theta_i} = -V_i \sum_{j=1}^{N} V_j (G_{ij} \sin\theta_{ij} - B_{ij} \cos\theta_{ij}) - V_i^2 B_{ii} \tag{2.18}$$

$$\frac{\partial P_i}{\partial \theta_j} = V_i V_j (G_{ij} \sin\theta_{ij} - B_{ij} \cos\theta_{ij}) \tag{2.19}$$

$$\frac{\partial P_i}{\partial V_i} = \sum_{j=1}^{N} V_j (G_{ij} \cos\theta_{ij} + B_{ij} \sin\theta_{ij}) + V_i G_{ii} \tag{2.20}$$

$$\frac{\partial P_i}{\partial V_j} = V_i (G_{ij} \cos\theta_{ij} + B_{ij} \sin\theta_{ij}) \tag{2.21}$$

2. Jacobian elements of the reactive power injection measurements:

$$\frac{\partial Q_i}{\partial \theta_i} = V_i \sum_{j=1}^{N} V_j (G_{ij} \cos\theta_{ij} + B_{ij} \sin\theta_{ij}) - V_i^2 G_{ii} \tag{2.22}$$

$$\frac{\partial Q_i}{\partial \theta_j} = -V_i V_j (G_{ij} \cos\theta_{ij} + B_{ij} \sin\theta_{ij}) \tag{2.23}$$

$$\frac{\partial Q_i}{\partial V_i} = \sum_{j=1}^{N} V_j (G_{ij} \sin\theta_{ij} - B_{ij} \cos\theta_{ij}) - V_i B_{ii} \tag{2.24}$$

$$\frac{\partial Q_i}{\partial V_j} = V_i (G_{ij} \sin\theta_{ij} - B_{ij} \cos\theta_{ij}) \tag{2.25}$$

3. Jacobian elements of the active power flow measurements:

$$\frac{\partial P_{ij}}{\partial \theta_i} = -\frac{V_i V_j}{a_{ij}}(-g_{ij}\sin\theta_{ij} + b_{ij}\cos\theta_{ij}) \tag{2.26}$$

$$\frac{\partial P_{ij}}{\partial \theta_j} = -\frac{V_i V_j}{a_{ij}}(g_{ij}\sin\theta_{ij} - b_{ij}\cos\theta_{ij}) \tag{2.27}$$

$$\frac{\partial P_{ij}}{\partial V_i} = 2\frac{V_i}{a_{ij}^2}(g_{si} + g_{ij}) - \frac{V_j}{a_{ij}}(g_{ij}\cos\theta_{ij} + b_{ij}\sin\theta_{ij}) \tag{2.28}$$

$$\frac{\partial P_{ij}}{\partial V_j} = -\frac{V_i}{a_{ij}}(g_{ij}\cos\theta_{ij} + b_{ij}\sin\theta_{ij}) \tag{2.29}$$

4. Jacobian elements of the reactive power flow measurements:

$$\frac{\partial Q_{ij}}{\partial \theta_i} = -\frac{V_i V_j}{a_{ij}}(g_{ij}\cos\theta_{ij} + b_{ij}\sin\theta_{ij}) \tag{2.30}$$

$$\frac{\partial Q_{ij}}{\partial \theta_j} = \frac{V_i V_j}{a_{ij}}(g_{ij}\cos\theta_{ij} + b_{ij}\sin\theta_{ij}) \tag{2.31}$$

$$\frac{\partial Q_{ij}}{\partial V_i} = -2\frac{V_i}{a_{ij}^2}(b_{si} + b_{ij}) - \frac{V_j}{a_{ij}}(g_{ij}\sin\theta_{ij} - b_{ij}\cos\theta_{ij}) \tag{2.32}$$

$$\frac{\partial Q_{ij}}{\partial V_j} = -\frac{V_i}{a_{ij}}(g_{ij}\sin\theta_{ij} - b_{ij}\cos\theta_{ij}) \tag{2.33}$$

5. Jacobian elements of the voltage magnitude measurements:

$$\frac{\partial V_i}{\partial V_i} = 1 \tag{2.34}$$

$$\frac{\partial V_i}{\partial \theta_i} = \frac{\partial V_i}{\partial \theta_j} = \frac{\partial V_i}{\partial V_j} = 0 \tag{2.35}$$

2.1.5 The WLS State Estimation Algorithm

Based on the network model and the mathematical models given in the previous sub-sections, the algorithm for WLS state estimation is outlined as follows [4]:

1. Start iterations, set the iteration index $k = 0$.
2. Initialize the state vector $\mathbf{x}^k$, typically as a flat start (all voltage angles equal to 0, and all voltage magnitudes equal to 1).
3. Formulate the Jacobian matrix, $\mathbf{H}$, according to (2.17) to (2.35).
4. Calculate the gain matrix, $\mathbf{G}(\mathbf{x}^k)$, using (2.14).
5. Calculate the estimated measurements based on $\mathbf{x}^k$, $\mathbf{h}(\mathbf{x}^k)$, according to (2.1) to (2.9).
6. Calculate the right hand side $\mathbf{t}^k$ using (2.15).
7. Decompose $\mathbf{G}(\mathbf{x}^k)$ and solve for $\Delta\mathbf{x}^k$ using (2.13).
8. Test for convergence, max $(|\Delta\mathbf{x}^k|) \leq \varepsilon$?
9. If Step 8 is not satisfied, update $\mathbf{x}^{k+1} = \mathbf{x}^k + \Delta\mathbf{x}^k$, $k = k + 1$, and go to Step 3. Else stop and output the state estimate.

2.2 Observability Analysis

Prior to state estimation, it must be guaranteed that a unique solution can be found with measurements received. The observability analysis is established for this purpose. The observability of the network can be defined on two levels. The first level is topological observability. A network is said to be *topologically observable* as long as enough measurements are placed at the right locations for a given network topology. The second level is numerical observability. The *numerical observability* requires the gain matrix as defined in (2.14) to be non-singular, i.e. invertible. This not only requires the network to be topologically observable, but also free of outliers and gross measurement errors. As such cases are not likely to happen and could be easily prevented by checking the robustness of the state estimator and bad data analysis, only the topological observability is required and thus analysed for state

estimation. In the following parts of the thesis, observability or network observability refers to topological observability for the sake of convenience.

In the case where the measurements available are not enough to support observability of the system, the network is divided into several *Observable Islands* separated by unobserved branches. Each of the observable islands has its individual reference angle, and the state estimation might still be performed within the observable islands. The observability analysis is also responsible for identifying the observable islands and finding measurements to restore the network observability.

As detailed in the Introduction, (topological) observability analysis can be carried out directly with the topological method that is based on the graphical theory, or using the numerical method based on the decoupled DC state estimation model and the measurement Jacobian matrix / the gain matrix.

The numerical observability analysis was first proposed in [26], where the theory behind observability analysis was presented, and the decoupled DC state estimation model was proposed for observability analysis. The observable islands and the unobserved branches are identified by partitioning the gain matrix and testing the observability of the sub-networks iteratively. The authors of [26] later improved the matrix partitioning process by using triangular factorisation [33]. Several methods based on the gain matrix have been proposed in [32], [34]-[35]. The other methods, which use alternative methods instead of analysing the gain matrix [36]-[37], include Hachtel's augmented matrix method [38]-[40], the gram matrix method and binary arithmetic [41].

It is reported in [42] that the classical method for observability analysis as proposed in [33] might incorrectly integrate the buses that belong to different observable islands into the same observable island. The cases in which the particular network topology and measurement placement would lead to misidentification of the observable islands are termed as *pathological cases*. It is stated in [42] that the pathological cases can be avoided by using the inverse

triangular factors of the gain matrix instead of using the gain matrix directly, and the observable islands can be identified without iteration using the new method.

However, it is found that the method proposed in [42] still cannot prevent all pathological cases. In this section, a review of the classical method proposed in [33], and the improved method proposed in [42] is presented. A new method is proposed in this thesis, which is completely free of pathological cases and significantly faster than the existing methods, will be discussed in detail in Chapter 3.

2.2.1 Decoupled DC Model for Numerical Observability Analysis

The decoupled DC model was proposed in [96] as the simplified network model for observability analysis in state estimation. A linear relationship between the active power measurements and the states of voltage angle is assumed. As it is recognized that PV and Qθ are weakly coupled, while Pθ and QV are strongly coupled, only the equations related to active power measurements and voltage angle states are considered to further simplify the model. The decoupled DC model is helpful for numerical observability analysis because of its simplification in calculations without loss of topological information of the network. By neglecting the positions of the circuit breaker position, the observability of the network is not affected by the branch parameters and the values of the states. So, the decoupled DC model can be applied for simplifying observability analysis without introducing any error in terms of topological observability.

Using the decoupled DC model, the measurement equation as defined in (2.2) can be simplified as follows:

$$\mathbf{z} = \mathbf{H}\boldsymbol{\theta} + \mathbf{e} \tag{2.36}$$

where $\mathbf{z}$ is the measurement vector containing the power injection and flow measurements only, $\mathbf{H}$ denotes the DC measurement Jacobian, $\boldsymbol{\theta}$ is the state vector of voltage angles, and $\mathbf{e}$ is the error vector.

As the value of the state estimate does not affect the network topology and measurement locations, and thus the network observability, the measurement error covariance matrix (**R**) as defined after (2.10) can be assumed to be an identity matrix and this process does not introduce any errors. The gain matrix can then be simplified as follows:

$$\mathbf{G} = \mathbf{H}^T\mathbf{H} \tag{2.37}$$

With unity branch reactance, the derivative of the power flow measurement is 1 for element corresponding to the sending bus, -1 for the receiving bus, and 0 for the other buses. As the power injection is the sum of the power flows into that bus, the derivative of the power injection measurement is *N* for the incident bus, -1 for the other ends of connected branches, and 0 for the other buses, where *N* is the number of the connecting branches of the incident bus. Examples of a power flow measurement and a power injection measurement are shown in (2.38) and (2.39), respectively.

$$\mathbf{h} = \begin{bmatrix} 0 & 0 & 0 & 0 & 1 & -1 \end{bmatrix} \tag{2.38}$$

$$\mathbf{h} = \begin{bmatrix} -1 & \cdots & -1 & N & 0 & \cdots & 0 & -1 & 0 & \cdots & 0 \end{bmatrix} \tag{2.39}$$

2.2.2 Factorisation of the Gain Matrix

In numerical observability analysis, a network can be seen as a combination of *N* observable islands (*N*=1 for fully observable case, *N*>1 for not fully observable case), each of the islands having their own reference angle. Thus, the gain matrix is always singular, and is required to be factorised in order to find information about the reference angles. In the classical method and the direct method presented in this section, Cholesky factorisation is used since the gain matrix is symmetrical. However, the prerequisite for Cholesky factorisation is that the matrix to be factorised must be positive definite. This problem is countered by skipping the zero pivot, and adding 0 into the corresponding diagonal element of the resulting diagonal matrix. For example, consider the case when the first zero pivot is encountered during factorisation as shown in (2.40).

$$\mathbf{D}_i = \mathbf{L}_1^{-1} \cdots \mathbf{L}_i^{-1} \mathbf{G} \mathbf{L}_i^{-T} \cdots \mathbf{L}_1^{-T} = \begin{bmatrix} d_1 & & & & \\ & \ddots & & & \\ & & d_i & & \\ & & & 0 & \mathbf{0} \\ & & & \mathbf{0} & \mathbf{G}_{i+1} \end{bmatrix} \tag{2.40}$$

where $\mathbf{D}_i$ is the semi-factorised diagonal matrix whose first i elements have been factorised, d_i is the i^{th} diagonal element, $\mathbf{G}_i$ is the sub-matrix to be factorised in the i^{th} step, and $\mathbf{L}_i$ is the Cholesky factor during the i^{th} step, whose structure is given in (2.41):

$$\mathbf{L}_i = \begin{bmatrix} \mathbf{I} & & \\ & 1 & \\ & \mathbf{l}_i & \mathbf{I} \end{bmatrix} \tag{2.41}$$

$$\mathbf{l}_i^T = \begin{bmatrix} L_{i+1,i} & \cdots & L_{N,i} \end{bmatrix} \tag{2.42}$$

where N is the number of buses in the system, $\mathbf{I}$ denotes identity matrix of arbitrary size, $\mathbf{l}_i$ is a nonzero sub-vector under the element of 1 in the i^{th} column (size of (N-i-1)*1).

In this case, the factorisation process is continued by setting the i+1$^{\text{th}}$ element of the diagonal matrix to be zero and i^{th} Cholesky factor to be an identity matrix (2.43)-(2.44). In such a way, the factorisation at the i^{th} step is skipped, and the process may continue to factorise $\mathbf{G}_{i+1}$.

$$d_{i+1} = 0 \tag{2.43}$$

$$\mathbf{L}_{i+1} = \mathbf{I} \tag{2.44}$$

Using this method for every zero pivot encountered, the resulting diagonal matrix can be expressed as follows:

$$\mathbf{D} = \mathbf{L}_1^{-1} \cdots \mathbf{L}_N^{-1} \mathbf{G} \mathbf{L}_N^{-T} \cdots \mathbf{L}_1^{-T} = \mathbf{L}^{-1} \mathbf{G} \mathbf{L}^{-T} \tag{2.45}$$

where **D** is the resulting singular diagonal matrix, and **L** is the resulting lower triangular Cholesky factor. For analysis purposes, the zero pivots can be moved to the bottom of the **D** after proper matrix permutations (2.46); correspondingly the structure of **L** is given by (2.47):

$$\mathbf{D} = \begin{bmatrix} d_1 & & & \\ & \ddots & & \\ & & d_{N-k} & \\ & & & \mathbf{0}_k \end{bmatrix} \tag{2.46}$$

$$\mathbf{L} = \begin{bmatrix} 1 & & & \\ & \ddots & & \\ & & 1 & \\ \mathbf{l}_1 & \cdots & \mathbf{l}_{N-k} & \mathbf{I}_k \end{bmatrix} \tag{2.47}$$

Both **D** and **L** contain observability information of the network. How these matrices are used to identify the unobservable branches and the observable islands by the classical method and the direct method for observability analysis are described in detail in the following subsections. Details of each step of Cholesky factorisation are given in Appendix A.

2.2.3 The Classical Numerical Method for Observability Analysis

The classical numerical method for observability analysis is based on analysing the gain matrix. The network is observable if all branches are identified to be observable, or the observable islands are identified after the unobservable branches have been removed. The derivation of the classical model is given as follows [4]:

Consider the normal equation (2.16) expressed in the decouple DC model with all power flows set at 0:

$$\mathbf{G\theta} = \mathbf{t} = \mathbf{0} \tag{2.48}$$

As the angle of the reference bus is also included in the state vector, the gain matrix, **G**, is still singular even for the fully observable case. Thus, it is possible to partition the gain matrix after permuting the rows and columns properly:

$$\begin{bmatrix} \mathbf{G}_{11} & \mathbf{G}_{12} \\ \mathbf{G}_{21} & \mathbf{G}_{22} \end{bmatrix} \begin{bmatrix} \boldsymbol{\theta}_1 \\ \boldsymbol{\theta}_2 \end{bmatrix} = \begin{bmatrix} \mathbf{0} \\ \mathbf{0} \end{bmatrix} \tag{2.49}$$

$$\mathbf{G}_{22} \equiv \mathbf{0} \tag{2.50}$$

where $\mathbf{G}_{11}$ is the maximum size non-singular submatrix within $\mathbf{G}$. The sub state vector, $\boldsymbol{\theta}_2$, is free to change its values as it is proved in [33] that its corresponding submatrix of the gain matrix is always a zero matrix (2.50). Thus the value of $\boldsymbol{\theta}_1$ can also be determined by assigning arbitrary but different values to $\boldsymbol{\theta}_2$ as $\bar{\boldsymbol{\theta}}_2$:

$$\hat{\boldsymbol{\theta}}_1 = -\mathbf{G}_{11}^{-1}\mathbf{G}_{12}\bar{\boldsymbol{\theta}}_2 \tag{2.51}$$

Then the power flows of all branches with the solution can be calculated:

$$\mathbf{A}\begin{bmatrix} \hat{\boldsymbol{\theta}}_1^T & \bar{\boldsymbol{\theta}}_2^T \end{bmatrix}^T = \mathbf{A}\hat{\boldsymbol{\theta}}^* = \mathbf{P}_{branch} \tag{2.52}$$

where $\mathbf{A}$ is the branch to bus incident matrix. Since it is assumed that all power flows in the network are equal to 0, the corresponding branches of the zero elements in $\mathbf{P}_{branch}$ are identified as the *unobservable branches*.

As it is difficult to find $\mathbf{G}_{11}$, $\hat{\boldsymbol{\theta}}^*$ can be solved using an alternative method, i.e. Cholesky factorisation of the gain matrix, $\mathbf{G}$. The zero pivots in the resulting singular diagonal matrix, $\mathbf{D}$, are replaced with 1's so that the gain matrix becomes invertible, and the corresponding elements of $\mathbf{t}$ are assigned with arbitrary but distinct values. The estimate of the state can be found using (2.53), and the values of $\bar{\mathbf{t}}$ are typically set as 0 for elements corresponding to positive pivots, and natural numbers starting from 1, as is shown in (2.54):

$$\hat{\boldsymbol{\theta}}^* = \left(\mathbf{L}\mathbf{D}\mathbf{L}^T\right)^{-1}\bar{\mathbf{t}} \tag{2.53}$$

$$\bar{\mathbf{t}}^T = \begin{bmatrix} 0 & \cdots & 0 & 1 & \cdots & N_{zp} \end{bmatrix} \tag{2.54}$$

where N_{zp} is the number of zero pivots.

The unobservable branches identified that follow the above procedure might not include all unobservable branches. This is because the identification might be affected by the *irrelevant injection measurements*, the injection measurements incident to the unobservable branches. Thus, it is necessary to repeatedly identify the unobservable branches, eliminating the irrelevant injection measurements at the end of each time, until no more irrelevant injection measurements are identified.

Based on the methods introduced in this sub-section, the algorithm for classical numerical observability analysis is presented as follows:

1. Set the iteration number $k = 1$.
2. Form the gain matrix in decoupled DC model using (2.48).
3. Perform Cholesky factorisation on the gain matrix, substitute the zero pivots with 1, and assign natural numbers to the vector, **t**. If $k = 1$ and only one zero pivot is identified, stop the program, the network is fully observable. Else if $k = 1$ and more than one zero pivot is identified, go to Step 4, the network is not fully observable.
4. Identify the unobservable branches using (2.52) and (2.53), and the irrelevant injection measurements separated by the unobservable branches.
5. If no more unobservable branches are identified, then identify the observable islands separated by the unobservable branches. Else, $k = k + 1$, go to Step 2.

2.2.4 The Direct Numerical Method for Observability Analysis

As suggested in [42], the classical method for observability analysis may incorrectly identify buses that belong to different observable islands in the same observable island. Consider a network with its gain matrix expressed by (2.55), the estimated angles can be derived as given in (2.56).

$$\mathbf{G} = \mathbf{L}\bar{\mathbf{D}}\mathbf{L}^T = \begin{bmatrix} 1 & & & \\ & \ddots & & \\ & & 1 & \\ \mathbf{l}_1 & \cdots & \mathbf{l}_{N-k} & \mathbf{I}_k \end{bmatrix} \begin{bmatrix} d_1 & & & \\ & \ddots & & \\ & & d_{N-k} & \\ & & & \mathbf{I}_k \end{bmatrix} \begin{bmatrix} 1 & & & \mathbf{l}_1^T \\ & \ddots & & \vdots \\ & & 1 & \mathbf{l}_{N-k}^T \\ & & & \mathbf{I}_k \end{bmatrix} \tag{2.55}$$

$$\begin{aligned} \hat{\boldsymbol{\theta}}^* &= \left(\mathbf{L}\bar{\mathbf{D}}\mathbf{L}^T\right)^{-1}\bar{\mathbf{t}} \\ &= \begin{bmatrix} 1 & & & \mathbf{m}_1^T \\ & \ddots & & \vdots \\ & & 1 & \mathbf{m}_{N-k}^T \\ & & & \mathbf{I}_k \end{bmatrix} \begin{bmatrix} d_1^{-1} & & & \\ & \ddots & & \\ & & d_{N-k}^{-1} & \\ & & & \mathbf{I}_k \end{bmatrix} \begin{bmatrix} 1 & & & \\ & \ddots & & \\ & & 1 & \\ \mathbf{m}_1 & \cdots & \mathbf{m}_{N-k} & \mathbf{I}_k \end{bmatrix} \begin{bmatrix} 0 \\ \vdots \\ 0 \\ \mathbf{n}_k \end{bmatrix} \\ &= \begin{bmatrix} 1 & & & \mathbf{m}_1^T \\ & \ddots & & \vdots \\ & & 1 & \mathbf{m}_{N-k}^T \\ & & & \mathbf{I}_k \end{bmatrix} \begin{bmatrix} 0 \\ \vdots \\ 0 \\ \mathbf{n}_k \end{bmatrix} \\ &= \begin{bmatrix} 1 & & \mathbf{u}_1^T & \mathbf{w}_1^T \\ & \ddots & \vdots & \vdots \\ & \ddots & \mathbf{u}_{N-k+1}^T & \mathbf{w}_{N-k+1}^T \\ & & 1 & \mathbf{w}_{N-k}^T \\ & & & \mathbf{I}_k \end{bmatrix} \begin{bmatrix} 0 \\ \vdots \\ \vdots \\ 0 \\ \mathbf{n}_k \end{bmatrix} \\ &= \begin{bmatrix} \mathbf{w}_1^T\mathbf{n}_k \\ \vdots \\ \mathbf{w}_{N-k}^T\mathbf{n}_k \\ \mathbf{n}_k \end{bmatrix} \end{aligned} \tag{2.56}$$

where $\mathbf{m}_i$ is the sub-vector under the diagonal element of the i^{th} column of the matrix, $\mathbf{L}^{-1}$, $\mathbf{w}_i$ is the sub-vector of $\mathbf{m}_i$ corresponding to the zero pivots, and $\mathbf{u}_i$ is the sub-vector of $\mathbf{w}_i$ that consists of the remaining elements, and $\mathbf{n}_k$ is a vector of natural numbers as given by (2.57).

$$\mathbf{n}_k^T = \begin{bmatrix} 1 & 2 & \cdots & k \end{bmatrix} \tag{2.57}$$

It can be seen from (2.56) that, although the values of the $\mathbf{w}_i$'s can be different, the results of the product might be the same. As will be proved in the next chapter, one of the properties of the $\mathbf{w}_i$ is that its sum of elements is always 1. Thus, it can be easily proved that for $k > 2$, such

pathological cases might happen as multiple solutions can be found for $\mathbf{w}_i$ because its elements are only constrained by two equations.

$$\sum_{k=1}^{N} k w_{i,k} = C \tag{2.58}$$

$$\sum_{k=1}^{N} w_{i,k} = 1 \tag{2.59}$$

where C is any real constant.

The above derivation also reveals that the sub-vectors, $\mathbf{w}_i$'s, might be the very key factors that contain information about observable islands. In [42], these sub-vectors and the bottom identity matrix are grouped together as the *Test Matrix* (2.60), and it is defined as the sub-matrix of the inverse of the Cholesky factor corresponding to the zero pivots. Note that, generally, the zero pivots might appear at any place on the diagonal matrix, $\mathbf{D}$, and the columns of $\mathbf{I}_k$ might appear in any column in the test matrix.

$$\mathbf{W} = \begin{bmatrix} \mathbf{w}_1 & \mathbf{w}_2 & \cdots & \mathbf{w}_{N-k} & \mathbf{I}_k \end{bmatrix} \tag{2.60}$$

According to [42], the test matrix has the following two properties:

Property 1: The columns of $\mathbf{W}$ corresponding to buses that belong to the same observable island will have the same numerical values.

Property 2: The columns of $\mathbf{W}$ corresponding to buses that belong to different observable islands will have different numerical values, as long as these buses are connected by a common branch. If the buses are topologically separated, then their corresponding column vectors might be the same even though they belong to different observable islands.

Property 2 suggests that the observable islands might not be correctly identified even by directly comparing the column vectors of the test matrix. However, the identification of the

unobservable branches can be directly identified using (2.61): the branches corresponding to non-zero row vectors are unobservable branches.

$$\mathbf{C} = \mathbf{A}\mathbf{W}^T \tag{2.61}$$

where **A** is the branch to bus incident matrix.

Based on the two properties as proved in [42], the algorithm for the direct numerical observability analysis is presented as follows:

1. Form the gain matrix in decoupled DC model using (2.48).
2. Perform Cholesky factorisation on the gain matrix. If there is only one zero pivot, stop the program, the network is fully observable. Else, calculate the inverse matrix of the Cholesky factor and obtain the test matrix, **W**.
3. Calculate **C** using (2.61), find the non-zero row vectors of **C**, their corresponding branches are unobservable branches.
4. Identify the observable island separated by the unobservable branches.

2.2.5 Measurement Replacement

After the observable islands are identified, additional measurements should be replaced in order to restore the observability of the network. The candidate measurements include the power injection measurements incident to the border buses of the observable islands, and the power flow measurements that connect two observable islands. These candidate measurements can be expressed in a single matrix, $\mathbf{H}_c$.

Now consider the new gain matrix after all candidate measurements have been added into the network as expressed in (2.62).

$$
\begin{aligned}
\mathbf{G}_{new} &= \mathbf{G} + \mathbf{H}_c^T \mathbf{H}_c \\
&= \mathbf{L}\left(\mathbf{D} + \mathbf{L}^{-1}\mathbf{H}_c^T\left(\mathbf{L}^{-1}\mathbf{H}_c^T\right)^T\right)\mathbf{L}^T \\
&= \mathbf{L}\left(\begin{bmatrix}\bar{\mathbf{D}} & \\ & \mathbf{0}\end{bmatrix} + \begin{bmatrix}\mathbf{U}\mathbf{H}_c^T \\ \mathbf{W}\mathbf{H}_c^T\end{bmatrix}\begin{bmatrix}\mathbf{U}\mathbf{H}_c^T \\ \mathbf{W}\mathbf{H}_c^T\end{bmatrix}^T\right)\mathbf{L}^T \\
&= \mathbf{L}\begin{bmatrix}\bar{\mathbf{D}} + \mathbf{U}\mathbf{H}_c^T\mathbf{H}_c\mathbf{U}^T & \mathbf{U}\mathbf{H}_c^T\mathbf{H}_c\mathbf{W}^T \\ \mathbf{W}\mathbf{H}_c^T\mathbf{H}_c\mathbf{U}^T & \mathbf{W}\mathbf{H}_c^T\mathbf{H}_c\mathbf{W}^T\end{bmatrix}\mathbf{L}^T \\
&= \mathbf{L}\mathbf{E}\mathbf{L}^T
\end{aligned}
\tag{2.62}
$$

where $\bar{\mathbf{D}}$ is the maximum non-singular submatrix of the singular diagonal matrix, **D**, **L** is the Cholesky factor, **W** is the test matrix, and **U** is the remaining part of $\mathbf{L}^{-1}$ except for the test matrix.

In order to analyse the observability of the new gain matrix, the following elementary transformations are performed for the middle matrix of the final expression, **E**.

1. Subtract $\mathbf{U}\mathbf{W}^{-1}$ times the second row from the first row:

$$
\mathbf{E} = \begin{bmatrix}\bar{\mathbf{D}} + \mathbf{U}\mathbf{H}_c^T\mathbf{H}_c\mathbf{U}^T & \mathbf{U}\mathbf{H}_c^T\mathbf{H}_c\mathbf{W}^T \\ \mathbf{W}\mathbf{H}_c^T\mathbf{H}_c\mathbf{U}^T & \mathbf{W}\mathbf{H}_c^T\mathbf{H}_c\mathbf{W}^T\end{bmatrix} \sim \begin{bmatrix}\bar{\mathbf{D}} & \mathbf{0} \\ \mathbf{W}\mathbf{H}_c^T\mathbf{H}_c\mathbf{U}^T & \mathbf{W}\mathbf{H}_c^T\mathbf{H}_c\mathbf{W}^T\end{bmatrix} \tag{2.63}
$$

2. Subtract $\bar{\mathbf{D}}^{-1}\mathbf{W}\mathbf{H}_c^T\mathbf{H}_c\mathbf{U}^T$ times the first row from the second row

$$
\mathbf{E} \sim \begin{bmatrix}\bar{\mathbf{D}} & \mathbf{0} \\ \mathbf{W}\mathbf{H}_c^T\mathbf{H}_c\mathbf{U}^T & \mathbf{W}\mathbf{H}_c^T\end{bmatrix} \sim \begin{bmatrix}\bar{\mathbf{D}} & \mathbf{0} \\ \mathbf{0} & \left(\mathbf{H}_c\mathbf{W}^T\right)^T\mathbf{H}_c\mathbf{W}^T\end{bmatrix} \tag{2.64}
$$

As $\bar{\mathbf{D}}$ and **L** are positive definite and rank(**A**) = rank($\mathbf{A}^T\mathbf{A}$), the new gain matrix will be observable, or it is 1 rank less than its dimension, as long as the matrix **B** as defined in (2.65) is observable. Since it is always more than enough to include all candidate measurements to restore network observability, only parts of them are required to be replaced. The selection of the necessary measurements can be done by computing the reduced echelon form $\mathbf{B}_e$ of **B**. The

measurements corresponding to the linearly independent rows of $\mathbf{B}_e$ are the necessary measurements to be replaced.

$$\mathbf{B} = \mathbf{H}_c \mathbf{W}^T \tag{2.65}$$

Assuming the identification of observable islands have been done before the measurement replacement process, the algorithm for measurement replacement can be summarised as follows:

1. Find a list of candidate measurements, including the power flow and injection measurements incident to the observable islands that have been identified in the previous steps of observability analysis.
2. Form the candidate measurement Jacobian matrix, $\mathbf{H}_c$.
3. Assuming the test matrix **W** has already been calculated while identifying the observable islands, calculate **B** using (2.65), and its reduced echelon, $\mathbf{B}_e$. The measurements corresponding to the linearly independent rows of $\mathbf{B}_e$ are the minimum number of measurements that can restore the network observability.

2.2.6 Redundancy analysis

After observability analysis a unique solution can be guaranteed with the measurements available. However, it is possible that some of the measurements might be lost due to telecommunication errors or failure of the measurement device. If a state is observed by only one measurement, then the loss of this measurement would make the system unobservable. In redundancy analysis, these measurements are termed as *critical measurements*, and the other type of measurements are termed as *redundant measurements* which can be removed without affecting the observability of the network [98].

Measurement redundancy is important for state estimation because it not only improves the reliability of state estimation, but also allows one of the essential functions of bad data

detection. As will be discussed in detail in the next section, bad data detection uses measurement residuals to evaluate the magnitude of measurement errors. However, the residual of the critical measurement is always 0, making it impossible to detect any error in the critical measurements even if in the presence of large errors.

The redundant measurements can also be classified into different redundancy levels, including critical pairs, critical trios, and critical *k*-tuples, $k = 4, 5, 6 \ldots$ They are respectively defined as a set of two, three, and *k* measurements whose simultaneous removal from the measurement set would make the system unobservable. After the critical measurements are eliminated, the measurement redundancy level of the network could be enhanced by reducing the number of critical pairs, critical trios and critical *k*-tuples.

Assuming the network is fully observable after observability analysis, the reduced measurement Jacobian matrix, $\mathbf{H}_r$, with the column corresponding to the reference angle removed can be decomposed as expressed in (2.66) [98].

$$\mathbf{H}_d = \mathbf{L}^{-1}\mathbf{H}_r = \begin{bmatrix} \mathbf{I}_{N-1} \\ \mathbf{K}_{red} \end{bmatrix} \tag{2.66}$$

where $\mathbf{I}_{N\text{-}1}$ is the identity matrix of size N-1, and $\mathbf{K}_{red}$ is the matrix of redundant measurements [99].

After the decomposition, the columns of $\mathbf{H}_d$ still correspond to the buses, and the rows of $\mathbf{H}_d$ still correspond to the measurements. The measurements corresponding to the identity matrix $\mathbf{I}_{N\text{-}1}$ are the selected set of basic of measurements that can make the system fully observable. If the elements of a column of $\mathbf{K}_{red}$ are all zeros, the corresponding state is a *critical state*, and the only measurement observing it, as indicated in the identity matrix, is a critical measurement. If a column of $\mathbf{K}_{red}$ contains k-1 nonzero elements, then the corresponding state of this column is a *redundant state*, and the basic measurement and the associated k-1 measurement form a critical *k*-tuple.

Extra measurements can be placed to eliminate the critical measurements and improve the measurement redundancy level. Similar to measurement replacement for network observability, the first step of redundancy improvement is to find a list of candidate measurements and form a reduced measurement Jacobian matrix $\mathbf{H}_{cr}$ excluding the reference angle. $\mathbf{H}_{cr}$ is combined to the bottom of $\mathbf{H}_r$, and the same triangular decomposition is performed for the augmented matrix as shown in (2.67):

$$\mathbf{H}_{ad} = \mathbf{L}^{-1}\begin{bmatrix}\mathbf{H}_r \\ \mathbf{H}_{cr}\end{bmatrix} = \begin{bmatrix}\mathbf{I}_{N-1} \\ \mathbf{K}_{red} \\ \mathbf{K}_c\end{bmatrix} \tag{2.67}$$

where $\mathbf{H}_{ad}$ is the decomposed augmented measurement Jacobian matrix, and $\mathbf{K}_c$ is the matrix of candidate redundant measurements .

From $\mathbf{I}_{N\text{-}1}$, $\mathbf{K}_{red}$ and $\mathbf{K}_c$, a critical state to candidate measurement incident matrix $\mathbf{R}$ can be formed. The optimal placement of the measurements that eliminates the critical measurements can be found using integer linear programming (ILP) as stated below:

$$\begin{aligned}&\text{minimize } \mathbf{c}^T\mathbf{X} \\ &\text{subject to } \mathbf{RX} \geq \mathbf{1}\end{aligned} \tag{2.68}$$

where $\mathbf{c}$ is a vector of costs for installing the measurements, $\mathbf{1}$ denotes a vector whose elements are all equal to 1, $\mathbf{X}$ is the vector consisting of binary decision variables x_i that is defined as:

$$x_i = \begin{cases}1 \text{ if Measurement } i \text{ is included} \\ 0 \text{ if Measurement } i \text{ is not included}\end{cases} \tag{2.69}$$

Similar methods can be developed for improving the measurement redundancy to higher levels so as to eliminate the critical pairs, critical trios and so on by forming different incident matrices according to the redundancy level required.

2.3 Bad Data Detection and Identification

Measurements used in state estimation are constantly exposed to errors caused by different reasons, including the finite accuracy capability of the meters and the telecommunication medium. One of the most important functions of state estimation is to detect, identify and eliminate these errors. It is expected that a state estimator can filter out large errors, or bad data, as long as sufficient measurement redundancy is guaranteed.

The detection of the presence of data can be carried out using the statistical method of chi-squared distribution test, which will be discussed in Section 2.3.1. The following step of identification of the data that contains large errors using the normalised residual method is described further in Section 2.3.2.

Gross measurement errors can also be caused by meter wrong connections, telecommunication system failure, or topology and line parameter errors. Such errors are more complex, and must be handled by means of topology estimation. Details of topology estimation will not be given in this work; readers can find them in [4], [100].

2.3.1 Bad Data Detection Using Chi-squared Distribution

Consider a vector **x** consisting of M random independent variables, in which every element x_i follows the standard normal distribution [4], [101]:

$$x_i \sim N(0,1) \tag{2.70}$$

Then, a new random variable y following the chi-squared distribution of N degrees of freedom can be defined as:

$$y = \sum_{i=1}^{N} x_i^2 \sim \chi_N^2 \tag{2.71}$$

The degree of freedom *M* is decided by the number of independent random variables. Thus, if these variables are constrained by *N* independent equations, the degree of freedom would be reduced to *M-N*.

To illustrate the characteristics of chi-squared distribution, the chi-squared probability density function (p.d.f.) with 10 degrees of freedom is shown in Figure 2-4. The area under the p.d.f. is the probability of *y* having the value within the corresponding range. Since the tail of the curve is decaying, a threshold y_t can be set so that there is only a slight chance that the value of *y* will be greater than y_t. For example, in Figure 2-4 the threshold that divides the curve into the 95% region and 5% region is found at 18.3 for chi-squared distribution with 10 degrees of freedom. If the value of *y* is greater than this threshold, it is suspected that bad data exists in **x**.

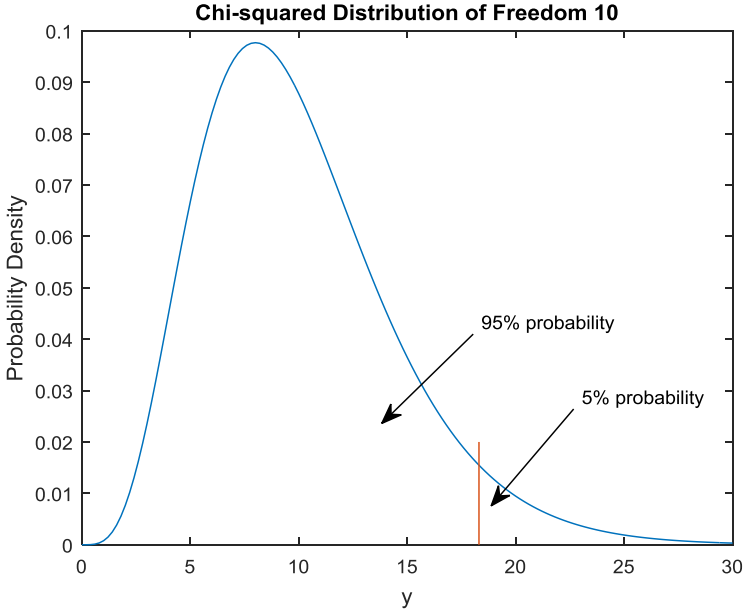

Figure 2-4: Chi-Squared Probability Density Function

Based on the assumption that measurement errors follow a Gaussian distribution, it can be found that the objective function as defined in (2.10) follows the chi-squared distribution with the degree of *M-N*:

$$\begin{aligned} J(\mathbf{x}) &= [\mathbf{z} - \mathbf{h}(\mathbf{x})]^T \cdot \mathbf{R}^{-1} \cdot [\mathbf{z} - \mathbf{h}(\mathbf{x})] \\ &= \mathbf{r}^T \mathbf{R}^{-1} \mathbf{r} \\ &= \sum_{i=1}^{M} \left(\frac{r_i}{\sqrt{R_{ii}}} \right)^2 \end{aligned} \tag{2.72}$$

$$\mathbf{r} = \mathbf{z} - \mathbf{h}(\mathbf{x}) \tag{2.73}$$

where M is the number of measurements, N is the number of states, $\mathbf{r}$ is defined as the residual vector consisting of r_i's, $i = 1, 2, \ldots M$, and the covariance matrix $\mathbf{R}$ is assumed to be diagonal and R_{ii} is its i^{th} diagonal element.

The degree of freedom of $J(\mathbf{x})$ is M-N because the measurement equations must follow the N power balance equations. Thus, a threshold can be set according to the degree of freedom and the confidence level. The confidence level is usually set to be 95%, or it can be set to any number as required. The measurements are determined to be free of errors if $J(\mathbf{x})$ is smaller than the threshold, or the existence of at least one set of bad data is detected.

2.3.2 Bad Data Identification with Largest Normalised Residual Test

The direct use of the objective function for chi-squared test might be inaccurate since the measurement error covariance matrix, $\mathbf{R}$, is used to approximate the covariance of the measurement residuals, $\mathbf{\Omega}$. Consider the linearised measurement equation as given in (2.74). Using the WLS method, the estimate of $\Delta\mathbf{x}$ can be expressed as given in (2.75), and the estimate of $\Delta\mathbf{z}$ can be calculated as given in (2.76). The measurement residual can then be expressed as given in (2.77), and the exact expression of $\mathbf{\Omega}$ is derived as given in (2.78).

$$\Delta\mathbf{z} = \mathbf{H}\Delta\mathbf{x} + \mathbf{e} \tag{2.74}$$

$$\Delta\hat{\mathbf{x}} = \left(\mathbf{H}^T\mathbf{R}^{-1}\mathbf{H}\right)^{-1}\mathbf{H}^T\mathbf{R}^{-1}\Delta\mathbf{z} \tag{2.75}$$

$$\Delta\hat{\mathbf{z}} = \mathbf{H}\Delta\hat{\mathbf{x}} = \mathbf{H}\left(\mathbf{H}^T\mathbf{R}^{-1}\mathbf{H}\right)^{-1}\mathbf{H}^T\mathbf{R}^{-1} \tag{2.76}$$

$$\begin{aligned}\mathbf{r} &= \Delta\mathbf{z} - \Delta\hat{\mathbf{z}} = \left(\mathbf{I}-\mathbf{K}\right)\Delta\mathbf{z} \\ &= \left(\mathbf{I}-\mathbf{K}\right)\left(\mathbf{H}\Delta\mathbf{x}+\mathbf{e}\right) \\ &= \left(\mathbf{I}-\mathbf{K}\right)\mathbf{e}+\left[\mathbf{H}\left(\mathbf{H}^T\mathbf{R}^{-1}\mathbf{H}\right)^{-1}\mathbf{H}^T\mathbf{R}^{-1}\mathbf{H}+\mathbf{H}\right]\Delta\mathbf{x} \\ &= \left(\mathbf{I}-\mathbf{K}\right)\mathbf{e} \\ &= \mathbf{S}e\end{aligned} \tag{2.77}$$

$$\mathbf{\Omega} = \mathrm{cov}\left(\mathbf{r}\right) = \mathbf{SRS}^T = \mathbf{SR} \tag{2.78}$$

where **I** is the identity matrix, $\Delta\hat{\mathbf{x}}$ and $\Delta\hat{\mathbf{z}}$ denote the estimate of $\Delta\mathbf{x}$ and $\Delta\mathbf{z}$, respectively, and the matrix **S**=**I**-**K** is defined as the *Residual Sensitivity Matrix* [4].

Given the expression of $\mathbf{\Omega}$, the normalised residuals are defined as follows:

$$r_i^N = \frac{|r_i|}{\sqrt{\Omega_{ii}}} = \frac{|r_i|}{\sqrt{S_{ii}R_{ii}}} \tag{2.79}$$

where Ω_{ii} is the diagonal element of $\mathbf{\Omega}$ and r_i^N is the normalised residual of the i^{th} element, which follows the Standard Normal Distribution:

$$r_i^N \sim N\left(0,1\right) \tag{2.80}$$

One of the most important properties of the normalised residuals is that the largest normalised residual will always correspond to the bad data. Consider the case where a large error is introduced in Measurement i: $e_i \neq 0$, while the errors existing in all of the other measurements are negligible: $e_j=0$, $j \neq i$. It is shown in (2.81) that the normalised residual of the bad data, which is Measurement k in this case, is always the largest among the normalised residuals of all measurements [4].

$$
\begin{aligned}
r_j^N &= \frac{|r_j|}{\sqrt{S_{jj}R_{jj}}} = \frac{S_{ji}e_i}{\sqrt{S_{jj}R_{jj}}} = \frac{\Omega_{ji}e_i}{\sqrt{\Omega_{jj}}R_{ii}} \\
&\le \frac{\sqrt{\Omega_{jj}}\sqrt{\Omega_{ii}}e_i}{\sqrt{\Omega_{jj}}R_{ii}} \qquad \text{since } \Omega_{ji}^2 \le \Omega_{jj}\Omega_{ii} \\
&= \frac{\sqrt{\Omega_{ii}}e_i}{R_{ii}} = \frac{S_{ii}e_i}{\sqrt{\Omega_{ii}}} = r_i^N
\end{aligned}
\tag{2.81}
$$

This property can be used to identify bad data for any other types of redundant measurements except for critical measurements and critical pairs [102]. This is because, for the critical measurements, the normalised residual will always be 0, while for the critical pairs, the corresponding columns of $\mathbf{\Omega}$ will be linearly dependant. The linear dependency can be expressed as given in (2.82), and it can be straightforwardly derived that the inequality in (2.81) becomes strict equality.

$$
\begin{aligned}
&\frac{\Omega_{ij}}{\Omega_{jj}} = \frac{\Omega_{ii}}{\Omega_{ji}} \\
&\rightarrow \Omega_{ji}^2 = \Omega_{jj}\Omega_{ii}
\end{aligned}
\tag{2.82}
$$

Based on the properties of the normalised residuals described above, the algorithm for bad data identification can be summarised in the following steps:

1. Calculate the measurement residuals using (2.73).
2. Calculate the normalised residuals using (2.79).
3. Find the largest normalised residual $r_{\max}^N$.
4. If $r_{\max}^N > C$, then the corresponding measurement is identified as bad data, else stop the program, no bad data is detected, where C is the threshold usually set to 3.
5. Eliminate or replace the erroneous measurement identified, and go back to Step1.

2.4 Summary

This chapter has given an overview of the classical state estimator that is realised by the WLS method, observability analysis and bad data detection and identification. In the following chapters, the network model, power flow equations as well as the WLS method will also be applied for constructing hybrid state estimators and dynamic state estimators. Based on the existing methods described in this chapter, new methods for numerical observability analysis are developed, and a new scheme for bad data detection and identification for dynamic state estimation is established.

Chapter 3 Numerical Observability Analysis

This chapter presents a novel method for numerical observability analysis. The proposed method is guaranteed to correctly identify the observable islands, in contrast to the existing methods that may produce incorrect identification results for the so called pathological cases. The proposed method is also faster than the existing method in terms of execution speed. This novel method was published in [A.1]. In addition to the novel method published in [A.1], this thesis also proposes a new scheme that allows observability analysis to be performed in networks with synchronised measurements.

3.1 Introduction

As an essential function of state estimation, observability analysis determines if it is possible to find a unique solution with the measurements available. If the network is not fully observable, the network is separated into a number of observable islands. Each of the observable islands can be estimated with reference to their own reference angles. The identification of observable islands is important since it provides information for the following steps of measurement replacement for restoring the network observability and redundant analysis as well as the function of optimal PMU placement in the presence of existing measurements. This process could be achieved by using either the topological methods or the numerical methods. Although both categories of these methods were proposed at almost the same time, the numerical methods have received the most attention because of their higher computational efficiency, and better compatibility with other related state estimation functions.

There have been plenty of methods for numerical observability analysis, which can be roughly divided into three categories: the gain matrix method [26], [32], [34], [35], the gram matrix method [103]-[105], and the test matrix method [42], [106]-[110]. All of these methods are based on the decoupled DC model as introduced in Chapter 2. The gain matrix method is the

first type of method proposed for numerical observability analysis, in which the gain matrix is used directly for identifying the observable islands. In numerical observability analysis, the gram matrix can be expressed as given in (3.1). Since the measurement Jacobian matrix **H** might not be a square matrix, the gram matrix is usually different from the transpose of the gain matrix as given in (2.37). Apart from the dimension, a significant difference in the gram matrix in comparison to the gain matrix is that its diagonal pivots correspond to the measurements, while those of the gain matrix correspond to the states. This gives the gram matrix method an edge in measurement replacement for restoring network observability and improving measurement redundancy. However, in terms of identifying observable islands, the gram matrix method is essentially the same as the gain matrix method. As discussed in Chapter 2, the test matrix method is an improved method developed from the gain matrix method. Instead of applying the gain matrix directly, the test matrix method obtains the test matrix from the inverse matrix of the lower triangular matrix of the gain matrix, and uses the test matrix to directly identify the observable islands.

$$\mathbf{A}_{gram} = \mathbf{H}\mathbf{H}^{T} \tag{3.1}$$

As demonstrated in Section 2.2.4, the identification of the observable islands by the gain matrix method might be incorrect in the so called pathological cases. It is stated in [42] that the pathological cases can be avoided by using the test matrix instead of the gain matrix, and thus the identification of the observable islands can be finished without any iteration. However, it is discovered in this PhD that the observable islands identified by the test matrix method might still be incorrect in certain cases. The research shows that pathological cases can be further classified into two different categories:

1. Pathological cases where there is no pathological branch in the network
2. Pathological cases where some observable islands are connected by pathological branches

A pathological branch is defined as an unobservable branch that is incorrectly identified as the observable branch in numerical observability analysis. The test matrix method can successfully prevent Type 1 pathological cases that might occur in the gain matrix method. However, it is

unable to detect the pathological branches, and thus it may cause incorrect results due to Type 2 pathological cases. In [106]-[110], several improved methods have been proposed based on the triangular factorisation of the gain matrix. But the major contributions of these papers are concerned with the improvement of the factorising procedure as the final resulting matrices are effectively the same as the test matrix. Hence, these methods might still incorrectly identify the observable islands due to Type 2 pathological cases.

It was reported in [110] that a correct identification of the observable islands can be guaranteed by using the iterations. However, there is no proof to support this statement. Following this discovery, this PhD work develops an iteration based method for observability analysis according to the corrected properties of the test matrix. It was mathematically proven that all pathological cases can be avoided if the network does not possess any irrelevant injection measurements. Thus, the iteration based method will always find the correct solution if all the irrelevant injection measurements can be removed through the iterations. However, the iteration procedure could significantly slow down the execution speed, which would undermine the overall functionality of observability analysis when applied online. To address this problem, a pathological case identification rule (*PCIR*) was proposed that can precisely discriminate pathological cases and normal cases. If a pathological case is identified at a certain round of iteration, an additional round of iteration will be required after the removal of the irrelevant injection measurements. Or, if a normal case is identified, the program can be terminated in advance, and it is guaranteed that the identified observable islands are correct even if in the existence of irrelevant injection measurements.

To avoid Type 1 pathological cases, the test matrix methods must identify the observable islands in two steps. With the help of *PCIR*, the new iterative method proposed here is allowed to directly identify the observable islands from the test matrix. Thus, in the majority of cases the new iterative method is even faster than the existing test matrix methods that do not require iterations.

In the following sections of this chapter, the flaws in the properties of the test proposed in [42] will be discussed in Section 3.2; the revised property of the test matrix and a fully iterative

method for numerical observability analysis will be proposed in Section 3.3; a novel pathological case identification rule will be proposed in Section 3.4; some examples of the pathological cases will be given in Section 3.5; a direct island identification method and the proposed method for numerical observability analysis will be discussed in Section 3.6; the simulation results will be given in Section 3.7; a new scheme for including the synchronised measurements in observability analysis will be proposed in Section 3.8; some alternative methods for Cholesky factorisation will be discussed in Section 3.9; the effect of branch reactance on observability analysis will be discussed in Section 3.10; and finally Section 3.11 will summarise the chapter.

3.2 Flaws in the Properties of the Test Matrix

As it was discovered that the test matrix method might not identify the observable islands correctly, the test matrix properties, which form the theoretic foundation of the test matrix method, are re-examined. Two test matrix properties are proposed in [42] as presented in Section 2.2.4. Property 1 has been successfully proven in [42] by using a contradiction method. However, there are flawed arguments in the proof for Property 2 that uses a similar method. It is stated in the proof that when any pseudo measurement $\mathbf{h}_k$ incident to multiple observable islands is added, the rank of the gain matrix increases by 1. This statement might be wrong in certain cases. For example, consider the six-bus system with the measurement placements as shown in Figure 3-1.

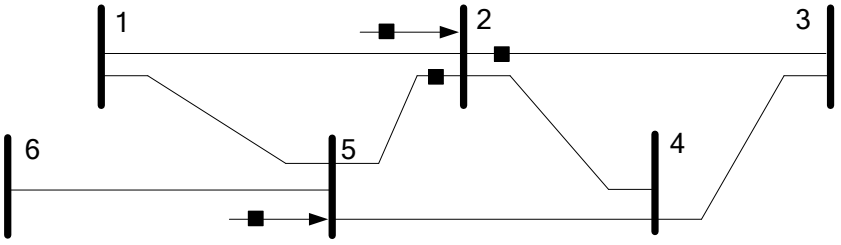

Figure 3-1: The Six Bus System and the Measurement Placements

The measurement Jacobian matrix can be expressed as given in (3.2):

$$\mathbf{H} = \begin{array}{c} \begin{matrix} \text{Bus 1} & \text{Bus 2} & \text{Bus 3} & \text{Bus 4} & \text{Bus 5} & \text{Bus 6} \end{matrix} \\ \begin{bmatrix} -1 & 4 & -1 & -1 & -1 & 0 \\ -1 & -1 & 0 & -1 & 4 & -1 \\ 0 & 1 & -1 & 0 & 0 & 0 \\ 0 & 1 & 0 & 0 & -1 & 0 \end{bmatrix} \end{array} \begin{matrix} p_2 \\ p_5 \\ p_{23} \\ p_{25} \end{matrix} \tag{3.2}$$

Following the steps given in Section 2.2.4, the test matrix and the matrix **C** are calculated as given in (3.4).

$$\mathbf{W} = \begin{bmatrix} -1 & 0 & 0 & 1 & 0 & 0 \\ 2 & 1 & 1 & 0 & 1 & 1 \end{bmatrix} \tag{3.3}$$

$$\begin{aligned} \mathbf{C} &= \mathbf{A}\mathbf{W}^T \\ &= \begin{array}{l} \begin{bmatrix} -1 & 1 \\ -1 & 1 \\ 0 & 0 \\ -1 & 1 \\ 0 & 0 \\ 1 & -1 \\ 0 & 0 \end{bmatrix} \begin{matrix} \text{Branch 1-2} \\ \text{Branch 1-5} \\ \text{Branch 2-3} \\ \text{Branch 2-4} \\ \text{Branch 2-5} \\ \text{Branch 4-5} \\ \text{Branch 5-6} \end{matrix} \end{array} \end{aligned} \tag{3.4}$$

where **A** is the branch to bus incident matrix whose values are given and explained in (3.5):

$$\mathbf{A} = \begin{array}{c} \begin{matrix} \text{Bus 1} & \text{Bus 2} & \text{Bus 3} & \text{Bus 4} & \text{Bus 5} & \text{Bus 6} \end{matrix} \\ \begin{bmatrix} 1 & -1 & 0 & 0 & 0 & 0 \\ 1 & 0 & 0 & 0 & -1 & 0 \\ 0 & 1 & -1 & 0 & 0 & 0 \\ 0 & 1 & 0 & -1 & 0 & 0 \\ 0 & 1 & 0 & 0 & -1 & 0 \\ 0 & 0 & 0 & 1 & -1 & 0 \\ 0 & 0 & 0 & 0 & 1 & -1 \end{bmatrix} \end{array} \begin{matrix} \text{Branch 1-2} \\ \text{Branch 1-5} \\ \text{Branch 2-3} \\ \text{Branch 2-4} \\ \text{Branch 2-5} \\ \text{Branch 4-5} \\ \text{Branch 5-6} \end{matrix} \tag{3.5}$$

Because their corresponding rows in **C** are not zero vectors, Branch 1-2, Branch 1-5, Branch 2-4, Branch 4-5 are identified as the unobservable branches. After removing these unobservable

branches, the network is separated into 3 observable islands: {1}, {2; 3; 5; 6}, {4}. However, for the subnetwork {2; 3; 5; 6} the incident measurements p_{23}, p_{25} and p_5 are not able to make it observable. This is because the injection measurement p_5 is incident to two buses outside the subnetwork, making it an irrelevant injection measurement with respect to the subnetwork. After removing p_5, Bus 6 is separated from the subnetwork, and Branch 5-6 is identified to be an unobservable branch. The unobservable branches like Branch 5-6 that cannot be identified are called *pathological branches*. Now an additional pseudo flow measurement $\mathbf{h}_k$ from Bus 5 to Bus 6 is added which can be expressed by:

$$\mathbf{h}_k = \begin{bmatrix} 0 & 0 & 0 & 0 & 1 & -1 \end{bmatrix} \tag{3.6}$$

$\mathbf{h}_k$ can be linearly expressed by the existing measurements as follows:

$$\mathbf{h}_k = -p_2 + p_5 + p_{23} + 4p_{25} \tag{3.7}$$

Thus, the addition of $\mathbf{h}_k$ will not change the rank of the measurement Jacobian matrix. So, it is demonstrated that the proof for Property 2 is flawed.

3.3 Revised Property of the Test Matrix and the Fully Iterative Method

This PhD has revised Property 2 of the test matrix as follows:

Property 2': The columns of **W** corresponding to buses in different observable islands will have different numerical values if the network does not possess irrelevant injection measurements.

Proof for Property 2':

For any network consisting of *n* observable islands, the measurement Jacobian matrix **H** can be divided as expressed in (3.8):

$$\mathbf{H} = \begin{bmatrix} \mathbf{H}_1 & & \\ & \ddots & \\ & & \mathbf{H}_n \\ & \mathbf{H}_{irr} & \end{bmatrix} \tag{3.8}$$

where the rows containing $\mathbf{H}_1$, …, $\mathbf{H}_n$ correspond to the measurements relevant to the n observable islands, and $\mathbf{H}_{irr}$ is formulated by the irrelevant injection measurements. Since each observable island contains and only contains one reference angle, the rank deficiency for any $\mathbf{H}_i$ is equal to 1. So, if the network does not have an irrelevant injection measurement, $R_d(\mathbf{H}) = n_{OI}$, where $R_d(\mathbf{H})$ represents the rank deficiency of the measurement Jacobian matrix, while n_{OI} represents the number of observable islands. Because rank($\mathbf{G}$) = rank($\mathbf{H}^T\mathbf{H}$) = rank ($\mathbf{H}$), we have $R_d(\mathbf{G}) = R_d(\mathbf{H}) = n_{OI}$ when $n_{II} = 0$, Where $R_d(\mathbf{G})$ represents the rank deficiency of the gain matrix and n_{II} represents the number of irrelevant injection measurements.

The gain matrix $\mathbf{G}$ can be factorised using Cholesky factorisation for singular matrices according to the steps described in Section 2.2.2. According to [111] and by grouping the columns corresponding to the zero pivots together and by row permutations, the Cholesky factor $\mathbf{L}$ can be expressed as:

$$\mathbf{L} = \begin{bmatrix} \mathbf{L}_{NZ} & \\ \mathbf{M} & \mathbf{I} \end{bmatrix} \tag{3.9}$$

where $\mathbf{L}_{NZ}$ is the lower triangular matrix whose columns correspond to the nonzero pivots, $\mathbf{M}$ is a rectangular matrix, and $\mathbf{I}$ represents an identity matrix with the same size as $\mathbf{G}$. The inverse matrix of $\mathbf{L}$ and the test matrix can then be calculated as given in (3.10) and (3.11), respectively.

$$\mathbf{L}^{-1} = \begin{bmatrix} \mathbf{L}_{NZ}^{-1} & \\ -\mathbf{M}\mathbf{L}_{NZ}^{-1} & \mathbf{I} \end{bmatrix} \tag{3.10}$$

$$\mathbf{W} = \begin{bmatrix} -\mathbf{M}\mathbf{L}_{NZ}^{-1} & \mathbf{I} \end{bmatrix} \tag{3.11}$$

Since the dimension of $\mathbf{I}$ is equal to that of the gain matrix, it can be derived that $n_{UC} \geq R_d(\mathbf{G})$, where n_{UC} is the abbreviation of the number of unique columns of $\mathbf{W}$. Supposing $n_{II} = 0$, the numerical values of the two columns of the test matrix that belong to different observable

islands happen to be the same. Then it follows that $n_{UC} < n_{OI} = R_d(\mathbf{G})$, where a contradiction can be drawn since it is assumed that $n_{UC} \geq R_d(\mathbf{G})$. So, if the network does not have an irrelevant injection measurement, it is impossible for numerical values of the columns of the test matrix that belong to different observable islands to be the same, and Property 2' is proved.

End of the Proof

The identify matrix of the test matrix corresponds to the reference buses of the n observable islands. In fact, $n_{UC} = R_d(\mathbf{G}) = n_{OI}$ when $n_{II} = 0$, which forces every column of the remaining part of the test matrix to be a singleton vector (a vector whose elements are equal to 0 except for one element equal to 1). Although in most cases the measurement set does include the irrelevant injection measurements, these measurements can be removed without changing the observability of the network. This can be explained by the fact that an irrelevant injection measurement measures the sum of power injections into multiple observable islands, making it an incorrect injection measurement of its incident observable island. So, in order to identify all the observable islands correctly, the observability analysis algorithm has to iteratively remove all irrelevant injection measurements.

A fully iterative algorithm for numerical observability analysis is proposed based on the revised properties of the test matrix (Property 1 and Property 2') [112]:

1. Create the measurement Jacobian matrix **H** and then the gain matrix **G** according to the decoupled DC model, and perform Cholesky factorisation.
2. If the resulting diagonal matrix **D** possesses one zero pivot, the network is observable. Else obtain the test matrix **W** from the Cholesky factor **L**.
3. Find the candidate observable islands: Group the buses into an observable island if the numerical values of their corresponding columns in the test matrix are the same.
4. Find the irrelevant injection measurements that are incident to multiple observable islands. If the network does not have any irrelevant injection measurements, go to the next step. Else go back to Step 1.
5. Output the observable islands identified and stop the program.

3.4 Pathological Case Identification Rule

The fully iterative method developed based on the corrected properties of the test matrix guarantees a correct solution of the observable islands. However, the introduction of iteration significantly increases the execution time. As a matter of fact, in normal cases where $n_{UC} = n_{OI}$, the observable islands can be found directly as it follows that $n_{UC} = n_{OI} = R_d(\mathbf{G})$ according to Property 1. In this case if $n_{II} \neq 0$ the fully iterative method would enter extra unnecessary iterations. Hence, a "pathological case identification rule" (*PCIR*) is proposed that can precisely distinguish pathological cases and normal cases, and thereby allow the accurate identification of observable islands without wasting computational resources:

$$PCIR = R_d\left(G\right) + n_{III} - n_{UC} \tag{3.12}$$

where n_{III} is the number of identifiable irrelevant injection measurements, where the attribute "identifiable" specifically refers to "identifiable from analysing the test matrix". The properties of the test matrix are presented as follows:

$$PCIR \begin{cases} > 0 & \text{for pathological cases (iterations are required)} \\ = 0 & \text{for normal cases (no iterations required)} \end{cases} \tag{3.13}$$

The formal definition of *PCIR* is given in (3.14). The $PCIR_{formal}$ also has the properties as given in (3.13).

$$PCIR_{formal} = NOI - NUC \tag{3.14}$$

The *PCIR* is proposed instead of $PCIR_{formal}$ because of the difficulty in calculating n_{OI}, which can be expressed as:

$$n_{OI} = R_d\left(\mathbf{G}\right) + n_{CII} \tag{3.15}$$

where n_{CII} is the abbreviation of the number of critical irrelevant injection measurements, which refers to the maximum number of linearly independent injection measurements.

Proof for (3.15) [112]:

In the case $n_{CII} = 0$, $n_{II} = 0$ This is because the power flow measurements cannot express the redundant irrelevant injection measurements, and if there is any irrelevant injection measurements, one of these measurements must be critical. So (3.15) holds when $n_{CII} = 0$ according to the proof for Property 2' given in the previous section. From its definition, the critical injection measurements cannot be linearly expressed by other measurements. In other words, every critical irrelevant injection measurement increases the rank of gain matrix by 1, or reduces the value of $R_d(\mathbf{G})$ by 1. Thus the sum of n_{CII} and $R_d(\mathbf{G})$ is unchanged, and is equal to n_{OI}.

End of the Proof

Since the test matrix rows correspond to the zero pivots of the gain matrix, $R_d(\mathbf{G})$ can be obtained by just counting the number of test matrix rows; while n_{UC} can be obtained by counting the number of unique columns according to its definition. However, it might be that n_{CII} cannot be calculated due to two obstacles: The first obstacle is that in some special pathological cases there might be some unidentifiable irrelevant injection measurements. The second obstacle is that it is difficult to identify the critical measurements from the test matrix or any other variable available. So, n_{III} is used in placement of n_{CII} in (3.15), which leads to the expression of *PCIR* as given in (3.12).

Since n_{III} might be different from n_{CII}, *PCIR*'s value might also be different from $PCIR_{formal}$. Nevertheless, the property of *PCIR* and $PCIR_{formal}$ for distinguishing normal and pathological cases as given by (3.13) is the same. This conclusion can be derived from the relationships between n_{II}, n_{III} and n_{CII} as presented in Lemma 3.1, Lemma 3.2 and Theorem 3.1 [112].

Lemma 3.1: In normal cases $n_{III} = n_{II} = n_{CII}$.

Proof for Lemma 3.1:

For an arbitrary irrelevant injection measurement which can be expressed as a linear combination of other measurements, the expression can be generalised as given in (3.16):

$$J_i = \sum_j F_j + \sum_k P_k \tag{3.16}$$

where J_i denotes an arbitrary irrelevant injection measurement, Fj represents an arbitrary power flow measurement, and P_k is the sum of pseudo flow measurements incident to the unobservable branches which are incident to J_i, as such P_k cannot be linearly expressed by other measurements for any k given.

If there is only one element in the sum for P_k, by definition the unobservable branch it is incident to will be a pathological branch. This is not possible because in normal cases the pathological branch will cause the incorrect identification of its connected observable islands as one observable island. Now consider the case where the sum of P_k contains two pseudo flow measurements, as shown in Figure 3-2.

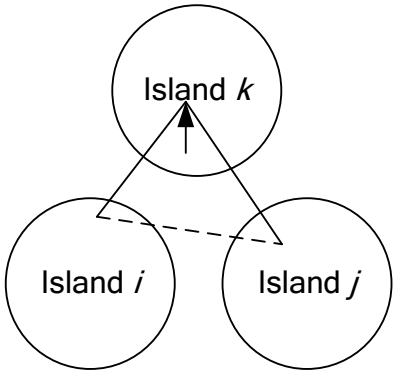

Figure 3-2: Power System Containing Three Observable Islands and One Irrelevant Injection Measurement

If there is no direct connection between the buses in Island *i* and the buses in Island *j*, as denoted by the dashed line in Figure 3-2, it would be impossible to express P_k without a pathological branch. If any bus in Island *i* and any bus in Island *j* is connected by a branch, it is possible to express P_k as given in (3.17). However, Island *i*, Island *j* and Island *k* will still be wrongly identified as one observable island because the rank deficiency of the gain matrix of the subnetwork containing the three observable islands has dropped to 1 after the two sums of pseudo flow measurements are added: (p_{ik}+p_{ij}) and (p_{ji}+p_{jk}).

$$P_k = -\left[\left(p_{ik} + p_{ij}\right) + \left(p_{ji} + p_{jk}\right)\right] \tag{3.17}$$

where p_{ij} represents the pseudo power flow measurement incident to the branch connecting Island *i* and Island *j*, and in the same way p_{ik} represents Island *i* and Island *k*, p_{ji} Island *j* and Island *i*, p_{jk} Island *j* and Island *k*.

Therefore, P_k cannot be linearly expressed by two pseudo flow measurements in normal cases either. The same conclusion can be drawn for P_k which is linearly represented by any number of pseudo flow measurements using mathematical induction.

So, the criterion for the existence of redundant measurements is not fulfilled in the normal case: $n_{II} = n_{CII}$. By definition, every observable island, and thus every irrelevant injection measurement is identifiable in the normal case: $n_{III} = n_{II} = n_{CII}$.

End of the Proof

Lemma 5.2: $n_{II} \geq n_{CII}$ in pathological cases, and the equality is established if the network does not have a pathological branch.

Proof for Lemma 5.2:

If the network does not have a pathological branch, all unobservable branches can still be found even in the pathological case: $n_{III} = n_{II}$. As the critical irrelevant injection measurements are a subset of irrelevant injection measurements, it follows that $n_{II} \geq n_{CII}$. $n_{II} > n_{CII}$ is possible since the criterion for the presence of redundant irrelevant injection measurement is fulfilled in pathological cases.

End of Proof

Theorem 3.1 (the Theorem of Convergence): If the network has pathological branches at least one irrelevant injection measurement that incidents to one of the pathological branches is identifiable [112].

Proof for Theorem 3.1:

Suppose in an arbitrary network, $N_x = \{S_1, S_2, \ldots, S_{nsub}\}$ ($n_{sub}>1$), with measurement set, M, and topology, T, there is a subnetwork, S_y consisting of a number of observable islands, $S_y = \{O_{y1}, \ldots, O_{yn}\}$. All of these observable islands in S_y are connected by pathological branches $P_y^M = \{p_{y1}^M, \ldots, p_{ynpath}^M\}$, and $P_y^M \neq \emptyset$. Hence, a set of irrelevant injection measurements can be found in S_y, $J_y^M = \{ j_{y1}^M, j_{y2}^M, \ldots j_{ynj}^M\}$. This set can be divided into two mutually exclusive sets, including a set containing identifiable elements I_y and a set containing unidentifiable elements U_y with $J_y = I_y \cup U_y$, and $I_y \cap U_y = \emptyset$. Two functions are defined as follows:

1. $g_A(B, C)$: for a given topology of network, A, a given set of buses, B, and a given set of branches, C, the function returns the subset of B containing elements incident to any of the elements of C according to topology A.
2. $h_A(B)$: for a given network topology, A, bus set, B, the function returns a set where the union of B and a set consisting of all neighbouring buses of B's elements in the network with topology, A.

The statement of this theorem can be interpreted as given in (3.18):

$$h_T\left(g_T\left(J_y^M, P_y^M\right)\right) - S_y \neq \varnothing, \text{ if } P_y^M \neq \varnothing \tag{3.18}$$

Since the subnetwork is not fully observable, the following equations can be derived:

$$h_T\left(J_y^M\right) - S_y \neq \varnothing \tag{3.19}$$

$$h_T\left(U_y^M\right) \subseteq S_y \tag{3.20}$$

From (3.19) and (3.20) and the definition that $J_y = I_y \cup U_y$, and $I_y \cap U_y = \emptyset$, we can deduce the relationship given in (3.21):

$$h_T\left(I_y^M\right) - S_y \neq \varnothing \tag{3.21}$$

Moreover, divide I_y^M into two sets, I_{1y}^M and I_{2y}^M, according to whether their elements are incident to pathological branches:

$$I_{1y}^M = \left\{ a : a \in I_y^M, \mathrm{g}_T\left(a, P_y^M\right) \neq \varnothing \right\} \tag{3.22}$$

$$I_{2y}^M = \left\{ a : a \in I_y^M, \mathrm{g}_T\left(a, P_y^M\right) = \varnothing \right\} \tag{3.23}$$

According to (3.22), Equation (3.18) can be re-written as given in (3.24):

$$I_{1y}^M \neq \varnothing, \text{ if } P_y^M \neq \varnothing \tag{3.24}$$

Suppose $I_{1y}^M = \emptyset$ for M, then $\exists$ M' such that, $M' \subset M$, $I_{1y}^{M'} = \emptyset$, $I_{2y}^{M'} = \emptyset$, and $P_y^{M'} = P_y^M \neq \emptyset$. It is possible to find such M', since removing elements from I_{1y}^M does not change P_y^M, due to the assumption that $I_{1y}^M = \emptyset$. Then, a new relation can be derived as follows:

$$\mathrm{h}_T\left(I_y^{M'}\right) - S_y = \mathrm{h}_T\left(I_{1y}^{M'} \bigcup I_{2y}^{M'}\right) - S_y = \mathrm{h}_T\left(\varnothing\right) - S_y = \varnothing \tag{3.25}$$

It can be seen that (3.25) contradicts (3.21), and thus (3.24) has to be true. Since the network, its topology and the measurement set are arbitrarily given, (3.24) holds true for any network not fully observable and any measurement placement, and thus Theorem 3.1 is proved.

End of the Proof

Lemma 3.1 guarantees that *PCIR* = 0 in the normal cases as shown below:

$$n_{III} + R_d\left(\mathbf{G}\right) - n_{UC} = n_{CII} + R_d\left(\mathbf{G}\right) - n_{UC} = 0 \tag{3.26}$$

In the pathological case where some observable islands that are separate in locations but share the same numerical values in the test matrix (Type 1 pathological case), Lemma 3.2 guarantees that *PCIR* > 0, as demonstrated in (3.27):

$$n_{III} + R_d\left(\mathbf{G}\right) - n_{UC} \geq n_{CII} + R_d\left(\mathbf{G}\right) - n_{UC} > 0 \tag{3.27}$$

In the pathological case where some directly connected observable islands have the same numerical values in the test matrix (Type 2 pathological case), Theorem 3.1 ensures that *PCIR* > 0, as is shown in (3.28):

$$\begin{aligned}
&n_{III} + R_d\left(\mathbf{G}\right) - n_{UC} \\
&= n_{II} + R_d\left(\mathbf{G}\right) - n_{UC} - n_{UII} \\
&= n_{CII} + NRII - n_{UC} - n_{UII} \\
&= \left(n_{CII} - n_{UCII}\right) + \left(n_{RII} - n_{URII}\right) + R_d\left(\mathbf{G}\right) - n_{UC} \\
&\geq \left(n_{CII} + R_d\left(\mathbf{G}\right) - n_{UC}\right) - n_{UCII} \\
&= n_{PC} - n_{UCII} \\
&\geq n_{PB} - n_{UCII} \\
&= \sum_i \left(n_{PBi} - n_{UCII\,i}\right)
\end{aligned} \tag{3.28}$$

where n_{PC} is the abbreviation of the number of pathological connections, *NUII* is the abbreviation of the number of unidentifiable irrelevant injection measurements, which refers to the irrelevant injection measurement that cannot be identified from the test matrix, n_{PB} is the abbreviation of the number of pathological branches, and index *i* denotes the i^{th} subnetwork, n_{UCII} is the abbreviation of the number of unidentifiable critical irrelevant injection measurements, n_{RII} is the abbreviation of the number of redundant irrelevant injection measurements, n_{URII} is the abbreviation of the number of unidentifiable redundant irrelevant injection measurements.

For any subnetwork consisting of *k* observable islands that are connected by pathological branches, only *k*-1 pathological branches are counted, i.e. n_{PBi}=*k*-1. This is because any additional pathological branches can be linearly expressed with the pseudo measurements across the pathological branch and the other available measurements. In addition, only the critical injection measurements that are incident to the pathological branches are accounted for. Thus, $n_{CIIi} \leq k$-1, or the subnetwork considered will become observable. Theorem 3.1 makes sure that $n_{UCIIi} < n_{CIIi}$, and it can be directly derived that the expression of (3.28) is greater than 0:

$$\begin{aligned}&\sum_i \left(NPB_i - NUCII_i \right) \\ &> \sum_i \left(NPB_i - NCII_i \right) \geq 0\end{aligned} \tag{3.29}$$

From (3.26), (3.27) and (3.29) it is demonstrated that the *PCIR* has the same properties as the $PCIR_{formal}$.

As well as deriving one of the properties of *PCIR*, another significant meaning of Theorem 3.1 is that it demonstrates that, after a sufficient number of iterations, all irrelevant injection measurements can be identified, and thus the test matrix method based numerical observability analysis can always converge to the correct identification result after a finite number of iterations. Hence, Theorem 3.1 is also named here as *the convergence theorem for numerical observability*.

3.5 Examples of the Pathological Cases

Examples of using the *PCIR* for observability analysis for both types of pathological cases are given in this section. The examples below show the existence of the new concepts and variables proposed in the previous sections, such as the pseudo connection, critical and redundant irrelevant injection measurements, and identifiable and unidentifiable irrelevant injection measurements.

3.5.1 Type 1 Pathological Case (without pathological branch)

Consider a five-bus network with the measurement placement shown in Figure 3-3:

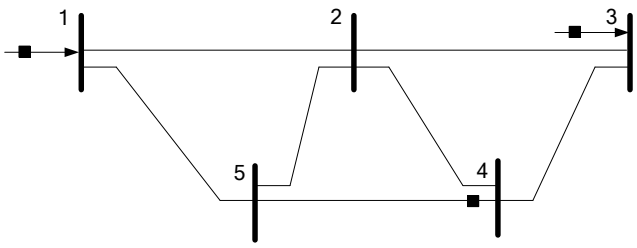

Figure 3-3 Five Bus Test System and the Measurement Placement

The measurement Jacobian matrix according to the DC decoupled model is given in (3.30):

$$\mathbf{H} = \begin{bmatrix} 2 & -1 & 0 & 0 & -1 \\ 0 & -1 & 2 & -1 & 0 \\ 0 & 0 & 0 & 1 & -1 \end{bmatrix} \tag{3.30}$$

The corresponding test matrix is given by (3.31):

$$\mathbf{W} = \begin{bmatrix} 1 & 2 & 1 & 0 & 0 \\ 0 & -1 & 0 & 1 & 1 \end{bmatrix} \tag{3.31}$$

By directly grouping the columns in **W** that have the same numerical values as one observable island, the following observable islands are identified: {1;3}, {2}, {4;5}. The identified irrelevant injection measurements are the injection measurements incident to Bus 1 and Bus 3 since they are incident to multiple observable islands. $PCIR = R_d(\mathbf{G}) + n_{III} - n_{UC} = 2 + 2 - 3 = 1 > 0$, which suggests the result is a pathological case, and the algorithm has to enter another round of iteration in order to find the correct identification result. After eliminating the identified irrelevant injection measurements, the new measurement Jacobian matrix and test matrix are calculated as given in (3.32):

$$\mathbf{H} = \begin{bmatrix} 0 & 0 & 0 & 1 & -1 \end{bmatrix} \tag{3.32}$$

$$\mathbf{W} = \begin{bmatrix} 1 & 0 & 0 & 0 & 0 \\ 0 & 1 & 0 & 0 & 0 \\ 0 & 0 & 1 & 0 & 0 \\ 0 & 0 & 0 & 1 & 1 \end{bmatrix} \tag{3.33}$$

From the new test matrix, four observable islands are found: {1}, {2}, {3}, {4;5}. In the previous iteration, Bus 1 and Bus 3, which form two separated observable islands, are incorrectly identified in one observable island. In the Type 1 pathological case, a pseudo connection between the observable islands, whose numerical values in the test matrix are the same, can be represented by the available measurements. In this example, the pseudo connection between Island {1} and Island {3} is expressed as:

$$\begin{aligned}\mathbf{h}_k &= \left(p_1 - p_3 - p_{45}\right)/2 \\ &= \begin{bmatrix}1 & 0 & -1 & 0 & 0\end{bmatrix}\end{aligned} \tag{3.34}$$

3.5.2 Type 2 Pathological Case (With pathological branches)

In Type 2 pathological cases, there might be some unidentifiable irrelevant injection measurements in the first few rounds of iteration, which are termed as the unidentifiable irrelevant injection measurements in the previous sections. To demonstrate the validity of this concept and the existence of such variables, consider a thirteen-bus system with the measurement placement, as shown in Figure 3-4.

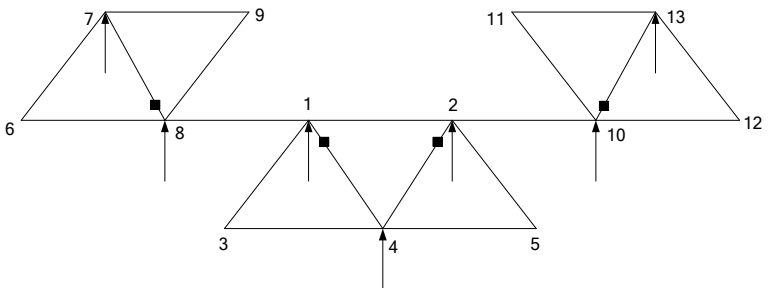

Figure 3-4: Thirteen Bus Test System and the Measurement Placement

The measurement Jacobian matrix and the corresponding test matrix are expressed as:

$$\mathbf{H} = \begin{bmatrix} 4 & -1 & -1 & -1 & 0 & 0 & 0 & -1 & 0 & 0 & 0 & 0 & 0 \\ -1 & 4 & 0 & -1 & -1 & 0 & 0 & 0 & 0 & -1 & 0 & 0 & 0 \\ -1 & -1 & -1 & 4 & -1 & 0 & 0 & 0 & 0 & 0 & 0 & 0 & 0 \\ 0 & 0 & 0 & 0 & 0 & -1 & 3 & -1 & -1 & 0 & 0 & 0 & 0 \\ -1 & 0 & 0 & 0 & 0 & -1 & -1 & 4 & -1 & 0 & 0 & 0 & 0 \\ 0 & -1 & 0 & 0 & 0 & 0 & 0 & 0 & 0 & 4 & -1 & -1 & -1 \\ 0 & 0 & 0 & 0 & 0 & 0 & 0 & 0 & 0 & -1 & -1 & -1 & 3 \\ 1 & 0 & 0 & -1 & 0 & 0 & 0 & 0 & 0 & 0 & 0 & 0 & 0 \\ 0 & 1 & 0 & -1 & 0 & 0 & 0 & 0 & 0 & 0 & 0 & 0 & 0 \\ 0 & 0 & 0 & 0 & 0 & 0 & -1 & 1 & 0 & 0 & 0 & 0 & 0 \\ 0 & 0 & 0 & 0 & 0 & 0 & 0 & 0 & 0 & 1 & 0 & 0 & -1 \end{bmatrix} \tag{3.35}$$

$$\mathbf{W} = \begin{bmatrix} 0 & 0 & 0 & 0 & 0 & -1 & 0 & 0 & 1 & 0 & 0 & 0 & 0 \\ 0 & 0 & 0 & 0 & 0 & 0 & 0 & 0 & 0 & 0 & -1 & 1 & 0 \\ 1 & 1 & 1 & 1 & 1 & 2 & 1 & 1 & 0 & 1 & 2 & 0 & 1 \end{bmatrix} \tag{3.36}$$

The following observable islands are found in the first iteration: {1; 2; 3;4;5;7;8;10;13}, {6}, {9}, {11} and {12}. According to their definitions, four irrelevant injection measurements are found: the injection measurements incident to Buses 7, 8, 10 and 13. $PCIR = R_d(\mathbf{G}) + n_{III} - n_{UC} = 3 + 4 - 5 = 2 > 0$, indicating that the result is a pathological case, which must be removed using iterations. After the irrelevant injection measurements are removed, the updated measurement Jacobian matrix and test matrix are computed as given in (3.37) and (3.38) respectively.

$$\mathbf{H} = \begin{bmatrix} 4 & -1 & -1 & -1 & 0 & 0 & 0 & 0 & 0 & 0 & 0 & 0 & 0 \\ -1 & 4 & 0 & -1 & -1 & 0 & 0 & 0 & 0 & -1 & 0 & 0 & 0 \\ -1 & -1 & -1 & 4 & -1 & 0 & 0 & 0 & 0 & 0 & 0 & 0 & 0 \\ 1 & 0 & 0 & -1 & 0 & 0 & 0 & 0 & 0 & 0 & 0 & 0 & 0 \\ 0 & 1 & 0 & -1 & 0 & 0 & 0 & 0 & 0 & 0 & 0 & 0 & 0 \\ 0 & 0 & 0 & 0 & 0 & 0 & 0 & -1 & 1 & 0 & 0 & 0 & 0 \\ 0 & 0 & 0 & 0 & 0 & 0 & 0 & 0 & 0 & 1 & 0 & 0 & -1 \end{bmatrix} \tag{3.37}$$

$$\mathbf{W} = \begin{bmatrix} 0 & 0 & 0 & 0 & 0 & 1 & 0 & 0 & 0 & 0 & 0 & 0 & 0 \\ 0.5 & 0.5 & 0 & 0.5 & 1 & 0 & 1 & 1 & 0 & 0 & 0 & 0 & 0 \\ 0 & 0 & 0 & 0 & 0 & 0 & 0 & 0 & 1 & 0 & 0 & 0 & 0 \\ 0 & 0 & 0 & 0 & 0 & 0 & 0 & 0 & 0 & 0 & 1 & 0 & 0 \\ 0 & 0 & 0 & 0 & 0 & 0 & 0 & 0 & 0 & 0 & 0 & 1 & 0 \\ 0.5 & 0.5 & 1 & 0.5 & 0 & 0 & 0 & 0 & 0 & 1 & 0 & 0 & 1 \end{bmatrix} \tag{3.38}$$

The updated observable islands in the second round of iteration includes {1, 2, 4}, {3, 10, 13}, {5, 7, 8}, {6}, {9}, {11} and {12}. According to this result, the remaining irrelevant injection measurements placed at Bus 1, Bus 2 and Bus 4 are also found to be irrelevant injection measurements. These measurements are not identifiable in the first round of iteration, and thus the existence of unidentifiable irrelevant injection measurements is demonstrated. $PCIR = R_d(\mathbf{G}) + n_{III} - n_{UC} = 6 + 3 - 7 = 2 > 0$, indicating that the result is still pathological, and the algorithm has to enter an additional round of iteration. Since all injection measurements have been removed, the observable islands identified after the third iteration are the final result, which are listed as follows: {1, 2, 4}, {3}, {5}, {6}, {7, 8}, {9}, {10, 13}, {11}, {12}.

The other two new concepts proposed in this thesis for observability analysis are the critical and redundant irrelevant injection measurements. In this example, the irrelevant injection measurements placed at Bus 1, Bus 2, Bus 7, Bus 8, Bus 10 and Bus 13 can be chosen to be the set of critical irrelevant injection measurements, then the remaining one incident to Bus 4 is redundant. The redundancy of this irrelevant injection measurement can be demonstrated as it can be linearly represented by the set of critical measurements and other available measurements:

$$\begin{aligned}\mathbf{h}_k &= p_1 + p_2 - p_7 + p_8 + p_{10} - p_{13} - 3p_{1-4} - 3p_{2-4} - 4p_{8-7} - 4p_{10-13} \\ &= \begin{bmatrix} -1 & -1 & -1 & 4 & -1 & 0 & 0 & 0 & 0 & 0 & 0 & 0 & 0 \end{bmatrix}\end{aligned} \tag{3.39}$$

where p_i denotes the power injection measurement at Bus i, and $p_{i\text{-}j}$ denotes the flow measurement connecting Bus i and Bus j.

Finally, the validity of (3.15) is also demonstrated: $9 = n_{OI} = R_d(\mathbf{G}) + n_{CII} = 3 + 6$. The example presented here uses a symmetrical network with the measurements also placed at the symmetrical locations. This is for the purpose of demonstrating how to use the *PCIR* to identify the observable islands and of explaining the related new concepts using the shortest possible mathematical expressions. Another Type 2 pathological case example is given in Appendix B, where only the identification results in each round of iteration are presented, while the mathematical expressions and the analysis are disregarded.

3.6 The Direct Island Identification Method and the Proposed Algorithm

The previous methods for observability analysis, including the classical method, the test method as well as the gram matrix method, use the Direct Branch (DB) method to identify the observable islands in two steps:

1. Find the unobservable branches: calculate the matrix **C** using (2.61), the corresponding branches of the nonzero rows of **C** are the unobservable branches.
2. Remove the unobservable branches from the network, and identify the observable islands.

This PhD has proposed a direct island method (DI) that identifies the observable islands directly from the test matrix in only one step:

1. Identify the observable islands according to the numerical values of the columns of the test matrix: the buses are grouped into one observable island if their corresponding columns are the same.

The benefit of DI is that it has a faster execution speed compared to DB as it only requires one step for identifying the observable islands, and the second step of DB usually needs iterations. However, DI has not been adopted by the previous numerical observability analysis methods since it cannot avoid the Type 1 pathological case. With the help of the *PCIR*, both DI and DB can detect and identify the pathological cases and thus correctly identify the observable islands.

Based on the *PCIR* and its associated theory, and the DI method, a novel algorithm for numerical observability analysis is proposed as follows:

The Proposed Algorithm:

1. Create the measurement Jacobian matrix **H** and calculate the gain matrix **G** according to (2.37). Perform Cholesky factorisation on **G**, and obtain the singular diagonal matrix **D** and the Cholesky factor **L**.
2. Check the number of zero pivots of **D**. If the number of zero pivots is one, the network is fully observable, stop the program. Else obtain the test matrix **W** from the inverse of **L**.
3. Use the DI method to identify the candidate observable islands from **W**.
4. Find the irrelevant injection measurements incident to multiple candidate observable islands. If no irrelevant injection measurement is found, go to Step 5. Else compute the *PCIR* using (3.12). If *PCIR* = 0, go to Step 5. Else if *PCIR* > 0, remove the irrelevant injection measurements found from the network and go back to Step 1.
5. Output the candidate observable islands identified as the final result, and stop the program.

3.7 Simulation Results

In this section, the simulation results and analysis of the execution time of both of the island identification methods, the DI method and DB method, are presented. The simulation results of the frequency of both types of pathological case in the IEEE 14 and 300 Bus Test Systems are also presented.

3.7.1 Execution Time of the Island Identification Methods

To demonstrate the speed advantage of the proposed direct island (DI) method, extensive simulations have been conducted on the execution time of both the DI and the direct branch (DB) method that has been widely adopted by the previous numerical observability analysis methods. For both island identification methods, the *PCIR* based iterative algorithm is adopted. In small networks such as the IEEE 14, 39, 57, 118 and 300 Bus Test Systems [113] the execution time tests are conducted with the number of measurements equal to the number of states in the system, and the number ratio of injection measurements to flow measurements is 1:4. For each network, the tests are conducted for both the DB method and the DI method. In addition, the execution time obtained for each test is the average of the results of 100 Monte

Carlo simulations. Furthermore, for each Monte Carlo simulation the execution time is recorded from the beginning to the end of the observability analysis program using the "start stopwatch timer" function in MATLAB.

The results of the execution time for each network and both types of identification method are shown in Table 3-1, which clearly indicate that the DI method is about 3 times faster than the DB method.

Table 3-1: Execution Time Test Results for Different Networks (milliseconds)

	IEEE 300	IEEE 118	IEEE 57	IEEE 39	IEEE 14
time(DB)	250.9	57.2	47.5	24.1	6. 9
time(DI)	84.9	22.0	15.6	9.7	2.5
time(DB)/time(DI)	3.0	2.6	3.1	2.5	2.8

The execution time test has also been conducted in a large network of the IEEE 2736 Bus Test System [113]. In these tests, two cases with different measurement configurations are considered: 1) the number ratio of injection measurements to flow measurements is 1:4 and 2) the number ratio of injection measurements to flow measurements is 4:1. In both cases the measurements are randomly added (while keeping the number ratio of the two types of measurements) from 0 to 3000 measurements, and each result is the average of 100 Monte Carlo simulations. The simulation results for case 1) and case 2) are presented in Figure 3-5 and Figure 3-6, respectively.

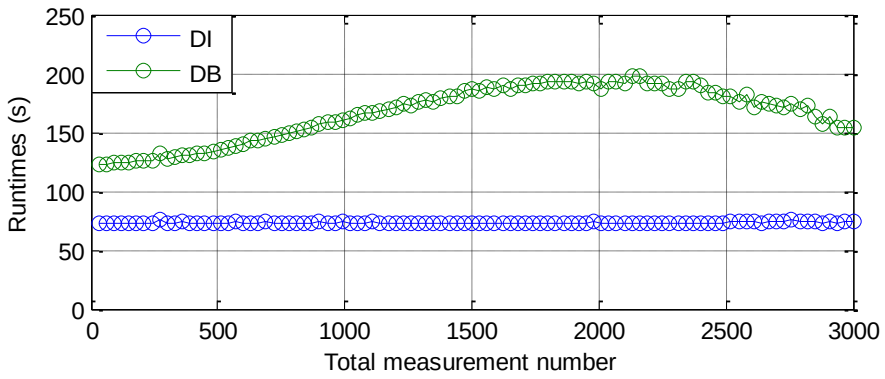

Figure 3-5: Execution Time Using DI and DB methods in the IEEE 2736 Bus Test System for Case 1)

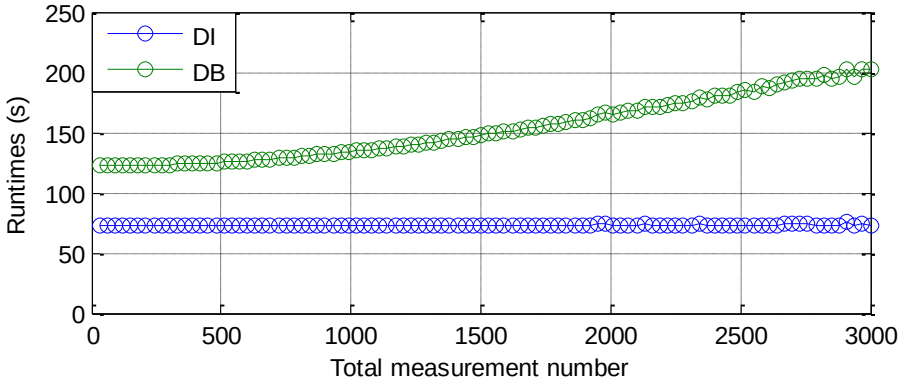

Figure 3-6: Execution Time when Using DI and DB Methods in the IEEE 2736 Bus Test System for Case 2)

It can be observed from Figure 3-5 and Figure 3-6 that DI is about 2 to 3 times faster than DB. In addition, the execution time of DI is almost the same for different numbers of measurements, while the execution time of DB increases significantly with the number of measurements. Such stability in execution time is desirable for the system operator in terms of knowing for sure how long the observability will take. As shown in both of the figures the execution time of DB is the least when there is no measurement and increases gradually when more measurements are added. The increasing trend becomes a decreasing trend when the number of measurements is about 2000 in case 1). This is due to the fact that when more measurements are added, the increased execution time, caused by the increased size of the measurement Jacobian matrix, becomes smaller than the time saving brought about by a smaller number of observable islands.

This phenomenon is only observed in case 1) since in this case the flow measurements constitute the majority of the measurements and the buses are more likely to form observable islands, while in Case 2) the injection measurements constitute the majority of the measurements, which are less likely to form observable islands. When the number of measurements is further increased, a peak in execution time can also be seen in Case 2). However, these cases might not be the ideal measurement placements.

As well as the number and the composition of the measurements, the value of the branch reactance affects the execution time. To investigate the impact of the branch reactance, 500 simulations are conducted for two cases respectively: case a) unit branch reactance is used, and case b) the real branch reactance is used. The average execution time for case a) is 80.3 s, and that for case b) is 97.8 s. This result shows that a simpler data of branch reactance could also reduce the amount of time for executing observability analysis. Thus the unit branch reactance is adopted in the two algorithms proposed in this thesis.

3.7.2 Frequency of Pathological Cases

Setting all the branch reactance equal to 1 p.u., the number of both Type 1 and Type 2 pathological cases are found for both the IEEE 14 Bus Test System and IEEE 2736 bus test system as given in Table 3-2. In the IEEE 14 Bus Test System, all possible placements of the flow and injection measurements are considered, while in the large network of the IEEE 2736 bus test system, 500 random placements are selected for the simulation.

Table 3-2 indicates that when the size of the network is small, the frequency of having pathological cases is low (less than 2%), and the occurrence of Type 1 pathological cases is about 6.4 times that of the other type. In comparison, in the 2736 bus network the percentage of pathological cases has increased to the significant number of 31%, while the ratio of Type 1 to Type 2 pathological cases remains almost the same (6.23 times more Type 1 cases). The reasons for the higher frequency of pathological cases in larger networks are the increased network topology complexity and increased number of measurements in large networks.

Table 3-2: Number of Pathological Cases Identified in the IEEE 14 Bus Test System and IEEE 2736 Bus Test System

Test System	IEEE 2736 Bus Test System		IEEE 14 Bus Test System	
Number of Simulations	500		2,605,911	
Pathological Case Type	Type 1	Type 2	Type 1	Type 2
Pathological Cases Identified	134	21	29,068	4553
Ratio	26.80%	4.20%	1.115%	0.175%

3.8 Inclusion of Synchronised Measurements

The increasing development of Wide Area Monitoring Systems (WAMS) [43], [97] means that modern power system observability analysis methods must be able to deal with synchronised measurements from Phasor Measurement Units (PMUs). In this section, a new method to include PMU measurements into conventional observability analysis methods without changing the formulation of the measurement Jacobian matrix is presented.

A PMU can measure both the voltage phasor of the bus where it is placed and the current phasors of the incident branches [98]. As shown in (3.40) $\overline{I_{ik}}$ is equivalent to P_{ik} and Q_{ik} in the DC model, as in the decoupled DC model the reactive variables are neglected.

$$\begin{aligned}\bar{I}_{ik} &= \frac{\overline{V}_i - \overline{V}_k}{jX} = \frac{V_i\cos\theta_i + jV_i\sin\theta_i - V_k\cos\theta_k - jV_k\sin\theta_k}{jX} \\ &= V_i\sin\theta_i - V_k\sin\theta_k - j\left(V_i\cos\theta_i - V_k\cos\theta_k\right) \\ &\approx \left(\theta_i - \theta_k\right) - j\left(V_i - V_k\right)\end{aligned} \tag{3.40}$$

Thus, for the purposes of observability analysis, $\overline{I_{ik}}$ becomes equivalent to P_{ik}. This equivalence between $\overline{I_{ik}}$ and P_{ik} holds even if both V_i and V_k are unknown. This is because, when assessing the observability between two buses, it must be determined if the relative voltage magnitude between the buses can be calculated (i.e. ΔV_{ik}) and not if the absolute voltage magnitude of the buses can be calculated.

For conventional measurements the rows of the measurement Jacobian matrix, **H**, have two standard forms: the flow form and the injection form. The flow form is shown in (3.41), the injection form is the sum of several row vectors in flow form. An example of the injection form is given in (3.42):

$$\mathbf{h} = \begin{bmatrix} 0 & \cdots & 0 & 1 & 0 & \cdots & 0 & -1 & 0 & \cdots & 0 \end{bmatrix} \tag{3.41}$$

$$\mathbf{h} = \begin{bmatrix} -1 & \cdots & -1 & N & 0 & \cdots & 0 & -1 & 0 & \cdots & 0 \end{bmatrix} \tag{3.42}$$

Using the approximation stated above, current measurements are readily available in flow form. However, the corresponding row in **H** for the voltage PMU measurements is in the form given in (3.43), which is neither of the two standard forms.

$$\begin{array}{c} \\ \theta_i \end{array} \quad \begin{array}{c} \theta_i \\ \begin{bmatrix} \cdots & 0 & 1 & 0 & \cdots \end{bmatrix} \end{array} \tag{3.43}$$

In order to convert the rows that correspond to complex voltage measurements into one of the standard forms, the following scheme is used:

> If there is only one PMU measurement, the complex voltage is regarded as one voltage magnitude measurement. The angle measurement is treated as the reference angle. If there is more than one PMU measurement, then the other complex voltage measurements can be regarded as fictional flow measurements between those buses and the reference bus since all angles measured by PMUs are synchronised using a common time signal (e.g. GPS). For example, although Bus *i* and Bus *j* are not connected by a

branch, the corresponding row can be written as shown in (3.44), provided that PMUs are placed at Bus *i* and Bus *j*.

$$\mathbf{H} = \begin{array}{c} \\ \theta_i \\ \\ \end{array} \begin{array}{c} \begin{array}{cccc} \theta_i & & \theta_j & \end{array} \\ \begin{bmatrix} \cdots & \cdots & \cdots & \cdots & \vdots \\ \cdots & -1 & \cdots & 1 & \vdots \\ \vdots & \vdots & \vdots & \vdots & \vdots \end{bmatrix} \end{array} \tag{3.44}$$

3.8.1 Inclusion of Current Phasor Measurements without Voltage Phasor Measurements at the Sending and Receiving Ends

The above analysis assumed that for any current phasor measurement there is always a voltage phasor measurement at its sending end. However, the voltage phasor measurement might be lost due to device damage or telecommunication errors. In these cases, the current phasor measurements cannot be simply regarded as power flow measurements since the voltages at both ends of the branch are unknown.

Consider the current between two buses, $\overline{I_{ik}}$. $\overline{I_{ik}}$ can be calculated using Ohm's law as given by (3.45), and the equation could be decomposed into real and imaginary parts, as given by (3.46) and (3.47).

$$\bar{V}_i - \bar{V}_k = Z_{ik}\bar{I}_{ik} \tag{3.45}$$

$$V_i \cos\theta_i - V_k \cos\theta_k = \mathrm{Re}\left\{Z_{ik}\bar{I}_{ik}\right\} \tag{3.46}$$

$$V_i \sin\theta_i - V_k \sin\theta_k = \mathrm{Im}\left\{Z_{ik}\bar{I}_{ik}\right\} \tag{3.47}$$

To solve (3.46) and (3.47), two of the four variables, V_i, V_k, θ_i and θ_k, should be known. Thus, the problem is discussed according to four different possible measurement placement cases as given in Table 3-3.

Table 3-3: Measurement Placement Cases for a Current Phasor Measurement

Case	Measurement Placement	Variable(s) Known
1	Bus *i* and Bus *k* are in the same observable island	V_i, $\theta_i - \theta_k$
2	Two voltage magnitude measurements, one at the sending end and the other at the receiving end of the current phasor measurement	V_i, V_k
3	One voltage magnitude measurement at the sending or receiving end of the current phasor measurement	V_i
4	The current phasor measurement is between two observable islands and no voltage magnitude measurement is available at either end	All of the four variables are unknown

In the first two cases, all four voltage variables of the two buses can be solved from (3.46) and (3.47), and they are all synchronised to the GPS reference bus. Thus, the current phasor measurement in these two cases is equivalent to a flow measurement between Bus *i* and Bus *k*, and a voltage phasor measurement at Bus *i*.

Equations (3.46) and (3.47) can be solved for Case 3 and Case 4, provided that a reference angle is available for Bus *i* in Case 3 and a reference voltage magnitude and a reference angle are available in Case 4. These requirements are exactly the same as those imposed when analysing the observability of two buses connected by a flow measurement. So, in these two cases, the current phasor measurement could also be treated as a power flow measurement when determining the observability.

Hence, two observable islands will form an observable island as long as they are connected by a current phasor measurement. However, the level of observability is different in different cases. The different observability levels in different cases and their characteristics are summarised in Table 3-4.

Table 3-4: Observability Levels and Their Characteristics.

Measurement Type	Case	Obser. Level	Characteristics
Current Phasor Measurements	1&2	3	The observable island is globally observable synchronised by the PMUs.
	3	2	The observable island is locally observable with its own reference angle.
	4	1	The observable island is locally observable with its own reference voltage angle and reference voltage magnitude.
Flow Measurements		2	The observable island is locally observable with its own reference angle.

In conclusion, if it is not guaranteed that there is a voltage phasor measurement at the sending end of the current phasor measurement, it is necessary to identify different levels of observability. In these cases, the algorithm proposed in Section 3.6 can be revised as follows:

The Algorithm Considering Special Current Phasor Measurements:

1. Form the measurement Jacobian matrix **H** in the decoupled DC model and calculate the gain matrix **G** according to (2.37). Perform Cholesky factorisation on **G**, and obtain the singular diagonal matrix **D** and the Cholesky factor **L**. Label the current phasor measurements without voltage measurements at the sending end.
2. Check the number of zero pivots of **D**. If **D** only has one zero pivot, the network is fully observable, stop the program. Else obtain the test matrix **W** from $\mathbf{L}^{-1}$.
3. Identify the candidate observable islands from **W** directly using the DI method.
4. Check if the labelled current phasor measurements are within one observable island or connecting two observable islands that have voltage magnitude measurements at both ends of the branch. If yes, merge the observable islands into the observable island that possesses the GPS bus. Else if there is a voltage magnitude measurement at either the sending end or receiving end, merge the observable islands into one observable island labelled as Level 2. Else merge the observable islands into a Level 1 observable island.

5. Identify the irrelevant injection measurements that are incident to more than one candidate observable island. If there is no irrelevant injection measurement, go to Step 6. Else compute the *PCIR* using (3.12). If *PCIR* = 0, go to Step 6. Else if *PCIR* > 0, remove the identified observable island from the network and go back to Step 1.
6. Output the candidate observable islands identified as the final result, and stop the program.

3.9 Alternative Methods for Cholesky Factorisation

The test matrix contains direct information about the observable islands, and constitutes the key component of the theory of the test matrix based numerical observability analysis methods. The test matrix can be derived from the inverse of the Cholesky factor according to its definition. However, Cholesky factorisation requires every pivot to be factorised in which vector multiplication is needed. This is time consuming especially in large networks such as the IEEE 2736 Bus Test System. In literature, several alternative methods are available for obtaining observable islands instead of Cholesky factorisation [107]-[109]. In [107], an integer arithmetic method for Cholesky factorisation is proposed. Using this method the elements of the obtained Cholesky factor are guaranteed to be integers. However, all pivots of the gain matrix still need to be factorised, and the Cholesky factor still needs to be inversed in order to obtain the test matrix. In [108]-[109], the null-space method is proposed as it can calculate the test matrix directly by only processing the nonzero pivots. This method is briefly introduced in the following subsection.

3.9.1 The Null-space Method

Using the DC decoupled model described in Subsection 2.2.1, the algorithm of the null-space method is shown as follows:

1. Set matrix **L** to be $\mathbf{I}_n$ (an identity matrix whose dimension is equal to the number of buses in the network n), **N** to be $\mathbf{0}_n$, and the iteration number to be 1.

2. Calculate the vector $\mathbf{t}_i = \mathbf{h}_i^T\mathbf{L}$, where $\mathbf{h}_i$ is the i^{th} row of the measurement Jacobian matrix.
3. Find the first positive element in $\mathbf{t}_i$, in the p^{th} position, t_i^p, and set the p^{th} element of **N**, $N_p = i$. If no positive element can be found in $\mathbf{t}_i$, go to Step 6.
4. Divide the p^{th} column of **L** by t_i^p.
5. For k =1 to n, $k \neq p$, $t_i^p \neq 0$ do, $\mathbf{l}_k = \mathbf{l}_k - t_i^j\ \mathbf{l}_p$, where $\mathbf{l}_k$ and $\mathbf{l}_p$ are the k^{th} and p^{th} column of **L**, respectively. Go to Step 2.
6. Set the test matrix $\mathbf{W} = \mathbf{N}^T$ and output **W**.

To illustrate the algorithm, an example that uses the null-space method to calculate the test matrix is given. The network and measurement placement is the same as the example given in Section 3.2 as shown in Figure 3-1. The iteration steps of this method are given below:

Iteration 1						
$\mathbf{h}_1$	0	0	0	0	0	0
–1	1	**0**	0	0	0	0
4	0	**1**	0	0	0	0
–1	0	**0**	1	0	0	0
–1	0	**0**	0	1	0	0
–1	0	**0**	0	0	1	0
0	0	**0**	0	0	0	1
$\mathbf{t}^1$	–1	4	–1	–1	–1	0

(3.48)

Iteration 2						
$\mathbf{h}_2$	0	1	0	0	0	0
–1	1	0	0	0	**0**	0
–1	$\frac{1}{4}$	$\frac{1}{4}$	$\frac{1}{4}$	$\frac{1}{4}$	$\mathbf{\frac{1}{4}}$	0
0	0	0	1	0	**0**	0
–1	0	0	0	1	**0**	0
4	0	0	0	0	**1**	0
–1	0	0	0	0	**0**	1
$\mathbf{t}^2$	$-\frac{5}{4}$	$-\frac{1}{4}$	$-\frac{1}{4}$	$-\frac{5}{4}$	$\frac{15}{4}$	–1

(3.49)

Iteration 3						
$\mathbf{h}_3$	0	1	0	0	2	0
0	1	**0**	0	0	0	0
1	$\frac{1}{3}$	$\frac{\mathbf{4}}{\mathbf{15}}$	$\frac{4}{15}$	$\frac{1}{3}$	$\frac{1}{15}$	$\frac{1}{15}$
–1	0	**0**	1	0	0	0
0	0	**0**	0	1	0	0
0	$\frac{1}{3}$	$\frac{\mathbf{1}}{\mathbf{15}}$	$\frac{1}{15}$	$\frac{1}{3}$	$\frac{4}{15}$	$\frac{4}{15}$
0	0	**0**	0	0	0	1
$\mathbf{t}^3$	$\frac{1}{3}$	$\frac{4}{15}$	$-\frac{11}{15}$	$\frac{1}{3}$	$\frac{1}{15}$	$\frac{1}{15}$

(3.50)

Iteration 4						
$\mathbf{h}_4$	3	1	0	0	2	0
0	3	–0.8	**2.2**	–1	–0.2	–0.2
1	1	0	**1**	0	0	0
0	0	0	**1**	0	0	0
0	0	0	**0**	1	0	0
–1	1	–0.2	**0.8**	0	0.2	0.2
0	0	0	**0**	0	0	1
$\mathbf{t}^4$	0	0.2	0.2	–1	–0.2	–0.2

(3.51)

Final Table					
3	1	4	0	2	0
3	–3	11	–1	2	2
1	–1	5	0	1	1
0	–1	5	0	1	1
0	0	0	1	0	0
1	–1	4	0	1	1
0	0	0	0	0	1

(3.52)

The corresponding null space matrix, **L**, is given by (3.53).

$$\mathbf{L}^T = \begin{bmatrix} -1 & 0 & 0 & -1 & 0 & 0 \\ 2 & 1 & 1 & 0 & 1 & 1 \end{bmatrix} \tag{3.53}$$

It can be verified that $\mathbf{L}^T = \mathbf{W}$ as given in (3.3). It is also shown that only the columns corresponding to the nonzero pivots are processed. Thus, the null-space method may be used to improve the efficiency in calculating the test matrix in observability analysis.

3.10 Discussion: Effect of Branch Reactance on Numerical Observability Analysis

In numerical observability analysis, the DC decoupled model and unit branch reactance are widely adopted for simplification of expressions and improvement of calculation efficiency. However, it has been discovered by the author during the research in observability analysis that the choice of the branch reactance does affect the values of the test matrix and thus the identification of observable islands (examples will be given in the following sections). It might be suggested by readers that it is not compulsory to correctly identify observable islands by using the proposed method based on the *PCIR*. These comments are given based on the fact that the measurement Jacobian matrix, the test matrix and thus the identified observable islands will be different if different values of branch reactance are used. There are two major concerns about the effect of branch reactance in numerical observability analysis: using alternative branch reactance and using real branch reactance to avoid pathological cases. It will be shown in the following subsections that both of the suggested methods cannot totally avoid both types of pathological case.

3.10.1 Alternative Branch Reactance for Numerical Observability Analysis

One of the major alternative methods for avoiding pathological cases is to use alternative / arbitrary branch reactance for building up the network model. However, after conducting extensive simulations for the IEEE 14 Bus Test System, it was concluded that varying the branch reactances could remove pathological cases for a certain scenario but could then result in different sets of pathological cases. As such, changing the branch reactances cannot guarantee that the existence of pathological cases is excluded. To demonstrate this, an example

is given below where the use of an alternative branch reactance can lead to a pathological case while the use of unit branch reactance can correctly identify observable islands:

Consider a six bus network and its measurement placement shown in Figure 3-7.

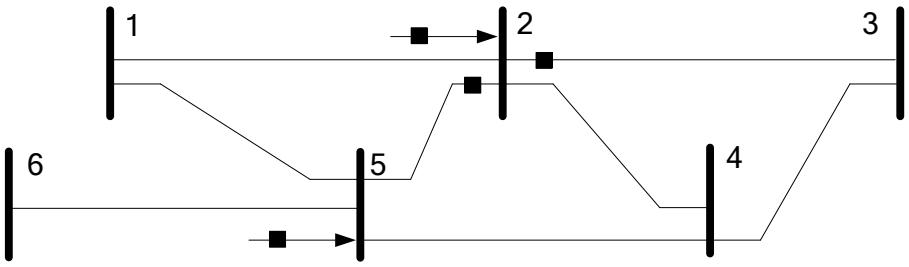

Figure 3-7: Six Bus System and the Measurement Placement

The measurement Jacobian matrix is given in (3.54) with all branch reactances equal to 1 per unit except for that of Branch 4-5, which is set to 2 per unit.

$$\mathbf{H} = \begin{bmatrix} -1 & 4 & -1 & -1 & -1 & -1 \\ -1 & -1 & 0 & -2 & 5 & -1 \\ 0 & 0 & 1 & -1 & 0 & 0 \\ 0 & 0 & 0 & 0 & 1 & -1 \end{bmatrix} \tag{3.54}$$

The corresponding test matrix is given by (3.55):

$$\mathbf{W} = \begin{bmatrix} -2 & 0 & 1 & 1 & 0 & 0 \\ 3 & 1 & 0 & 0 & 1 & 1 \end{bmatrix} \tag{3.55}$$

The identified observable islands are as follows: {1}, {2, 5, 6}, {3, 4}, and both of the injection measurements are determined to be irrelevant injection measurements. Thus, $PCIR = R_d(\mathbf{G}) + n_{III} - n_{UC} = 2+2-3=1>0$, indicating that this is a pathological case. After removing all irrelevant injection measurements, it is easy to find the 4 observable islands since there are only flow measurements: {1}, {2}, {3, 4}, {5, 6}. This implies that Branch 2-5 is a pathological branch. In contrast, when unit reactances are used for every branch, all 4 observable islands could be

successfully identified without iterations. The measurement Jacobian matrix and the test matrix for the unit branch reactance case are given in (3.56) and (3.57) respectively.

$$\mathbf{H} = \begin{bmatrix} -1 & 4 & -1 & -1 & -1 & -1 \\ -1 & -1 & 0 & -1 & 4 & -1 \\ 0 & 0 & 1 & -1 & 0 & 0 \\ 0 & 0 & 0 & 0 & 1 & -1 \end{bmatrix} \tag{3.56}$$

$$\mathbf{W} = \begin{bmatrix} -1.2 & 0.2 & 1 & 1 & 0 & 0 \\ 2.2 & 0.8 & 0 & 0 & 1 & 1 \end{bmatrix} \tag{3.57}$$

3.10.2 Actual Branch Reactance for Numerical Observability Analysis

The other alternative method for preventing pathological cases in the test matrix based observability analysis is to use actual branch reactances. However, when actual reactances are used, it is still possible to have pathological cases and pathological branches because of the coincidence of linear combinations.

Although intuitively it seems impossible to have such coincidences, since the branch reactances are almost random (with precision to 10^{-6}), it is still possible to find a number of pathological cases in the very simple IEEE 14 Bus Test system such as given in the example below:

The diagram of the IEEE 14 Bus Test System and the measurement placement are shown in Figure 3-8.

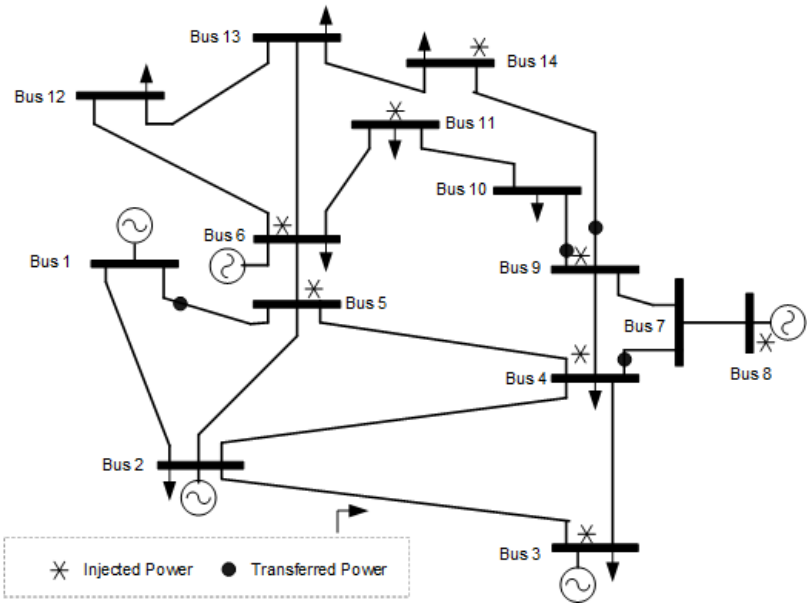

Figure 3-8: IEEE 14 Bus Test System and the Measurement Placement

The reactances of the branches in the IEEE 14 Bus Test System are given in the table below:

Table 3-5: Branch reactance for IEEE 14 Bus Test System

Branch #	From Bus #	To Bus #	Reactance (per unit)
1	1	2	0.05917
2	1	5	0.22304
3	2	3	0.19797
4	2	4	0.17632
5	2	5	0.17388
6	3	4	0.17103
7	4	5	0.04211
8	4	7	0.20912
9	4	9	0.55618
10	5	6	0.25202
11	6	11	0.19890
12	6	12	0.25581
13	6	13	0.13027
14	7	8	0.17615
15	7	9	0.11001
16	9	10	0.08450
17	9	14	0.27038
18	10	11	0.19207
19	12	13	0.19988
20	13	14	0.34802

3.10.2.1 Results When Actual Branch Reactances Are Used

When actual branch reactances are used, the measurement Jacobian matrix is calculated and is given by:

$$\mathbf{H}=\begin{bmatrix}
0 & -0.19797 & 0.369 & -0.17103 & 0 & 0 & 0 & 0 & 0 & 0 & 0 & 0 & 0 & 0\\
0 & -0.17632 & -0.17103 & 1.15476 & -0.04211 & 0 & -0.20912 & 0 & -0.55618 & 0 & 0 & 0 & 0 & 0\\
-0.22304 & -0.17388 & 0 & -0.04211 & 0.69105 & -0.25202 & 0 & 0 & 0 & 0 & 0 & 0 & 0 & 0\\
0 & 0 & 0 & 0 & -0.25202 & 0.837 & 0 & 0 & 0 & 0 & -0.1989 & -0.25581 & -0.13027 & 0\\
0 & 0 & 0 & 0 & 0 & 0 & -0.17615 & 0.17615 & 0 & 0 & 0 & 0 & 0 & 0\\
0 & 0 & 0 & -0.55618 & 0 & 0 & -0.11001 & 0 & 1.02107 & -0.0845 & 0 & 0 & -0.27038 & 0\\
0 & 0 & 0 & 0 & 0 & -0.1989 & 0 & 0 & 0 & -0.19207 & 0.39097 & 0 & 0 & 0\\
0 & 0 & 0 & 0 & 0 & 0 & 0 & 0 & -0.27038 & 0 & 0 & 0 & -0.34802 & 0.6184\\
0.22304 & 0 & 0 & 0 & -0.22304 & 0 & 0 & 0 & 0 & 0 & 0 & 0 & 0 & 0\\
0 & 0 & 0 & 0.20912 & 0 & 0 & -0.20912 & 0 & 0 & 0 & 0 & 0 & 0 & 0\\
0 & 0 & 0 & 0 & 0 & 0 & 0 & 0 & 0.0845 & -0.0845 & 0 & 0 & 0 & 0\\
0 & 0 & 0 & 0 & 0 & 0 & 0 & 0 & 0.27038 & 0 & 0 & 0 & 0 & -0.27038
\end{bmatrix} \tag{3.58}$$

According to its definition, the test matrix is calculated as given in (3.59):

$$\mathbf{W}=\begin{bmatrix}
0.21421835 & -0.03364963 & 0.01805316 & 0 & 0.21421835 & 0.42102742 & 0 & 0 & 0 & 0 & 0.21421835 & 1 & 0 & 0\\
0.78578165 & 1.03364963 & 1.01805316 & 1 & 0.78578165 & 0.57897258 & 1 & 1 & 1 & 1 & 0.78578165 & 0 & 1 & 1
\end{bmatrix} \tag{3.59}$$

By grouping the buses whose columns in the test matrix are the same as one observable island, the following observable islands are identified: {1, 5, 11}, {2}, {3}, {4, 7, 8, 9, 10, 13, 14}, {6} and {12} (which are incorrect). The irrelevant injection measurements in this case are the injection measurements located at Buses 3, 4, 5, 6 and 11. Thus, $PCIR = R_d(\mathbf{G}) + n_{III} - n_{UC} = 2+5-6 = 1 > 0$, indicating this is a pathological case. After removing the irrelevant injection measurements from the measurement set, the new measurement Jacobian matrix is formed as given by (3.60):

$$\mathbf{H}=\begin{bmatrix}
0 & 0 & 0 & 0 & 0 & 0 & -0.17615 & 0.17615 & 0 & 0 & 0 & 0 & 0 & 0\\
0 & 0 & 0 & -0.55618 & 0 & 0 & -0.11001 & 0 & 1.02107 & -0.0845 & 0 & 0 & 0 & -0.27038\\
0 & 0 & 0 & 0 & 0 & 0 & 0 & 0 & -0.27038 & 0 & 0 & 0 & -0.34802 & 0.6184\\
0.22304 & 0 & 0 & 0 & -0.22304 & 0 & 0 & 0 & 0 & 0 & 0 & 0 & 0 & 0\\
0 & 0 & 0 & 0.20912 & 0 & 0 & -0.20912 & 0 & 0 & 0 & 0 & 0 & 0 & 0\\
0 & 0 & 0 & 0 & 0 & 0 & 0 & 0 & 0.0845 & -0.0845 & 0 & 0 & 0 & 0\\
0 & 0 & 0 & 0 & 0 & 0 & 0 & 0 & 0.27038 & 0 & 0 & 0 & 0 & -0.27038
\end{bmatrix} \tag{3.60}$$

The new test matrix is given by：

$$\mathbf{W} = \begin{bmatrix} 0 & 1 & 0 & 0 & 0 & 0 & 0 & 0 & 0 & 0 & 0 & 0 & 0 & 0 \\ 0 & 0 & 1 & 0 & 0 & 0 & 0 & 0 & 0 & 0 & 0 & 0 & 0 & 0 \\ 1 & 0 & 0 & 0 & 1 & 0 & 0 & 0 & 0 & 0 & 0 & 0 & 0 & 0 \\ 0 & 0 & 0 & 0 & 0 & 1 & 0 & 0 & 0 & 0 & 0 & 0 & 0 & 0 \\ 0 & 0 & 0 & 0 & 0 & 0 & 0 & 0 & 0 & 0 & 1 & 0 & 0 & 0 \\ 0 & 0 & 0 & 0 & 0 & 0 & 0 & 0 & 0 & 0 & 0 & 1 & 0 & 0 \\ 0 & 0 & 0 & 1 & 0 & 0 & 1 & 1 & 1 & 1 & 0 & 0 & 1 & 1 \end{bmatrix} \tag{3.61}$$

From the new test matrix, a different set of observable islands is identified: {1, 5}, {2}, {3}, {4, 7, 8, 9, 10, 13, 14}, {6}, {11} and {12}. Since there is no irrelevant injection measurement, the observable islands identified after this iteration are correct according to Property 2' of the test matrix as proposed in the manuscript. This can also be verified with *PCIR*: $PCIR = R_d(\mathbf{G}) + n_{III} - n_{UC} = C = 7+0-7 = 0$.

3.10.2.2 Results When Branch Reactances Are 1 Per Unit

When the reactance of all branches is changed to 1 per unit, the corresponding measurement Jacobian matrix is given by:

$$\mathbf{H} = \begin{bmatrix} 0 & -1 & 2 & -1 & 0 & 0 & 0 & 0 & 0 & 0 & 0 & 0 & 0 & 0 \\ 0 & -1 & -1 & 5 & -1 & 0 & -1 & 0 & -1 & 0 & 0 & 0 & 0 & 0 \\ -1 & -1 & 0 & -1 & 4 & -1 & 0 & 0 & 0 & 0 & 0 & 0 & 0 & 0 \\ 0 & 0 & 0 & 0 & -1 & 4 & 0 & 0 & 0 & 0 & -1 & -1 & -1 & 0 \\ 0 & 0 & 0 & 0 & 0 & 0 & -1 & 1 & 0 & 0 & 0 & 0 & 0 & 0 \\ 0 & 0 & 0 & -1 & 0 & 0 & -1 & 0 & 4 & -1 & 0 & 0 & -1 & 0 \\ 0 & 0 & 0 & 0 & 0 & -1 & 0 & 0 & 0 & -1 & 2 & 0 & 0 & 0 \\ 0 & 0 & 0 & 0 & 0 & 0 & 0 & 0 & -1 & 0 & 0 & 0 & -1 & 2 \\ 1 & 0 & 0 & 0 & -1 & 0 & 0 & 0 & 0 & 0 & 0 & 0 & 0 & 0 \\ 0 & 0 & 0 & 1 & 0 & 0 & -1 & 0 & 0 & 0 & 0 & 0 & 0 & 0 \\ 0 & 0 & 0 & 0 & 0 & 0 & 0 & 0 & 1 & -1 & 0 & 0 & 0 & 0 \\ 0 & 0 & 0 & 0 & 0 & 0 & 0 & 0 & 1 & 0 & 0 & 0 & 0 & -1 \end{bmatrix} \tag{3.62}$$

The test matrix in this case is given by:

$$\mathbf{W} = \begin{bmatrix} 0.08450704 & -0.05633803 & -0.02816901 & 0 & 0.08450704 & 0.30985915 & 0 & 0 & 0 & 0 & 0.15492958 & 1 & 0 & 0 \\ 0.91549296 & 1.05633803 & 1.02816901 & 1 & 0.91549296 & 0.69014085 & 1 & 1 & 1 & 1 & 0.84507042 & 0 & 1 & 1 \end{bmatrix} \quad (3.63)$$

Observing the columns of the test matrix, the identified observable islands are: {1, 5}, {2}, {3}, {4, 7, 8, 9, 10, 13, 14}, {6}, {11} and {12}. This is the correct solution and is the same as that of the previous case. The irrelevant injection measurements are the injection measurements at Buses 3, 4, 5, 6 and 11. Thus, it is verified that the identification result using unit reactances is correct: $PCIR = R_d(\mathbf{G}) + n_{III} - n_{UC} = 7+0-7 = 0$.

In conclusion, if all possible pathological cases are expressed as a certain set of branch reactances, say Set *k*, as the set P_k, then the following three sets, P_k, P_i -P_k and P_k –P_i, are not all guaranteed to be empty sets, regardless of the choice of branch reactances, especially for large systems with more complex topologies. The most reliable and convenient way to identify pathological cases is to use *PCIR*, as it can guarantee the removal of pathological cases, regardless of the chosen branch reactances.

3.11 Summary

In this chapter, a new numerical method for observability analysis has been proposed based on the pathological case identification rule (*PCIR*). The existing numerical method for observability analysis is found to be flawed and may cause incorrect results of identified observable islands in some certain cases that are named *pathological cases*. The underlying theorem of the existing numerical method is revised, and a new fully iterative method for numerical observability analysis has been proposed that guarantees the correct identification of observable islands. However, unnecessary iterations drastically slow down the execution speed, and affect the observability analysis when it is applied online. For this purpose, a screening rule, *PCIR*, is proposed that is capable of sifting out normal cases while giving extra iterations for pathological cases. In addition, with the help of *PCIR*, observable islands can be identified directly from the test matrix using the direct island (DI) method. The simulation results

demonstrate that the proposed iterative algorithm that combines the *PCIR* based screening rule and the DI method is 2 to 3 times faster than the direct branch (DB) method which is widely adopted by the existing numerical methods in multiple networks ranging from IEEE 14 Bus Test System to 2736 bus test system. The limitations of the existing numerical observability methods are taken into account as well as the limitations of the proposed method that is designed for networks with only conventional measurements. Thus, a new scheme for including the synchronised measurements from the PMUs is also proposed. A highly efficient alternative method for Cholesky factorisation is also presented, and some discussions are given about the effect of branch reactance in numerical observability analysis and the reasons why pathological cases cannot be avoided by changing the values of branch reactance.

Chapter 4 Optimal Phasor Measurement Unit Placement

This chapter presents a new method for optimal Phasor Measurement Unit (PMU) placement in the presence of conventional measurements. The proposed method can guarantee that the PMU placement found can support full network observability in networks with existing conventional measurements. It also reduces the occurrence of suboptimal solutions compared to the existing methods.

4.1 Introduction

As the core and enabler of the Wide Area Monitoring System (WAMS) Synchronised Measurement Technology (SMT) is closely associated with the development of a range of processes including economic evaluation, feasibility and gap analyses, implementation schedule planning and system studies. Thus, research into optimal PMU placement could benefit a large number of SMT applications such as open and closed loop control, post-disturbance event analysis, protection, situational awareness, system model validation, visualisation and early warning systems.

The methodologies of optimal PMU placement must consider two different types of criteria, the application criteria and infrastructure criteria as listed below:

- Application Criteria
  - Angular Separations
  - Black Start
  - Critical Paths
  - FACTS Controls
  - Islanding, Separation and Restoration
  - Major Generation and Load

  - Oscillations
  - Renewable Integration
  - State Estimation
  - Tie Line Flows
- Infrastructure Criteria
  - Aggregate Sites
  - Automated P&C Systems
  - NERC PRC – 002
  - Security

The application criteria are based on the application to be used. In addition, the effectiveness of the PMU is highly dependent on the used application it will support. Thus, it is possible that, with the one placement, the PMU placement will be highly efficient for one application but inefficiently for another application. In this thesis, only the application criterion for state estimation, which is network observability, is considered. Thus, objective the optimal PMU placement considered in this Thesis is to minimise the number of PMUs placed in the network while ensuring network observability. The effects of the locations of the PMUs on other application criteria will not be considered.

There is extensive literature on optimal PMU placement for network observability that considers different constraints, optimisation algorithms and scenarios (such as loss of branch and loss of PMUs). Integer linear programming (ILP) is the most popular optimisation algorithm because of its high accuracy, ease of implementation and flexibility. In 2012 a taxonomy [114] of the optimal PMU placement methods classified the existing methods into six categories according to the scenarios considered: single branch loss contingency [115]-[125], PMU outage contingency [116]-[119], [122]-[126], single line outage or single PMU loss contingency [116], [118]-[121], [127] the limits of PMU channel capacity (the maximum number of current phasor measurements that can be measured by the PMU) [116], [128]-[129], the effect of virtual measurements such as zero injection measurements [115]-[117], [126], [128], [130]-[146], and the effect imposed by the conventional measurements [118]-[119], [126], [134], [140], [143]-[150]. Recently, research on optimal PMU placement has given

increasing attention to solving the problem in the presence of conventional measurements. This is mainly because of the interest in developing hybrid state estimators that use a mixture of conventional measurements and PMU measurements. In addition, zero injection measurements, which have the same effect in observability analysis as the injection measurement, can be assumed for any bus that has neither generation nor load. These measurements do not provide direct observability of the buses in the network, but they allow fewer PMUs to be placed if the PMUs are properly placed.

Most of the algorithms for optimal PMU placement in the presence of conventional measurements are developed based on Kirchhoff's Current Law (KCL) [117]-[120]. According to KCL, a group of buses will be fully observable if one of the buses has an injection measurement or is neighbouring to a bus incident with an injection measurement, and the rest of the buses are observed by the PMUs, then all of these buses will be observable. However, the KCL based method can only guarantee optimal PMU placement when no bus incident with an injection measurement neighbours to another bus incident with an injection measurement, which is quite unrealistic in real networks. If this condition is not satisfied, the KCL based method might not give correct placements, the placements that can ensure full observability of the network. There are also some other methods that are developed based on observability analysis of the network [120], [134]. The observable islands identified in the observability analysis are regarded as individual buses in the new network. It is also assumed that there is no existing conventional measurement in the new reduced network. However, this assumption might not always hold. As mentioned in the previous chapter there might be irrelevant injection measurements that are incident to multiple observable islands, which means that they will increase the rank of the gain matrix, and must not be neglected when finding the optimal PMU placement.

In this thesis, an efficient method is proposed that overcomes the problems of the existing methods by using a network transformation scheme and a novel global observability criterion. The network transformation scheme creates a reduced network model that contains only injection measurements. It is also based on the observability analysis, but it also considers the effect of irrelevant injection measurements, while the other measurements which do not affect

the observability of the network are discarded. The network transformation scheme is required for the algorithm because it is difficult to find a global observability criterion for a network with multiple types of conventional measurement, and it will be difficult to implement it with ILP even if such an observability criterion exists. A global observability criterion is thus designed for networks that only possess irrelevant injection measurements. Global observability means that it considers the observability of the entire network rather than that of a group of buses near a particular injection measurement. Hence, the proposed algorithm can offer better placement solutions than the existing two types of method for the following two reasons, respectively.

1 The proposed method can guarantee that the PMU placement solution can always support network observability, while the KCL based methods might give the wrong solutions that cannot make the system observable due to its local observability criterion used.
2 The proposed method considers the effects of the irrelevant injection measurements while the observability analysis based method does not take these measurements into consideration. Furthermore, the proposed method can also reduce the execution time due to the reduced size of the network especially in cases where the number of observable islands is much smaller than the number of buses in the network.

Regarding the later sections of this chapter, a new network transformation scheme will be presented in Section 4.2, a new network observability criterion will be proposed in Section 4.3, the proposed algorithm will be presented in Section 4.4, the advantages of the proposed method compared to the existing methods will be discussed in Section 4.5, the simulation results will be presented in Section 4.6, and a summary of this chapter will be given in Section 4.7.

4.2 The Network Transformation Scheme

The network transformation scheme is proposed as follows:

1. Identify the observable islands and irrelevant injection measurements using observability analysis.
2. Create a reduced network, where the buses are the observable islands in the original network, and the injection measurements that measure the power flow injected from parts of its connected branches are the irrelevant injection measurements in the original network.
3. Form the bus to placement incident matrix, **A**.

The aim of the network transformation scheme is to transform the network, which consists of multiple types of conventional measurements, into a reduced network that only has injection measurements. This makes it possible to use the global observability criterion proposed in the next section. An example of using the network transformation in the IEEE 14 Bus Test System is presented below:

Consider the IEEE 14 Bus Test System with the measurements shown in Figure 4-1, five observable islands are identified after observability analysis: {1;2;3;4;5}, {6;12;13;14}, {7;8}, {9;10} and {11}, and the injection measurements incident to Bus 4, Bus 9, Bus 11 are identified to be irrelevant injection measurements. As discussed in the previous chapter, the irrelevant injection measurements are defined as the injection measurements incident to multiple observable islands [110]. Following the steps set out above, the network is transformed into a network of reduced size as shown in Figure 4-2.

Since in the transformed network every bus represents an observable island in the original network, a PMU placed in the transformed network might not be able to measure the current phasors of all the branches connected. For example a PMU placed at Bus 5 of Island 1 (Bus 1 in the transformed network) can only measure the current phasor incident to Island 2 (Bus 2 in the transformed network). Here *placement* is defined as a PMU placed at a given bus measuring the current phasors incident to given branches. Thus, a bus can have multiple placements, and each placement is unique. The bus to placement incident matrix is expressed and explained in (4.1) and (4.2) respectively.

$$\mathbf{A} = \begin{bmatrix} 1 & 1 & 1 & 0 & 1 & 1 & 0 & 0 \\ 0 & 1 & 1 & 1 & 0 & 1 & 0 & 1 \\ 1 & 0 & 0 & 0 & 1 & 1 & 0 & 0 \\ 1 & 0 & 0 & 1 & 1 & 1 & 1 & 1 \\ 0 & 0 & 1 & 0 & 0 & 0 & 1 & 1 \end{bmatrix} \tag{4.1}$$

$$\mathbf{A}_{ij} = \begin{cases} 0 \text{ if Bus } i \text{ is not measured by PMU with Placement } j \\ 1 \text{ if Bus } i \text{ is measured by PMU with Placement } j \end{cases} \tag{4.2}$$

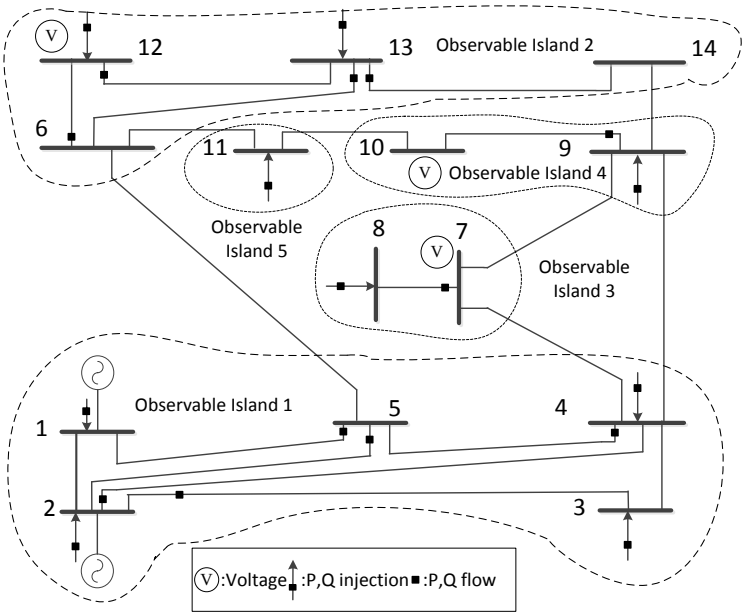

Figure 4-1: IEEE 14 Bus Test System and the Measurement Placement

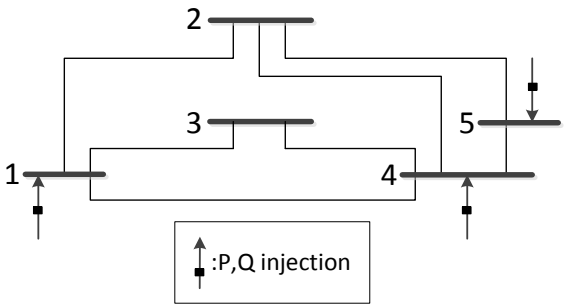

Figure 4-2: Transformed Five Bus Network and the Measurement Placement

Eight placements are found in the transformed network, as summarised in Table 4-1. Each placement in the transformed network represents a PMU placement in the original network that

connects two observable islands. For example, Placement 1 that only measures the current phasor of the branch connecting Bus 2 in the transformed network represents a PMU placed at Bus 5 in Observable Island 1 in the original network, while Placement 2 that measures that connecting Bus 3 and Bus 4, represents a PMU placed at Bus 4. The irrelevant injection measurements incident to Bus 4, Bus 5 and Bus 11 are represented as injection measurements incident to their corresponding placements in the transformed network, as shown in Table 4-1. The placements incident with the injection measurements will be treated differently from the other placements and this will be explained in the next section.

Table 4-1: Placement Available in the Transformed Network

	At Bus #	To Bus #	With injection measurement?
Placement 1	1	2	No
Placement 2	1	3,4	Yes
Placement 3	2	1,5	No
Placement 4	2	4	No
Placement 5	3	4	No
Placement 6	4	1,2,3	No
Placement 7	4	5	Yes
Placement 8	5	2,4	Yes

4.3 Network Observability Criterion

For any network that only has injection measurements (including the zero injection measurements), the optimal PMU placement can be found following the observability criterion presented below:

Theorem 4.1: A network with q buses incident with injection measurements will be fully observable if the remaining p buses that are not incident with injection measurements are observed by the PMUs.

Proof for Theorem 4.1:

Define matrix **C** as the network connection matrix. The definition of the entries of **C** is given in (4.3):

$$C_{ik} = \begin{cases} 1 & \text{Bus } k \text{ is the sending bus of Branch } i \\ -1 & \text{Bus } k \text{ is the receiving bus of Branch } i \\ 0 & \text{Otherwise} \end{cases} \tag{4.3}$$

Define matrix $\mathbf{C}_q$ as the sub-matrix of **C** consisting of the columns corresponding to the q buses incident with injection measurements. Then, the sub-matrix of the measurement Jacobian matrix corresponding to the placements with the q injection measurements, $\mathbf{H}_q$, can be expressed as given in (4.4):

$$\mathbf{H}_q = \mathbf{C}_q^T \mathbf{C}_q \tag{4.4}$$

After a number of row eliminations and matrix permutations, the measurement Jacobian matrix, **H**, of all measurements including the injection measurements and the newly placed PMU measurements are given in (4.5):

$$\mathbf{H} = \begin{bmatrix} \mathbf{I}_p & \mathbf{0} \\ \mathbf{0} & \mathbf{C}_q^T \mathbf{C}_q \end{bmatrix} \tag{4.5}$$

H is of full rank because $\mathbf{C}_q$ is of full rank, and for any vector or matrix, **x**, rank(**x**) = rank($\mathbf{x}^T\mathbf{x}$). After a number of row eliminations and matrix permutations, any **C** can be expressed by (4.6):

$$\mathbf{C} = \begin{bmatrix} 1 & -1 & & \\ & \ddots & \ddots & \\ & & 1 & -1 \\ & \mathbf{R} & & \end{bmatrix} \tag{4.6}$$

where **R** represents the redundant part of **C**. rank(**C**)=rank($\mathbf{C}_{p+q-1}$) = p+q-1 because the sum of each row of **c** is 0 and an identity matrix of dimension p+q-1 can be obtained after deleting one

column from **C** and performing Gaussian elimination. Since $\mathbf{C}_{p+q-1}$ is of full rank, the matrix composed by any columns of $\mathbf{C}_{p+q-1}$ is also of full rank. So $\mathbf{C}_q$ has full rank.

End of the Proof

The observability criterion proposed above can be easily implemented with ILP as expressed in (4.7) and (4.8):

$$\min \mathbf{c}^{T}\mathbf{x} \tag{4.7}$$

$$s.t.\ \mathbf{A}\mathbf{x} \geq \mathbf{b} \tag{4.8}$$

where **c** is the placement cost coefficient vector, **x** is the vector of placements, **A** is the bus to placement incidence matrix, and **b** is the vector consisting of linear equality constraints, in which the elements corresponding to placements incident with injection measurements are set to be 0 and the other elements are set to be 1. Since the elements of **A** and **x** can are non-negative the zero constraints in **b** are released constraints. In other words, the constraints corresponding to the buses incident with injection measurements could be removed without changing the final result of PMU placement.

4.4 The Proposed Algorithm

Based on the network transformation scheme presented in Section 4.2 and the new observability criterion proposed in Section 4.3, A new algorithm for optimal PMU placement taking the presence of conventional measurement into account is described as follows:

1. Transform the network into a reduced form following the steps as described in Sections 4.2.
2. Obtain the optimal placement in the transformed network using ILP according to the optimisation function and constraints given in (4.7) and (4.8), respectively.
3. Obtain the optimal PMU placement in the original network.

The steps presented above can be summarised in Figure 4-3.

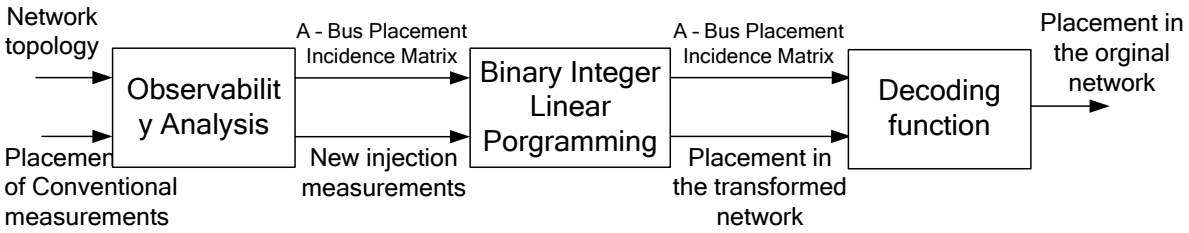

Figure 4-3: Block Diagram of the Proposed Algorithm for Optimal PMU Placement

4.5 Advantages of the Proposed Method Compared to the Existing Methods

4.5.1 KCL Based Methods: Possible Failure for Correct Placement Solution

The major problem of the KCL based methods (algorithm given in Appendix D.1) is that its PMU placement results can fail to make the network observable. The basic aspects of the KCL based method are given below:

If a bus is placed with a PMU or directly neighbouring a bus placed with a PMU, this bus is said to be *reached* by PMU. Define the number of times of Bus i reached by PMUs, y_i. To ensure observability, for buses not incident with any conventional measurements, y_i should be not less than 1, while for a group of n buses associated with conventional measurements they should obey the following constraint:

$$y_{i1} + y_{i2} + \cdots + y_{in} \geq n - 1 \tag{4.9}$$

According to KCL, n buses that are incident with an injection measurement or that neighbour a bus incident with an injection measurement will be observable if any n-1 of them are observed by PMUs. This condition is not always true with the constraint expressed by (4.9), since it is possible that $y_i > 1$. For example, let $y_{i1} = 2$, $y_{i2} = 0$, $y_{i3} = 0$, and $y_i = 1$, for $i > 4$, the inequality constraint shown by (4.9) still holds but 2 of the n buses are not observed by PMUs. In these cases the PMU placement obtained with the KCL method might fail to make the system fully observable.

Simulations have been conducted in the IEEE 14 Bus Test System to check the correctness of both the proposed method and the KCL based methods. All 2^{14} possible placements of

injection measurements without the presence of other types of conventional measurement are investigated in the simulations. The simulation results are summarised in Table 4-2 and Table 4-3.

Table 4-2: Correct Placement Found

	KCL based method	Proposed method
Correct Solutions Found	96.71%	100%

Table 4-3: Examples of Failed PMU Placements Using the KCL Method

	Injection measurements placed at Buses	PMU placement at Buses
Case 1	3, 11	5, 7, 13
Case 2	3, 5	6, 7, 9
Case 3	2, 11	5, 7, 13

4.5.2 Sub-Optimal Solutions of KCL Based Methods and Observability Analysis Based Methods

The placement given by the KCL based methods might not restore the observability of the network with the minimum number of PMUs. This is shown with an example given below:

Consider a six bus network with the measurement placement shown in Figure 4-4.

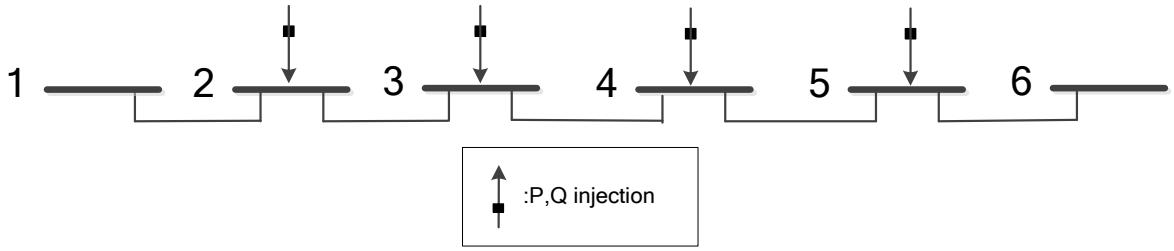

Figure 4-4: Six Bus Network and the Measurement Placement

According to Theorem 1, the network will be fully observable by placing a PMU at either Bus 1, Bus 2, Bus 5 or Bus 6. This can be easily validated by checking the rank of the measurement Jacobian matrix that consists of both the conventional measurements and the added PMU measurements. The constraints of the proposed method are given by:

$$\begin{cases} y_1 \geq 1 \\ y_6 \geq 1 \end{cases} \tag{4.10}$$

In comparison, the KCL based method has the following constraints:

$$\begin{cases} y_1 + y_2 + y_3 \geq 2 \\ y_2 + y_3 + y_4 \geq 2 \\ y_3 + y_4 + y_5 \geq 2 \\ y_4 + y_5 + y_6 \geq 2 \end{cases} \tag{4.11}$$

It can be observed that it is impossible to satisfy every constraint given in (4.11) with only one PMU because a PMU at the given six-bus network can only reach three buses at most. Thus, the KCL based method suggests that two PMUs are placed in the network to restore system observability.

As mentioned in the previous sections, the obvious flaw of the observability analysis based method (algorithm given in Appendix D.2) in finding the optimal PMU placement is that the effects of the irrelevant injection measurements are neglected. In the example in Section 4.2, the constraints of the proposed method in the transformed network and the observability analysis based method are given in (4.12) and (4.13) respectively.

$$\begin{cases} x_1 + x_2 + x_3 + x_5 + x_6 \geq 1 \\ x_2 + x_3 + x_4 + x_6 + x_8 \geq 1 \\ x_1 + x_5 + x_6 \geq 1 \\ x_1 + x_4 + x_5 + x_6 + x_7 + x_8 \geq 1 \\ x_3 + x_7 + x_8 \geq 1 \end{cases} \tag{4.12}$$

$$\begin{cases} x_2 + x_3 + x_4 + x_6 + x_8 \geq 1 \\ x_1 + x_5 + x_6 \geq 1 \end{cases} \tag{4.13}$$

where x_i constitutes the placement decision vector, **x**, $x_i = 1$ means that the i^{th} placement is placed with a PMU, and $x_i = 0$ means that it is not. It can be observed that at least two PMUs are needed to satisfy the five constraints given by (4.12), while only one PMU in Placement 6, which in the original network corresponds to Bus 9, is required to satisfy the constraints given in (4.13).

4.6 Simulation Results

In this section, the results of two simulations are presented, which are conducted for the IEEE 14 and 57 Bus Test Systems [151], respectively. The integer linear programming function in MATLAB is applied to solve the optimisation problem.

4.6.1 IEEE 14 Bus Test System

In this simulation both flow measurements and injection measurements are considered. Details of the measurement placement and the result of PMU placement are included in Table 4-4 and the network topology of the IEEE 14 Bus Test System (data sheets given in Appendix C.1) is shown in Figure 4-1.

It was also discovered in the simulations that the execution time of the proposed method and the existing methods change significantly with different placements of conventional measurements. The conclusion is that the observability analysis based method and the proposed method require less time to identify the optimal placement for networks with fewer observable islands, and vice versa.

Table 4-4: Details of the Simulation in the IEEE 14 Bus Test System

Injection measurement at Bus#	1, 6, 7, 8, 9, 11, 13
Flow measurement From Bus# to Bus#	4-5, 10-11, 13-6
PMU suggested to be placed at Bus# (Proposed method)	4, 13
PMU suggested to be placed at Bus# (KCL based method)	3, 6, 9
PMU suggested to be placed at Bus# (Observability analysis based method)	2, 6, 9

4.6.2 IEEE 57 Bus Test System

The simulation in the IEEE 57 Bus Test System (network diagram given in Appendix C.3) [113] involves 50 conventional measurements, including 40 power flow measurements and 10 injection measurements. The measurement placement and the PMU placement results are given in Table 4-5 and the topology of the IEEE 57 Bus Test System is shown in Figure 4-5:

Table 4-5: Details of the Simulation in the IEEE 57 Bus Test System

Injection measurement at Bus#	23, 26, 31, 33, 34, 36, 38, 48, 55, 57
Flow measurement at Branch #	1, 2, 6, 8, 11, 12, 14, 16, 17, 18, 19, 21, 24, 25, 28, 30, 32, 38, 40, 42, 44, 46, 50, 51, 53, 56, 59, 60, 64, 65, 66, 67, 68, 69, 70, 71, 72, 73, 74, 75
PMU suggested to be placed at Bus# (Proposed method)	12, 15, 19, 24, 29, 33, 34
PMU suggested to be placed at Bus# (KCL based method)	3, 7, 10, 15, 21, 24, 34, 37, 41, 47, 53
PMU suggested to be placed at Bus# (Observability analysis based method)	19, 24, 29, 32, 36, 38, 49, 57

Figure 4-5: IEEE 57 Bus Test System

4.7 Summary

In this chapter, a new method for optimal PMU placement in the presence of conventional measurements is proposed. The proposed method is used to solve the problem of optimal PMU placement for both IEEE 14 and 57 Bus Test Systems using integer linear programming (ILP) implemented in MATLAB. It is shown that the two types of existing method in literature, Kirchoff Law Current (KCL) based methods and observability analysis based methods, are

susceptible to sub-optimal problems, i.e. they might not give the placement that can restore network observability with the least number of PMUs. The sub-optimal problem of the observable analysis based method is solved with a network transformation scheme, while that of the KCL based method is tackled by proposing a global observability criterion which considers the eligible PMU placements that might be neglected by the KCL based methods. The global observability criterion is proved mathematically, and demonstrated with simulations in the IEEE 14 Bus Test System, taking into consideration all possible existing placements of injection measurements. The shortcoming of the proposed method is that it might also omit some eligible PMU placements. Thus, it is possible that in certain cases the proposed method has sub-optimal problems while the KCL based method can obtain the right solution. Nevertheless, the biggest problem of the KCL based method is that it cannot guarantee that the placement solution can restore the network observability. The simulation results show that the KCL based method will obtain erroneous solutions for 3.29% of the possible injection measurement placements in the IEEE 14 Bus Test System, while the proposed method can always guarantee a correct placement solution. This number is quite high since ensuring observability is the substantial task of optimal PMU placement. So, it is concluded that the method proposed in this chapter provides better overall results than the two types of existing methods for optimal PMU placement in the presence of conventional measurements. The future work on this topic would focus on defining the value of the PMUs placing at each of the buses, and thus finding the best solution from all eligible PMU placements.

Chapter 5 Hybrid State Estimation

The existing open literature offers a number of solutions for designing hybrid state estimators (HSEs) and it is not clear which one and why can be considered as more appropriate for practical applications. That is why such an assessment has a particular value, particularly for electrical power industry, keen to design as efficient as possible Energy Management Systems (EMS). So, this chapter provides a comparison of the performance of five different formulations of in terms of their estimation accuracy, execution time and convergence. A comprehensive simulation study was conducted for the IEEE 14 Bus Test System considering all possible PMU placements. The conclusions drawn in this simulation study are then verified using further simulations for the IEEE 118 Bus Test System. Furthermore, the conclusions regarding the estimation accuracies of the HSEs are then verified and explained using mathematical derivations. In addition to this, this chapter also presents research results about the performance of the HSEs in the presence of gross errors and model errors.

5.1 Introduction

The development of Synchronised Measurement Technology (SMT) has received much attention in recent years [152]-[153]. One of the applications in the EMS that directly benefits from SMT is state estimation. This is because the PMU measurements are reported at a rate of 50 to 100 Hz and these measurements (voltage phasors and current phasors) are linearly related to the states [154]. Therefore, provided a power system is completely observable using PMUs, a linear state estimator can solve the system state using a non-iterative procedure [155]-[156]. LSE greatly reduces the calculation load of the online state estimation process. In addition, the high sampling rate of the PMU measurements (100 times faster than that provided by the RTUs) allows real-time monitoring of the system. However, the high cost of installing the PMUs is a barrier to implementing LSE in the near future [157]. In response to this, the concept of hybrid state estimators (HSEs), which use both conventional and synchronised

measurements, began to be developed. An HSE uses existing state estimation resources (e.g. monitoring and communication assets) and new resources (e.g. PMUs and new computational assets) that may one day support LSE. Therefore, it is now more realistic and economically sound to exploit the advantages of both PMUs and the existing SCADA system by using a HSE that may serve as a transition from classical SE to LSE.

Current research into hybrid state estimation can be classified into three categories:

1. New methods for state estimation instead of the weighted least square method,
2. The applications for HSE, and
3. Methods of how to optimally integrating the conventional and synchronised measurements into the HSE.

As mentioned in the Introduction, the alternative methods for state estimation include HSE applying the Taguchi differential evolution algorithm and HSE using Cubature Kalman Filter in a multi-agent system. The HSE has also been applied to enhance the performance of dynamic state estimation, and state estimation in the presence of HVDC links. Finally, in literature there are four different types of methods for integrating the synchronised measurements into a HSE, including the post-processing (PP) HSE, integrated HSE, fusion HSE [158], and distributed HSE [159].

The aim of this chapter is to provide a comprehensive analysis of the different formulations of HSEs, including the estimation accuracy under Gaussian errors, parameter errors and gross errors, as well as the execution time and convergence property.

In the following sections of this chapter, an overview of the HSEs will be presented in Section 5.2, a comparison of HSE performance using exhaustive simulations in the IEEE 14 Bus Test System will be provided in Section 5.3, validation of the results using the IEEE 118 Bus Test System will be given in Section 5.4, mathematical analyses of the results regarding estimation accuracy will be provided in Section 5.5, the effect of gross errors and parameter errors will be

discussed in Section 5.6, and the summary of the research results presented in this chapter will be provided in Section 5.7.

5.2 Overview of Hybrid State Estimators

In this section, the structure and mathematical formulations of the abovementioned HSEs are presented.

5.2.1 Post Processing HSE

A post processing hybrid state estimator is composed of a classical state estimator and a linear state estimator that are executed in sequence. The output of the classical state estimator, the operation of which is unchanged by the HSE, is combined with the available PMU measurements to create a linear state estimator, see in Figure 5-1.

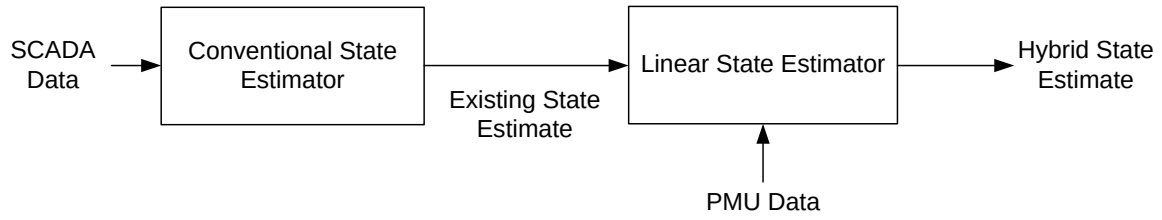

Figure 5-1: Post Processing Hybrid State Estimator

The obvious advantage of a post processing HSE is that it continues to make use of the existing conventional state estimator. This should mean that a post processing HSE should be less complex / expensive to develop than other HSEs, as the LSE required for post processing is less complex than the new estimators required by integrated HSE. Furthermore, it does not require full observability from synchronised measurements, as a fusion estimator does, nor does it entail a shift away from centralised calculation.

An operational advantage of leaving the conventional state estimator unchanged may be that it reduces the impact of any failures during the initial deployment of any post processing HSE, as the existing state estimate will still be available. However, the use of two stages of estimation

makes the post processing HSE more computationally complex than other HSEs. A disadvantage of using a post processing HSE in the long term is that the conventional state estimator, using measurements from RTUs, must have complete observability of the system. In the short term this will not be an issue, as the existing conventional state estimator will already have complete observability with a significant degree of redundancy. However, in the long term, as RTUs begin to age and fail, this complete observability may no longer be available and PMUs will be unable to compensate for this, as the conventional estimator will be unable to incorporate their measurements directly. Therefore, it may be necessary to invest in new RTUs, at a time when they have become an obsolete technology, to preserve the operation of the HSE until the system is able to gradually undergo the transition to a LSE.

As the classical state estimator has been discussed in Chapter 2, in the remainder of this sub-section, the formulation of a LSE and, how a classical state estimator and a LSE form a post processing HSE, are discussed in detail.

5.2.1.1 Linear State Estimator

If the input to an estimator solely consists of PMU data then the problems of time skew are avoided. The PMU data is time-tagged using the global positioning system (GPS) and updated at a rate that is approximately 100 times faster than that of the remote terminal units (RTUs) used in the existing SCADA system. A linear state estimator (LSE) is so named because of the linear relationship between the measurements and the states. The linearity of the estimator eliminates the need for iterations. It will be shown in the later part of this section that the estimation of LSE is only a single step matrix multiplication, although this step does depend on the results of some previous off-line calculations.

The equations for a LSE will now be given, with reference to the pi equivalent circuit shown in Figure 5-2 [1], [160]-[162].

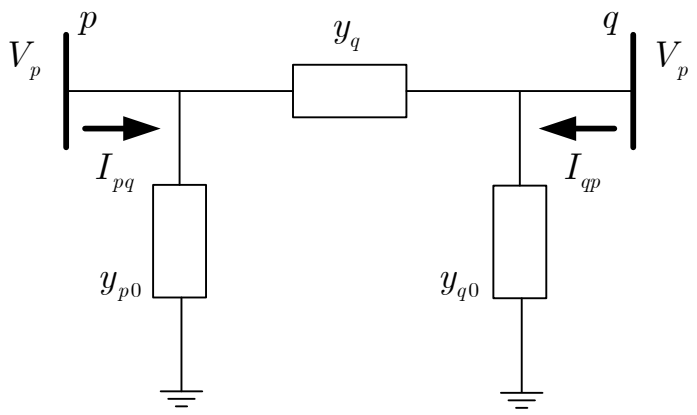

Figure 5-2: Pi Equivalent Circuit

The linear relationship between the voltage and current measurements and the states are given as:

$$\begin{bmatrix} V_p \\ V_q \\ I_{pq} \\ I_{qp} \end{bmatrix} = \begin{bmatrix} 1 & 0 \\ 0 & 1 \\ y_{pq} + y_{p0} & -y_{pq} \\ -y_{pq} & y_{pq} + y_{q0} \end{bmatrix} \begin{bmatrix} V_p \\ V_q \end{bmatrix} \tag{5.1}$$

Define the incident matrix, $\mathbf{A}$, whose elements are 1 for the transmitting bus of a current, -1 for the receiving bus of a current, an 0 for unrelated buses. In the case shown by Figure 5-2 the incident matrix $\mathbf{A} = \begin{bmatrix} 1 & -1 \\ -1 & 1 \end{bmatrix}$. Define two vectors: the admittance vector, **y**, whose elements are the admittance that the currents are incident to; and the shunt admittance vector, $\mathbf{y_s}$, whose elements are the shunt admittance that the buses are incident to. Here $\mathbf{y} = \begin{bmatrix} y_{pq} & y_{pq} \end{bmatrix}^T$ and $\mathbf{y}_s = \begin{bmatrix} y_{p0} & y_{q0} \end{bmatrix}^T$. Now, define $\mathbf{z} = \begin{bmatrix} V_p & V_q & I_{pq} & I_{qp} \end{bmatrix}^T$ as the measurement vector and $\mathbf{x} = \begin{bmatrix} V_p & V_q \end{bmatrix}^T$ as the states. From this, the following relationship can be discovered:

$$\mathbf{z} = \begin{bmatrix} \mathbf{I} \\ \mathbf{yA} + \mathbf{y}_s \end{bmatrix} \mathbf{x} \tag{5.2}$$

where **I** is the identity matrix. Since any complex electric circuit can be regarded as an assembly of many pi equivalent circuits, (5.2) is deduced from this simple pi equivalent circuit and can be extended for any power network without changing its matrix form. The only difference is that some voltage measurements might be missing, since not all buses will have their voltage phasors directly measured. In this case, matrix **II**, an identity matrix from which rows corresponding to missing bus voltages are removed, is used instead of **I**. Define $\mathbf{B}=\begin{bmatrix}\mathbf{II}\\ \mathbf{yA}+\mathbf{y}_s\end{bmatrix}$ and the linear equation set is shown in (5.3):

$$\mathbf{z}=\mathbf{Bx} \tag{5.3}$$

Equation (5.3) is also a set of over-determined equations. Similar to the classical state estimator, the estimate of the states can be obtained using the WLS method as given by (5.4):

$$\hat{\mathbf{x}}=\left(\mathbf{B}^T\mathbf{R}^{-1}\mathbf{B}\right)^{-1}\mathbf{B}^T\mathbf{R}^{-1}\mathbf{z}=\mathbf{Mz} \tag{5.4}$$

Since the placement of measurement units is fixed at the time of the state estimate, the matrix $\mathbf{M}$ can be calculated off-line and saved as a constant for calculating the states directly in the later state estimations if the topology of the system does not change.

The variance of the magnitudes and angles of the voltages and the magnitudes and angles of the currents are usually given separately for classical state estimators. However, the states are all in rectangular form for the linear estimator. So, a problem is faced when representing the variance of the measurements in the LSE in a compatible way. This can be overcome by defining an area in the complex number space that is based on the standard deviations of the magnitude and angle of the measurements, as shown in Figure 5-3.

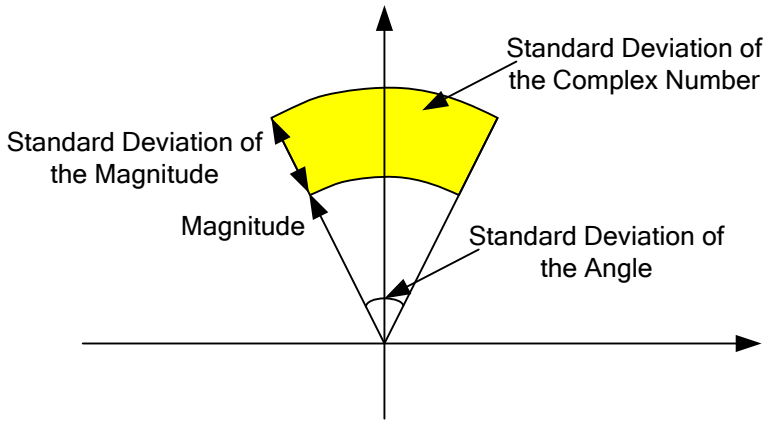

Figure 5-3: Standard Deviation of a Complex Number

According to Figure 5-3, the standard deviation of a complex voltage is defined as: $\sigma_C = 2\sigma_a\left(V_m + \sigma_m\right)^2 - 2\sigma_a\left(V_m - \sigma_m\right)^2 = 8V_m\sigma_a\sigma_m$. Similarly, the standard deviation of a complex current is defined as: $\sigma_C = 8I_m\sigma_a\sigma_m$. Because the variances are only used for weightings, dividing them by a common factor does not affect the final estimate. So, the variance of the complex voltages and currents are as given in (5.5) and (5.6):

$$\sigma_C^2 = V_m^2\sigma_a^2\sigma_m^2 \tag{5.5}$$

$$\sigma_C^2 = I_m^2\sigma_a^2\sigma_m^2 \tag{5.6}$$

5.2.1.2 Integration of Classical SE and Linear SE

A post-processing HSE uses the output of a classical SE and PMU data as the input to a LSE. However, whilst the LSE uses a rectangular form to describe the complex voltages, both the PMUs and classical SE use a polar form. Therefore, the measurements from the PMUs and the output of the classical SE must be transformed from polar form into rectangular form before they can be used by the LSE. The variance of the voltage magnitudes and angles are given by (5.7):

$$\mathbf{P} = \mathbf{G}^{-1} = \left(\mathbf{H}^{\mathbf{T}}\mathbf{R}^{-1}\mathbf{H}\right)^{-1} \tag{5.7}$$

Assuming that there is no correlation between these pseudo voltage measurements, the off-diagonal elements are all replaced by 0 and the diagonal elements of $\mathbf{P}$ are the variance of the voltage magnitudes and angles of all buses in the system. Combining this with (5.5) allows the variances of the complex voltages to be obtained. These variances of the pseudo voltages are then combined with those of the PMU measurements to construct a new variance matrix, $\mathbf{P}'$.

Once transformed, the pseudo voltage measurements from the classical SE and the voltage and current phasor measurements from the PMUs are combined together to form the input of the LSE. The measurement-to-state equation for the LSE in a post processing HSE is given in (5.8):

$$\mathbf{z}' = \begin{bmatrix} \mathbf{I} \\ \mathbf{II} \\ \mathbf{yA} + \mathbf{y_s} \end{bmatrix} \mathbf{x} = \mathbf{B}'\mathbf{x} \tag{5.8}$$

The final estimation is given by (5.9):

$$\hat{\mathbf{x}}' = \left(\mathbf{B}'^{T}\,\mathbf{P}'^{-1}\mathbf{B}'\right)^{-1}\mathbf{B}'^{T}\,\mathbf{P}'^{-1}\mathbf{z} = \mathbf{M}'\mathbf{z}' \tag{5.9}$$

5.2.2 Challenge of Including Current Phasor Measurements

The various forms of integrated HSE described in the following section were all developed in an attempt to find the best way to address the challenge of including the phasor measurements of current into the HSE formulation. The inclusion of these current phasor measurements into the problem formulation is challenging because the partial derivatives of polar form variables (i.e. vector variables defined by a magnitude and angle $\bar{I} = I\angle\varphi$) are vulnerable to singular points, see Figure 5-4 and Figure 5-7. These partial derivatives form the elements of the Jacobian matrix **H** and, as such, are integral to ensuring the proper behaviour of the state estimator. If singular points appear in the Jacobian matrix then the convergence and accuracy of the state estimator will be jeopardised. In contrast, if the current phasors are expressed in rectangular form then no singular points will appear, see Figure 5-8 – Figure 5-11.

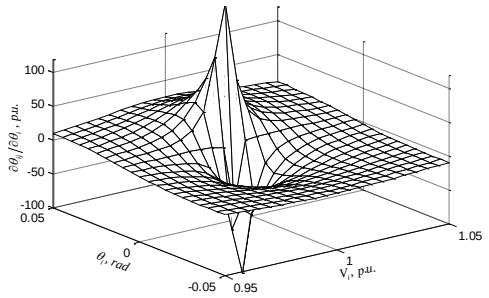

Figure 5-4: Variation of Jacobian element $\partial\,\theta_{ij}/\partial\,\theta_i$ with respect to small changes of θ_i and V_i

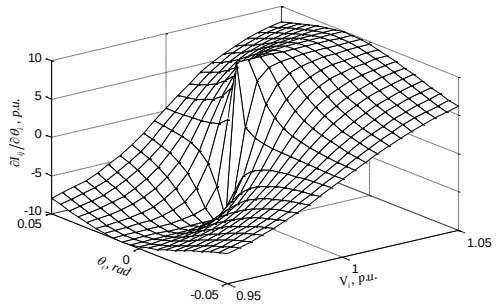

Figure 5-5: Variation of Jacobian element $\partial\,I_{ij}/\partial\,\theta_i$ with respect to small changes of θ_i and V_i

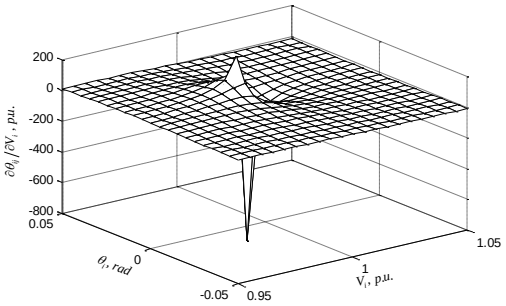

Figure 5-6: Variation of Jacobian element $\partial\,\theta_{ij}/\partial\,V_i$ with respect to small changes of θ_i and V_i

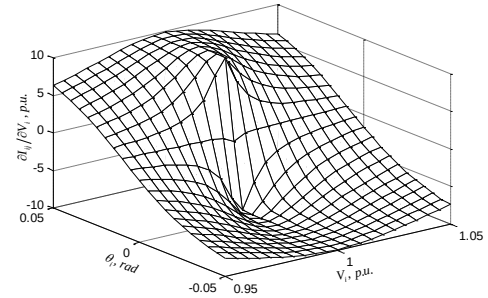

Figure 5-7: Variation of Jacobian element $\partial\,I_{ij}/\partial\,V_i$ with respect to small changes of θ_i and V_i

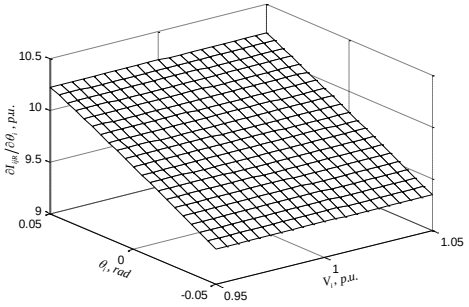

Figure 5-8: Variation of Jacobian element $\partial\,I_{ijR}/\partial\,\theta_i$ with respect to small changes of θ_i and V_i

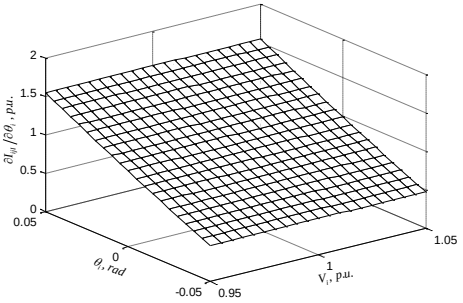

Figure 5-9: Variation of Jacobian element $\partial\,I_{ijI}/\partial\,\theta_i$ with respect to small changes of θ_i and V_i

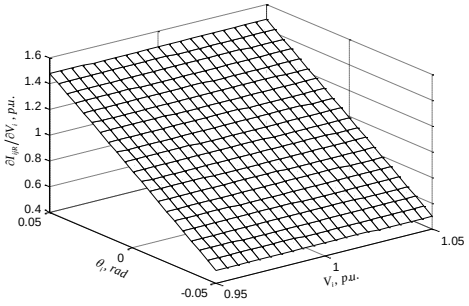

Figure 5-10: Variation of Jacobian Element $\partial\,I_{ijR}/\partial\,V_i$ with Respect to Small Changes of θ_i and V_i

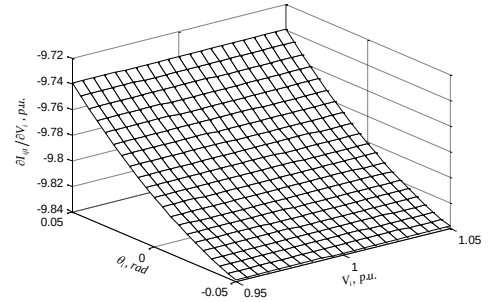

Figure 5-11: Variation of Jacobian Element $\partial\,I_{ijI}/\partial\,V_i$ with Respect to Small Changes of θ_i and V_i

5.2.3 Integrated Hybrid State Estimator

An integrated hybrid state estimator is so called because it combines (integrates) the SCADA data and PMU data into a single, iterative estimation process, as shown in Figure 5-12.

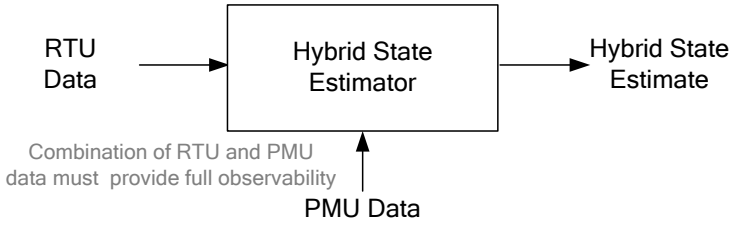

Figure 5-12: Generic Diagram of an Integrated Hybrid State Estimator

The common advantages of all forms of integrated HSE are reduced execution time, as only a single stage of calculation is required and the fact that both PMUs and RTUs can contribute to ensuring the state estimator has full observability. This will avoid the issues of ensuring observability in the long term that are faced by post processing HSEs. However, a common disadvantage is that completely new state estimator software must be developed. This software will be more complex than the new LSE software required by post processing and fusion HSEs and its development may prove quite expensive and may initially entail significant risk due to the introduction into a normal operation of a radically different state estimator.

Furthermore, while a variety of methods have been proposed, the inherent complexity involved in combining dissimilar measurements into a single calculation will mean that the computational complexity of this type of HSE will be relatively high.

The challenge of integrating polar form measurements into the state estimation procedure has resulted in a variety of integrated HSEs being proposed, each of which attempts to address this challenge in a different way. They exist in two groups: those methods that transform the current measurements into another form of measurement (e.g. rectangular current, power flow and voltage) or those that change the formulation of the HSE to accommodate the current phasors in their polar form. These variations are:

- Rectangular Current (RC)
- Pseudo Flow (PF)
- Pseudo Voltage (PV)
- Constrained Formulation (CF)

5.2.4 Rectangular Current HSE

A simple idea for integrating the current measurements into the estimation procedure is to transform them from their original polar form into a rectangular form, which can be expressed alongside the states (voltage magnitudes and angles) in very simple mathematical expressions.

A generalised formulation of the measurement vector, $\mathbf{z}$, including the injection measurements and flow measurements from SCADA and the voltage and current measurements from PMUs is:

$$\mathbf{z} = \begin{bmatrix} \mathbf{P}_{flow}^T & \mathbf{Q}_{flow}^T & \mathbf{P}_{inj}^T & \mathbf{Q}_{inj}^T & \boldsymbol{\theta}_{Vpmu}^T & \mathbf{V}_{Vpmu}^T & \mathbf{I}_{real}^T & \mathbf{I}_{imag}^T \end{bmatrix}^T \tag{5.10}$$

where the state vector, $\mathbf{x}$, is identical to the one used for classical state estimation. The transformation of the RC HSE can be expressed as:

$$I_{ik\,\mathrm{Re}al} = I_{ik}\cos\theta_{Iik} \tag{5.11}$$

$$I_{ik\,\mathrm{Im}ag} = I_{ik}\sin\theta_{Iik} \tag{5.12}$$

The relationship between the currents and the system states is given by (5.13) and (5.14):

$$I_{ij\,\mathrm{Re}al} = g_{ij}\left(V_i\cos\theta_i - V_j\cos\theta_j\right) - b_{ij}\left(V_i\sin\theta_i - V_j\sin\theta_j\right) - b_{si}V_i\sin\theta_i + g_{si}V_i\cos\theta_i \tag{5.13}$$

$$I_{ij\,\mathrm{Im}ag} = g_{ij}\left(V_i\sin\theta_i - V_j\sin\theta_j\right) + b_{ij}\left(V_i\cos\theta_i - V_j\cos\theta_j\right) + b_{si}V_i\cos\theta_i + g_{si}V_i\sin\theta_i \tag{5.14}$$

The corresponding Jacobian Matrix elements are given in Table 5-1.

Table 5-1: Elements of Jacobian Matrix corresponding to rectangular currents

$\frac{\partial I_{\text{ijReal}}}{\partial \theta_{\text{i}}} = -\left(g_{ij} V_i \sin\theta_i + b_{ij} V_i \cos\theta_i + b_{si} V_i \cos\theta_i + g_{si} V_i \sin\theta_i \right)$	
$\frac{\partial I_{\text{ijReal}}}{\partial V_{\text{i}}} = g_{ij} \cos\theta_i - b_{ij} \sin\theta_i - b_{si} \sin\theta_i + g_{si} \cos\theta_i$	
$\frac{\partial I_{\text{ijReal}}}{\partial \theta_{\text{j}}} = g_{ij} V_j \sin\theta_j + b_{ij} V_j \cos\theta_j$	$\frac{\partial I_{\text{ijReal}}}{\partial V_{\text{j}}} = -g_{ij} \cos\theta_j + b_{ij} \sin\theta_j$
$\frac{\partial I_{\text{ijImag}}}{\partial \theta_{\text{i}}} = g_{ij} V_i \cos\theta_i - b_{ij} V_i \sin\theta_i - b_{si} V_i \sin\theta_i + g_{si} V_i \cos\theta_i$	
$\frac{\partial I_{\text{ijImag}}}{\partial V_{\text{i}}} = g_{ij} \sin\theta_i + b_{ij} \cos\theta_i + b_{si} \cos\theta_i + g_{si} \sin\theta_i$	
$\frac{\partial I_{\text{ijImag}}}{\partial \theta_{\text{j}}} = -g_{ij} V_j \cos\theta_j + b_{ij} V_j \sin\theta_j$	$\frac{\partial I_{\text{ijImag}}}{\partial V_{\text{j}}} = -\left(g_{ij} \sin\theta_j + b_{ij} \cos\theta_j \right)$

5.2.4.1 Propagation of Uncertainty

When a random variable is transformed from one form to another form, or it is a function of other variables, the uncertainty in this variable will be propagated through this transformation. The uncertainty in measurements is often expressed as the variance of these measurements (σ). The variance of the transformed measurements must be calculated because their reciprocals are used as the weightings in WLS and they are usually different from those of the original measurements.

The propagation of uncertainty from polar form to rectangular form is given by:

$$\sigma_{real}^2 = \cos^2\theta \sigma_{mag}^2 + mag^2 \sin^2\theta \sigma_\theta^2 \tag{5.15}$$

$$\sigma_{imag}^2 = \sin^2\theta \sigma_{mag}^2 + mag^2 \cos^2\theta \sigma_\theta^2 \tag{5.16}$$

5.2.5 Pseudo Flow HSE

The Pseudo Flow HSE integrates the current measurements into the HSE formulation by transforming them into pseudo flow measurements. The corresponding measurement vector, **z**, is:

$$\mathbf{z} = \begin{bmatrix} \mathbf{P}_{flow}^T & \mathbf{Q}_{flow}^T & \mathbf{P}_{inj}^T & \mathbf{Q}_{inj}^T & \boldsymbol{\theta}_{pmu}^T & \mathbf{V}_{pmu}^T & \mathbf{P}_{flow,pseudo}^T & \mathbf{Q}_{flow,pseudo}^T \end{bmatrix}^T \tag{5.17}$$

The elements in $\mathbf{h(x)}$ that correspond to the pseudo flow measurements are:

$$P_{ij,pseudo} = V_i I_{ij} \cos\left(\theta_i - \theta_{ij}\right) \tag{5.18}$$

$$Q_{ij,pseudo} = V_i I_{ij} \sin\left(\theta_i - \theta_{ij}\right) \tag{5.19}$$

The Jacobian Matrix elements that correspond to the pseudo flow measurements are calculated in the same way as they are for the conventional flow measurements, which is given in (2.26) - (2.33) .

The calculation of the elements in $\mathbf{h(x)}$ is much simpler, from a direct mathematical point of view, for the pseudo flow integrated HSE than it is for the pseudo voltage HSE. However, the corresponding rows in the Jacobian Matrix of the pseudo flows type are more complicated. In other words, the level of nonlinearity of the Jacobian matrix of the pseudo flows type is higher than that of the pseudo voltage type.

5.2.5.1 Propagation of uncertainty

The propagation of uncertainty from current measurements to pseudo flows measurements is shown in (5.20) and (5.21):

$$\sigma\left(P_{ij,\,pseudo}\right)=\sqrt{\sum_{k=1}^{4}\left[\partial P_{ij,\,pseudo}/\partial\mathbf{p}(k)\right]^2\cdot\left[\sigma\left(\mathbf{p}(k)\right)\right]^2} \tag{5.20}$$

$$\sigma\left(Q_{ij,\,pseudo}\right)=\sqrt{\sum_{k=1}^{4}\left[\partial Q_{ij,\,pseudo}/\partial\mathbf{p}(k)\right]^2\cdot\left[\sigma\left(\mathbf{p}(k)\right)\right]^2} \tag{5.21}$$

where $\mathbf{p}(k)=\begin{bmatrix}V_i & \theta_i & I_{ij} & \theta_{ij}\end{bmatrix}$, $\sigma(\bullet)$ denotes the standard deviation of the variable specified.

5.2.6 Pseudo Voltage HSE

The pseudo voltage type of integrated HSE handles the current measurements by transforming them into pseudo voltage measurements of the adjacent buses. For this HSE, the formulation of the measurement vector, **z**, becomes:

$$\mathbf{z}=\begin{bmatrix}\mathbf{P}_{flow}^T & \mathbf{Q}_{flow}^T & \mathbf{P}_{inj}^T & \mathbf{Q}_{inj}^T & \boldsymbol{\theta}_{pmu}^T & \mathbf{V}_{pmu}^T & \boldsymbol{\theta}_{pseudo}^T & \mathbf{V}_{pseudo}^T\end{bmatrix}^T \tag{5.22}$$

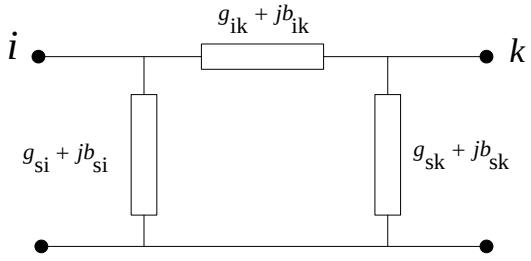

Figure 5-13: Pi Equivalent Circuit of a Transmission Line

With reference to Figure 5-13, assuming that Bus i has a PMU installed and Bus k does not, the voltage magnitude and angle of Bus i are known, as it can be assumed they are directly measured by the PMU. Although Bus k is not directly monitored by the PMU, its voltage magnitude and angle can be calculated using the voltage phasor from Bus i, the current phasor between the two buses, and the line parameters shown in Figure 5-13 using this expression:

$$\bar{V}_k=\frac{\bar{V}_i(g_{si}+jb_{si}+g_{ik}+jb_{ik})-\bar{I}_{ik}}{g_{ik}+jb_{ik}} \tag{5.23}$$

where $\bar{V}_{\mathrm{i}}$ and $\bar{V}_{\mathrm{k}}$ are the voltage phasors of Bus i and Bus k; $\bar{I}_{\mathrm{ik}}$ is the current phasor between the two buses measured by the PMU at Bus i; $(g_{si} + jb_{si})$ is the shunt admittance connected at Bus i, and $(g_{ik} + jb_{ik})$ is the admittance of the transmission line from Bus i to Bus k. For simplification of the expressions, three parameters are defined as in (5.24) and (5.25):

$$a + jb = (g_{si} + jb_{si} + g_{ik} + jb_{ik})(g_{ik} - jb_{ik}) \tag{5.24}$$

$$c = g_{ik}^2 + b_{ik}^2 \tag{5.25}$$

Equation (5.24) is separated into the real part and imaginary part, which are expressed in (5.26) and (5.27):

$$a = g_{ik}(g_{si} + g_{ik}) + b_{ik}(b_{si} + b_{ik}) \tag{5.26}$$

$$b = g_{ik}(b_{si} + b_{ik}) - b_{ik}(g_{si} + g_{ik}) \tag{5.27}$$

V_{kR} and V_{kI} can then be calculated by:

$$V_{kR} = (aV_i \cos\theta_i - bV_i \sin\theta_i - g_{ik} I_{ik} \cos\theta_{ik} - b_{ik} I_{ik} \sin\theta_{ik})/c \tag{5.28}$$

$$V_{kI} = (bV_i \cos\theta_i + aV_i \sin\theta_i + b_{ik} I_{ik} \cos\theta_{ik} - g_{ik} I_{ik} \sin\theta_{ik})/c \tag{5.29}$$

The magnitude and angle of $\bar{V}_{\mathrm{k}}$ can be obtained from its real part and imaginary part in rectangular form as is shown in (5.30) and (5.31):

$$V_{k,pseudo} = \sqrt{V_{kR}^2 + V_{kI}^2} \tag{5.30}$$

$$\theta_{k,pseudo} = \tan^{-1}\left(\frac{V_{kI}}{V_{kR}}\right) \tag{5.31}$$

Although it seems quite complicated to calculate the pseudo voltages, this method has great advantages during the iterative procedure because the corresponding Jacobian elements of the pseudo voltages are very simple, as shown in Table 5-2.

Table 5-2: Elements of the Jacobian Matrix Corresponding to the Pseudo Voltages

$\frac{\partial V_k}{\partial V_k} = 1$	$\frac{\partial V_k}{\partial V_i} = 0, i \neq k$	$\frac{\partial V_k}{\partial \theta_i} = 0$
$\frac{\partial \theta_k}{\partial \theta_k} = 1$	$\frac{\partial \theta_k}{\partial \theta_i} = 0, i \neq k$	$\frac{\partial \theta_k}{\partial V_i} = 0$

5.2.6.1 Propagation of Uncertainty

The equations for the propagation of uncertainty for the PV HSE are:

$$\sigma(V_{kR}) = \sqrt{\sum_{k=1}^{4}\left[\partial V_{kR} / \partial \mathbf{p}(k)\right]^2 \cdot \left[\sigma(\mathbf{p}(k))\right]^2} \tag{5.32}$$

$$\sigma(V_{\mathrm{kI}}) = \sqrt{\sum_{k=1}^{4}\left[V_{\mathrm{kI}} / \partial \mathbf{p}(k)\right]^2 \cdot \left[\sigma(\mathbf{p}(k))\right]^2} \tag{5.33}$$

where $\mathbf{p}(k) = \begin{bmatrix} V_i & \theta_i & I_{ij} & \theta_{ij} \end{bmatrix}$, $\sigma(\bullet)$ denotes the standard deviation of the variable specified.

5.2.7 Constrained Formulation HSE

The constrained formulation of integrated HSE was proposed in [25]. Unlike the other Integrated HSEs which are described above, and which transform the current measurements into other forms, the constrained formulation integrates them directly into the state vector, **x**, and this compensates for the increase in the number of states by introducing a set of equality constraints. The newly defined state vector is:

$$\mathbf{x}^{new} = [\mathbf{x}, \mathbf{x}^{aux}]^T \tag{5.34}$$

in which,

$$\mathbf{x}^{aux} = [\theta_{ij}, \cdots, \theta_{lk}, I_{ij}, \cdots, I_{lk}]^T \tag{5.35}$$

where:

i,…,*l* are PMU buses

j,…,*k* are buses adjacent to PMU buses.

The auxiliary states cannot only express the current magnitudes and angles directly in polar form but they also participate in the expressions of the constraints and the voltage-current relationship between the adjacent buses. The measurement vector, **z**, and the measurement-to-state function, **h(x)** , are given in (5.36) and (5.37) respectively:

$$\mathbf{z} = \begin{bmatrix} \mathbf{P}_{flow}^T & \mathbf{Q}_{flow}^T & \mathbf{P}_{inj}^T & \mathbf{Q}_{inj}^T & \boldsymbol{\theta}_{Vpmu}^T & \mathbf{V}_{Vpmu}^T & \boldsymbol{\theta}_{Ipmu}^T & \mathbf{V}_{Ipmu}^T \end{bmatrix}^T \tag{5.36}$$

$$\mathbf{h(x)} = \begin{bmatrix} \mathbf{h}_{conv}^T\mathbf{(x)} & \boldsymbol{\theta}^T & \mathbf{V}^T & \boldsymbol{\theta}_I^T & \mathbf{I}^T \end{bmatrix}^T \tag{5.37}$$

where $\boldsymbol{\theta}_{Ipmu}$ and $\mathbf{I}_{pmu}$ are current angles and magnitudes measured by PMUs and $\boldsymbol{\theta}_I$ and $\mathbf{I}$ are defined as the auxiliary state variables as shown in (5.35).

The increase in the number of states requires the same number of additional measurements or additional constraints, or the observability of the estimator will be compromised. Furthermore, although the current measurements can now be expressed directly, adding the current magnitudes and angles into the state vector has caused the current measurements and voltage states to become unrelated. These two problems are solved simultaneously by exploiting the voltage-current relationship between the two adjacent buses whose currents are measured by PMUs. These relationships are expressed as the equality constraints shown in (5.38) and (5.39). Obviously, the number of equality constraints is equal to the number of states. Thus, the problem introduced by the increased number of states is resolved (via an increase in the number of constraints) and these constraints reintroduce the relationship between current measurements and voltage states.

$$V_k - V_{k,pseudo} = 0 \tag{5.38}$$

$$\theta_k - \theta_{k,pseudo} = 0 \tag{5.39}$$

where V_k and θ_k are the voltage state variables corresponding to Bus k. $V_{k,pseudo}$ and $\theta_{k,pseudo}$ are a set of pseudo voltage measurements expressed by the adjacent voltage states and the corresponding current states in the way given by (5.28) to (5.31). These equality constraint equations are combined in a new vector **t**, and the optimisation problem should be subject to the following equality constraint (5.40):

$$\mathbf{t}(\mathbf{x}^{new}) = \mathbf{0} \tag{5.40}$$

5.2.7.1 Propagation of Uncertainty

There is no propagation of uncertainty in the constrained integrated HSE, as there is no transformation of current measurements into other forms or other types of measurements.

5.2.7.2 Constrained State Estimation

Constrained state estimation has been used to deal in the presence of null injection measurements. Null injection measurements are used to describe buses where the power injections are known to be zero, as these buses have no generation or load. Null injection measurements, when correctly identified, are extremely accurate because they are determined rigorously by analysis of the system rather than being measured by equipment. Thus they are always included in state estimation as equality constraints, or the state estimator's robustness will be impaired.

The same method could be applied for the constrained formulation form of integrated HSE described in this section. The optimisation problem (as defined for the classical state estimator) is now subject to a set of equality constraints. Lagrange multipliers are used to express the constraints and the performance index in only one expression:

$$L(\mathbf{x},\boldsymbol{\lambda}) = \frac{1}{2}[\mathbf{z}-\mathbf{h}(\mathbf{x})]^{\mathrm{T}}\mathbf{R}^{-1}[\mathbf{z}-\mathbf{h}(\mathbf{x})] - \boldsymbol{\lambda}^{\mathrm{T}}\mathbf{t}(\mathbf{x}) \tag{5.41}$$

where λ is the Lagrange multiplier vector. The partial derivative of $L(\mathbf{x},\boldsymbol{\lambda})$ with respect to $\mathbf{x}$ and λ can be calculated for the original optimisation problem given by (2.10). The difference in the k^{th} iteration, $\Delta\mathbf{x}^k$ and $\boldsymbol{\lambda}^{k+1}$ is given in (5.42):

$$\begin{bmatrix}\Delta\mathbf{x}^k \\ \boldsymbol{\lambda}^{k+1}\end{bmatrix} = \begin{bmatrix}\mathbf{H}_x^T\mathbf{R}^{-1}\mathbf{H}_x & -\mathbf{T}_x^T \\ \mathbf{T}_x & \mathbf{0}\end{bmatrix}^{-1}\begin{bmatrix}\mathbf{H}_x^T\mathbf{R}^{-1}(\mathbf{z}-\mathbf{h}(\mathbf{x}^k)) \\ -\mathbf{t}(\mathbf{x}^k)\end{bmatrix} \tag{5.42}$$

where $\mathbf{H}_x$ is the derivative of $\mathbf{h}(\mathbf{x})$ with respect to $\mathbf{x}$, and $\mathbf{T}_x$ is the derivative of $\mathbf{t}(\mathbf{x})$ with respect to $\mathbf{x}$. Note that the derivative of $\frac{1}{2}[\mathbf{z}-\mathbf{h}(\mathbf{x})]^{\mathrm{T}}\mathbf{R}^{-1}[\mathbf{z}-\mathbf{h}(\mathbf{x})]$ with respect to λ is $\mathbf{0}$, and the derivative of $\boldsymbol{\lambda}^{\mathrm{T}}\mathbf{t}(\mathbf{x})$ with respect to λ is $\mathbf{t}(\mathbf{x})$.

Combining the performance index in (5.41), the iteration difference given in (5.42) and the variables and functions specified for the original the state estimation problem, allows the states of this constrained problem to be solved.

5.3 Comparison of HSE Performance Using Exhaustive Simulations in the IEEE 14 Bus Test System

This section presents the results of exhaustive simulations in the IEEE 14 Bus Test System that were used to investigate the performance of the different HSEs. Performance is observed through the accuracy of the state estimates, the execution time and convergence for each bus.

5.3.1 Simulation Settings

The simulations test all possible PMU placements (2^{14}=16384 in total) using a fixed redundant set of conventional measurements in the IEEE 14 Bus Test System (data sheets given in Appendix C.1) as illustrated in Figure 5-14. Full redundancy is required to enable all functions of the HSEs, including bad data detection.

In the simulations, random Gaussian errors are included in both conventional and PMU measurements noise, the standard deviation of any error is set to be the value of the measurement times a coefficient factor according to the different types of measurement defined as follows:

- SCADA: P, Q measurements (0.02) and V (0.002)
- PMU: 0.0002 for magnitudes, and 0.01 for angles

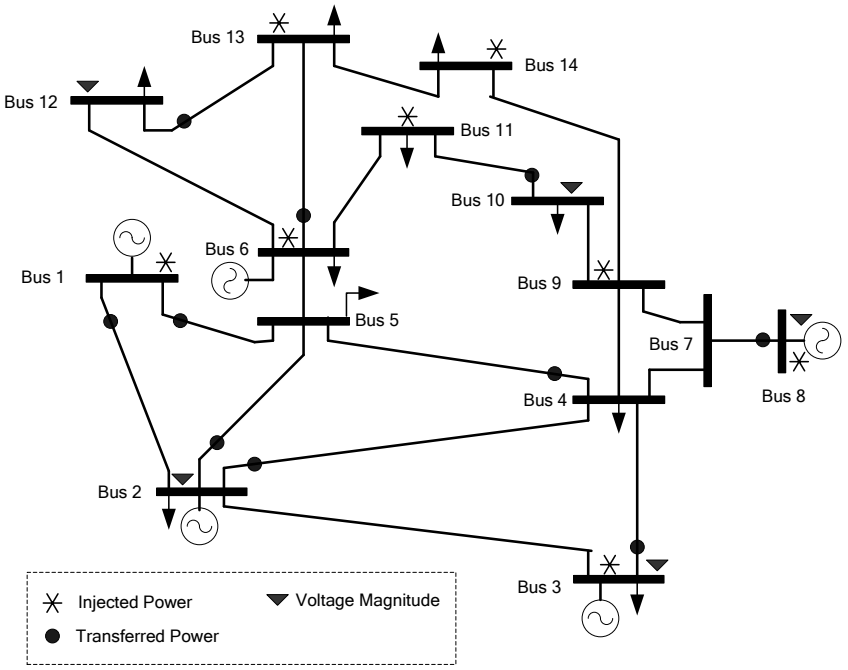

Figure 5-14: IEEE 14 Bus Test System and the Measurement Placement

The HSEs were simulated for 100 Monte Carlo trials for every possible PMU placement, and the average of the absolute values of the errors of the estimates at each bus, the execution time and the condition number are recorded. Here, the condition number is the measurement of HSE convergence, whose definition will be given in Section 5.3.6. Note that the time skew errors exist in the conventional measurements, but not in the PMU measurements due to their synchronisation nature. Thus, the conventional measurements are assigned with errors of larger magnitude compared to the PMU measurements.

5.3.2 Best Accuracy

Having simulated every possible PMU placement for every number of PMUs, it was possible to select the best accuracy that could be achieved by each HSE for each PMU number, where accuracy is described in terms of the variance of all of the states as defined in (5.43) and the lower the variance the better the accuracy. This best accuracy for each HSE is plotted in Figure 5-15.

$$\sigma^2 = \frac{\sum_{i=1}^{n}\left[\left(\hat{V}_i - V_i^{true}\right)^2 + \left(\hat{\theta}_i - \theta_i^{true}\right)^2\right]}{2n-1} \tag{5.43}$$

where $\hat{V}_i$ and V_i^{true} are the estimate and the true value of the magnitude of the voltage at Bus *i*, respectively, $\hat{\theta}_i$ and θ_i^{true} are the estimate and the true value of the angle of the voltage at Bus *i*, respectively, and *n* is the number of buses in the network.

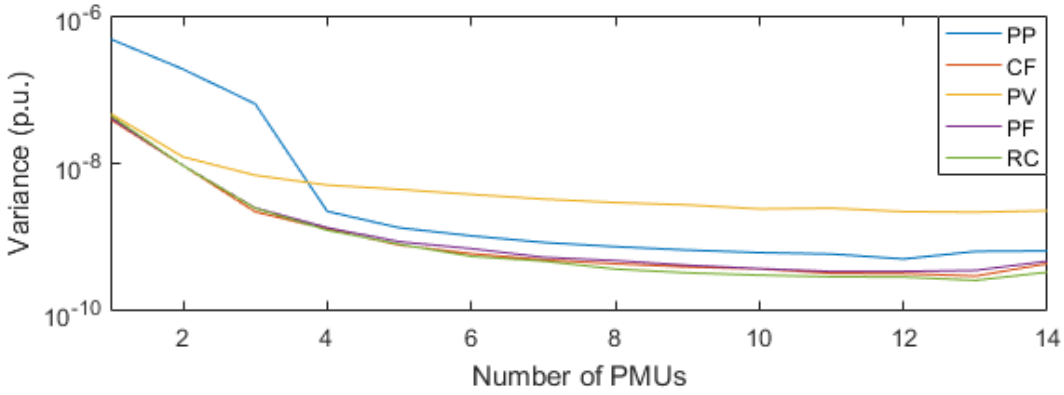

Figure 5-15: Best Accuracy for each HSE as the PMU number is varied

Figure 5-15 shows that the Rectangular Current HSE (RC) offers the best accuracy, but it is only marginally better than the Constrained Formulation HSE (CF), which is in turn marginally better than the Pseudo Flow HSE (PF). However, the Pseudo Voltage HSE (PV) is noticeably less accurate and as the PMU number increases it becomes less accurate than the Post Processing HSE (PP).

In general, Figure 5-15 shows that, as the number of PMUs is increased, the accuracy of the HSEs increases. This increase is characterised by a knee point, where the first PMU leads to a significant increase in accuracy over the classical state estimator (which has an accuracy of approximately 10^{-5}) and after this the improvement offered by each PMU is reduced, until approximately four PMUs where the increase becomes negligible. This knee point exists because the accuracy of the HSEs when estimating the state of a bus is improved if the bus is observed by a PMU (i.e. if a PMU is placed at that bus or a neighbouring bus) and the minimum number of PMUs required to make the system fully observable is four. After four

PMUs have been placed and the system is fully observable for the best case placement, any further PMU can obviously not make more buses observed and so offers a reduced benefit. This knee point is most distinct for the post processing HSE, as after four PMUs have been placed its accuracy approaches that of the RC, CF, PF HSEs and it outperforms the PV HSE. While the first four PMUs offer a significant improvement in accuracy, as they make new buses PMU observable, the 5^{th} to 7^{th} PMUs to be added offer noticeably more benefit than the 8^{th} to 14^{th} PMUs to be added. This is because these PMUs enable buses to be observed by two PMUs, which helps to mitigate the impact of the Gaussian noise and, given the random nature of this noise, it is unlikely that two measurements will both contain the same random error, so making the bus observable by a third PMU offers little benefit. Based on this, the benefit offered by a PMU can be separated into three stages:

1. Significant benefit – until full observability is achieved;
2. Marginal benefit – until all buses are observed by two PMUs (redundant observability);
3. Minimal benefit.

The results show that, in terms of accuracy in the presence of Gaussian noise, the PV HSE make poorer use of the PMU measurements than the other integrated HSEs when the number of PMUs increases. This is because the PV HSE cannot use the current phasor measurements and the equations derived from the network structure to increase the estimation accuracy as the other HSEs. This limitation of the PV HSE results in only a small loss of performance of one to two PMUs, but as the PMU number increases the difference in accuracy increases quickly, as the other HSEs are able to use combinations of other measurements to improve their accuracy (compensating for the Gaussian errors in the measurements) while the PV HSE must still depend on the accuracy of individual measurements. Note that eventually the difference in performance stops increasing as the PMU number does (at the 7^{th} PMU), because little to no new information is added by the further PMUs.

5.3.3 HSE Performance for each Bus for Different Placements

This section uses the error in the bus angle estimates for different PMU placements to demonstrate the impact on accuracy of a bus being observable using a PMU and why the PP HSE is the most sensitive to this observability. The placements considered are:

- Bus 2 and Bus 9, and thus all buses are observed by PMUs except for Buses 6, 8 11 and 12,
- Buses 2, 6 and 9 making all buses except Bus 8 observed by PMUs, and
- Buses 2, 6, 7 and 9, which ensures full network observability from PMUs.

Figure 5-16, Figure 5-17 and Figure 5-18 show the bus voltage angle residues for each HSE for these placements. Note that these figures include two different approaches for implementing the PV HSE (i.e. direct derivation and unscented transform); these were included to verify the conclusion that the PV error arises from the fundamental properties of its measurement Jacobian and not the implementation used.

It can be observed that the estimation accuracy of all of the states (the same results can be achieved for the voltage magnitudes) are improved for integrated HSEs even for those buses that are not directly observed by PMUs. For the PP HSE the residuals of the states of the buses observed by PMUs are almost as small as those of the integrated HSEs, but the residuals of the states of the buses not observed by PMUs are much larger. In addition, it can be seen that when all buses are observable with PMUs the residuals of the PP HSE are smaller than those of the PV integrated HSE but larger than those of the other integrated HSEs.

This behaviour causes the average estimation accuracy of the PP HSE to be worse than the integrated HSEs, when the number of PMUs is small, due to the very large residuals of the buses not observed by PMUs. However, as the number of buses observed by PMUs increases, the average accuracy of the PP HSE will exceed that of the PV integrated HSE and approach that of the other integrated HSEs, as the likelihood of full system observability by PMUs increases as the number of PMUs is increased. This property of the PP HSE means that it is more sensitive to the placement than the integrated HSEs.

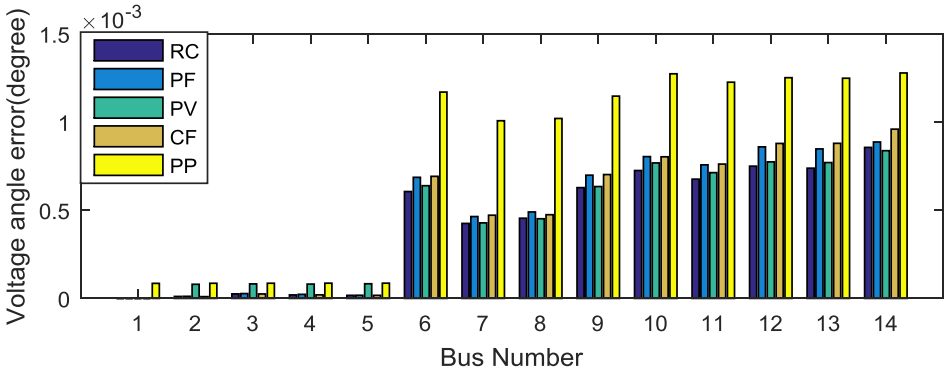

Figure 5-16: Voltage Angle Residuals of the HSEs with PMUs at Bus 2 and Bus 9. All buses are observed by PMUs except for Buses 6, 8, 11, 12 and 13

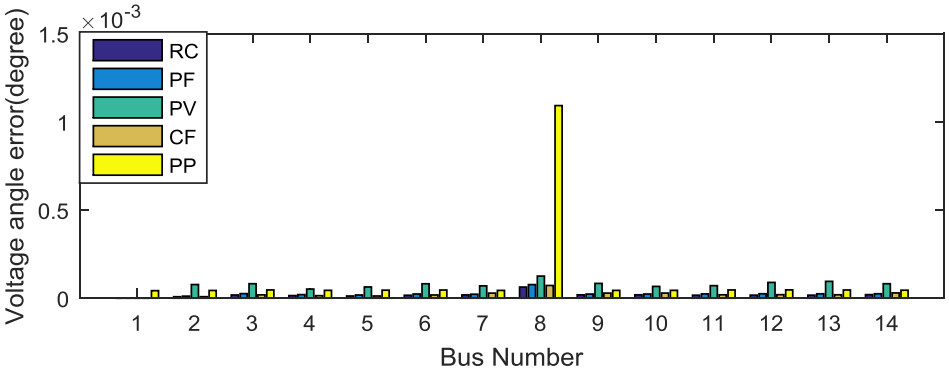

Figure 5-17: Voltage Angle Residuals of the HSEs with the PMUs Placed at Bus 2, 6 and 9. All buses are observed by PMUs except for Bus 8

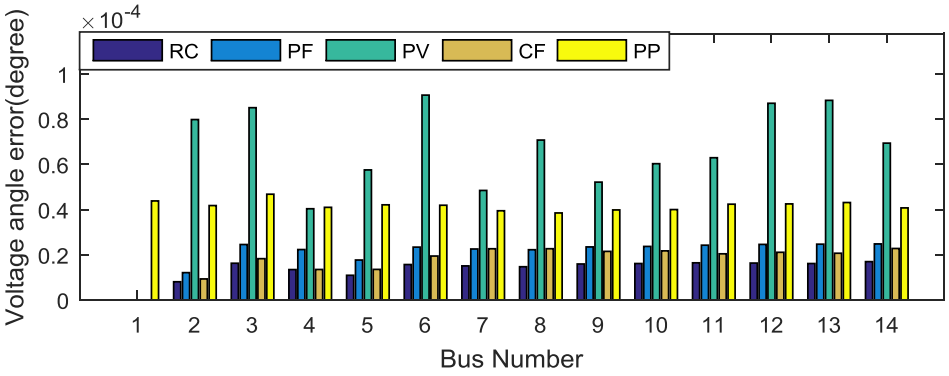

Figure 5-18: Voltage Angle Residuals of the HSEs with the PMUs Placed at Bus 2, 6, 7 and 9. All buses are observed by PMUs

5.3.4 Distribution of Error with PMU Placement

The best accuracy that was presented in Section 5.3.2 is useful for understanding the performance of the HSEs when they have the optimal PMU placement, but does not give any insight into their performance of a sub-optimal or even random PMU placement.

In this section histograms are used to study the distribution of the HSE accuracy when four, seven and twelve PMUs are placed in the system. These results are shown in Figure 5-19 for all five HSEs.

These histograms demonstrate that, in addition to being the most accurate HSE, the RC HSE offers the most reliable accuracy for a large number of PMUs. Furthermore, these distributions show significantly poorer accuracy of the PV HSE and its less efficient use of the PMU data. Note that the performance of the PV HSE for twelve PMUs is lower than the performance of the other integrated HSEs for the majority of the seven PMU placements. This can be interpreted as follows: a PP HSE equipped with the optimal placement of twelve PMUs will usually perform more poorly than other types of integrated HSE that has a random placement of seven PMUs.

The wide variation seen for four PMUs further demonstrates the importance of the accuracy improvement offered by HSEs when a bus is observed by a PMU. The best cases for four PMUs are fully observable, while the worst cases have as few as five of the fourteen buses observed by PMUs. This is further supported by the ‘tail’ observed in the placements for seven PMUs, as many types of seven-PMU placements do not offer full observability. The HSE performance becomes more reliable as the number of PMUs is increased to twelve. This means that optimal placement becomes less relevant as the number of PMUs increases, which is not surprising. However, for smaller PMU numbers optimal placement can improve performance by two orders of magnitude.

Furthermore, the large split in the distribution of seven PMU cases for the PP HSE is due to the issue of observability. The PP HSE requires that a bus be observed by a PMU to offer a

significant improvement in the estimation of the state of that bus. The nature of Bus 8 (only connected to Bus 7) in the IEEE 14 Bus Test System means that only placements that include either Bus 7 or Bus 8 can offer observability of Bus 8. This means that any placement that does not include Bus 7 or Bus 8 will have a poor average variance for the PP HSE. This also explains the very poor performance seen for a 12 PMU case for the PP HSE (these isolated points are also observed for the integrated HSEs but they are far less severe). Figure 5-20 shows these outlying cases more clearly. The impact of this is less severe for the integrated HSEs due to their ability to improve the state estimation at buses that are not directly observed. Indeed, this property of the PP HSE makes it particularly poorly suited for state estimation in systems with significant radial sections.

PMU placements that observe the same number of buses do not always have the same performance. This is due to the benefits of multiple PMUs observing the same bus. As discussed in previous sections, this significantly reduces the impact of the Gaussian noise that is added to the measurement. This contributes to the particularly wide distribution seen for four PMUS. The variation of placement is less significant for the PV HSE, which offers the most reliable performance for a given number of PMUs. The PV HSE is less sensitive to the placement, as it does not use the virtual measurements effectively. The reasons and the definition of the virtual measurements will be discussed in Section 5.5. So, the performance will vary less for placements with the same observable buses for the PV HSE than they will for the other integrated HSEs.

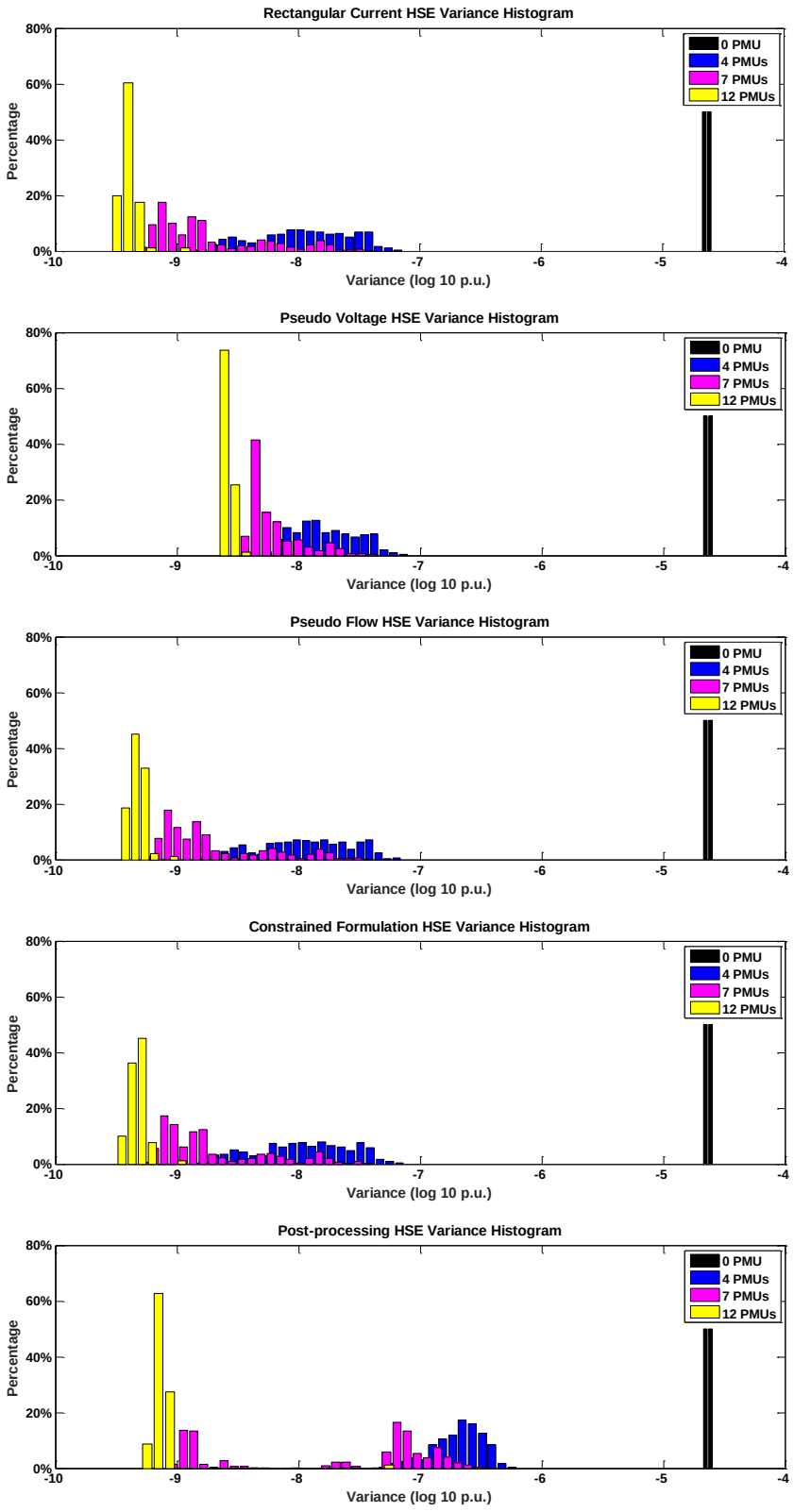

Figure 5-19: Histogram of Variation in HSE Accuracy for Different PMU Numbers and All Placements

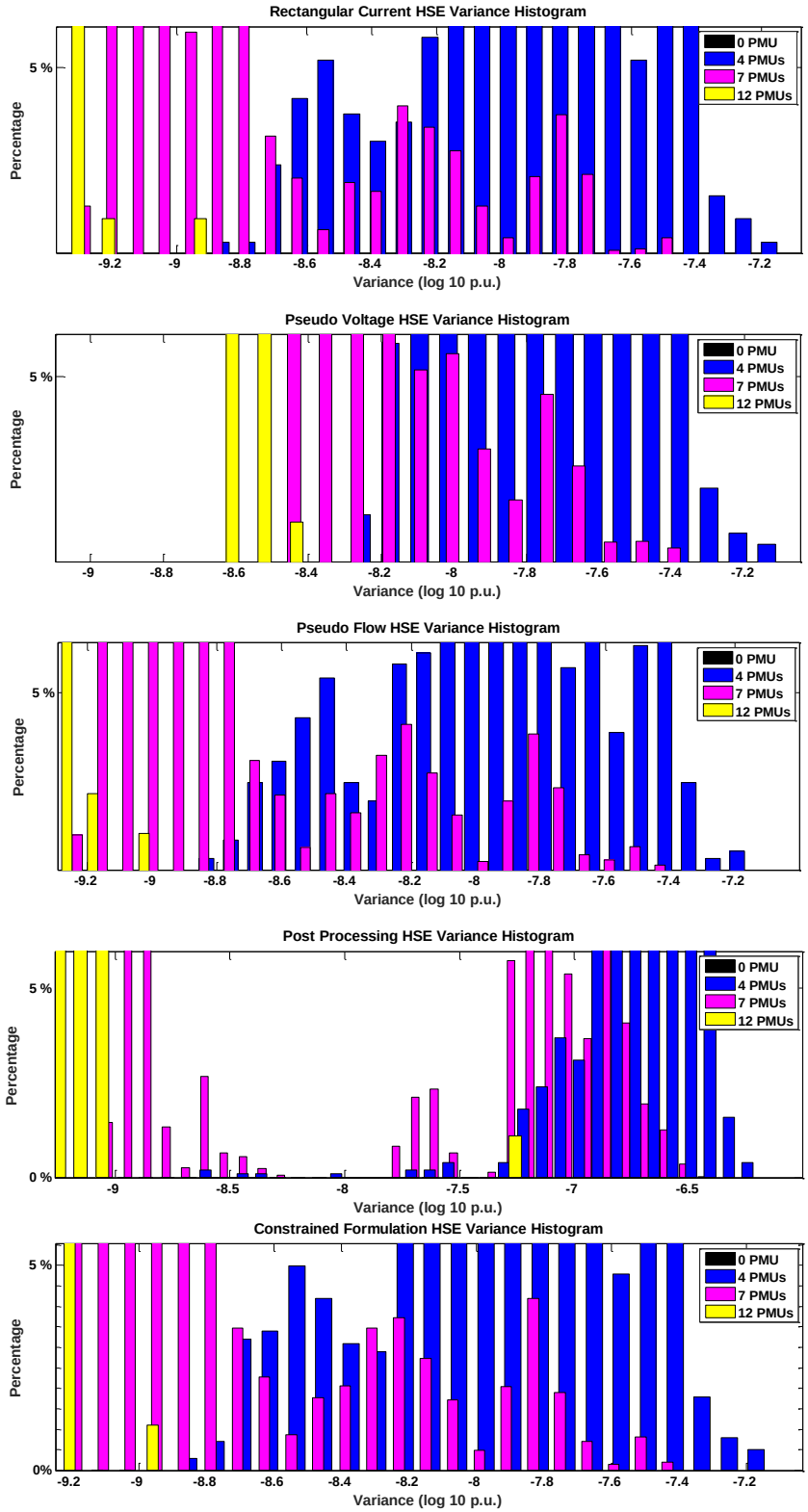

Figure 5-20: Focused View of Histograms of Variation in HSE Accuracy for Different PMU Placements. The Outliers are Placements with High/Low Numbers of Observable Buses.

5.3.5 Execution Time

The convergence of an HSE is described in two aspects: the overall execution time and the possibility to encounter divergence. The execution time must be considered when evaluating the performance of an HSE since a long execution time would mean that the HSE is not applicable in real practice. The other aspect will be quantified using the condition number discussed in the next sub-section.

In the case of the PP HSE, it can be observed that the convergence time does not vary with the number of PMUs. This is unsurprising as the classical SE in the PP HSE will not be affected in any way by the PMU number and the LSE does not use iterations, so no matrix inversion is required.

As shown in Figure 5-21, for all four integrated HSEs the average convergence time increases as more PMUs are added. This is because the gain matrix becomes less sparse when more PMU measurements are integrated into the HSE and, as such, the length of time required for executing the required matrix inversion and multiplication becomes greater. However, the CF integrated HSE, which uses an augmented state vector with current phasors, is the most sensitive to the increase in the number of PMUs because the size of its state vector increases with the number of PMU measurements. Furthermore, the PV HSE shows a more significant increase in execution time than the other integrated HSEs.

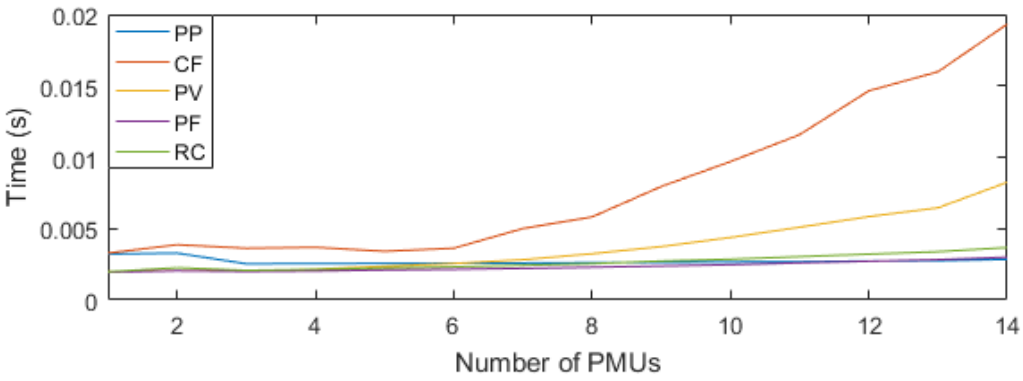

Figure 5-21: Average Convergence Time as PMU Number is Increased

5.3.6 Condition Number

Apart from the execution time, the convergence of an HSE can also be described by the HSE's possibility to diverge, which is quantified by the condition number of the gain matrix in this PhD. A high condition number of the gain matrix indicates that the gain matrix is ill-conditioned, and the HSE is likely to diverge. If a matrix, **A**, is non-singular, its condition number is defined by (5.44). Since the gain matrix is always normal due to its definition, the definition can also be expressed as given in (5.45).

$$\mathrm{cond}(\mathbf{A}) = \|\mathbf{A}\|\|\mathbf{A}^{-1}\| \tag{5.44}$$

$$\mathrm{cond}(\mathbf{A}) = |\lambda_{A\max}| / |\lambda_{A\min}| \tag{5.45}$$

In the exhaustive simulation in the IEEE 14 Bus Test System, the condition numbers for each PMU placement and each HSE are recorded, which are expressed in log 10 scale (CNlog10) in the plot against the number of PMUs (Figure 5-22). The figure shows that CNlog10 of the PP, PF and RC HSE are around the value of 5, while CNlog10 of the PV HSE decreases from 5 to about 1 when the number of PMUs increases. Thus, the PP, PF, RC and PV HSE are not likely to experience divergence due to bad data. However, the CNlog10 is significantly larger than the other HSEs, which is about 13 for 0 PMUs and increases to about 20 when all 14 buses are placed with PMUs. This might also be explained by the augmented state vector of the CF HSE, which increases the size of the gain matrix where the ratio of the largest and least eigenvalues becomes larger. Note that for PP HSE, only CNlog10 of the CSE part is presented in the figure since the LSE does not use iterations to estimate the states.

In general, in spite of the CF HSE that uses augmented state vector, the PMUs improve the estimation accuracy of the HSEs at the cost of less estimation stability: the RC and PF HSE have better estimation accuracy but less resistance to bad data, the PV HSE has less accurate estimate but a smaller condition number.

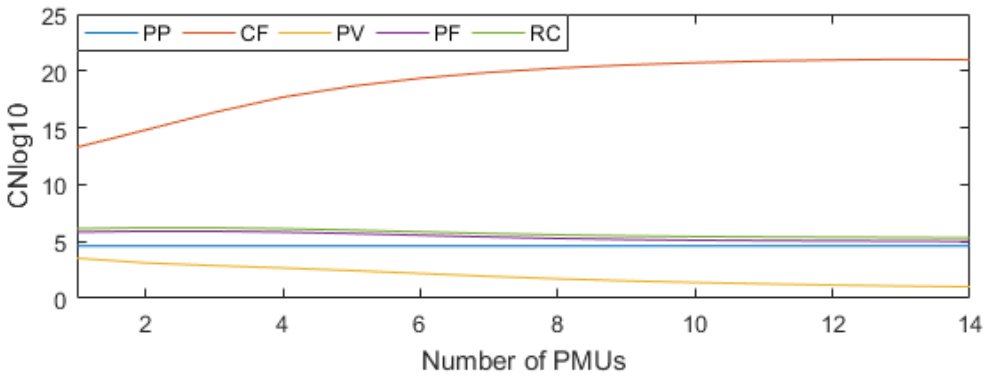

Figure 5-22: Condition Number in Log 10 Scale as the PMU Number is Increased

5.4 Validation of the Results Using IEEE 118 Bus Test System

In this section, the conclusions drawn for the best accuracy, execution time and condition number in the previous section are validated using the IEEE 118 Bus Test System [113].

5.4.1 Simulation Settings

With reference to the topology of the IEEE 118 Bus Test System as shown in Figure 5-23, the simulation presented in this section also uses a fixed set of conventional measurements as given in Table 5-3. These conventional measurements also ensure fully redundant network observability.

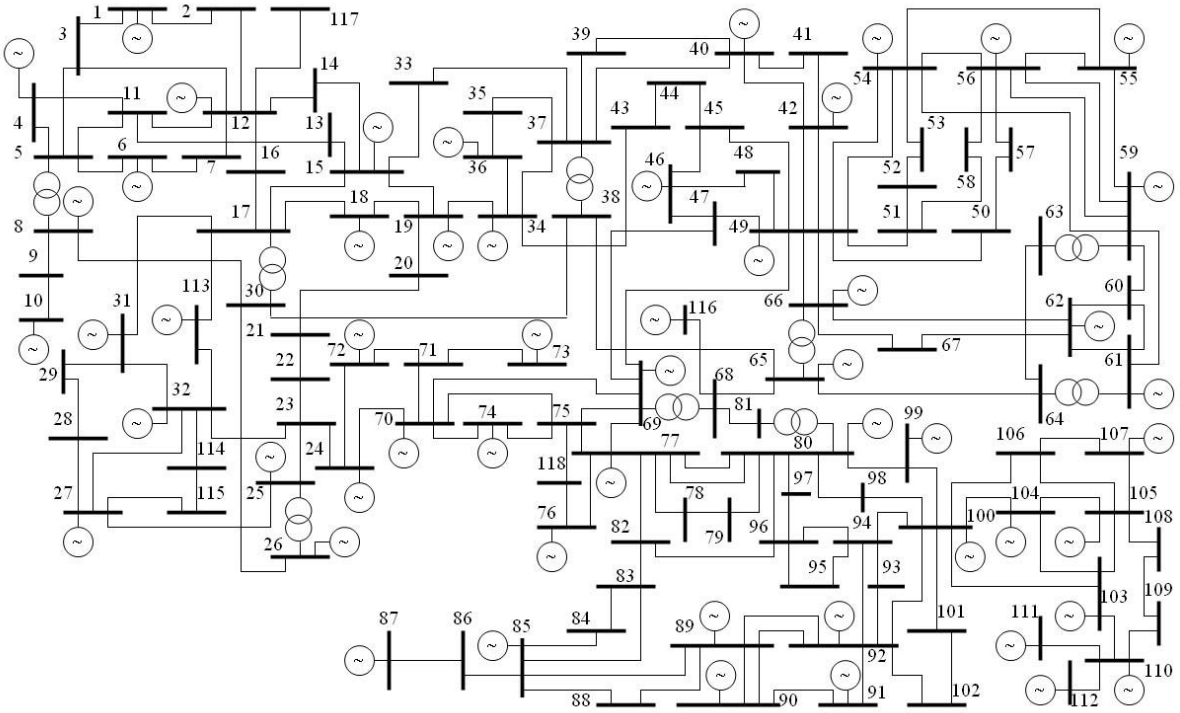

Figure 5-23: Network Diagram for IEEE 118 Bus Test System

Table 5-3: Conventional Measurement Placement in the IEEE 118 Bus Test System

Injection meas.at Bus #	2;5;7;10;12;15;16;17;19;23;25;27;31;33;34;39;44;45;47;49;51;52;59;61;64;66;69;71;72;74;75;77;80;85;90;93;96;101;102;105;110;111;113;115;116
Flow meas.at Branch #	1;5;7;10;15;16;19;24;25;27;31;33;37;43;45;46;49;51;53;56;57;61;66;71;72;75;80;81;84;87;92;95;100;102;104;110;111;114;116;118;119;126;131;134;135;137;140;142;144;147;149;152;158;159;163;165;169;172;174;177;179;182;184
Voltage magnitude meas. at Bus #	1;4;7 … 115;118 (with common difference of 3)

In the IEEE 118 Bus Test System, it is no longer possible to run exhaustive simulations for every possible PMU placement due to the large number of simulations required ($2^{118}=3.3*10^{35}$

in total) and increased execution time for each simulation. Thus, a set of measurements including an approximate best placement (in terms of estimation accuracy), 99 suboptimal placements and 100 random placements are used for each number of PMUs instead. To further reduce the number of simulations, only 15 selected PMU numbers are tested (0, 1, 2, 5, 10, 20, 25, 30, 35, 40, 45, 60, 80, 100, 118).

Based on empirical observations from the results of the exhausted simulation in the IEEE 14 Bus Test System, a simple optimisation algorithm was developed to find the best placement of the PMUs in terms of HSE estimation accuracy. The best placement is found at the point where the number of observable branches and the number of observable buses are maximised subject to a given number of PMUs as shown in (5.46) and (5.47). The proposed method does not ensure that the result will allow the HSEs to estimate the best accuracy due to the method's simple and empirical based nature; however, the result will be a close approximation to the best estimate. Further research will be needed to establish a complete method for optimal PMU placement for HSE estimation accuracy; however, the result is sufficient in terms of meeting the needs of this PhD.

$$\max N_{obr} + MN_{ob} \tag{5.46}$$

$$s.t. \quad N_{PMU} = N \tag{5.47}$$

where N_{obr} is the number of branches observable by PMUs, M is a large positive number (M=10 here) to enforce the priority of observable buses, N_{ob} is the number of observable buses by PMUs, N_{PMU} is the number of PMUs to be placed, and N is the number of PMUs required to be placed.

The suboptimal placements are found by including an additional constraint:

$$N_{obr} + MN_{ob} \leq f_{\max} - k \tag{5.48}$$

where f_{max} is the maximised optimisation goal solved from (5.46) and (5.47), and k is the number of the sub-optimal case, which ranges from 1 to 99 here.

5.4.2 Simulation Results

Figure 5-24, Figure 5-25 and Figure 5-26 present the simulation results of best accuracy, execution time and condition number in the IEEE 118 Bus Test System, respectively. It is shown in Figure 5-24 that all the characteristics of the curves are the same as those presented in Figure 5-15, including a clear knee point as the number of PMUs is increased, RC HSE being the most accurate, PF being the least accurate before the knee point and PV being the least accurate after the knee point. As illustrated in Figure 5-25 the conclusions drawn for HSE execution time are also validated except that the PV HSE becomes slower than CF HSE when the number of PMUs is large. Similar characteristics of the curves are also observed in the condition number test as shown in Figure 5-26. The difference is that CNlog10 of the CF HSE approaches the steady state with a smaller number of PMUs; thus, the condition number of the CF HSE is large for almost any number of PMUs – CNlog10 is 20 when only 5 PMUs are placed.

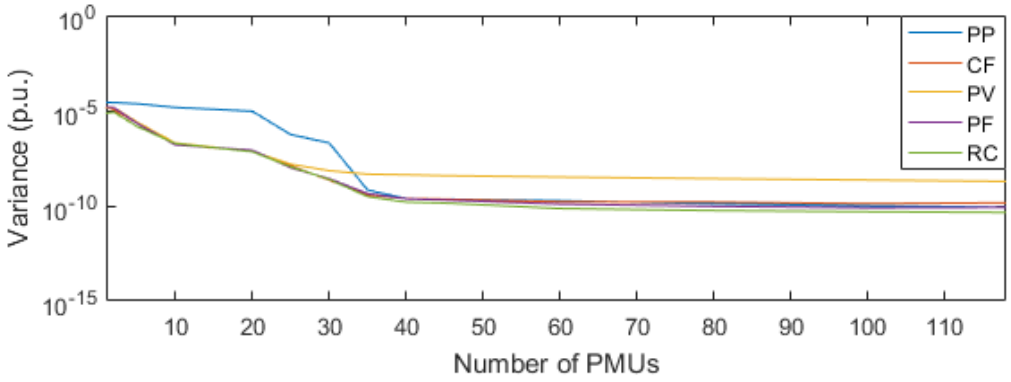

Figure 5-24: Best Accuracy of the HSEs against the number of PMUs in the IEEE 118 Bus Test System

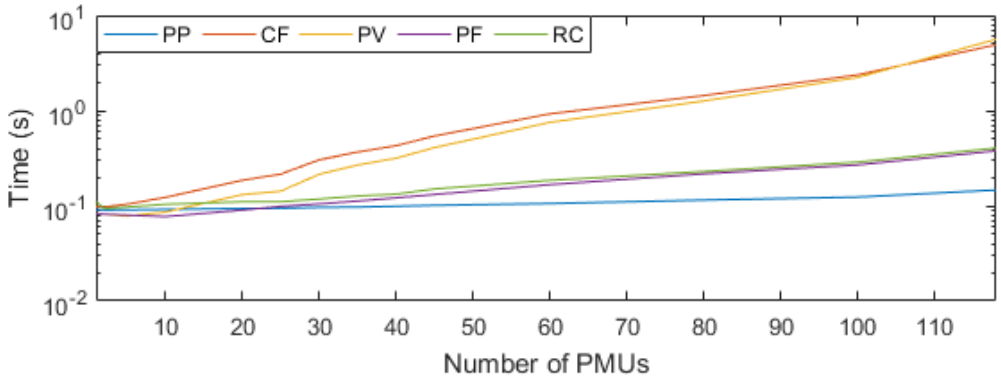

Figure 5-25: Execution Time of the HSEs against the Number of PMUs in the IEEE 118 Bus Test System

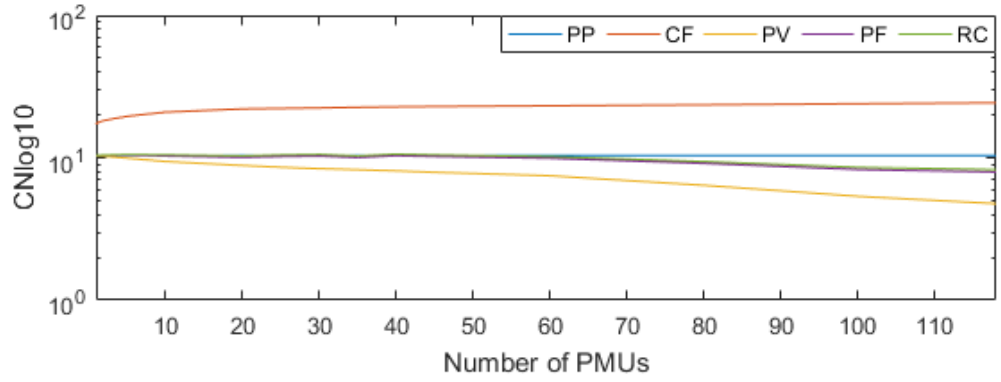

Figure 5-26: Condition Number in Log 10 Scale of the HSEs against the Number of PMUs in the IEEE 118 Bus Test System

5.5 Mathematical Analyses

This section presents the mathematical analysis to explain and further validate the important characteristics regarding the best accuracy of the HSEs shown in both the IEEE 14 and 118 Bus Test Systems. The first subsection will explain the small difference in accuracy between the RC, PF and PP HSEs and the reason why RC HSE has the best accuracy. The second subsection will explain the large difference in accuracy between the PV HSE and the other HSEs after the knee point and the large difference in accuracy between the PP HSE and the integrated HSEs before the knee point.

5.5.1 Analysis of RC, PF and CF Accuracy

The analysis considers the case where the PMU measurements decide the estimation accuracy of the HSEs. A two bus network with a single PMU as shown in Figure 5-27 is used to simplify the analysis for large networks. This simplification is valid if the following two assumptions can be made. First, at the sending end of a current phasor measurement there is always a voltage phasor measurement [163]. Second, the error-free equations (such as measurement equations for zero injection measurements and the slack bus) that are derived from the structure of the network are excluded from the measurement set. Based on the above assumptions and the fact that PMU measurements are more accurate than the conventional measurements, any network can be divided into a number of two bus networks, in which the current between the two buses can be expressed as given in (5.49):

$$\bar{I} = \left(\bar{V}_1 - \bar{V}_2\right) / \, jX = 10\left(\bar{V}_1 - \bar{V}_2\right) / \, j \tag{5.49}$$

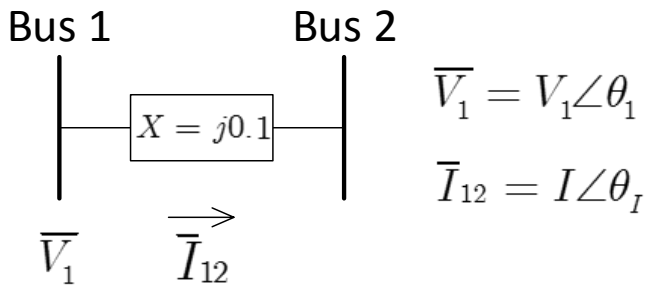

Figure 5-27: Two Bus Network with j0.1 Branch Reactance

To simplify the expression, let $I_{normalised}=I/10$, $X_{normalised}=1$ p.u., and (5.49) is transformed as given in (5.50). In the following part of this section, the subscript "normalised" will be dropped for brevity. The normalised current angle is the same as the original current angle, but the normalised current magnitude becomes 1/10 of its original value, making it much smaller than the voltage magnitudes. Note that the variance of the current magnitude measurement is still the same since the transformation only simplifies its expression but not the measurement itself.

$$\bar{I}_{normalised} = \left(\bar{V}_1 - \bar{V}_2\right) / \, jX_{normalised} = \left(\bar{V}_1 - \bar{V}_2\right) / \, j \tag{5.50}$$

The voltage phasor measurement at Bus 1 can be directly expressed as given by (5.51) and (5.52). The current phasor measurement at Bus 2 must be transformed into alternative forms according to different types of integrated HSEs used as listed from (5.53) to (5.60). In addition, the CF HSE requires two equality constraints to be satisfied, as expressed by (5.61) and (5.62).

$$z_1 = \theta_1 + e_{\theta 1} \tag{5.51}$$

$$z_2 = V_1 + e_{V1} \tag{5.52}$$

$$z_{3,RC} = I\cos\theta_I = V_1\sin\theta_1 - V_2\sin\theta_2 + e_{3,RC} \tag{5.53}$$

$$z_{4,RC} = I\sin\theta_I = -V_1\cos\theta_1 + V_2\cos\theta_2 + e_{4,RC} \tag{5.54}$$

$$z_{3,PF} = \hat{V}_1 I\cos\left(\hat{\theta}_1 - \theta_I\right) = V_1V_2\sin\left(\theta_1 - \theta_2\right) + e_{3,PF} \tag{5.55}$$

$$z_{4,PF} = V_1 I\sin\left(\hat{\theta}_1 - \theta_I\right) = V_1^2 - V_1V_2\cos\left(\theta_1 - \theta_2\right) + e_{4,PF} \tag{5.56}$$

$$z_{3,PV} = \tan^{-1}\left(\frac{V_{kI}}{V_{kR}}\right) = \tan^{-1}\left(\frac{V_1\sin\theta_1 - I\cos\theta_I}{V_1\cos\theta_1 + I\sin\theta_I}\right) = \theta_2 + e_{3,PV} \tag{5.57}$$

$$z_{4,PV} = \sqrt{V_{kR}^2 + V_{kI}^2} = \sqrt{V_1^2 + I^2 - 2VI\sin\left(\theta_1 - \theta_I\right)} = V_2 + e_{4,PV} \tag{5.58}$$

$$z_{3,CF} = \theta_I + e_{\theta I} \tag{5.59}$$

$$z_{4,CF} = I + e_I \tag{5.60}$$

$$t_1 = \tan^{-1}\left(\frac{V_1\sin\theta_1 - I\cos\theta_I}{V_1\cos\theta_1 + I\sin\theta_I}\right) - \theta_2 = 0 \tag{5.61}$$

$$t_2 = \sqrt{V_1^2 + I^2 - 2V_1I\sin\left(\theta_1 - \theta_I\right)} - V_2 = 0 \tag{5.62}$$

Take the partial derivative of the measurement equations from (5.53) to (5.58) which corresponds to the RC, PF and PV HSEs with respect to the state vector, $\mathbf{x}=[\theta_1\ V_1\ \theta_2\ V_2]^T$, and also take the partial derivative of the measurement equations of (5.59) and (5.60) and the equality constraint equations of (5.61) and (5.62), the measurement Jacobian matrices of the measurement equations and constraints of the HSEs are obtained as given in (5.63) to (5.67):

$$\mathbf{H}_{RC}=\begin{bmatrix} 1 & 0 & 0 & 0 \\ 0 & 0 & 1 & 0 \\ V_1\cos\theta_1 & -V_2\cos\theta_2 & \sin\theta_1 & -\sin\theta_2 \\ V_1\sin\theta_1 & -V_2\sin\theta_2 & -\cos\theta_1 & \cos\theta_2 \end{bmatrix} \tag{5.63}$$

$$\mathbf{H}_{PF}=\begin{bmatrix} 1 & 0 & 0 & 0 \\ 0 & 0 & 1 & 0 \\ V_1V_2\cos\theta_{12} & -V_1V_2\cos\theta_{12} & V_2\sin\theta_{12} & V_1\sin\theta_{12} \\ V_1V_2\sin\theta_{12} & -V_1V_2\sin\theta_{12} & 2V_1-V_2\cos\theta_{12} & -V_1\cos\theta_{12} \end{bmatrix} \tag{5.64}$$

$$\mathbf{H}_{PV}=\begin{bmatrix} 1 & 0 & 0 & 0 \\ 0 & 0 & 1 & 0 \\ 0 & 1 & 0 & 0 \\ 0 & 0 & 0 & 1 \end{bmatrix} \tag{5.65}$$

$$\mathbf{H}_{CF}=\begin{bmatrix} 1 & 0 & 0 & 0 & 0 & 0 \\ 0 & 1 & 0 & 0 & 0 & 0 \\ 0 & 0 & 0 & 0 & 1 & 0 \\ 0 & 0 & 0 & 0 & 0 & 1 \end{bmatrix} \tag{5.66}$$

$$\mathbf{T}=\begin{bmatrix} \left(I\sin\theta_I+1\right)/c^2, -I\cos\theta_I/c^2, -1, 0, \left(I^2+I\sin\theta_I\right)/c^2, -\cos\theta_I/c^2 \\ -I\cos\theta_I/c, \quad \left(I\sin\theta_I+1\right)/c, 0, -1, I\cos\theta_I/c, \quad \left(I+\sin\theta_I\right)/c \end{bmatrix} \tag{5.67}$$

where c is a constant defined by:

$$c=\sqrt{V_1^2+I^2-2VI\sin\left(\theta_1-\theta_I\right)}\approx 1 \tag{5.68}$$

Assuming the uncertainties of the original measurements, θ_1, V_1, θ_I and I, are known to be $\sigma^2_{\theta 1}$, σ^2_{V1}, $\sigma^2_{\theta I}$ and σ^2_I, respectively. The uncertainty of the transformed measurements can be obtained by propagating the original measurements through the equation by assuming that $\theta_1\approx 0$ and $V_1\approx 1$. Thus, the calculated variances of the transformed measurements are given in (5.70) to (5.75), and the residual matrix of the HSEs can be expressed by (5.76) to (5.79).

$$\mathrm{var}\left(z_{tran}\right)=\sqrt{\sum_{k=1}^{n}\left[\partial z_{tran}/\partial \mathbf{z}\left(k\right)\right]^{2}\left[\mathrm{var}\left(\mathbf{z}\left(k\right)\right)\right]} \tag{5.69}$$

$$\mathrm{var}\left(z_{3,RC}\right)=I^{2}\sin^{2}\theta_{I}\sigma_{\theta I}^{2}+\cos^{2}\theta_{I}\sigma_{\theta I}^{2} \tag{5.70}$$

$$\mathrm{var}\left(z_{4,RC}\right)=I^{2}\cos^{2}\theta_{I}\sigma_{\theta I}^{2}+\sin^{2}\theta_{I}\sigma_{\theta I}^{2} \tag{5.71}$$

$$\mathrm{var}\left(e_{3,PF}\right)=I^{2}\sin^{2}\theta_{I}\sigma_{\theta I}^{2}+\cos^{2}\theta_{I}\sigma_{\theta I}^{2}+I^{2}\sin^{2}\theta_{I}\sigma_{\theta 1}^{2}+I^{2}\cos^{2}\theta_{I}\sigma_{V1}^{2} \tag{5.72}$$

$$\mathrm{var}\left(z_{4,PF}\right)=I^{2}\cos^{2}\theta_{I}\sigma_{\theta I}^{2}+\sin^{2}\theta_{I}\sigma_{\theta I}^{2}+I^{2}\cos^{2}\theta_{I}\sigma_{\theta 1}^{2}+\sin^{2}\theta_{I}\sigma_{V1}^{2} \tag{5.73}$$

$$\mathrm{var}\left(z_{3,PV}\right)=\left[\left(1+I\sin\theta_{I}\right)^{2}\sigma_{\theta 1}^{2}+I^{2}\cos^{2}\theta_{I}\sigma_{V1}^{2}+\left(I^{2}+I\sin\theta_{I}\right)^{2}\sigma_{\theta I}^{2}+\cos^{2}\theta_{I}\sigma_{I}^{2}\right]/c^{2} \tag{5.74}$$

$$\mathrm{var}\left(z_{4,PV}\right)=\left[I^{2}\cos^{2}\theta_{I}\sigma_{\theta 1}^{2}+\left(1+I\sin\theta_{I}\right)^{2}\sigma_{V1}^{2}+I^{2}\cos^{2}\theta_{I}\sigma_{\theta I}^{2}+\left(I+\sin\theta_{I}\right)^{2}\sigma_{I}^{2}\right]/c \tag{5.75}$$

$$R_{RC}=\mathrm{diag}\left(\left[\sigma_{\theta 1}^{2}\quad\sigma_{V1}^{2}\quad\mathrm{var}\left(e_{3,RC}\right)\quad\mathrm{var}\left(e_{4,RC}\right)\right]\right) \tag{5.76}$$

$$R_{PF}=\mathrm{diag}\left(\left[\sigma_{\theta 1}^{2}\quad\sigma_{V1}^{2}\quad\mathrm{var}\left(e_{3,PF}\right)\quad\mathrm{var}\left(e_{4,PF}\right)\right]\right) \tag{5.77}$$

$$R_{PV}=\mathrm{diag}\left(\left[\sigma_{\theta 1}^{2}\quad\sigma_{V1}^{2}\quad\mathrm{var}\left(e_{3,PV}\right)\quad\mathrm{var}\left(e_{4,PV}\right)\right]\right) \tag{5.78}$$

$$R_{CF}=\mathrm{diag}\left(\left[\sigma_{\theta 1}^{2}\quad\sigma_{V1}^{2}\quad\sigma_{\theta i}^{2}\quad\sigma_{I}^{2}\right]\right) \tag{5.79}$$

where z_{tran} represents a transformed measurement of z_3 or z_4, e denotes the error of a measurement, the subscripts 3 and 4 are the measurement numbers.

The variance of the estimated states of any WLS state estimator is given by (5.80) [4], while that of a constrained formulation state estimator can be derived as shown in (5.81) and (5.82). Applying these general equations, the variances of the estimated states of the integrated HSEs are summarised in Table 5-4.

$$\mathrm{cov}\left(\hat{\mathbf{x}}\right)=\left(\mathbf{H}^{T}\mathbf{R}^{-1}\mathbf{H}\right)^{-1} \tag{5.80}$$

$$\mathbf{H}_{aug}=\begin{bmatrix}\mathbf{H}^{T}\mathbf{R}^{-1}\mathbf{H} & -\mathbf{T}^{T}\\ \mathbf{T} & \mathbf{0}\end{bmatrix} \tag{5.81}$$

$$\mathrm{cov}\left(\hat{\mathbf{x}}_{CF}\right)=\mathbf{P}\mathbf{H}^{T}\mathbf{R}^{-1}\mathbf{H}\mathbf{P}^{T} \tag{5.82}$$

where **P** is a matrix consisting of the rows taken from the inverse of $\mathbf{H}_{aug}$ corresponding to the state vector, **x**.

Table 5-4: HSE Estimate Covariance in Two Bus Network with Single PMU at Bus 1

	Voltage Angle 1	Voltage Mag. 1	Voltage Angle 2	Voltage Mag. 2
RC	$\sigma_{\theta 1}^2$	σ_{V1}^2	$\sigma_{\theta 1}^2 + I^2 \sin^2\theta_I \sigma_{\theta I}^2 + \cos^2\theta_I \sigma_I^2$	$\sigma_{V1}^2 + I^2 \cos^2\theta_I \sigma_{\theta I}^2 + \sin^2\theta_I \sigma_I^2$
PF	$\sigma_{\theta 1}^2$	σ_{V1}^2	$\left(1+I^2\sin^2\theta_I\right)\sigma_{\theta 1}^2 + I^2\cos^2\theta_I\sigma_{V1}^2$ $+I^2\sin^2\theta_I\sigma_{\theta I}^2 + \cos^2\theta_I\sigma_I^2$	$I^2\cos^2\theta_I\sigma_{\theta 1}^2 + \left(1+I^2\sin^2\theta_I\right)\sigma_{V1}^2$ $+I^2\cos^2\theta_I\sigma_{\theta I}^2 + \sin^2\theta_I\sigma_I^2$
PV	$\sigma_{\theta 1}^2$	σ_{V1}^2	$\left(1+I\sin\theta_I\right)^2\sigma_{\theta 1}^2 + I^2\cos^2\theta_I\sigma_{V1}^2$ $+\left(I^2+I\sin\theta_I\right)^2\sigma_{\theta I}^2 + \cos^2\theta_I\sigma_I^2$	$I^2\cos^2\theta_I\sigma_{\theta 1}^2 + \left(1+I\sin\theta_I\right)^2\sigma_{V1}^2$ $+I^2\cos^2\theta_I\sigma_{\theta I}^2 + \left(I+\sin\theta_I\right)^2\sigma_I^2$
CF	$\sigma_{\theta 1}^2$	σ_{V1}^2	$\left(1+I\sin\theta_I\right)^2\sigma_{\theta 1}^2 + I^2\cos^2\theta_I\sigma_{V1}^2$ $+\left(I^2+I\sin\theta_I\right)^2\sigma_{\theta I}^2 + \cos^2\theta_I\sigma_I^2$	$I^2\cos^2\theta_I\sigma_{\theta 1}^2 + \left(1+I\sin\theta_I\right)^2\sigma_{V1}^2$ $+I^2\cos^2\theta_I\sigma_{\theta I}^2 + \left(I+\sin\theta_I\right)^2\sigma_I^2$

It can be easily observed from the left side of Table 5-4 that the transformation of the current phasor measurement does not affect the estimation accuracy of the state at Bus 1, where the variance of the states is only determined by the uncertainty of the incident voltage phasor measurement. In comparison, the error of the state estimate for Bus 2 is determined by both the voltage phasor measurement at Bus 1 and the current phasor measurement connecting the two buses. What is more, the RC HSE has the least error for the estimates at Bus 2 compared to the other integrated HSEs. This is because it does not use the states at Bus 1 for transforming the current phasor measurement like the other integrated HSEs, which brings extra errors as shown in the corresponding expressions in Table 5-4. However, the estimation errors among the different integrated HSEs are small if only the effects of the PMU measurements are accounted for. The relative magnitudes of the estimate errors of the four integrated HSEs, for states at Bus 2 quantified by variance, are given in (5.83) and (5.84).

$$\operatorname{cov}\left(\hat{\theta}_{2,RC}\right) < \operatorname{cov}\left(\hat{\theta}_{2,PF}\right) \approx \operatorname{cov}\left(\hat{\theta}_{2,PV}\right) = \operatorname{cov}\left(\hat{\theta}_{2,CF}\right) \tag{5.83}$$

$$\operatorname{cov}\left(\hat{V}_{2,RC}\right) < \operatorname{cov}\left(\hat{V}_{2,PF}\right) \approx \operatorname{cov}\left(\hat{V}_{2,PV}\right) = \operatorname{cov}\left(\hat{V}_{2,CF}\right) \tag{5.84}$$

5.5.2 Analysis of PV and PP HSE Accuracy

As well as the *real* measurements collected from the measurement units such as the conventional measurements and the PMU measurements, the measurement set used for state estimation involves the *virtual* measurements that are mathematically derived from the topology of the network. For example, if a bus is known to have no generation or load a zero injection measurement can be assumed for this bus. A virtual measurement can also be assumed for the reference angle of the slack bus, which is usually set to be always 0 regardless of the changing states of the network. The real measurements contain a certain degree of errors due to the accuracy limit of the measurement device, telecommunication errors and loss of data; the virtual measurements are free of errors and are usually treated as equality constraints. In this analysis, the effect of virtual measurements is represented as a voltage phasor measurement at Bus 2 with a fundamentally lesser degree of error than that of the PMU measurements, as shown in Figure 5-28.

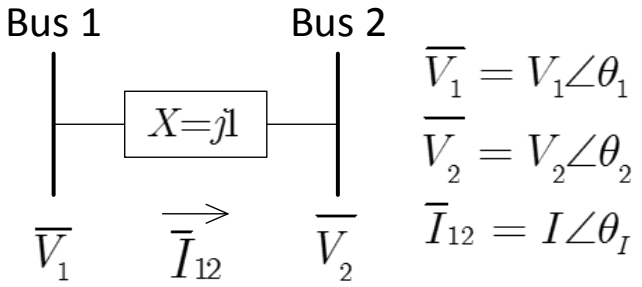

Figure 5-28: Two Bus Network with a Virtual Voltage Phasor Measurement

Following the same procedure described in the previous subsection, the variance of the state estimate of the four integrated HSEs is calculated as summarised in Table 5-4. Because of the complexity of the original expressions, the expressions listed are obtained after substituting $I \approx 0$ (I is much smaller than V_1) and making other approximations based on the magnitude difference between the variables.

Table 5-5: HSE Estimate Variance in Two Bus Network with a PMU at Bus 1 and a Virtual Voltage Phasor Measurement at Bus 2

	Voltage Angle 1	Voltage Mag. 1	Voltage Angle 2	Voltage Mag.2
RC	$\sigma_{\theta 2}^2 + \cos^2\theta_I \sigma_I^2$	$\sigma_I^2 \sigma_{V1}^2 / \sigma_I^2 + \sigma_{V1}^2$	$\sigma_{\theta 2}^2$	σ_{V2}^2
PF	$\sigma_{\theta 2}^2 + \cos^2\theta_I \sigma_I^2$	$\sigma_I^2 \sigma_{V1}^2 / \sigma_I^2 + \sigma_{V1}^2$	$\sigma_{\theta 2}^2$	σ_{V2}^2
PV	$\sigma_{\theta 1}^2$	σ_{V1}^2	$\sigma_{\theta 2}^2$	σ_{V2}^2
CF	$\sigma_{\theta 2}^2 + \cos^2\theta_I \sigma_I^2$	$\sigma_I^2 \sigma_{V1}^2 / \sigma_I^2 + \sigma_{V1}^2$	$\sigma_{\theta 2}^2$	σ_{V2}^2

Table 5-5 shows that after the inclusion of the virtual voltage phasor measurement at Bus 2, the approximated expressions of the variance of the state estimate at Bus 2 are all the same. This result is expected since the virtual measurements are fundamentally more accurate than the PMU measurements, and thus their very small uncertainty will dominate the estimate accuracy of their incident buses. In terms of the variance of the state estimates at Bus 1, the left two columns of Table 5-5 show that the variance of the RC, PF and CF HSE have been reduced significantly to about the same values, while the variance of the PV HSE has the same value as it was before the inclusion of the virtual measurement. To summarise these results, the RC, PF and PV HSE are able to "propagate" the accuracy of the virtual measurements to the neighbouring buses with the help of current phasor measurements, while the PV HSE obviously does not have this important capability. In large networks accurate measurements improve the accuracy of the state estimates of the neighbouring buses, and gradually propagate the enhanced accuracy through the network.

The accuracy propagation mechanism is not just limited to the virtual measurements and the PMU measurements; it also applies to the PMU measurements and the conventional measurements as the former is also fundamentally more accurate than the latter. When the number of PMUs is small, most of the states are monitored by conventional measurements, and only a small proportion of the states are monitored by the PMUs. In this case, the estimation

accuracies of the different HSEs are mainly affected by the accuracy gap between the PMU measurements and the conventional measurements. As most of the conventional measurements are power flow or power injection measurements, the integrated HSEs that make direct use of them are said to use the conventional measurements in the "flow form". Similar to the full PMU observability case where the PF HSE can make use of the virtual measurements to improve its estimation accuracy, the integrated HSEs are found, through mathematical derivation, to be capable of utilizing the PMU measurements to enhance their estimation accuracies. In comparison, the PP HSE transforms these measurements into "voltage phasor form" by using the CSE in the first stage. Therefore, by depriving itself of the ability to use these flow measurements to propagate accuracy of the PMU measurements, the PP HSE will have poorer estimation accuracy, unless the network is fully observable by PMUs.

5.6 The Effect of Gross Errors and Parameter Errors

The general errors caused by the accuracy limit of the meters, time skew errors and telecommunication errors are commonly modelled as Gaussian errors. As well as the general errors, the HSEs might also be affected by gross errors and parameter errors. The effects of these two types of error on the HSEs will be discussed in detail according to the exhausted simulation in the IEEE 14 Bus Test System. The simulations use the same setting as introduced in Section 5.3.1 except for the new errors included.

5.6.1 Including Gross Measurement Errors

In this subsection, the performance of the HSEs is studied when gross measurement errors are integrated into the conventional measurements for the IEEE 14 Bus Test System. While state estimators do have bad data detection capabilities that will usually prevent gross errors from entering the state estimator, it is useful to determine if any of the HSEs are inherently more resilient against gross errors that may be included in the estimation procedure, either through

misfortune or malicious actions. The test setup is the same as in Section 5.3.1 and two cases are considered:

1 A single Conventional Measurement is set to Zero
2 A single Conventional Measurement is set to Two thirds of its True Value

The results for the Case 1 are given in Figure 5-29 and the results for Case 2 are given in Figure 5-30. Both of these cases returned similar results in terms of the trends observed, although the two thirds case led to smaller errors for most placements. These results show that the gross errors are capable of severely undermining the accuracy of the HSEs. However, if the voltage magnitude cases are neglected, these outliers are on a par with the performance of the conventional state estimator with only Gaussian noise.

Furthermore, for the integrated HSEs it can be seen that some placements can make the HSE resilient to gross error. However, the placements that make the HSE resilient to one error do not make it resilient to all of the others. The errors of the estimated results from the integrated HSE can, for the most part, be characterised as possessing accuracy that is nearly equivalent to the base case (without gross errors) with a few outliers with poor or very poor accuracy. This is supported by the median accuracy of the data points, where the outliers distort the mean. This contrasts to the PP HSE, for which the errors can be described as primarily poor or very poor with a few outliers that approach the accuracy of the base case, as in previous cases this is due to the ability of the PP HSE to improve a state estimate being dependent on the bus being observable by a PMU.

Some cases do not have outliers; this is because the significance of the gross errors considered are not all equal, e.g. setting the power flow of a lightly loaded line to zero is not an equivalent error to setting the power flow of a heavily loaded branch to zero.

In general, errors in voltage magnitude measurements are clearly the most significant. It is expected that this is because these measurements are more directly connected to the states. The PV HSE is noticeably more resilient to the gross errors in voltage magnitude. This trend needs further investigation. Indeed, further analysis of these results (e.g. to determine why some

placements are better than others) requires more detailed study of the cases. Furthermore, this study will likely require the development of new tools for studying the HSEs and their performance, as it is a complex interaction between the conventional measurement placements, the PMU placement, the system properties (e.g. topology and power flow) and the error in question. At this time, participation factors appear to be the best avenue to pursue when creating these new tools.

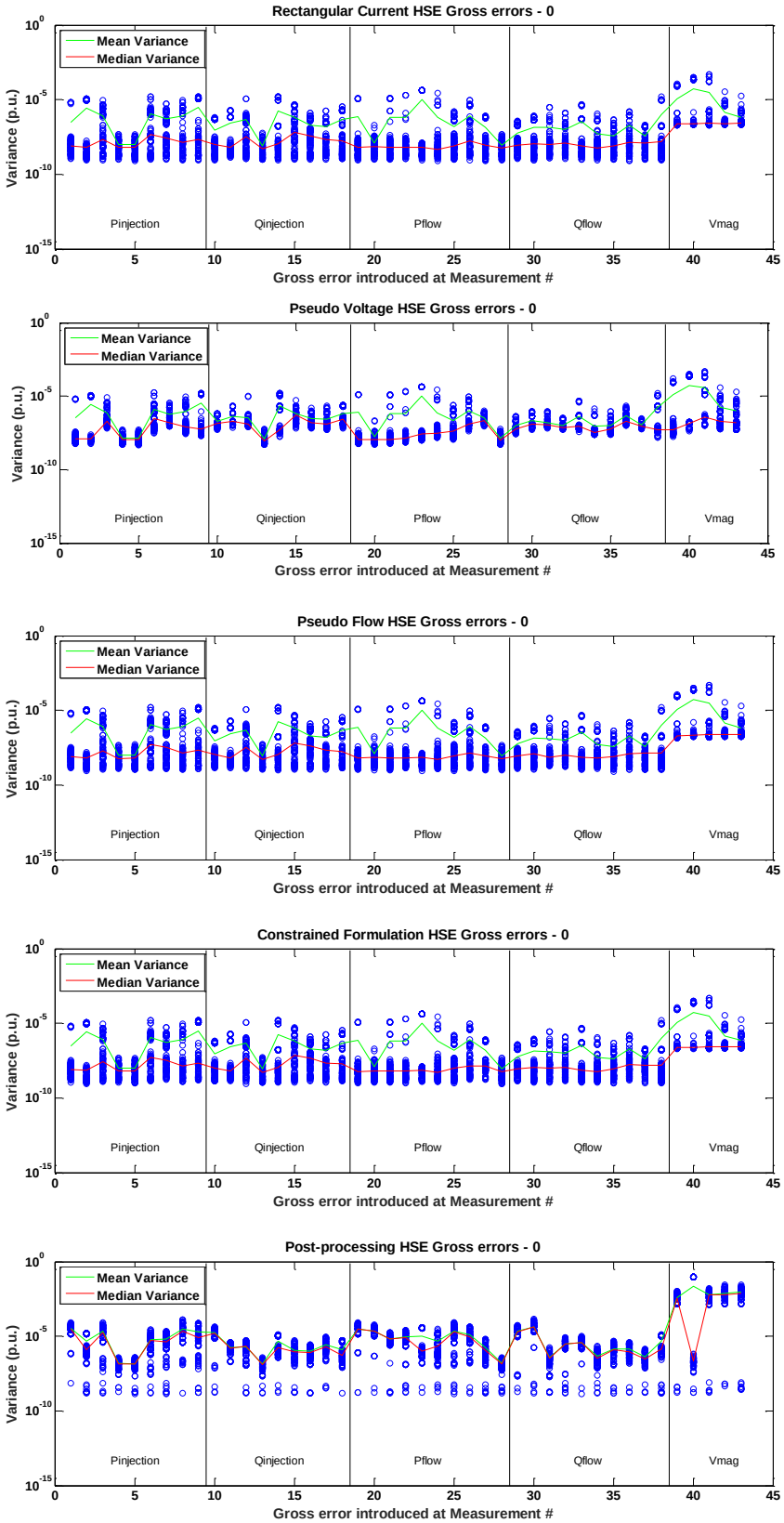

Figure 5-29: Figures for Gross Error in Case 1

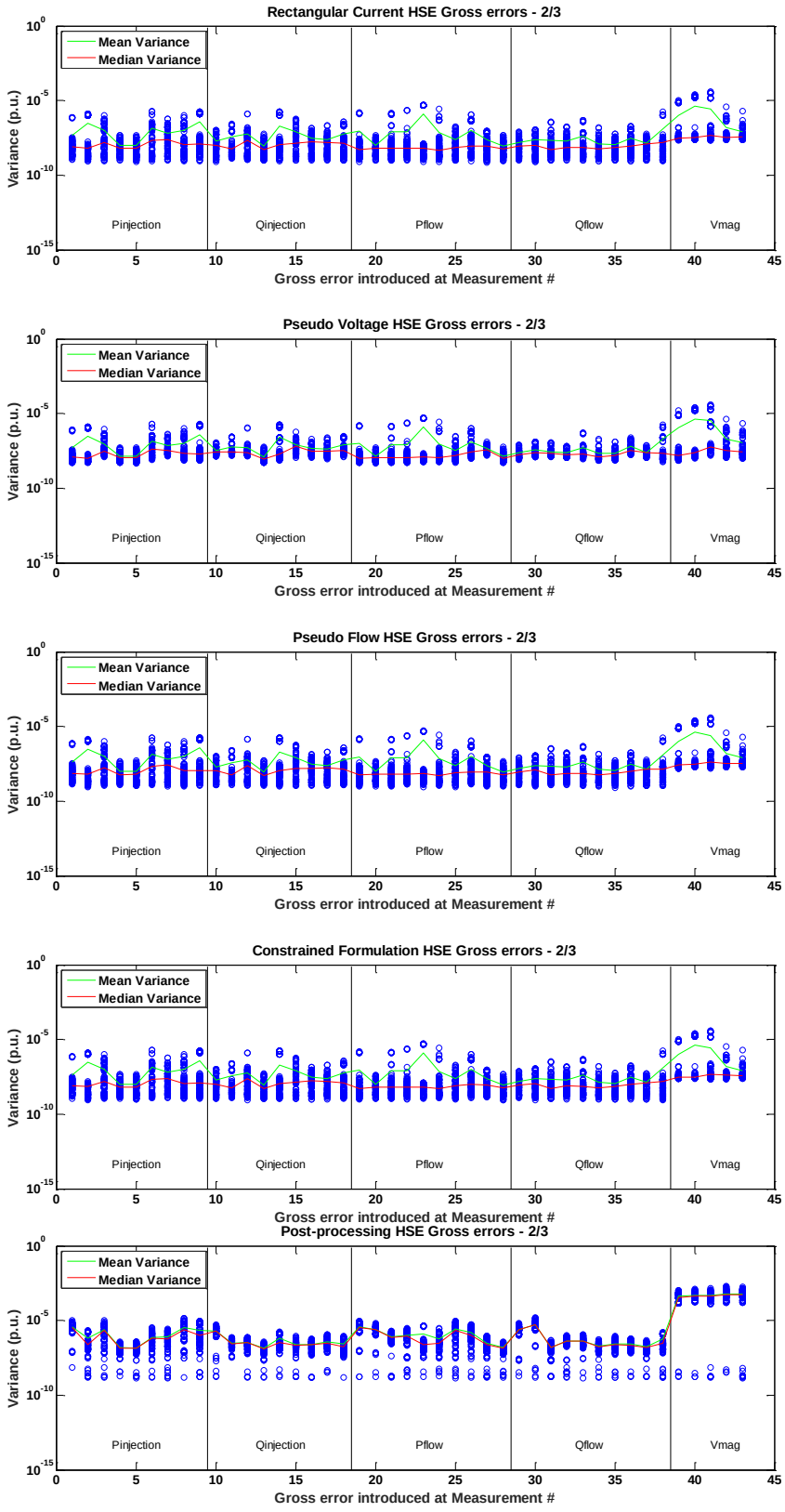

Figure 5-30: Figures for Gross Errors in Case 2

5.6.2 Parameter Errors – Branch Impedance

In this subsection the performance of the HSEs is studied when errors are introduced into the branch impedances of the IEEE 14 Bus Test System. These errors must be considered as network models can use outdated impedance estimates that do not reflect the changing nature of line impedance (particularly as they age), it is useful to determine if any of the HSEs are inherently more resilient against these parameter errors. The test setup is the same as in Section 3.2 and a Gaussian error with a standard deviation of 10% of the branch impedance is added to one branch at a time.

The results of this test are presented in Figure 5-31. The errors seen for this case have a very different distribution to those observed in the gross error case. The worst case is far more severe and the distribution of errors is more uniform (no clear outliers in most cases) and the median is skewed toward the worst case (for gross errors the integrated HSEs had the median skewed toward the best case). This suggests that parameter errors have a more significant impact than gross errors; however, it should be noted that some PMU placements allow the HSEs to perform as well as in the base case, despite the branch impedance error.

Integrated HSEs, except PV, are consistently poor for Branch 14. While the PV and PP HSEs do not exhibit any particular behaviour for this branch, the lack of sensitivity to PMU placement for the RC, CF and PF HSEs make this case a candidate for further investigation. To this end, the correlation coefficients between the HSE error and the branch properties of impedance magnitude, impedance angle, current magnitude and current angle were calculated as given in Table 5-6 and plotted in Figure 5-32. These results show that the HSE accuracy in a case with a branch impedance error is largely independent of these parameters, with only a small positive correlation to current magnitude and an even smaller positive correlation to impedance angle.

Table 5-6: Pearson Correlation Coefficients for Rectangular Current

Impedance	Impedance Angle	Current	Current Angle
0.0008	0.1378	0.3397	0.0046

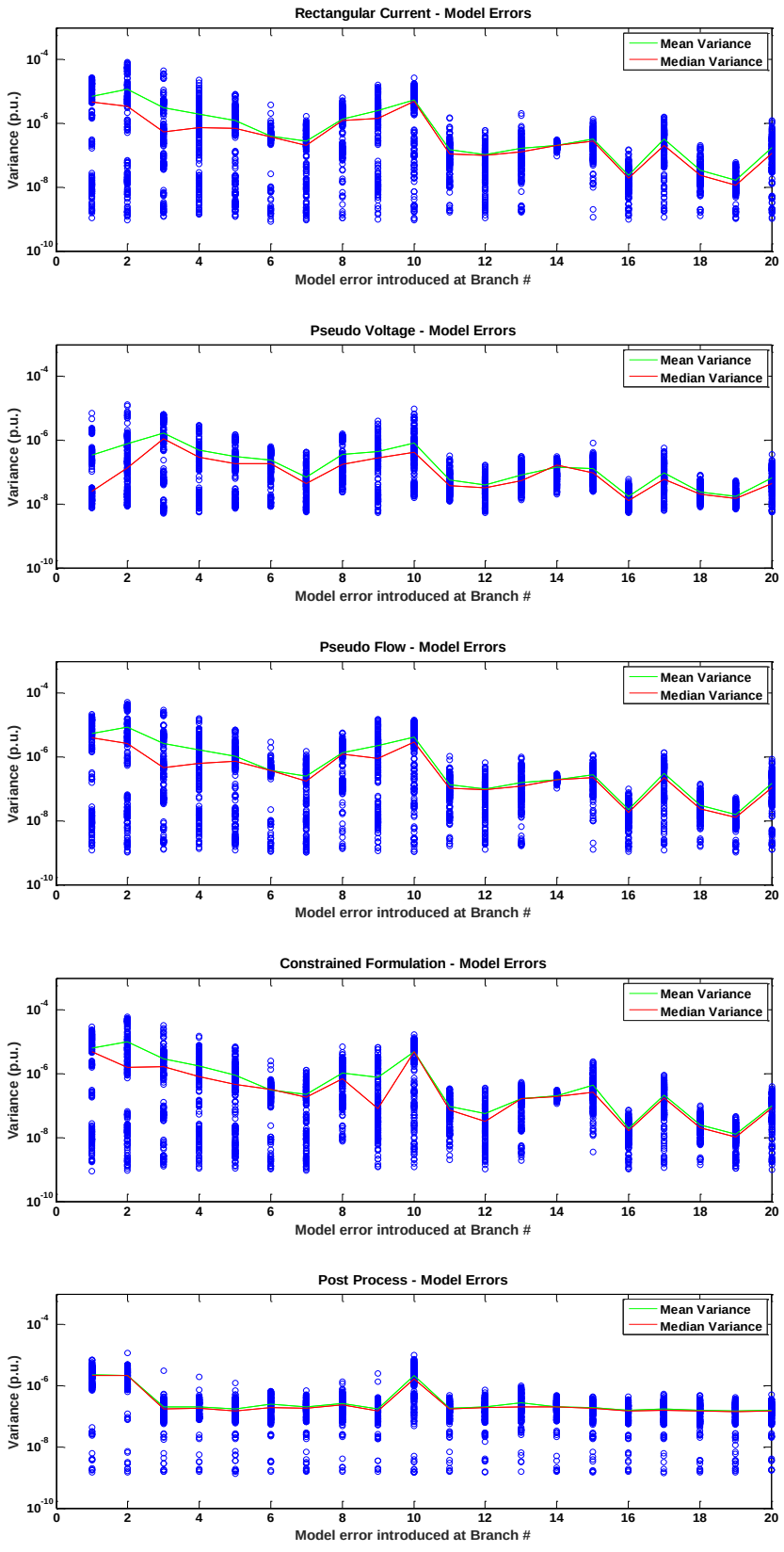

Figure 5-31: Impact of Errors in Branch Impedance on HSEs

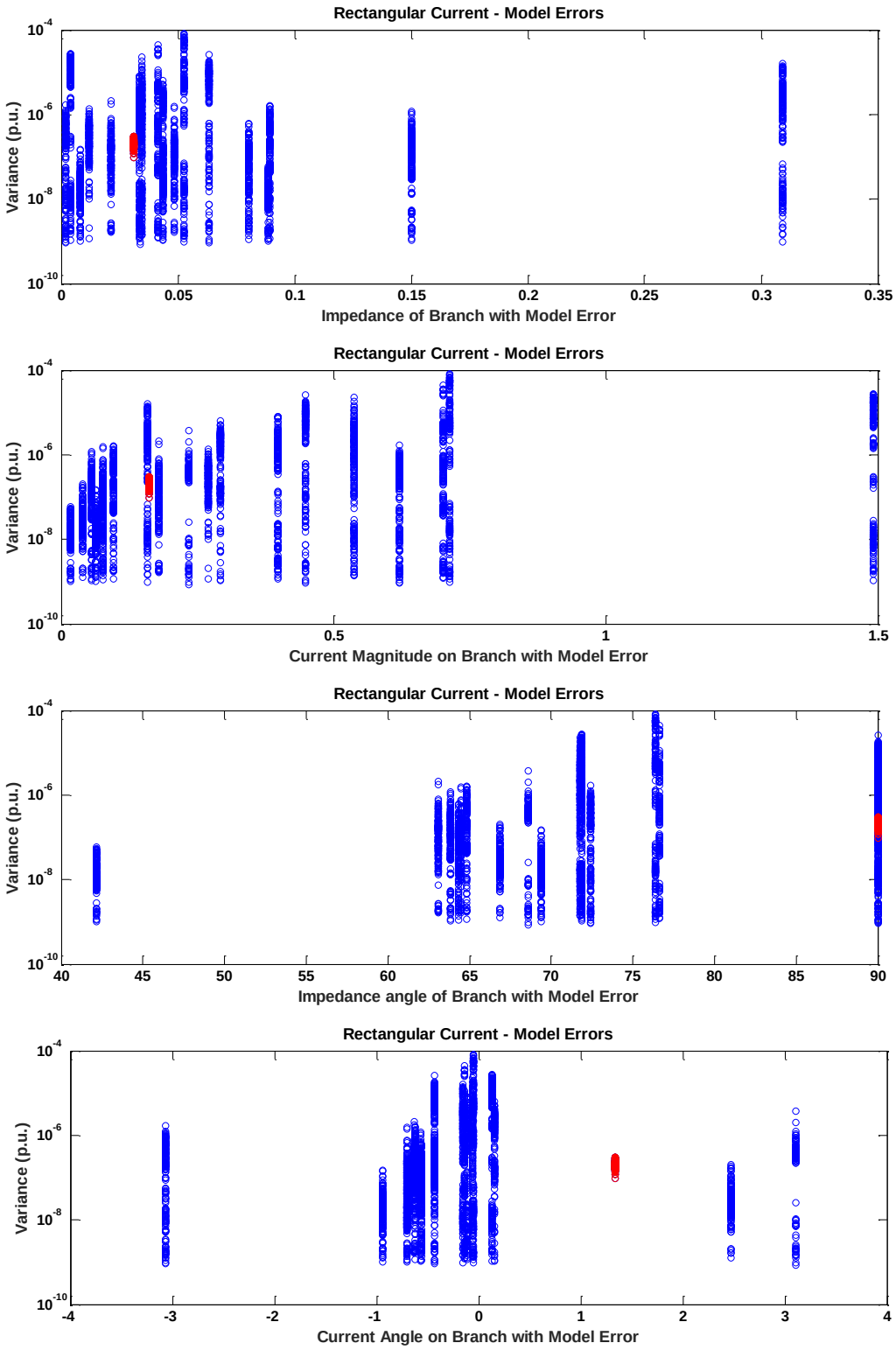

Figure 5-32: Examples of Low Correlation between Variance and Branch Properties (the Points for Branch 14 are Marked in Red)

As in the gross error case, it would appear that further study will depend upon developing new tools for defining HSE performance, due to the complex interaction between the conventional measurement placements, the PMU placement, the system properties (e.g. topology and power flow) and the error in question.

5.7 Summary

This chapter has provided comparisons and an analysis of five hybrid state estimators (HSEs). A post processing hybrid state estimator and four integrated hybrid state estimators have been identified in literature, which are:

- Rectangular Current (RC)
- Pseudo Flow (PF)
- Pseudo Voltage (PV)
- Constrained Formulation (CF)

The performance of the HSEs is studied in terms of their accuracy, execution time and condition number using mathematical analysis and simulations in both the IEEE 14 and 118 Bus Test Systems. Cases studied include Gaussian errors, gross measurement errors and parameter errors.

In general, the results of this comparison show that the accuracy of the HSEs is greater than the conventional state estimator by up to several orders of magnitude, and it increases with the number of PMUs and will saturate after a knee point. The knee point is about the same as the number of PMUs required to make the system fully observable.

The exhaustive simulation in the IEEE 14 Bus Test System show that the RC HSE is the most accurate HSE, the PF and CF HSE have slightly worse estimation accuracy, while the PP and PV HSE have the least estimation accuracy when the number of PMUs is smaller and larger than the knee point, respectively. These conclusions are validated in the IEEE 118 Bus Test System using a selected set of PMU placements obtained from an optimal and suboptimal

PMU placement method proposed in Section 5.4.1. The conclusions are further demonstrated and explained by mathematical analysis. It is concluded from the analysis that the RC HSE has the best estimation accuracy because the direct transformation of its current phasor measurements, without the help of other variables, introduces less error compared to the other HSEs. The PP and PV HSE have very poor estimation accuracy because they cannot use the PMU measurements and virtual measurements to improve the accuracy of their state estimates.

The simulations for execution time and condition number clearly show that the CF HSE will require a longer execution time and be vulnerable to convergence problems, especially when more PMUs are placed in the network. These problems can be explained by its augmented state vector, which resulted in a large and ill-conditioned gain matrix.

The study of sensitivity to PMU placement in Section 5.3.4 shows that the optimal placement becomes less relevant as the number of PMUs increases, which is not surprising. However, for smaller PMU numbers (e.g. four in the fourteen bus system) optimal placement can improve performance by two orders of magnitude. This sensitivity is most pronounced for the PP HSE, which means it will perform far more poorly than the integrated HSEs if a random or unplanned PMU placement is used. The PV HSE is the least sensitive to the PMU placement, as it makes poor use of the phasor data. In other words, a PV HSE equipped with the optimal placement of twelve PMUs will usually perform more poorly than other types of integrated HSE that have a random placement of seven PMUs.

Studies of gross measurement errors in the form of severely erroneous conventional measurements and parameter errors in the form of branch impedance errors are presented in Sections 5.6.1 and 5.6.2, respectively. The results have shown that parameter errors will have a more severe impact on HSE performance than gross errors and that gross errors in voltage magnitude are the most severe form of conventional measurement error. These results also show that, whilst gross and parameter errors can cause the HSE to perform poorly, the proper PMU placement can allow them to offer accuracy that is close to the base cases (Gaussian errors but no gross/model error). Furthermore, the poor performance that is observed as outliers in the gross error case is equivalent to the performance of the conventional state estimator in

the base case. However, further study that may reveal exactly why some placements are advantageous and why errors in certain measurement and branches have a more severe impact will require the development of new tools for studying HSE performance.

Chapter 6 Dynamic State Estimation

This chapter presents a new algorithm for dynamic state estimation using Cubature Kalman Filter (CKF). It is demonstrated that the proposed dynamic state estimator (DSE) using CKF is more accurate than other DSEs that use different nonlinear filters, which are in turn more accurate than the static state estimator (SSE). However, it was also discovered that CKF is more vulnerable to anomalies, including bad data, sudden changes of load, and sudden changes of network topology due to faults. Thus, the algorithm also includes a new scheme with a set of methods that can accurately detect, discriminate and identify the different types of anomaly.

6.1 Introduction

To ensure secure and economic operation, power systems need real-time monitoring of the states, the voltage magnitudes and angles, of all substations in the network. This important function has been performed using the static state estimator (SSE) since the establishment of state estimation in the early 1970s. However, the SSE requires a single redundant set of measurements to enable all of its functions, including state estimation solution and bad data detection. In addition, the SSE can only perform state estimation after receiving the measurements. The dynamic state estimator (DSE), which uses not only the measurements but also the predictions based on state estimates of previous time steps, provides a possible solution to the problems of using the SSE. However, although the DSE was also proposed in the early 1970s, it was not developed and widely deployed as the SSE because of the limit of computation capability of the control centre at that time. Nowadays, the barrier of computation capability has been surmounted with the advancements of information and communication technology. In addition, recently with the open access to the operation of transmission network the prediction of power generation and load has become much more accurate. Therefore, the pilot application of the DSE in power systems has been shown especially with the development of a wide area monitoring system (WAMS) [43], [97].

The DSE uses the Kalman Filter to estimate the states from the measurements and the predicted measurements based on the information of the previous time instant. The Kalman Filter must be linearized in order to be applied to dynamic state estimation since the power system is a nonlinear system. The most popular solutions for linearizing the Kalman Filter in literature are the Extended Kalman Filter (EKF) [164] and the Unscented Kalman Filter (UKF) [165]. However, the EKF linearizes the equations by only keeping the first order term of the Taylor Expansion, which limits its estimation accuracy especially in large power networks that are highly nonlinear. To overcome this drawback, the Iterated Extend Kalman Filter (IEKF) [166] and Second-order Kalman Filter (SKF) [167] have been proposed which might improve the estimation accuracy by iterations and including the second order term of the Taylor Expansion. The UKF simulates the process of uncertainty propagation using a set of sigma points and thus the error will be smaller than that introduced during the linearization process of EKF. However, the UKF is still susceptible to problems including numerical inaccuracy and unavailability of a square root solution due to negatively weighted sigma points. Thus, the Cubature Kalman Filter (CKF) that optimally chooses the locations of the sigma point is proposed in this paper to enhance the performance of dynamic state estimation.

Besides the selection of nonlinear filters, the performance of the DSE is also significantly affected by a sudden change of loads [172]. In normal conditions, the power system is assumed to be in a quasi-steady state. In other words, the variation of the state of the system is slow in comparison to the update rate of state estimation. However, this assumption might not be satisfied in the cases where there is a sudden change of load(s), or a removal of a branch to clear the fault. In these cases, the prediction which is made based on the normal operating condition will be erroneous, and will significantly degrade the performance of the DSE. Apart from the sudden change of load which results in the wrong prediction of the states, the measurements might also be smeared (i.e. the quality of the measurements is degraded) due to the existence of bad data. So, it is crucial for the DSEs to accurately detect, discriminate and identify these anomalies. Reference [69] assigns different weighting factors for the predictions and measurements so that those containing large errors are depressed after they are given smaller weightings. The drawback of this method is that not all predictions are rejected when a

sudden change of states happens, and the varied weightings only take effect at the next iteration making it difficult to detect and minimize the effect of the anomalies. It is pointed out in [76] and [77] that the anomalies can be detected and identified using normalised innovations of the measurements. However, methods are not given for identifying the anomalies, and there is no further study or assessment of different scenarios.

In this chapter, a new algorithm for dynamic state estimation based on the CKF using the normalised innovation of the measurements and the skewness for accurately detecting and identifying the anomalies, is proposed. The proposed algorithm would detect, discriminate and take different actions for the three different types of anomaly: reject the prediction for sudden change of load, identify the removed branch and update the topology after the fault, and reject the identified bad data. The simulation also compares the performance of CKF and other nonlinear filters including EKF, IEKF, SKF and UKF. It is demonstrated that the CKF has better performance in terms of estimation accuracy, and higher sensitivity for detecting anomalies.

In the following sections of this chapter, system dynamic models will be firstly discussed in Section 6.3, five different types of nonlinear filter will then be discussed in Section 6.4, then methods for anomaly identification will be presented in Section 6.5, then the proposed algorithm for dynamic state estimation will be presented in Section 6.6, then simulation settings will be presented in Section 6.7, after that simulation results and analysis will be discussed in Section 6.8, finally this chapter will be summarised in Section 6.9.

6.2 Dynamic State Estimators

While the SSE only uses the measurements to produce the state estimate, the DSE estimates the states of the system based on both the measurements but also the changing / dynamic behaviour of the states. Since state estimation is performed discontinuously at an interval of a few minutes, a discrete DSE is used in Thesis. A general structure of the discrete DSE is illustrated in Figure 6-1. The structure can be divided into two parts. The first part is a dynamic

model. It describes the dynamic behaviour by a set of state transition functions, which can be used to calculate the predicted state at Time k ($\bar{\mathbf{x}}_k$) based on the input at Time k ($\mathbf{u}_k$) and the estimate at Time k-1 ($\hat{\mathbf{x}}_{k-1}$). Details about the dynamic models will be discussed in Section 6.3, and the expression of the state transition function will be given in (6.1). The second part of the DSE is a nonlinear filter. It is capable of calculating an unbiased estimate of the states ($\hat{\mathbf{x}}_k$) combining the predictions ($\bar{\mathbf{x}}_k$) and the measurements ($\mathbf{z}_k$). A detailed description of five nonlinear filters available for power system DSE will be given in Section 6.4.

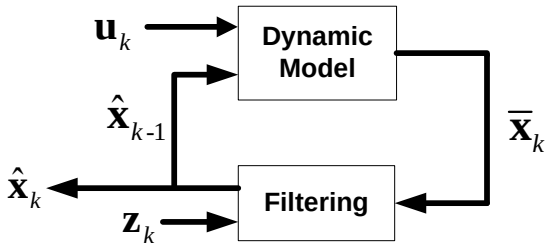

Figure 6-1: General Structure of the Discrete DSE

6.3 System Dynamic Models

This section introduces the dynamic model used in the DSEs, based on which the prediction of the states is made.

The first question which must be answered for developing a dynamic model is what kind of dynamics of the system should be considered, or what kind of dynamics are relevant for the purpose of power system state estimation. As introduced at the beginning of Chapter 2, the power system operates in either normal state or in emergency state when perturbations happen. Although the dynamics of the voltage and other variables such as the angle of the internal emf, δ, and the rotor angular speed ω_m, of the perturbed bus can be described by a set of dynamic equations, only a small proportion of the perturbations can be perceived by the system operator through the measurement system. In addition, security analysis needs records of the operation conditions of the power system as a reference base case. Furthermore, the power system operates in quasi steady states. In other words, the changing of the states is very slow in comparison to the update rate of state estimators. Thus, it is reasonable to model the dynamics of the power system as a succession of correlated steady states. Therefore, the aim of the

dynamic model for power system state estimation should be to track the trend of changes rather than track the dynamic responses of the states to the random disturbances. It is true that in literature some new DSEs have been proposed that use dynamic models considering the dynamics of the generator [170]-[171]. However, these methods only consider the states and parameters of a single bus that is connected to a generator. So, this PhD work adopted a prediction model named Holt's Linear Exponential Smoothing technique [171] as the dynamic model for DSE, which predicts the states based on the trend indicated by the previous states and parameters. The mathematical expressions of this dynamic model are described below:

The discrete state transition function can be generally represented by a difference equation given by (6.1):

$$\mathbf{x}_{k+1} = \mathbf{F}_k \mathbf{x}_k + \mathbf{g}_k + \mathbf{q}_k \tag{6.1}$$

where **x** is the state vector, **F** is the state transition matrix, **g** is the input vector, **q** is the process error vector, and the subscript represents the number of the time instant.

The parameters, **F** and **g**, are derived as given in (6.2)-(6.3):

$$\mathbf{F}_k = \alpha_k (1+\beta_k) \cdot \mathbf{I} \tag{6.2}$$

$$\mathbf{g}_k = (1+\beta_k)(1-\alpha_k)\mathbf{x}_k^- - \beta_k \mathbf{a}_{k-1} + (1-\beta_k)\mathbf{b}_{k-1} \tag{6.3}$$

where **I** is the identity matrix of the size of the state vector, and α_k and β_k are two scaler parameters in the range from 0 to 1, $\mathbf{x}_k^-$ is the state of predicted states at time k, and parameter vectors **a** and **b** at time k can be obtained according to (6.4)-(6.5):

$$\mathbf{a}_k = \alpha_k \mathbf{x}_k + (1-\alpha_k)\mathbf{x}_k^- \tag{6.4}$$

$$\mathbf{b}_k = \beta_k (\mathbf{a}_k - \mathbf{a}_{k\text{-}1}) + (1-\beta_k)\mathbf{b}_{k\text{-}1} \tag{6.5}$$

In the simulations presented in this chapter, $\alpha_k = 0.8$, $\beta_k = 0.5$ for $k = 1, 2, 3 \ldots$ The choice of these parameters are explained in [171].

6.4 Nonlinear Filters

This section discusses the mathematical formulations of the five nonlinear Kalman Filters introduced at the beginning of this chapter. All of the nonlinear Kalman Filters are capable of solving the dynamic state estimation problem as expressed in (6.6)-(6.9):

$$\mathbf{x}_k = \mathbf{f}\left(\mathbf{x}_{k-1}, k-1\right) + \mathbf{q}_{k-1} \tag{6.6}$$

$$\mathbf{z}_k = \mathbf{h}\left(\mathbf{x}_k, k\right) + \mathbf{r}_k \tag{6.7}$$

$$\sigma^2\left(\mathbf{q}_{k-1}\right) = \mathbf{Q}_{k-1} \tag{6.8}$$

$$\sigma^2\left(\mathbf{r}_{k-1}\right) = \mathbf{R}_{k-1} \tag{6.9}$$

where **f** is the general expression for the system state transition matrix as detailed in (6.1)-(6.5), **q** is a vector consisting of the zero-mean Gaussian errors, **z** is the measurement vector, **h** is the nonlinear measurement function, and **r** is the vector consisting of measurement errors.

6.4.1 Extended Kalman Filter

The estimation process of Extended Kalman Filter (EKF) can be roughly divided into two steps of prediction and correction as shown in the equations below:

Prediction:

$$\mathbf{x}_{\mathrm{k}}^{-} = \mathbf{f}\left(\mathbf{x}_{k-1}, k-1\right) \tag{6.10}$$

$$\mathbf{P}_k^{-} = \mathbf{F}_k \mathbf{P}_{k-1} \mathbf{F}_k^T + \mathbf{Q}_{k-1} \tag{6.11}$$

Correction:

$$\mathbf{K}_k = \mathbf{P}_k^{-} \mathbf{H}_k^T \left(\mathbf{H}_k \mathbf{P}_k^{-} \mathbf{H}_k^T + \mathbf{R}_k\right)^{-1} \tag{6.12}$$

$$\mathbf{x}_k^{+} = \mathbf{x}_k^{-} + \mathbf{K}_k \left[\mathbf{z}_k - \mathbf{h}\left(\mathbf{x}_k^{-}\right)\right] \tag{6.13}$$

$$\mathbf{P}_k^{+} = \left(\mathbf{I} - \mathbf{K}_k \mathbf{H}_k\right) \mathbf{P}_k^{-} \tag{6.14}$$

where $\mathbf{P}_k^-$ is the covariance matrix of $\mathbf{x}_k^-$, $\mathbf{F}$ is the Jacobian matrix of $\mathbf{f}$ with respect to $\mathbf{x}$, $\mathbf{H}$ is the Jacobian matrix of $\mathbf{h}$ with respect to $\mathbf{x}$, $\mathbf{K}_k$ is the Kalman gain, $\mathbf{z}_k$ is the measurement vector, $\mathbf{x}_k^+$ is the final estimate of the states after correction, $\mathbf{I}$ is the identity matrix, and $\mathbf{P}_k^+$ is the covariance matrix of $\mathbf{x}_k^+$.

6.4.2 Iterated Extend Kalman Filter

In highly nonlinear systems, the estimate given by the EKF may not be accurate due to its practice of first order approximation of the Taylor Expansion of the equations, one of the methods that could improve the estimate, $\mathbf{x}_k$, given by (6.13) is to iteratively calculate $\mathbf{x}_k$ until the difference between $\mathbf{x}_{k,i}$ and $\mathbf{x}_{k,i\text{-}1}$ is within a given threshold, where the subscript i denotes the number of iteration. Thus, this alternative form of the EKF is called Iterated Extended Kalman Filter (IEKF). The IEKF can also be divided in the prediction and correction stages, and the expressions are given as:

Prediction

$$\mathbf{x}_{\mathrm{k}}^{-} = \mathbf{f}\left(\mathbf{x}_{k-1}, k-1\right) \tag{6.15}$$

$$\mathbf{P}_k^{-} = \mathbf{F}_k \mathbf{P}_{k-1} \mathbf{F}_k^T + \mathbf{Q}_{k-1} \tag{6.16}$$

Correction

$$\mathbf{K}_{k,i} = \mathbf{P}_k^{-} \mathbf{H}_{k,i}^T \left(\mathbf{H}_{k,i} \mathbf{P}_k^{-} \mathbf{H}_{k,i}^T + \mathbf{R}_k\right)^{-1} \tag{6.17}$$

$$\mathbf{x}_{k,i+1}^{+} = \mathbf{x}_k^{-} + \mathbf{K}_{k,i}\left[\mathbf{z}_k - \mathbf{h}\left(\mathbf{x}_{k,i+1}^{+}\right) - \mathbf{H}_{k,i}\left(\mathbf{x}_k^{-} - \mathbf{x}_{k,i+1}^{+}\right)\right] \tag{6.18}$$

$$\mathbf{P}_{k,i+1} = \left(\mathbf{I} - \mathbf{K}_{k,i}\mathbf{H}_{k,i}\right)\mathbf{P}_k^{-} \tag{6.19}$$

$$\mathbf{x}_{k,0}^{+} = \mathbf{x}_k^{-} \tag{6.20}$$

6.4.3 Second-order Extend Kalman Filter

Another way to reduce the estimation error of the EKF during linearization is to introduce higher order terms of the Taylor Expansion of the measurement function. The most widely used high-order EKF is the second-order EKF (SKF).

Prediction:

$$\mathbf{x}_{\mathrm{k}}^{-} = \mathbf{f}\left(\mathbf{x}_{k-1}, k-1\right) \tag{6.21}$$

$$\mathbf{P}_{k}^{-} = \mathbf{F}_{k}\mathbf{P}_{k-1}\mathbf{F}_{k}^{T} + \mathbf{Q}_{k-1} \tag{6.22}$$

Correction:

$$\mathbf{K}_{k} = \mathbf{P}_{k}^{-}\mathbf{H}_{k}^{T}\left(\mathbf{H}_{k}\mathbf{P}_{k}^{-}\mathbf{H}_{k}^{T} + \mathbf{R}_{k} + \mathbf{A}_{k}\right)^{-1} \tag{6.23}$$

$$\mathbf{x}_{k-1}^{+} = \mathbf{x}_{k}^{-} + \mathbf{K}_{k}\left[\mathbf{z}_{k} - \mathbf{h}\left(\mathbf{x}_{k}^{-}\right) - \frac{1}{2}\partial^{2}\left(\mathbf{h}_{k}, \mathbf{P}_{k}^{-}\right)\right] \tag{6.24}$$

$$\mathbf{P}_{k}^{+} = \left(\mathbf{I} - \mathbf{K}_{k}\mathbf{H}_{k}\right)\mathbf{P}_{k}^{-} \tag{6.25}$$

where $\partial^{2}\left(\mathbf{f}, \mathbf{B}\right)$ is the second-order term operator, for any function **f**(**x**) and any matrix, **B**, whose i^{th} term is defined as given in (6.26) and the matrix, $\mathbf{A}_k$, is defined in (6.27).

$$\partial_{i}^{2}\left(\mathbf{f}, \mathbf{B}\right) = \operatorname{trace}\left[\frac{\partial^{2} f_{i}}{\partial \mathbf{x} \partial \mathbf{x}^{T}}\mathbf{B}\right] \tag{6.26}$$

$$\begin{aligned}\mathbf{A}_{k} = {} & \frac{1}{4}\mathrm{E}\left[\partial^{2}\left(\mathbf{h}_{k}, \tilde{\mathbf{x}}_{k}^{-}\left(\tilde{\mathbf{x}}_{k}^{-}\right)^{T}\right)\partial^{2}\left(\mathbf{h}_{k}, \tilde{\mathbf{x}}_{k}^{-}\left(\tilde{\mathbf{x}}_{k}^{-}\right)^{T}\right)^{T}\right] \\ & -\frac{1}{4}\mathrm{E}\left[\partial^{2}\left(\mathbf{h}_{k}, \mathbf{P}_{k}^{-}\right)\partial^{2}\left(\mathbf{h}_{k}, \mathbf{P}_{k}^{-}\right)^{T}\right]\end{aligned} \tag{6.27}$$

where f_i is the i^{th} element of **f**, E is the expectation function, and $\tilde{\mathbf{x}}_{k}^{-}$ is the predicted state residual vector as given by (6.28):

$$\tilde{\mathbf{x}}_{k}^{-} = \mathbf{x}_{k,true} - \mathbf{x}_{k}^{-} \tag{6.28}$$

The ij^{th} element of $\mathbf{A}_k$, $a_{k,ij}$,can be approximated by (6.29). To avoid massive loop calculations, $a_{k,ij}$ can be expressed in a compact way as given in (6.30):

$$a_{k,ij} \approx \frac{1}{4}\left[\sum_{p,q,m,n} \frac{\partial^2 h_{k,i}}{\partial x_p \partial x_q} \left(p_{k,pm} p_{k,qn} + p_{k,pn} p_{k,qm} \right) \frac{\partial^2 h_{k,i}}{\partial x_m \partial x_n} \right] \tag{6.29}$$

$$a_{k,ij} \approx \frac{1}{4}\left[sum\left(\left(\ddot{\mathbf{H}}_{k,i} \mathbf{P}_k^- \right) .* \left(\ddot{\mathbf{H}}_{k,j} \mathbf{P}_k^- \right)^T + \left(\ddot{\mathbf{H}}_{k,i} \mathbf{P}_k^- \right)^T .* \left(\ddot{\mathbf{H}}_{k,j} \mathbf{P}_k^- \right) \right) \right] \tag{6.30}$$

where $h_{k,i}$ is the i^{th} element of $\mathbf{h}_k$, $p_{k,ij}$ is the ij^{th} element of $\mathbf{P}_k^-$, the operator .* denotes element-wise multiplication, the function *sum* obtains the sum of all elements in the matrix, and $\ddot{\mathbf{H}}_{k,i}$ is defined in (6.31):

$$\ddot{\mathbf{H}}_{k,i} = \frac{\partial^2 h_{k,i}}{\partial \mathbf{x} \partial \mathbf{x}^T} \tag{6.31}$$

6.4.4 Unscented Kalman Filter

The Unscented Kalman Filter (UKF) is developed based on the Unscented Transform (UT) theory. Instead of using the Taylor expansion to linearize the measurement function the UKF propagates a set of sigma points generated according to the statistical distribution of the states through nonlinear functions. Thus, the UKF does not need to calculate the Jacobian matrices to estimate the states and the covariance. Therefore, the UKF could improve the performance of the DSE in terms of both accuracy and execution speed especially for the highly nonlinear systems. The procedure of the UKF involves four steps of sigma point generation, state prediction, measurement prediction, and correction. Each of the steps is formulated as follows:

Sigma Point Generation:

The first step of UKF is to generate a set of $2n+1$ (n is the number of states) sigma points, which can be expressed in a compact form as shown in (6.32):

$$\begin{aligned} \mathbf{X}_{\text{k-1}} &= [\boldsymbol{\chi}_0 \quad \cdots \quad \boldsymbol{\chi}_{2n}] \\ &= [\mathbf{x}_{k-1}^+ \quad \cdots \quad \mathbf{x}_{k-1}^+] + \sqrt{3}[\mathbf{0} \quad \sqrt{\mathbf{P}_{k-1}^+} \quad -\sqrt{\mathbf{P}_{k-1}^+}] \end{aligned} \tag{6.32}$$

State Prediction:

$$\mathbf{X}_k^- = \mathbf{f}(\mathbf{X}_{k-1}, k-1) \tag{6.33}$$

$$\mathbf{x}_k^- = \hat{\mathbf{X}}_k \boldsymbol{\omega}_m \tag{6.34}$$

$$\mathbf{P}_k^- = \mathbf{X}_k^- \mathbf{W} \left(\mathbf{X}_k^-\right)^T + \mathbf{Q}_{k-1} \tag{6.35}$$

$$\begin{aligned} \mathbf{W} &= (\mathbf{I} - [\boldsymbol{\omega}_m \quad \cdots \quad \boldsymbol{\omega}_m]) \cdot diag(W_0^c \cdots \quad W_{2n}^c) \\ &\cdot (\mathbf{I} - [\boldsymbol{\omega}_m \quad \cdots \quad \boldsymbol{\omega}_m])^T \end{aligned} \tag{6.36}$$

where $\mathbf{X}_k^-$ is the prediction of $\mathbf{X}_k$, $\mathbf{W}$ is the weighting matrix, the definitions of the weighting vector, $\boldsymbol{\omega}_m$, and $W_0^c \ldots W_{2n}^c$ are defined below:

$$\boldsymbol{\omega}_m = [W_0^m \; W_1^m \cdots W_{2n}^m]^T \tag{6.37}$$

$$W_0^m = 1 - n/3 \tag{6.38}$$

$$W_i^m = 1/6, i = 1, 2, ..., 2n \tag{6.39}$$

$$W_0^c = 3 - n/3 \tag{6.40}$$

$$W_i^c = 1/6, i = 1, 2, ..., 2n \tag{6.41}$$

Measurement Prediction:

$$\boldsymbol{\Gamma}_k^- = \mathbf{h}(\mathbf{X}_k^-, k) \tag{6.42}$$

$$\mathbf{z}_k^- = \boldsymbol{\Gamma}_k^- \boldsymbol{\omega}_m \tag{6.43}$$

$$\mathbf{P}_{z,k}^- = \boldsymbol{\Gamma}_k^- \mathbf{W} \left(\boldsymbol{\Gamma}_k^-\right)^T + \mathbf{R}_k \tag{6.44}$$

$$\mathbf{P}_{xz,k}^- = \mathbf{X}_k^- \mathbf{W} \left(\boldsymbol{\Gamma}_k^-\right)^T \tag{6.45}$$

where $\boldsymbol{\Gamma}_k^-$ is the resulting matrix after propagating $\mathbf{X}_k^-$ through $\mathbf{h}$, $\mathbf{z}_k^-$ is the predicted measurement vector, $\mathbf{P}_{z,k}^-$ is the covariance of the predicted measurements, and $\mathbf{P}_{xz,k}^-$ is the covariance between the predicted states and the predicted measurements.

Correction:

$$\mathbf{K}_k = \mathbf{P}_{xz,k}^- \left(\mathbf{P}_{z,k}^-\right)^{-1} \tag{6.46}$$

$$\mathbf{x}_k^+ = \mathbf{x}_k^- + \mathbf{K}_k\left(\mathbf{z}_k - \mathbf{z}_k^-\right) \tag{6.47}$$

$$\mathbf{P}_k^+ = \mathbf{P}_k^- - \mathbf{K}_k\mathbf{P}_{xz,k}^- \tag{6.48}$$

6.4.5 Cubature Kalman Filter

The Cubature Kalman Filter (CKF) is a new accurate and highly efficient nonlinear filter proposed in 2009 [172]. It was developed based on the spherical-radial cubature rule which allows the CKF to quickly and accurately calculate multivariate moment integrals within the Bayesian filtering paradigm. In contrast to the other nonlinear filters, the CKF requires the process noises and measurement noises to be Gaussian noises to ensure an accurate estimate of the states. Thus, under the common assumption of Gaussian noises, the estimation process of the CKF is expressed in three steps as follows:

State Prediction:

$$\mathbf{x}_{\mathrm{k}}^- = \int_{\mathbb{R}^n} \mathbf{f}\left(\mathbf{x}_{k-1}, k-1\right) N\left(\mathbf{x}_{k-1}; \mathbf{x}_{k-1}^+, \mathbf{P}_{k-1}^+\right) d\mathbf{x}_{k-1} \tag{6.49}$$

$$\begin{aligned}\mathbf{P}_k^- = &\int_{\mathbb{R}^n} \mathbf{f}\left(\mathbf{x}_{k-1}, k-1\right)\mathbf{f}^T\left(\mathbf{x}_{k-1}, k-1\right) \\ &\cdot N\left(\mathbf{x}_{k-1}; \mathbf{x}_{k-1}^+, \mathbf{P}_{k-1}^+\right) d\mathbf{x}_{k-1} - \mathbf{x}_k^-\left(\mathbf{x}_k^-\right)^T\end{aligned} \tag{6.50}$$

where $N(\mathbf{x};\boldsymbol{\mu},\mathbf{P})$ represents the Gaussian density for variable $\mathbf{x}$ with the mean value of $\boldsymbol{\mu}$, and covariance of $\mathbf{P}$,

Measurement Prediction:

$$\mathbf{z}_k^- = \int_{\mathrm{R}^n} \mathbf{h}\left(\mathbf{x}_k, k\right) N\left(\mathbf{x}_k; \mathbf{x}_k^-, \mathbf{P}_k^-\right) d\mathbf{x}_k \tag{6.51}$$

$$\mathbf{P}_{z,k}^- = \int_{\mathrm{R}^n} \mathbf{h}\left(\mathbf{x}_k, k\right)\mathbf{h}^T\left(\mathbf{x}_k, k\right) N\left(\mathbf{x}_k; \mathbf{x}_k^-, \mathbf{P}_k^-\right) d\mathbf{x}_k - \mathbf{z}_k^-\left(\mathbf{z}_k^-\right)^T \tag{6.52}$$

$$\mathbf{P}_{xz,k}^- = \int_{\mathrm{R}^n} \mathbf{x}_k\mathbf{h}^T\left(\mathbf{x}_k, k\right) N\left(\mathbf{x}_k; \mathbf{x}_k^-, \mathbf{P}_k^-\right) d\mathbf{x}_k - \mathbf{x}_k^-\left(\mathbf{z}_k^-\right)^T \tag{6.53}$$

Correction:

$$\mathbf{K}_k = \mathbf{P}_{xz,k}^{-} \left(\mathbf{P}_{z,k}^{-} \right)^{-1} \tag{6.54}$$

$$\mathbf{x}_k^{+} = \mathbf{x}_k^{-} + \mathbf{K}_k [\mathbf{z}_k - \mathbf{z}_k^{-}] \tag{6.55}$$

$$\mathbf{P}_k^{+} = \mathbf{P}_k^{-} - \mathbf{K}_k \mathbf{P}_{xz,k}^{-} \tag{6.56}$$

Because of the difficulty in directly calculating the multivariate integrals as listed in (6.51)-(6.56), they can be very accurately approximated using the spherical-radial cubature rule, and the procedures are given in (6.57)-(6.59).

$$\begin{aligned} I_N(\mathbf{f}) &= \int_{\mathbb{R}^n} \mathbf{f}(\mathbf{x}) N(\mathbf{x}; \boldsymbol{\mu}, \mathbf{P}) d\mathbf{x} \\ &\approx \sum_{i=1}^{2n} \omega_i \mathbf{f}\left(\boldsymbol{\mu} + \sqrt{\mathbf{P}} \xi_i \right) \end{aligned} \tag{6.57}$$

$$\xi_i = \begin{cases} -\sqrt{n} e_i & \text{for } i = 1, ..., n \\ \sqrt{n} e_{i-n} & \text{for } i = n+1, ..., 2n \end{cases} \tag{6.58}$$

$$\omega_i = \frac{1}{2n}, i = 1, ..., 2n \tag{6.59}$$

where e_i is a singleton vector where all of its elements are 0's except for its i^{th} element being 1, ξ_i, i=1, ... 2n, are the cubature points, ω_i, i=1, ... 2n, are the weightings of the cubature points.

The cubature points can be generated in a similar way to the way in which the sigma points are generated in the UKF. However, they choose different locations for the cubature / sigma points with different weightings. For instance, the cubature points (6.60) and sigma points (6.62) and their corresponding weightings ((6.61) and (6.63) respectively) of a four-state vector with 0 mean and unity covariance can be expressed as follows. Apart from the clear difference seen between the cubature points and the sigma points, it can also be observed that one element of the weighting vector of the sigma points is less than 0, which may result in a non-positive covariance matrix and eventually lead to non-convergence of the DSE.

$$\boldsymbol{\xi} = \begin{bmatrix} \xi_1 & \xi_2 & \cdots & \xi_8 \end{bmatrix} = \begin{bmatrix} -\mathbf{I}_{4\times4} & \mathbf{I}_{4\times4} \end{bmatrix} \tag{6.60}$$

$$\begin{bmatrix} \omega_1 & \omega_2 & \cdots & \omega_8 \end{bmatrix} = \begin{bmatrix} \frac{1}{8} & \frac{1}{8} & \cdots & \frac{1}{8} \end{bmatrix} \tag{6.61}$$

$$\mathbf{X} = \begin{bmatrix} \boldsymbol{\chi}_0 & \boldsymbol{\chi}_1 & \boldsymbol{\chi}_2 & \cdots & \boldsymbol{\chi}_8 \end{bmatrix} = \sqrt{3}\begin{bmatrix} \mathbf{0}_{4\times 1} & -\mathbf{I}_{4\times 4} & \mathbf{I}_{4\times 4} \end{bmatrix} \tag{6.62}$$

$$\begin{bmatrix} W_0 & W_1 & W_2 & \cdots & W_8 \end{bmatrix} = \begin{bmatrix} -\frac{1}{3} & \frac{1}{6} & \frac{1}{6} & \cdots & \frac{1}{6} \end{bmatrix} \tag{6.63}$$

6.5 Anomaly Identification

In this section, new methods for detection, discrimination and identification of the three different types of anomalies including sudden change of load, sudden change of topology after the clearance of fault and bad data, will be discussed. The purpose of identifying the anomalies is that the existence of these anomalies will severely degrade the estimation accuracy of the DSEs, which will be demonstrated in Section 6.8.

6.5.1 Anomaly Detection and Discrimination

The anomalies of different types are detected and identified based on their different impacts on the estimation errors of the different measurements. Since the true values of the measurements are unknown, the absolute values of the errors of the measurements are also unknown. Thus, the normalised innovations (NIs), which is defined as the normalised difference between the measurements and the predicted measurements, are used to quantify the magnitude of the errors instead. The NIs can be obtained from the normalised innovation vector, which can be calculated following (6.64).

$$\boldsymbol{\tau}_k = \left(\mathbf{z}_k - \mathbf{z}_k^-\right) / \sqrt{\mathbf{P}_{z,k}^-} \tag{6.64}$$

where the definition of the predicted measurement $\mathbf{z}_k^-$, and its covariance, $\mathbf{P}_{z,k}^-$, of the UKF and the CKF have already been given in (6.43)-(6.44) and (6.51)-(6.52) respectively, and that of the EKF, IEKF and SKF are given in (6.65) and (6.66) respectively.

$$\mathbf{z}_k^- = \mathbf{h}\left(\mathbf{x}_k^-\right) \tag{6.65}$$

$$\mathbf{P}_{z,k}^- = \mathbf{H}_k \mathbf{P}_k^- \mathbf{H}_k^T + \mathbf{R}_k \tag{6.66}$$

All three types of anomalies could significantly increase the NIs. As well as this, they could affect the distribution of the elements in the normalised innovation vector. The skewness of the normalised innovation vector is introduced to quantify the asymmetry of the affected distribution as defined in (6.67)-(6.69).

$$M_{3,k} = \mathrm{E}\left[\left(\boldsymbol{\tau}_k\right)^{.*3}\right] - 3v_k\,\mathrm{E}\left[\left(\boldsymbol{\tau}_k\right)^{.*2}\right] + 2v_k^3 \tag{6.67}$$

$$\sigma_k^2 = \mathrm{E}\left[\left(\boldsymbol{\tau}_k\right)^{.*2}\right] - v_k^2 \tag{6.68}$$

$$v_k = \mathrm{E}\left[\boldsymbol{\tau}_k\right] \tag{6.69}$$

where the operator, *.*n*, denotes elementwise exponential calculation with the exponent *n*.

It is assumed that the anomalies happen very rarely and even when they do, at most only one anomaly happens at any time. Assuming that the anomaly happens at time instant *k*, the impacts of the anomalies on the normalised innovation and its skewness are summarised in Table 6-1.

Table 6-1: The Effects of Different Types of Anomalies on Normalised Innovations and Skewness

Anomalies	Normalised Innovation	Skewness
Bad Data	Single NI much greater than the normal value	Skewness at Time *k* much greater than the normal value
Sudden Load Change	Multiple NIs greater than the normal value	No skewness beyond the normal value, or the skewness at Time *k* slightly greater than the normal value
Fault	Multiple NIs much greater than the normal value	The skewness at and after Time *k* all greater than the normal value

Bad data can only affect a single measurement at a given time instant; thus only the NI of the measurement smeared by the bad data and only the skewness at that time instant will be greater than their normal values. In comparison, the sudden change of load will change the overall power flow in the network, and thus many states and many predicted measurements will be affected. This results in multiple NIs greater than the normal values. Its impact on the skewness of the NIs is affected by the size of the network: if the size of the network is small, the skewness of the NIs will stay more or less the same since almost all states are evenly affected

by the sudden change of load; if the size of the network is large, then the skewness of the NIs will be slightly more than the normal value, since states will be affected differently by the sudden change of load according to their distance to the load.

The clearance of the fault can be done by removing one of the branches in the network. If such an action is not reported to the state estimator in time, then errors will happen persistently at both stages of state prediction and measurement prediction. This is because the measurements are made from the network with new topology, while the predictions of states and measurements are based on the old topology. So, both NI and its skewness at and after time instant k will be greater than their normal values. Based on the different responses of NI and the skewness to the different anomalies, a unified algorithm is proposed as shown in Figure 6-2. Note Ck_{th1} and Ck_{th2} are two thresholds for the skewness at Time k, and $Ck_{th1} < Ck_{th2}$. These two thresholds are set to identify sudden load change in small networks and large networks, respectively.

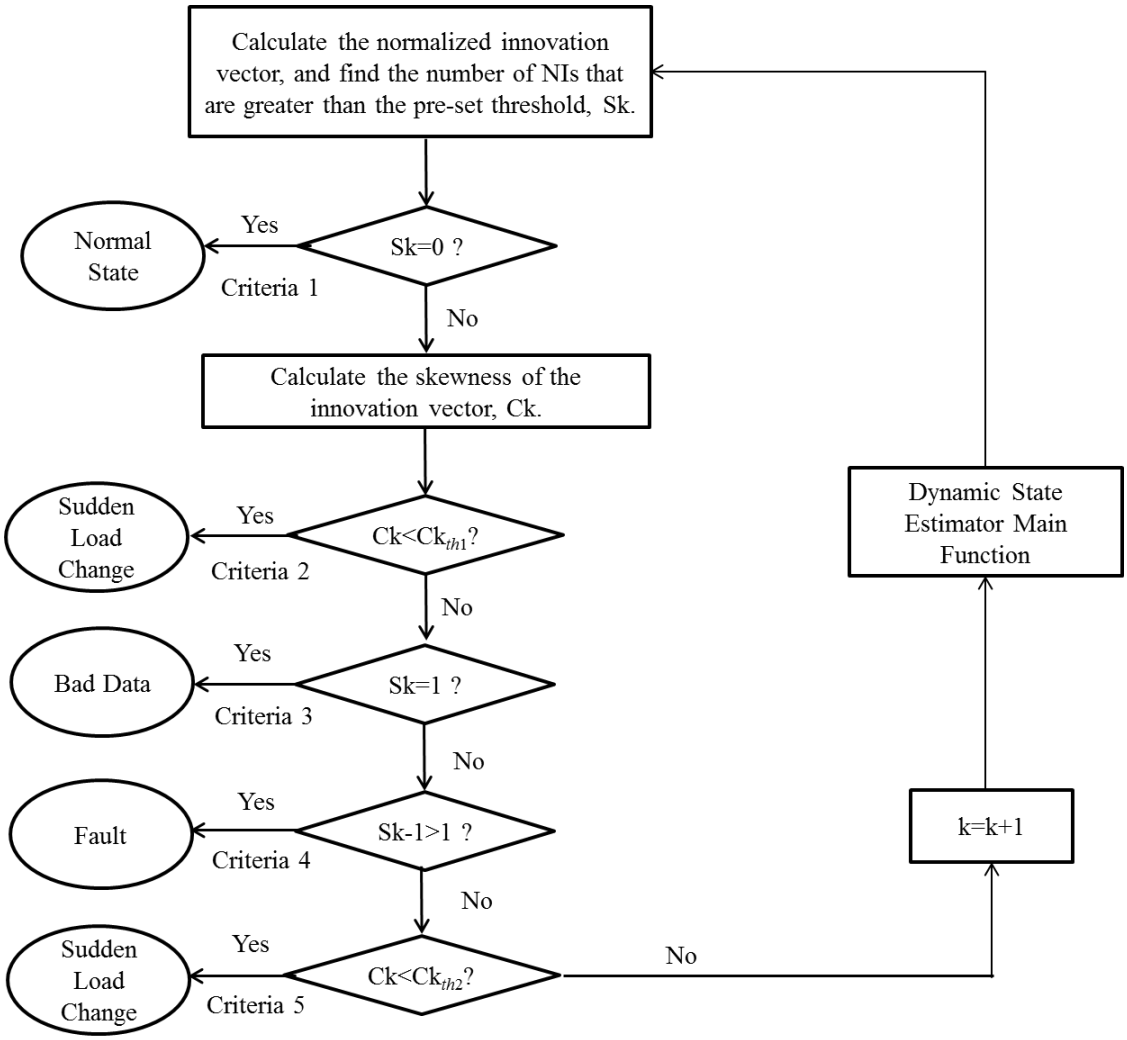

Figure 6-2: Algorithm for Anomaly Identification

6.5.2 Identification of the Anomalies

It was shown in Section 2.3 that bad data identification for SSE have been realised by using the largest normalised residual test method. Based on this method, the bad data identification for DSE can be done easily using a similar method of the largest normalised residual test: the measurement that has the largest NI is identified as the bad data since in this case only one NI will be greater than the normal value. However, the location where a sudden change of load or topology change cannot be identified directly because these events will cause multiple NIs

greater than their normal values. Two methods are proposed below to identify the location of the latter two types of anomalies.

6.5.2.1 Identification of Sudden Load Change Bus

A pseudo power injection method for the CKF is proposed below for identification of the bus that experienced sudden load change:

Step a. Identify the buses that possess load and calculate the average load of these buses, select the buses whose load is larger than 10% of the average load.

Step b. Compute the predicted active power injection measurements of the selected buses , $\mathbf{z}_l^-$, and the corresponding covariance matrix, $\mathbf{P}_l^-$, as shown in (6.70):

$$\mathbf{z}_l^- = \int_{\mathrm{R}^n} \mathbf{h}_l\left(\mathbf{x}_k, k\right) N\left(\mathbf{x}_k; \mathbf{x}_k^-, \mathbf{P}_k^-\right) d\mathbf{x}_k \tag{6.70}$$

where $\mathbf{h}_l$ consists of functions of the active power injection incident to the selected buses in Step a.

Step c. Compute the updated active power injection measurements, $\mathbf{z}_l^+$, as given in (6.71):

$$\mathbf{z}_l^+ = \int_{\mathrm{R}^n} \mathbf{h}_l\left(\mathbf{x}_k, k\right) N\left(\mathbf{x}_k; \mathbf{x}_k^+, \mathbf{P}_k^+\right) d\mathbf{x}_k \tag{6.71}$$

Step d. Compute the mutual covariance between $\mathbf{z}_l^-$ and $\mathbf{z}_l^+$, $\mathbf{P}_l$:

$$\mathbf{P}_l = \int_{\mathrm{R}^n} \mathbf{h}_l\left(\mathbf{x}_k, k\right) \mathbf{h}_l^T\left(\mathbf{x}_k, k\right) N\left(\mathbf{x}_k; \mathbf{x}_k^+, \mathbf{P}_k^+\right) d\mathbf{x}_k - \mathbf{z}_l^+\left(\mathbf{z}_l^+\right)^T \tag{6.72}$$

Step e. Compute the normalised innovation vector of the pseudo power injection measurements, $\boldsymbol{\tau}_l$.

$$\boldsymbol{\tau}_l = \left|\mathbf{z}_l^- - \mathbf{z}_l^+\right| / \sqrt{\mathbf{P}_l} \tag{6.73}$$

Step f. Find the largest NI, or the largest element of $\boldsymbol{\tau}_l$, its corresponding bus is identified at the bus where sudden load change happens.

6.5.2.2 Identification of the Removed Branch after Fault Clearance

The branch removed after the fault clearance can be identified before the update of the topology of the network if the power flows and currents in all branches are monitored. The procedures are shown in the following steps:

Step A. Select a set of uni-direct power flow measurements that cover all branches of the network, M.

Step B. Store the measurements received at time instant $k \in M$ into a vector, m_k.

Step C. If a fault is detected at time instant k, calculate the variation ratio, $\mathbf{r}_m$, according to (6.74). Find the largest element of $\mathbf{r}_m$, its corresponding branch is identified to be the removed branch.

$$\mathbf{r}_m = \left| \ln \left(\left| m_{k-1} / m_k \right| \right) \right| \tag{6.74}$$

6.6 Dynamic State Estimation Using the Cubature Kalman Filter

Based on the new algorithm for anomaly detection and identification presented in the previous section and the cubature spherical rule, a novel dynamic state estimation algorithm applying the CKF is proposed as follows:

Begin: Calculate $\mathbf{f}_k$ and $\mathbf{Q}_k$ according to (6.1)-(6.7), and $\mathbf{h}_k$ and $\mathbf{R}_k$ according to (6.8)-(6.9), respectively. $\mathbf{a}_0 = \mathbf{x}_{-1}$, $\mathbf{b}_0 = \mathbf{0}$, $\mathbf{x}_0^+ = \mathbf{x}_0^- = \mathbf{x}_0$, $\mathbf{P}_{k0}^+ = \mathbf{Q}_0$. Set $k = 1$, stop = 0, and define k_{max}

While (stop = 0)

{

Step 1. Generate the cubature points and the weightings as described in (6.58) and (6.59).

Step 2. Predict the states according to (6.49)-(6.50).

Step 3. Predict the measurements according to (6.51)-(6.53).

Step 4. Calculate the Kalman estimate according to (6.54)-(6.56).

Step 5. Detect and discriminate the anomaly using the algorithm shown in Figure 6-2.

Step 6. According to the type of anomaly detected in Step 5, use the normalised innovation method to identify the bad data, the pseudo power injection method to identify the sudden load change bus following Step a to Step f , and follow Step A to Step C to identify the removed bus after fault if possible.

Step 7. Reject the bad data and go back to Step 5 if the bad data is identified, reject the prediction and calculate the new state estimate using static state estimator if the sudden load change is identified, and update the network topology and use static state estimator to find the new state estimate if the removed branch is identified.

Step 8. Output $\mathbf{x}_k^+$ and $\mathbf{P}_k^+$. Set $k = k+1$.

Step 9. If a stop signal is received or $k = k_{max}$, set stop = 1.}

6.7 Simulation Settings

The objective of the simulations in the research is to demonstrate the advantage of the CKF based dynamic state estimator over the other nonlinear filters presented in Section 6.4, and how to use the anomaly identification algorithm to detect, discriminate and identify different types of anomaly.

In order to enable the function of bad data detection, a redundant set of conventional measurements and a redundant set of PMU measurements are chosen for the simulations in the IEEE 14 and 39 Bus Test Systems as shown in Table 6-2 and Table 6-3 respectively.

Table 6-2: Measurement Placement for the IEEE 14 Bus Test System

Voltage Magnitude at Bus #	2;3;8;10;12
Power Injection at Bus #	1;3;6;7;8;9;11;13;14
Power Flow #	1;2;4;5;6;7;13;18;19;34
PMU Voltage Phasor at Bus #	1;4
PMU Current Phasor at Branch #	1;2;7;8;9;24;26

Table 6-3: Measurement Placement for the IEEE 39 Bus Test System

Voltage Magnitude at Bus #	3;5;6;8;12;14;16;17;19;22;25;26;30;31;32;34;36;38;39
Power Injection at Bus #	3;4;7;8;12;15;16;18;20;21;23;24;25;28;29;30;31;32;33;34;36;37;38;39
Power Flow #	2;3;5;10;11;13;14;15;16;17;18;21;25;26;28;29;30;31;36;40;47;50;52;53;54;55;58;65;66;68;69;73;78;79;80;81;87;88;89;90;91;92
PMU Voltage Phasor at Bus #	2;6;9;12;14;17;22;23;29;32;33;34;37
PMU Current Phasor #	3;4;11;12;15;19;25;26;28;29;35;36;38;39;43;44;46;47;54;55;60;64;67;73;74;79;80;83;87;88;91

Note that in the IEEE 14 Bus Test System, there are 20 branches in the network. Thus, in Table 6-2 a power flow number or PMU current phasor number, *k*, which is not larger than 20, indicates the forward direction of Branch *k* defined in the test system. If the number, *k*, is larger than 20, it indicates the reversed power flow / current flow direction of Branch *k*-20. This notation also applies to the numbering of the power flow and current measurements in the IEEE 39 Bus Test System in Table 6-3, where the number of branches in the network is 46.

The assumption of a quasi-static state is represented by a gradual linear increase in some chosen loads by 20% over 50 time steps. To simulate the small fluctuations existing in the load, a random walk with a standard deviation of 3% of the magnitude of the load change is assigned to the load. It is also assumed that the generators will respond to the load increase by generating more power according to their participation factors, i.e. the proportion of power generations before the change of load.

The DSE is affected by two types of error, the process errors and measurement errors, which exist in the prediction stage and update stage respectively. The process error, **Q**, is assumed to be Gaussian error, and its covariance is set to be $1e10^{-6}$***I** in this research, where **I** is an identity matrix. The measurement errors are also assumed to be Gaussian errors, and each of their standard deviations is set to be the values of the magnitude of the measurement times a coefficient according to different types of measurement as shown below:

- SCADA: *P*, *Q* measurements (0.02) and *V* (0.002)
- PMU: 0.002 for magnitudes, and 0.01 for angles

To initialise Holt's method, it is assumed that the previous two states before the first state to be estimated by the DSE ($\mathbf{x}_{-1}$ and $\mathbf{x}_0$) are known. The performance index as defined in (6.75) is used to assess the performance of the DSE:

$$J_k = \frac{\sum \left| \mathbf{z}_k^+ - \mathbf{z}_{k,true} \right|}{\sum \left| \mathbf{z}_k - \mathbf{z}_{k,true} \right|} \tag{6.75}$$

The simulations consider four different cases, including the normal operation case, the presence of bad data, the presence of sudden load change, and the presence of a fault. The simulation settings stated above are applied to all of the four cases. At time instant 25, the corresponding anomalies are introduced for the last three cases respectively.

6.8 Simulation Results and Analysis

In this section, the simulation results and the analysis of the four cases as mentioned in the previous section are given.

6.8.1 Normal Operation Case

This subsection presents the simulation results for the normal case in the IEEE 14 Bus Test System (data sheets given in Appendix C.1). Figure 6-3 shows the OPIs of the five DSEs and the steady state estimator (SSE) over the 50 time steps. It is shown that all five DSEs have smaller OPI than the SSE. This demonstrates the effectiveness of Holt's method and higher estimation accuracy of the DSEs over the SSE in a quasi-steady state. It is also demonstrated that the CKF has the most accurate estimation accuracy among the five DSEs with the lowest average OPI at about 0.16. This is followed by the UKF with an OPI at about 0.20. What is notable is that the OPIs of the EKF, IEKF and the SKF have the same average value at about

0.22. This might because in the simulation case studied, the nonlinearity of the system is still not high enough to cause a significant difference among the three DSEs that are all based on Taylor Expansions of the equations. Since the same measurements are used for the DSEs, such estimation accuracy improvements offered by the CKF is significant. Figure 6-4 shows that the CKF also has the least skewness, while the UKF has the largest skewness among the DSEs. However, the differences in the skewness of the DSEs are small, and are all below the threshold of 3. As in the normal case, all measurements and predictions are basically accurate; it is shown in Figure 6-5 the NIs of all the DSEs over the 50 time instant are all well below the threshold of 3.

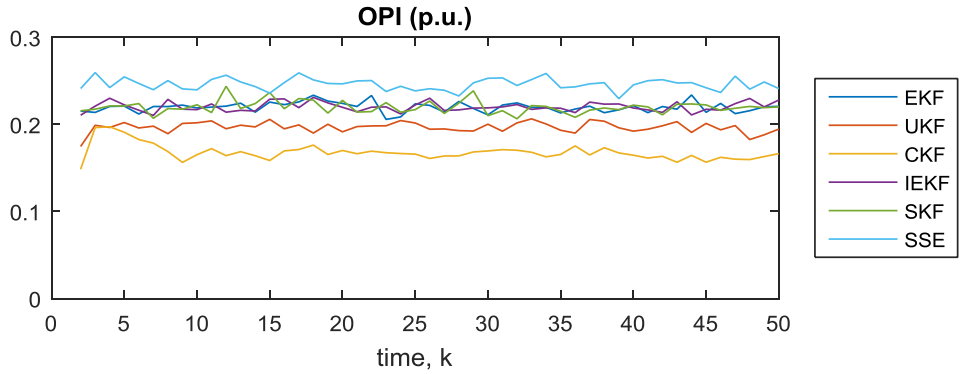

Figure 6-3: OPIs of the DSEs and the SSE in Normal Operation Case in the IEEE 14 Bus Test System

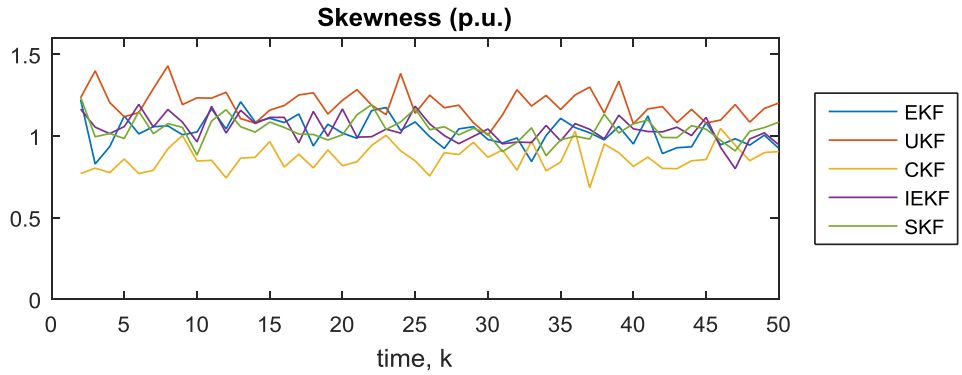

Figure 6-4: Skewness of the DSEs and the SSE in Normal Operation Case in the IEEE 14 Bus Test System

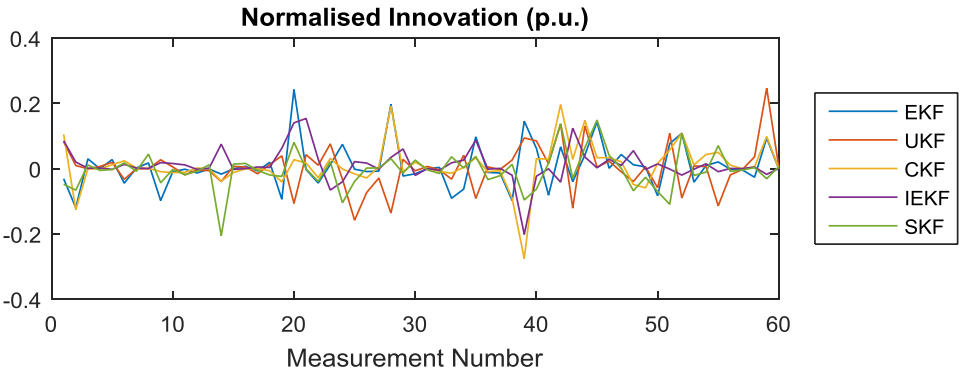

Figure 6-5: Normalised Innovations of the DSEs and the SSE in Normal Operation Case in the IEEE 14 Bus Test System

6.8.2 Presence of Bad Data

This section gives the simulation results in the case of bad data. A gross error (the measurement is set to 0) is introduced in the active power flow measurement connecting Bus 2 and Bus 4 at Time 25.

In Figure 6-6 a severe drop can be seen in the OPI curves of all DSEs and the SSE. This can be explained by the nature of the state estimation that errors existing in the measurements will be averaged out so that the overall error after the estimation will be smaller than that before the estimation. This effect will become more significant if any one of the measurements has significantly larger errors than the other measurements. However, the quality of the state estimate in this case is much worse than that in the normal operation case since the OPI quantifies the improvement of the data quality, but not the absolute size of the errors. So, the bad data has to be detected and identified in time.

As can be seen in Figure 6-7 and Figure 6-8, a single skewness and a single NI of a measurement become much larger than their normal values. According to the anomaly identification algorithm presented in Figure 6-2, the anomaly is identified to be bad data, and bad data exists in Measurement 21, which is the active power flow measurement between Bus 2 and Bus 4.

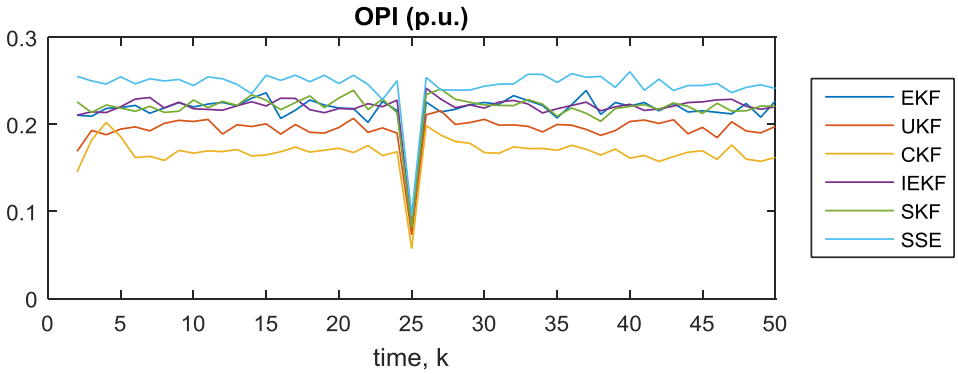

Figure 6-6 : OPIs of the DSEs and the SSE in the Presence of Bad Data in the IEEE 14 Bus Test System

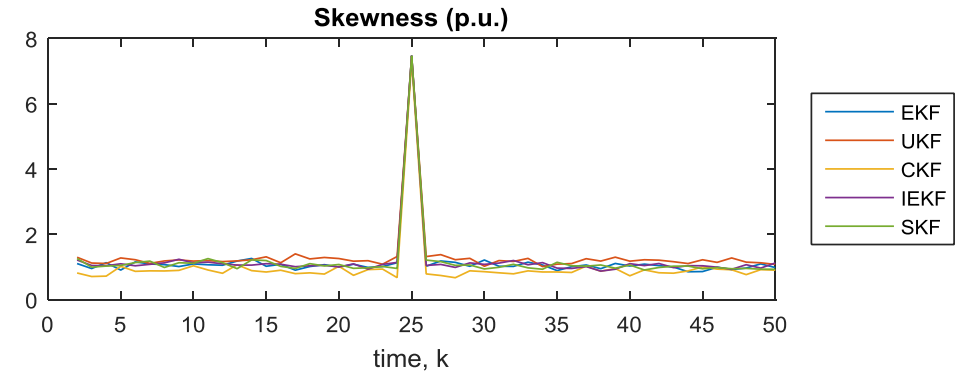

Figure 6-7: Skewness of the DSEs and the SSE in the Presence of Bad Data in the IEEE 14 Bus Test System

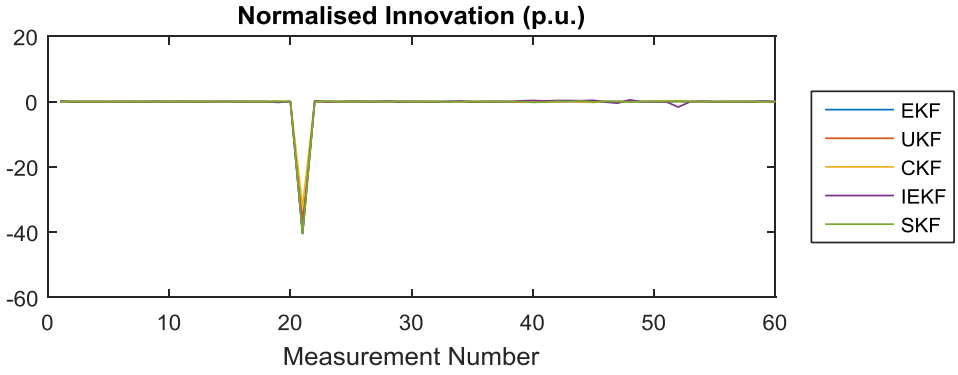

Figure 6-8: Normalised Innovations of the DSEs and the SSE in the Presence of Bad Data in the IEEE 14 Bus Test System

6.8.3 Presence of Sudden Load Change

6.8.3.1 IEEE 14 Bus Test System

This subsection discusses the simulation results of the third simulation case where a sudden load change of a 40% load reduction is introduced at the load at Bus 2 at Time 25 in the IEEE 14 Bus Test System. As shown in the previous subsection, the bad data have almost the same effect on the performance (OPI) of the DSEs and the SSE. In contrast, the sudden change of load affects and the DSEs and the SSE differently. As shown in Figure 6-9, the OPI of the CKF is the most sensitive to a nonlinear filter with its peak at about 0.7; the OPI of the UKF is also significantly affected, but its peak value is lower at about 0.5, the OPIs of EKF family (EKF, IEKF and SKF) at time Time 25 also increase, but the change is not obvious; the SSE is not affected by the sudden load change since it does not use the prediction of the states to produce the state estimate. This result of the relative OPI values of the DSEs and SSE is exactly the opposite to that in the normal operation case. That is to say, the more efficient a nonlinear filter is the more susceptible it is to the sudden change of load. Hence, in order to make use of the highly efficient nonlinear filters to improve the performance of the DSE it is crucial to accurately detect and identify the sudden change of load and make correct responses in time.

It is shown in Figure 6-10 that the skewness of the DSEs increases slightly at time Time 25 but is still within the threshold of 3. This is because in a small network such as the IEEE 14 Bus Test System the sudden change of load affects the states of all buses to more or less the same extent. Thus, the distribution of the normalised innovations does not change very much. The difference compared to the normal case is that several NIs are larger than the threshold of 3 as can be seen in Figure 6-11. According to Criteria 3 given in Figure 6-2, the anomaly is detected to be sudden change of load. Although the five measurements greater than 3, V_4, $I_{real,1\text{-}2}$, $I_{real1\text{-}5}$, $I_{imag,1\text{-}2}$ and $I_{imag,2\text{-}4}$, are near Bus 2, it is not obvious to directly identify the bus when the sudden change of load happens. Following Step a to Step f of the pseudo injection method given in Section 6.5.2.1, the normalised innovation vector of the pseudo injection measurements, $\boldsymbol{\tau}_l$, for the CKF is computed and summarised in Table 6-1. The results show that Load 1 at Bus 2 has much larger $\boldsymbol{\tau}_l$ than any other loads, which clearly indicates that the sudden change of load happens at Bus 2.

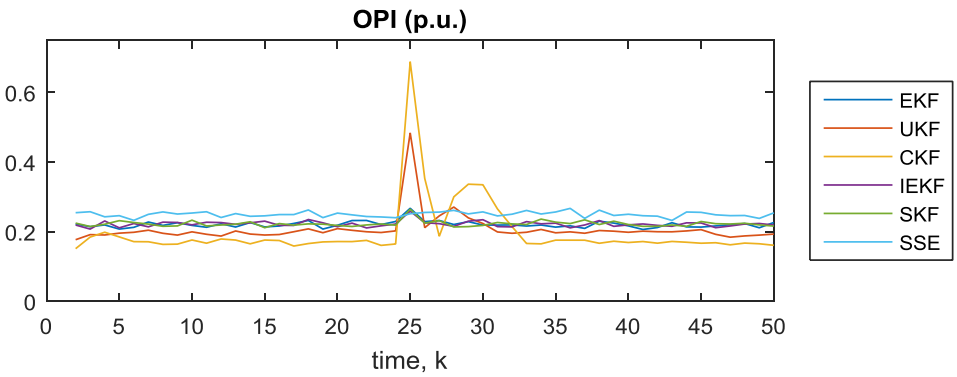

Figure 6-9: OPIs of the DSEs and the SSE in the Presence of Sudden Load Change in the IEEE 14 Bus Test System

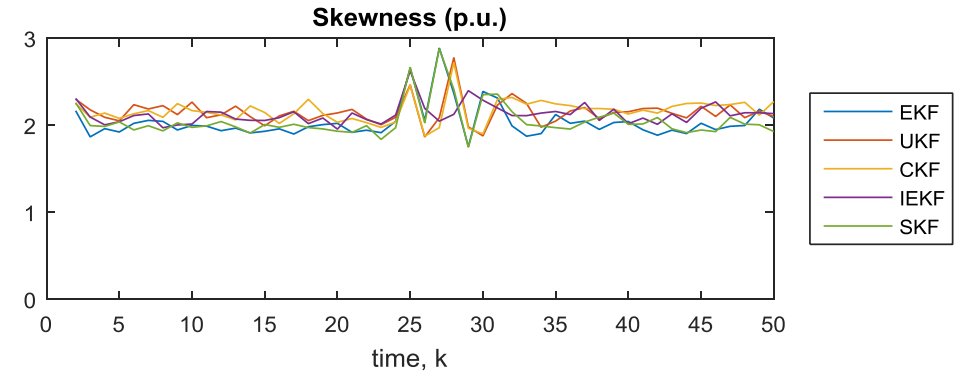

Figure 6-10: Skewness of the DSEs and the SSE in the Presence of Sudden Load Change in the IEEE 14 Bus Test System

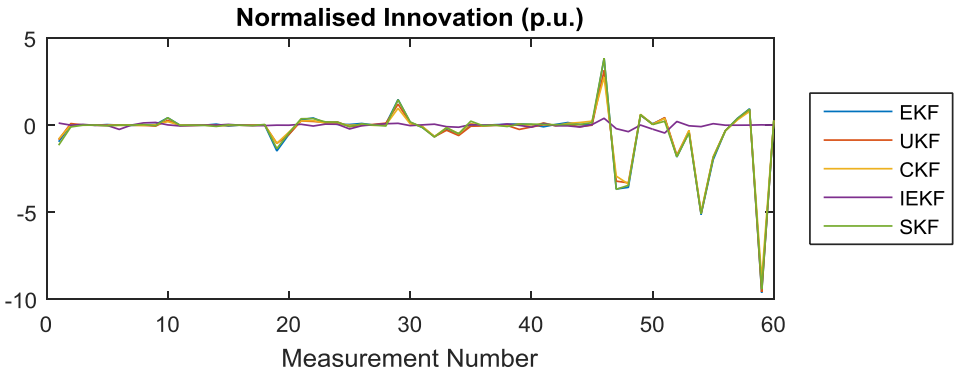

Figure 6-11: Normalised Innovation of the DSEs and the SSE in the Presence of Sudden Load Change in the IEEE 14 Bus Test System

Table 6-4: Normalise Innovation Vector of the Pseudo Injection Measurements

Load	1	2	3	4	5	6	7	8	9	10	11
Bus	2	3	4	5	6	9	10	11	12	13	14
$\boldsymbol{\tau}_l$	1.25	0058	0.026	0.103	0.160	0.257	0.704	0.114	0.075	0.123	0.200

6.8.3.2 IEEE 39 Bus Test System

In this subsection, the simulation is conducted again in the IEEE 39 Bus Test System (data sheets given in Appendix C.2). A 10% load reduction is introduced at Bus 27 at Time 25. In general, the OPIs of the DSEs increase significantly at Time 25 although the change of load is less severe compared to the 40% load reduction, as can be seen in Figure 6-12. In the previous simulation for sudden change of load in the IEEE 14 Bus Test System, two characteristics of the results are shown: multiple NIs are greater than the normal values, and the all skewness over the time is within the normal value. In the IEEE 39 Bus Test System, these characteristics become less obvious; rather, the effect of sudden change of load becomes similar to the effect of bad data. First, there is a significant increase in the value of skewness at Time 25 when the anomaly happens, but the peak value at about 3.5 is significantly smaller than the peak value of the skewness at about 7.5 in the bad data case. Second, there are multiple NIs greater than the threshold of 3, but the largest NI is much larger than the others making the shapes of the curves more similar to those of the bad data case. The reason for the differences compared to the 14 bus case and the similarities to the bad data case is that in a larger network, only a small proportion of the states are significantly affected by the sudden change of load, while most of the states are weakly or basically unaffected. The detection of the sudden change of load can still be realised according to Criteria 5 of the algorithm shown in Figure 6-2 as long as the thresholds of skewness, $C_{k,th1}$ and $C_{k,th2}$, are properly selected, for example 3 and 5 respectively in this case. Identification of the anomaly can be carried out following the same procedure as given in the previous subsection, and thus is not discussed here.

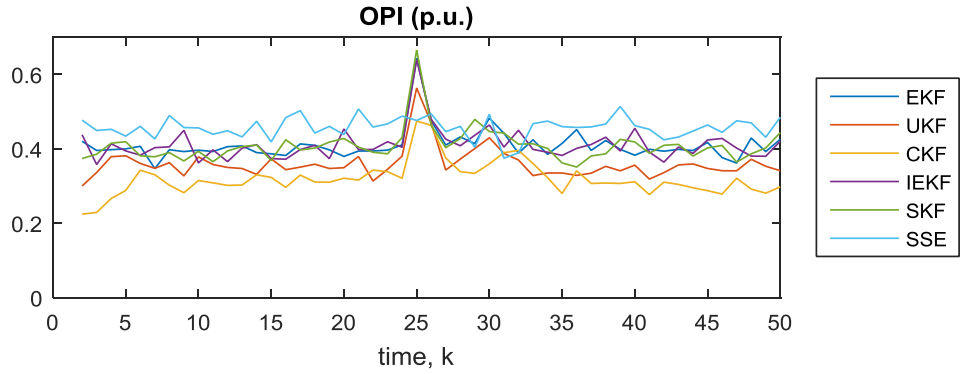

Figure 6-12: OPIs of the DSEs and the SSE in the Presence of Sudden Load Change in the IEEE 39 Bus Test System

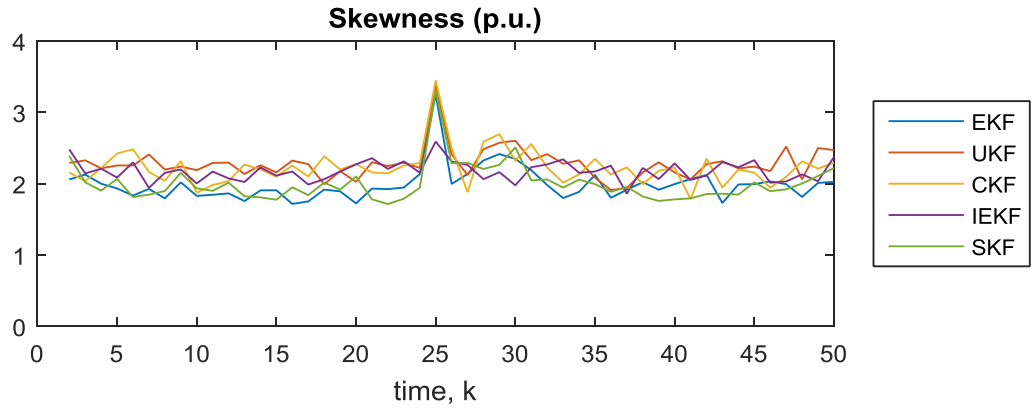

Figure 6-13: Skewness of the DSEs and the SSE in the Presence of Sudden Load Change in the IEEE 39 Bus Test System

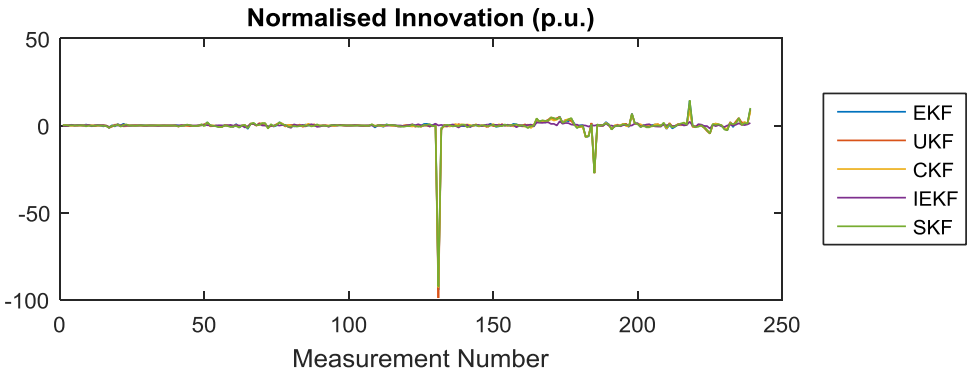

Figure 6-14: Normalised Innovations of the DSEs and the SSE in the Presence of Sudden Load Change in the IEEE 39 Bus Test System

6.8.4 Presence of a Fault in the Network

The final case studied in this chapter is in the presence of a single fault in the grid. It is assumed that the state estimator always receives the measurements of the power system in a steady state after the fault. This is because the transient response of the network to the fault is much faster than the update rate of the state estimator. It is also assumed that the fault is cleared by removing one of the branches. The scope of this study is to investigate the effect of such a topology change on the DSEs and how this type of anomaly can be detected and identified before the topology change is updated.

The simulation in this case is performed in the IEEE 14 Bus Test System where a topology change happens at Time 25 when the branch connecting Bus 3 and Bus 4 is removed. The topology change is not updated after Time 25 in order to clearly show its persistent impact on the DSE. As shown in Figure 6-15 the OPIs of all DSEs and the SSE have become much larger than the 1 after the topology change happens at Time 25, which indicates that the estimation is even worse than the measurements.

The topology change after the fault imposes persistent impact on not only the OPI but also on the skewness and the NIs, which can be used to detect and identify the anomaly. As shown in Figure 6-16, the skewness surges from the normal operation case value of around 2 to about 3.5 at Time 25, and continues to increase until a steady value of about 5 is reached at Time 30. In Figure 6-17 and Figure 6-18 it is shown that multiple NIs are greater than the normal value at Time 25, and this phenomenon still exists at Time 26. According to Criteria 5 of the anomaly detection algorithm shown in Figure 6-2, a topology change is detected at Time 25 that might be caused after the fault is cleared.

The removed branch can be identified following Step A to Step C given in Section 6.5.2.2; the variation ratios of the branches at Time 25 are computed as summarised in Table 6-5. Since its corresponding $\mathbf{r}_m$ is the largest, Branch 6 is identified to be the removed branch.

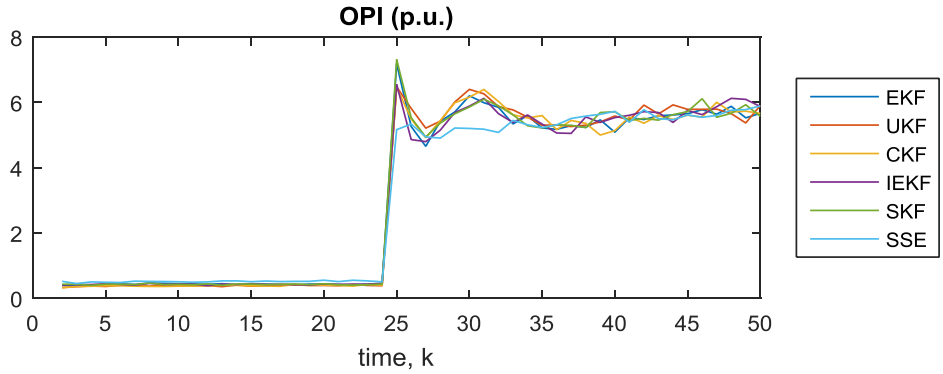

Figure 6-15: OPIs of the DSEs and the SSE in the Presence of Fault in the IEEE 14 Bus Test System

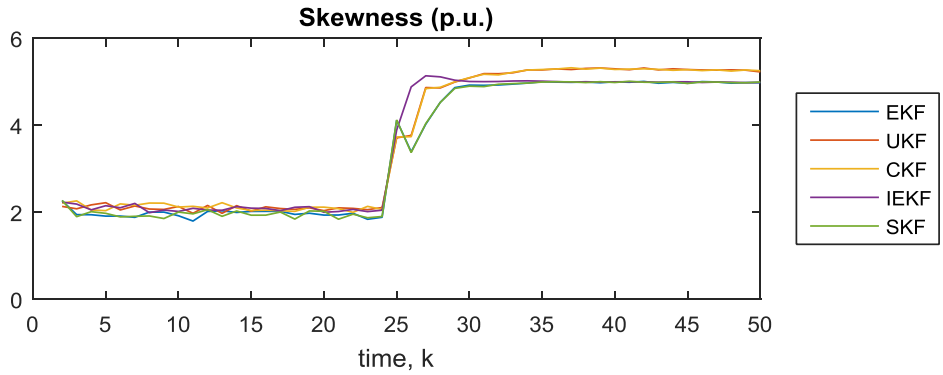

Figure 6-16: Skewness of the DSEs and the SSE in the Presence of Fault in the IEEE 14 Bus Test System

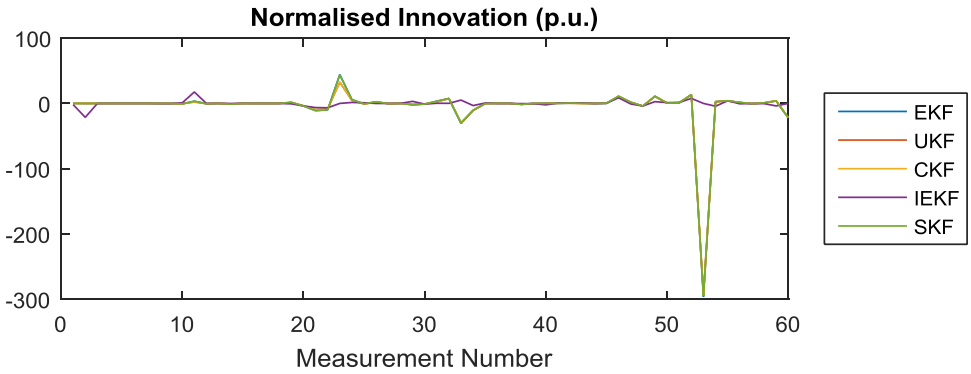

Figure 6-17: Normalised Innovations of the DSEs and the SSE in the Presence of Fault in the IEEE 14 Bus Test System at Time Instant 25

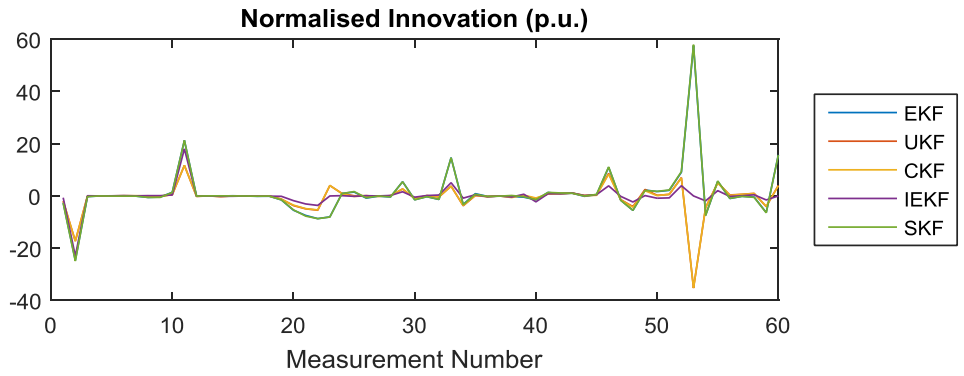

Figure 6-18: Normalised Innovations of the DSEs and the SSE in the Presence of Fault in the IEEE 14 Bus Test System at Time Instant 26

Table 6-5： Variation Ratios of the Branches After the Fault in the IEEE 14 Bus Test System

Branch	1	2	3	4	5	6	7	8	9	10
$\mathbf{r}_m$	0.0116	0.0124	0.0121	0.0120	0.0068	1.4350	0.0063	0.0435	0.0323	0.0002
Branch	11	12	13	14	15	16	17	18	19	20
$\mathbf{r}_m$	0.0345	0.0561	0.0169	0.7173	0.0374	0.0129	0.0208	0.0088	0.0105	0.0305

6.9 Summary

The development of the IT technology, SMT technology and the open access to the operation of transmission networks makes it feasible to develop a DSE in power systems in the future. The ability of the DSE to use the prediction for state estimation gives it advantages over the SSE in bad data detection and estimation of the branch parameters and generator parameters.

The performance of DSEs is mainly limited by two aspects; the efficiency of the nonlinear filter and the sudden change of states. This chapter proposed a new DSE algorithm using the Cubature Kalman Filter (CKF) as the nonlinear filter. The proposed algorithm is also capable of detecting, discriminating and identifying three types of anomaly, including bad data, sudden change of load and fault, where the latter two types are the reasons that can cause the sudden

change of states. Four other nonlinear filters that are often used in DSEs are also introduced in order to demonstrate the high efficiency of the CKF.

From the simulation results, it was found that in the normal operation case the estimation accuracy of the CKF is significantly higher than that of the other nonlinear filters with the same measurements. However, it was found that the high efficiency nonlinear filters, such as the CKF and UKF, are also more susceptible to anomalies. Thus, a novel anomaly detection algorithm is proposed based on the different responses of the normalised innovations of the measurements and their skewness to anomalies. In addition, anomaly identification methods are proposed for different anomalies: bad data can be identified using the existing largest normalised innovation method, the load that experiences sudden change can be identified using the pseudo injection measurement method. On the other hand, the removed branch after the fault can be identified using the branch power flow variation ratio method if all branch power flows or currents are monitored. So, the performance of DSE can be significantly improved with the algorithm proposed based on the CKF with the help of anomaly detection and identification methods.

Chapter 7 Thesis Summary

This chapter summarises the conclusions drawn from the results presented in the thesis (Chapter 7.1), the contributions achieved in this research (Chapter 7.2) and provides some suggestions for future work (Chapter 7.3).

7.1 Conclusions

This PhD thesis has discussed new algorithms to enhance the practice of power system state estimation considering the possible improvements for static state estimation (Section 7.1.1), the opportunities and challenges provided by synchronised measurement technology (Section 7.1.2 and Section 7.1.3) and future developments of dynamic state estimation (Section 7.1.4).

7.1.1 Observability Analysis

The first research topic of this thesis is observability analysis, a necessary function prior to the main function of state estimation. Observability analysis can be performed using either a numerical method or a topological method. The research of this thesis focuses on the numerical method because of its popularity in literature and its capability to analyse large networks.

The functions of observability analysis include checking network observability (if a unique solution can be found), identification of observable islands and measurement replacement. The existing numerical method for observability analysis can be classified into the gain matrix method, the gram matrix method and the test matrix method. It is demonstrated in this thesis that all of these methods may not correctly identify the observable islands in the so-called *pathological cases*. This thesis has established that, apart from the common pathological case

(Type 1 pathological case) recognised in literature where the observable islands are topologically separated, there is another type of pathological case (Type 2 pathological case) where some of the observable islands can be directly connected by branches. The gain matrix method and the gram matrix method are vulnerable to both types of pathological cases, while the test matrix method is vulnerable to Type 2 pathological case. The thesis identified the flaw in the theory of the test matrix method, revised the theory, and proposed a new fully iterative numerical method for observability analysis. However, the iterations can slow down the execution speed of observability analysis, and they are found to be unnecessary in most cases. To avoid unnecessary iterations and improve the efficiency of observability analysis, a pathological case identification rule (*PCIR*) is proposed that can precisely discriminate normal cases where iterations are not needed and pathological cases where iterations are needed.

The *PCIR* also allows observable islands to be identified directly from the test matrix. Such an observable island identification approach is called the direct island method, while the algorithms presented in literature use the direct branch method, which identifies observable islands in two steps. The simulations demonstrate that the direct island method assisted by the *PCIR* is up to 3 times faster than the direct branch method. Hence, the proposed method based on the *PCIR* and the direct island identification method not only guarantees accurate observable island identification but is also much faster execution than the existing numerical observability analysis methods in terms of execution speed.

Another major drawback of the existing numerical methods for observability analysis is that they cannot analyse network observability in the presence of PMU measurements since they are designed only to consider the conventional methods. The thesis considers all possible types of conventional and PMU measurement placements, studies the observability they provide, and proposes a new method to numerically express them in the same format used in existing observability analysis methods so that the PMU measurements can be included in the existing methods without the need to fundamentally change them.

The thesis also points out that the execution speed of the observability analysis can be further improved using highly efficient factorisation method instead of the widely used Cholesky

factorisation, and that the proposed method for numerical observability analysis based on the *PCIR* cannot be substituted by the other methods such as the methods using alternative or actual branch reactance.

7.1.2 Optimal PMU Placement

The second research topic in the thesis is optimal PMU placement. While the research topic of optimal PMU placement has been thoroughly studied in literature considering different optimisation algorithms, constraints and scenarios, the focus of this thesis is on optimal PMU placement in the presence of conventional measurements using integer linear programming (ILP). The purpose of this research is to find the minimum number of PMUs that can support the observability of the hybrid state estimators in the presence of existing conventional measurements.

There are two major types of methods for optimal PMU placement in the presence of conventional measurements, the Kirchoff Current Law (KCL) based methods and the observability analysis based methods. It is found in the research that both of these methods may give sub-optimal solutions, i.e. there are better PMU placements that can ensure network observability with a smaller number of PMUs. In addition, the KCL based methods may also obtain wrong placements that cannot make the system observable. A new method is proposed in the thesis based on a novel network transformation scheme and a new global network observability criterion. The new method is guaranteed to always obtain correct PMU placements, and it is demonstrated through simulations that it gives less sub-optimal solutions than the existing KCL and observability analysis based methods. The drawback of the proposed method is that it is still susceptible to the problem of sub-optimal solution. Nevertheless, the proposed method is still valuable for two reasons: first, the PMU placement obtained by this method can ensure network observability; second, the simplicity of the method gives it advantages in terms of execution time and allows it to be easily implemented with ILP.

7.1.3 Hybrid State Estimation

The third research topic in the thesis is hybrid state estimation. Hybrid state estimator (HSE) was proposed as a transitional product between the conventional state estimator (CSE) and the linear state estimator (LSE) due to the high costs to install a sufficient amount of PMUs to support LSE. There are three major research topics for HSE: improving the performance of the state estimator, exploring new applications of HSE and methods for optimally integrating the conventional measurements and PMU measurements into the HSE. The research presented in this thesis focuses on the third topic listed above.

The problem of directly using both types of measurements in HSE comes from the current phasor measurement. The current phasor measurements provided by the PMUs are in polar form, whose derivatives with respect to the states might be singular for certain values of states. Thus, the direct use of the polar current phasor measurements might result in non-convergence. Five different formulations of HSEs have been identified in literature that overcomes this problem, including the post-processing (PP) HSE and four integrated HSEs: rectangular current (RC) HSE, pseudo flow (PF) HSE, pseudo voltage (PV) HSE and constrained formulation (CF) HSE. Although in literature each of these methods has shown its advantage in comparison to the CSE, it is unknown yet which formulation can optimally use the PMU measurements to improve the performance of the HSE.

The thesis compares the performance of the HSEs in three aspects: the estimation accuracy, execution time and convergence. An exhaustive simulation of all possible PMU placements in the IEEE 14 bus test system was executed for this purpose. It is found that in general the placement of every additional PMU would significantly increase the estimation accuracy of the HSEs from 0 PMU, which is effectively a CSE, until a knee point, the minimum number of PMUs that can make the system fully observable. After the knee point, the accuracy improvement brought by placing an additional PMU becomes significantly smaller. In particular, after the point where the number of PMUs can make the network fully redundant the improvement in accuracy becomes negligible. In terms of the relative estimation accuracy of the HSEs, it is found that the RC HSE is the most accurate HSE, the PF HSE and CF HSE have

comparable estimation accuracy, but they are less accurate than the RC HSE, the PP HSE and PV HSE have the least estimation accuracy when the number of PMUs are smaller and larger than the knee point respectively. These conclusions are perfectly validated in the IEEE 118 Bus Test System. In addition, the conclusions are further proved by mathematical analysis, through which it is shown the reasons for these conclusions. The reason why the RC HSE is the most accurate is that it uses the simplest measurement transformation, and the reasons why PP HSE and PV HSE are the least accurate are that they cannot make good use of the PMU measurements and the virtual measurements, respectively.

As for the execution time and convergence, it is shown in the simulation results in both the IEEE 14 and 39 Bus Test Systems that the CF HSE and PV HSE take much more execution time than the other HSEs, and that the CF HSE is much less stable than the other HSEs. This result is explained by the characteristics of augmented state vector, whose length is up to more than 5 times the length of the other HSEs.

Apart from simulations with Gaussian errors in the measurements, the thesis also performed additional simulations with gross measurement errors and parameter errors. The results show that parameter errors will have more severe impact on the estimation accuracy of the HSEs than gross errors. It is also concluded that the PMU placement can significantly affect the impact of these two types of errors: a poor estimation accuracy of an HSE could be as low as that of a CSE, while a good estimation of an HSE could approach the base case (the case without being affected by parameter errors or gross errors). However, there is still not a clear conclusion on which PMU placements are more resilient to gross errors and parameter errors, and the reasons why they are more advantageous than the other placements. The answer to these questions would require the development of new tools and more research on HSE in the future.

7.1.4 Dynamic State Estimation

The fourth and final research topic in the thesis is on dynamic state estimation. In contrast to the static state estimator (SSE) that produces the state estimate using only measurements,

dynamic state estimator (DSE) estimates the states using both the measurements and predictions based on the information of the previous state estimate. The tasks of creating the prediction and estimating the states in DSE are undertaken by the dynamic model of the system and a nonlinear recursive filter, respectively. Thus, the challenge of the DSE is to ensure a correct and accurate prediction of the states and choose the most efficient nonlinear recursive filter. In literature, most DSEs choose extended Kalman filter (EKF) or unscented Kalman filter (UKF) as their nonlinear filters. However, the EKF is limited by its inaccurate estimation in highly nonlinear systems, while the UKF is vulnerable to convergence problems. It is also widely recognised in literature that the sudden change of states could lead to wrong predictions and significantly degrade the performance of the DSE. However, there is not an algorithm yet which can detect, discriminate and identify different types of anomaly in different scenarios.

To solve the abovementioned problems, the thesis proposes a new algorithm for DSE using the cubature Kalman filter (CKF) as the nonlinear recursive filter, which can systematically detect, discriminate and identify three different types of anomaly considered in the thesis, namely bad data, sudden change of load, and sudden change of topology due to a fault. The simulation results show that in normal operation cases the CKF is significantly more accurate than the UKF, the EKF and two revised formulations of the EKF (iterated EKF and second-order EKF), which are more accurate than the SSE. Although it is also shown that the CKF is more affected by the anomalies, a set of anomaly detection criteria is proposed to solve this problem according to the different responses of the normalised innovations of the estimation and their skewness. While bad data identification can be carried out using the existing largest normalised innovation method, a pseudo injection method and a branch power flow variation ratio method are proposed to identify the location of sudden change of load and the location of the sudden change of topology. All of these anomaly detection and identification methods have been demonstrated in different case studies in the IEEE 14 and / or 39 Bus Test Systems.

7.2 Thesis Contributions

The research presented in this thesis focuses on proposing new algorithms to improve the performance of power system state estimation. The contributions of this thesis can be divided into four parts:

1. Observability Analysis (Paper [A.1])
2. Optimal PMU Placement (Papers [A.2], [A.3], [A.7])
3. Hybrid State Estimation (Papers [A.2], [A.4], [A.7])
4. Dynamic State Estimation (Paper [A.5])

Details of these parts are given as follows.

1. New algorithms and theories for numerical observability analysis.
    a. Proposition of a fully-iterative method for numerical observability analysis, which can guarantee the correct identification of observable islands, after identifying and revising the flaw in the theory of the existing numerical method for observability analysis.
    b. Proposition of the convergence theorem for numerical observability analysis which proves the definite convergence of observability analysis.
    c. Proposition of the pathological case identification rule (*PCIR*) which can precisely distinguish normal cases and pathological cases.
    d. Proposition of the direct observable island identification method that identifies the observable islands in only one step.
    e. Proposition of a new algorithm for numerical observability analysis based on the *PCIR* and the direct observable island identification method.
    f. Proposition of a new method for integrating the PMU measurements into the algorithm of numerical observability analysis.
2. A new algorithm for optimal PMU placement in the presence of conventional measurements.
    a. Proposition of a new global network observability criterion.
    b. Proposition of a new network transformation scheme.

   c. Proposition of a new algorithm for optimal PMU placement in the presence of conventional measurements, which can ensure correct PMU placement with less sub-optimal problems compared to the existing methods, based on the new global network observability criterion and the new network transformation scheme.

3. A comprehensive analysis of the impact of estimator formulations on the performance of the hybrid state estimator (HSEs) taking the Gaussian measurement errors, gross measurement errors and parameter errors into account.
   a. Identification of the accuracy curves of five different formulations characterized by the knee point, which clearly indicates the benefits of using HSE compared to the conventional state estimator (CSE); that is to say, even with a small number of PMUs the state estimation accuracy can be significantly improved compared to the CSE.
   b. Identification of the relative estimation accuracy of the five different HSEs in the IEEE 14 Bus Test System. Before the knee point: Rectangular Current (RC) > Pseudo Flow (PF) ≈ Constrained Formulation (CF) ≈ Pseudo Voltage (PV) > Post-processing (PP); after the knee point: RC > PF ≈ CF > PP > PV.
   c. Validation of the knee point characteristic of the HSE accuracy curves and the relative estimation accuracy of the HSEs using simulations in the IEEE 118 Bus Test System and mathematical analysis.
   d. Setting out the reasons why the RC HSE is the most accurate while the PP HSE and PV HSE are the least accurate using mathematical analysis.
   e. Comparison of the execution time and convergence of the five HSE, and establishing that the CF HSE and PV HSE have poor performance in these two aspects.
   f. Recommendation of the RC HSE as the HSE to be implemented in the power system based on the comparison of the HSEs in terms of estimation accuracy, execution time and convergence.
   g. Discovering that the PMU placement can significantly affect the performance of the HSEs in the presence of gross measurement errors and parameter errors.
4. New algorithms for dynamic state estimation.

a. Proposition of a new algorithm for detecting different types of anomaly.
b. Proposition of the pseudo injection method for identifying the anomaly of sudden change of load.
c. Proposition of the branch power flow variation ratio method for identifying the anomaly of a sudden change of topology due to fault.
d. Proposition of a new algorithm for dynamic state estimation based on the Cubature Kalman Filter and the proposed anomaly detection and identification methods.

7.3 Future Work

This thesis has described an accurate and efficient method for observability analysis that is suitable for both conventional measurements, synchronised measurements and a combination of both measurements. This work can be further extended considering multi-area state estimation, and state estimation, and the presence of HVDC links.

Although the topic of optimal PMU placement has been extensively researched with a wide range of available literature, there has been little literature about how the PMU placement can affect the performance (especially accuracy) of the HSEs, and thus how to optimally place the PMUs. Although the simple optimal PMU placement method as discussed in Section 5.4, which aims to maximize the number of observed branches, successfully finds the PMU placements close to the optimal solution, it has not been rigorously proved and tested in other networks and considered all possible scenarios. In addition, it has been shown in Section 5.6.2 that the PMU placement determines the estimation accuracy level (the level of the HSE in normal cases and the level of CSE) of the HSE in the presence of gross measurement errors and parameter errors. However, it is still unknown how to optimally place the PMUs so that the effects of these two types of errors are minimised. One of the possible solutions is to derive and carry out a sensitivity analysis of the participation factors that describe the relationship between the states and the measurements and model parameters. These participation factors would enhance our understanding of the HSEs and their performance in different scenarios,

and thus help to develop optimal PMU placement strategies that are dedicated for each HSE and move beyond the benefits of observability that were established in the research presented in the thesis.

The thesis also shows the high sensitivity of the Cubature Kalman Filter (CKF) to the sudden change of states although it has a significant advantage in terms of estimation accuracy compared to the other nonlinear filters. Although anomalies can be detected and identified according to the response of the normalised innovations and the skewness of them, the actions are always taken after the execution of state estimation. Thus, new methods should be designed so that pre-emptive actions are taken before the anomaly can affect the estimate of the states.

The prediction step in the DSEs presented in this thesis uses Holt's linear smoothing technique based on the assumption that the states of the system progresses much more slowly than the updating rate of state estimation. However, this assumption limits the DSE's capability to track the transient behaviour of the power system. Thus, a more accurate and sophisticated dynamic model of the network will be required. It is expected that in the future the DSE will not only be able to precisely estimate the states during the transient period after disturbance but also to estimate the transient parameters of the generators and even the rate of change of frequency of any bus in the network.

References

[1] A. G. Phadke and J. S. Thorp, Synchronised Phasor Measurements and Their Applications: Springer, 2008.

[2] A. Monticelli, "Electric power system state estimation", Proc. IEEE, vol. 88, no. 2, pp. 262-282, 2000-Feb.

[3] Monticelli, A. (1999). State Estimation in Electric Power Systems, Springer US.

[4] A. Abur and A. Gomez-Exposito, Power System State Estimation: Theory and Implementation. New York: Marcel Dekker, 2004.

[5] A. Wood and B. F. Wollenberg, Power Generation Operation and Control, 2nd ed, 1996.

[6] F. C. Schweppe and J. Wildes, "Power System Static-State Estimation, Part I: Exact Model," in the IEEE Transactions on Power Apparatus and Systems, vol. PAS-89, no. 1, pp. 120-125, Jan. 1970.

[7] F. C. Schweppe and D. B. Rom, "Power System Static-State Estimation, Part II: Approximate Model," in the IEEE Transactions on Power Apparatus and Systems, vol. PAS-89, no. 1, pp. 125-130, Jan. 1970.

[8] F. C. Schweppe, "Power System Static-State Estimation, Part III: Implementation," in the IEEE Transactions on Power Apparatus and Systems, vol. PAS-89, no. 1, pp. 130-135, Jan. 1970.

[9] Y.-F. Huang, S. Werner, J. Huang, N. Kashyap, V. Gupta, "State estimation in electric power grids: Meeting new challenges presented by the requirements of the future grid" in the IEEE Signal Process. Mag., vol. 29, no. 5, pp. 33-43, 2012.

[10] A. Q. Huang, "Power Semiconductor Devices for Smart Grid and Renewable Energy Systems," in Proceedings of the IEEE, vol. 105, no. 11, pp. 2019-2047, Nov. 2017.

[11] E. Ghahremani and I. Kamwa, "Local and Wide-Area PMU-Based Decentralized Dynamic State Estimation in Multi-Machine Power Systems," in the IEEE Transactions on Power Systems, vol. 31, no. 1, pp. 547-562, Jan. 2016.

[12] M. Asprou, "Synchronised measurement technology: A blessing for power systems [Trends in Future I&M]," in the IEEE *Instrumentation & Measurement Magazine*, vol. 20, no. 3, pp. 25-42, June 2017.

[13] M. Asprou, S. Chakrabarti and E. Kyriakides, "A Two-Stage State Estimator for Dynamic Monitoring of Power Systems," in the IEEE Systems Journal, vol. 11, no. 3, pp. 1767-1776, Sept. 2017.

[14] F. F. Wu and W. H. E. Liu, "Detection of topology errors by state estimation power systems]," in the IEEE Transactions on Power Systems, vol. 4, no. 1, pp. 176-183, Feb 1989.

[15] R. E. Larson, W. F. Tinney and J. Peschon, "State Estimation in Power Systems Part I: Theory and Feasibility," in the IEEE Transactions on Power Apparatus and Systems, vol. PAS-89, no. 3, pp. 345-352, March 1970.

[16] R. E. Larson, W. F. Tinney, L. P. Hajdu and D. S. Piercy, "State Estimation in Power Systems Part II: Implementation and Applications," in the IEEE Transactions on Power Apparatus and Systems, vol. PAS-89, no. 3, pp. 353-363, March 1970.

[17] O. J. M. Smith, "Power System State Estimation," in the IEEE Transactions on Power Apparatus and Systems, vol. PAS-89, no. 3, pp. 363-379, March 1970.

[18] L. Zhang, A. Bose, A. Jampala, V. Madani and J. Giri, "Design, Testing, and Implementation of a Linear State Estimator in a Real Power System," in the IEEE Transactions on Smart Grid, vol. 8, no. 4, pp. 1782-1789, July 2017.

[19] T. Yang, H. Sun and A. Bose, "Transition to a Two-Level Linear State Estimator—Part I: Architecture," in the IEEE Transactions on Power Systems, vol. 26, no. 1, pp. 46-53, Feb. 2011.

[20] T. Yang, H. Sun and A. Bose, "Transition to a Two-Level Linear State Estimator—Part II: Algorithm," in the IEEE Transactions on Power Systems, vol. 26, no. 1, pp. 54-62, Feb. 2011.

[21] M. Zhou, V. A. Centeno, J. S. Thorp and A. G. Phadke, "An Alternative for Including Phasor Measurements in State Estimators," in the IEEE *Transactions on Power Systems*, vol. 21, no. 4, pp. 1930-1937, Nov. 2006.

[22] T.S. Bi, X.H. Qin, Q.X. Yang, A novel hybrid state estimator for including synchronised phasor measurements, Electric Power Systems Research, Volume 78, Issue 8, 2008, Pages 1343-1352, ISSN 0378-7796, http://dx.doi.org/10.1016/j.epsr.2007.12.002.

[23] M. Asprou and E. Kyriakides, "Enhancement of hybrid state estimation using pseudo flow measurements," 2011 IEEE Power and Energy Society General Meeting, San Diego, CA, 2011, pp. 1-7.

[24] S. Chakrabarti, E. Kyriakides, G. Ledwich and A. Ghosh, "Inclusion of PMU current phasor measurements in a power system state estimator," in IET Generation, Transmission & Distribution, vol. 4, no. 10, pp. 1104-1115, October 2010.

[25] G. Valverde, S. Chakrabarti, E. Kyriakides and V. Terzija, "A Constrained Formulation for Hybrid State Estimation," in the IEEE Transactions on Power Systems, vol. 26, no. 3, pp. 1102-1109, Aug. 2011.

[26] A. Monticelli and F. F. Wu, "Network Observability: Theory," Power Engineering Review, IEEE, vol. PER-5, pp. 32-33, 1985.

[27] G. R. Krumpholz, K. A. Clements, and P. W. Davis, "Power System Observability: A Practical Algorithm Using Network Topology," Power Apparatus and Systems, IEEE Transactions on, vol. PAS-99, pp. 1534-1542, 1980.

[28] A. M. Sasson, S. T. Ehrmann, P. Lynch, and L. S. Van Slyck, "Automatic Power System Network Topology Determination," Power Apparatus and Systems, IEEE Transactions on, vol. PAS-92, pp. 610-618, 1973.

[29] V. H. Quintana, A. Simoes-Costa, and A. Mandel, "Power System Topological Observability Using a Direct Graph-Theoretic Approach," Power Engineering Review, IEEE, vol. PER-2, pp. 23-23, 1982.

[30] K. A. Clements, G. R. Krumpholz, and P. W. Davis, "Power System State Estimation with Measurement Deficiency: An Algorithm that Determines the Maximal Observable Subnetwork," Power Apparatus and Systems, IEEE Transactions on, vol. PAS-101, pp. 3044-3052, 1982.

[31] K. A. Clements, G. R. Krumpholz, and P. W. Davis, "Power System State Estimation with Measurement Deficiency: An Observability/Measurement Placement Algorithm," Power Engineering Review, IEEE, vol. PER-3, pp. 28-28, 1983.

[32] I. W. Slutsker and J. M. Scudder, "Network Observability Analysis through Measurement Jacobian Matrix Reduction," IEEE Transactions on Power Systems, vol. 2, pp. 331-336, 1987.

[33] A. Monticelli and F. F. Wu, "Network Observability: Identification of Observable Islands and Measurement Placement," Power Engineering Review, IEEE, vol. PER-5, pp. 32-32, 1985.

[34] F. F. Wu, W. H. E. Liu, and S. M. Lun, "Observability analysis and bad data processing for state estimation with equality constraints," IEEE Transactions on Power Systems, vol. 3, pp. 541-548, 1988.

[35] D. M. Falcao and M. A. Arias, "State estimation and observability analysis based on echelon forms of the linearized measurement models," IEEE Transactions on Power Systems, vol. 9, pp. 979-987, 1994.

[36] F. F. Wu, W. H. E. Liu, L. Holten, L. Gjelsvik, and S. Aam, "Observability analysis and bad data processing for state estimation using Hachtel's augmented matrix method," IEEE Transactions on Power Systems, vol. 3, pp. 604-611, 1988.

[37] R. R. Nucera, V. Brandwajn, and M. L. Gilles, "Observability and bad data analysis using augmented blocked matrices [power system analysis computing]," IEEE Transactions on Power Systems, vol. 8, pp. 426-433, 1993.

[38] M. C. d. Almeida, E. N. Asada, and A. V. Garcia, "On the Use of Gram Matrix in Observability Analysis," IEEE Transactions on Power Systems, vol. 23, pp. 249-251, 2008.

[39] M. Almeida, E. Asada, and A. Garcia, "Power system observability analysis based on gram matrix and minimum norm solution," in Power & Energy Society General Meeting, 2009. PES '09. IEEE, 2009, pp. 1-1.

[40] G. N. Korres, "A Gram Matrix-Based Method for Observability Restoration," IEEE Transactions on Power Systems, vol. 26, pp. 2569-2571, 2011.

[41] C. Solares, A. J. Conejo, E. Castillo, and R. E. Pruneda, "Binary-arithmetic approach to observability checking in state estimation," IET Generation, Transmission & Distribution, vol. 3, pp. 336-345, 2009.

[42] B. Gou and A. Abur, "A Direct Numerical Method for Observability Analysis," IEEE TRANSACTIONS ON POWER SYSTEMS, VOL. 15, NO. 2, MAY 2000.

[43] V. Terzija et al., "Wide-Area Monitoring, Protection, and Control of Future Electric Power Networks," in Proceedings of the IEEE, vol. 99, no. 1, pp. 80-93, Jan. 2011.

[44] V. Terzija, Z. M. Radojević and G. Preston, "Flexible Synchronised Measurement Technology-Based Fault Locator," in the IEEE Transactions on Smart Grid, vol. 6, no. 2, pp. 866-873, March 2015.

[45] A. Moreno-Munoz, V. Pallares-Lopez, J. J. Gonzalez de la Rosa, R. Real-Calvo, M. Gonzalez-Redondo and I. M. Moreno-Garcia, "Embedding Synchronised Measurement Technology for Smart Grid Development," in the IEEE Transactions on Industrial Informatics, vol. 9, no. 1, pp. 52-61, Feb. 2013.

[46] S. Chakrabarti, E. Kyriakides, T. Bi, D. Cai and V. Terzija, "Measurements get together," in the IEEE Power and Energy Magazine, vol. 7, no. 1, pp. 41-49, January-February 2009.

[47] J. De La Ree, V. Centeno, J. S. Thorp and A. G. Phadke, "Synchronised Phasor Measurement Applications in Power Systems," in the IEEE *Transactions on Smart Grid*, vol. 1, no. 1, pp. 20-27, June 2010.

[48] J. S. Thorp, A. G. Phadke, S. H. Horowitz and M. M. Begovic, "Some applications of phasor measurements to adaptive protection," in the IEEE Transactions on Power Systems, vol. 3, no. 2, pp. 791-798, May 1988.

[49] W. Dickerson, "Effect of PMU analog input section performance on frequency and ROCOF estimation error," *2015 IEEE International Workshop on Applied Measurements for Power Systems (AMPS)*, Aachen, 2015, pp. 31-36.

[50] A. Sharma, S. C. Srivastava and S. Chakrabarti, "A multi-agent-based power system hybrid dynamic state estimator," in the IEEE *Intelligent Systems*, vol. 30, no. 3, pp. 52-59, May-June 2015.

[51] S. Naka, T. Genji, T. Yura and Y. Fukuyama, "A hybrid particle swarm optimisation for distribution state estimation," in the IEEE Transactions on Power Systems, vol. 18, no. 1, pp. 60-68, Feb 2003.

[52] C.-H. Lin, "A distributed state estimator for electric power systems" in the IEEE Trans. Power Syst., vol. 7, no. 2, pp. 551-557, May 1992.

[53] X. Li and A. Scaglione, "Robust Decentralized State Estimation and Tracking for Power Systems via Network Gossiping," in the IEEE Journal on Selected Areas in Communications, vol. 31, no. 7, pp. 1184-1194, July 2013.

[54] D. Falcao, F. Wu, L. Murphy, "Parallel and distributed state estimation" in the IEEE Trans. Power Syst., vol. 10, no. 2, pp. 724-730, May 1995.

[55] G. Korres, A. Tzavellas, E. Galinas, "A distributed implementation of multi-area power system state estimation on a cluster of computers", Elect. Power Syst. Res., vol. 102, pp. 20-32, Sep. 2013.

[56] W. Jiang, V. Vittal, G. Heydt, "A distributed state estimator utilizing synchronised phasor measurements" in the IEEE Trans. Power Syst., vol. 22, no. 2, pp. 563-571, May 2007.

[57] W. Jiang, V. Vittal, G. Heydt, "Diakoptic state estimation using phasor measurement units" in the IEEE Trans. Power Syst., vol. 23, no. 4, pp. 1580-1589, Nov. 2008.

[58] L. Xie, D.-H. Choi, S. Kar, H. V. Poor, "Fully distributed state estimation for wide-area monitoring systems" in the IEEE Trans. Smart Grid, vol. 3, no. 3, pp. 1154-1169, 2012.

[59] V. Basetti and A. K. Chandel, "Hybrid power system state estimation using Taguchi differential evolution algorithm," in IET Science, Measurement & Technology, vol. 9, no. 4, pp. 449-466, 7 2015.

[60] E. Ghahremani and I. Kamwa, "PMU analytics for decentralized dynamic state estimation of power systems using the Extended Kalman Filter with Unknown Inputs," 2015 IEEE Power & Energy Society General Meeting, Denver, CO, 2015, pp. 1-5.

[61] A. K. Singh and B. C. Pal, "Decentralized Dynamic State Estimation in Power Systems Using Unscented Transformation," in the IEEE *Transactions on Power Systems*, vol. 29, no. 2, pp. 794-804, March 2014

[62] E. Ghahremani and I. Kamwa, "Local and Wide-Area PMU-Based Decentralized Dynamic State Estimation in Multi-Machine Power Systems," in the IEEE Transactions on Power Systems, vol. 31, no. 1, pp. 547-562, Jan. 2016.

[63] Y. Chakhchoukh, V. Vittal and G. T. Heydt, "PMU Based State Estimation by Integrating Correlation," in the IEEE Transactions on Power Systems, vol. 29, no. 2, pp. 617-626, March 2014.

[64] E. Ghahremani and I. Kamwa, "PMU analytics for decentralized dynamic state estimation of power systems using the Extended Kalman Filter with Unknown Inputs," 2015 IEEE Power & Energy Society General Meeting, Denver, CO, 2015, pp. 1-5.

[65] J. Du, S. Ma, Y. C. Wu and H. V. Poor, "Distributed Hybrid Power State Estimation Under PMU Sampling Phase Errors," in the IEEE Transactions on Signal Processing, vol. 62, no. 16, pp. 4052-4063, Aug.15, 2014.

[66] V. Basetti and A. K. Chandel, "Hybrid power system state estimation using Taguchi differential evolution algorithm," in IET Science, Measurement & Technology, vol. 9, no. 4, pp. 449-466, 7 2015

[67] Wei Li, Luigi Vanfretti, A PMU-based state estimator considering classic HVDC links under different control modes, Sustainable Energy, Grids and Networks, Volume 2, June 2015, Pages 69-82, ISSN 2352-4677, http://dx.doi.org/10.1016/j.segan.2015.04.004.

[68] V. Donde, X. Feng, I. Segerqvist and M. Callavik, "Distributed State Estimation of Hybrid AC/HVDC Grids by Network Decomposition," in the IEEE Transactions on Smart Grid, vol. 7, no. 2, pp. 974-981, March 2016.

[69] S. J. Huang and K. R. Shih, "Dynamic-state-estimation scheme including nonlinear measurement-function considerations," in *IEE Proceedings - Generation, Transmission and Distribution*, vol. 149, no. 6, pp. 673-678, Nov 2002.

[70] P. Rousseaux, T. Van Cutsem, and T. E. Dy Liacco, "Whither dynamic state estimation?," *International Journal of Electrical Power & Energy Systems*, vol. 12, no. 2, pp. 104-116, Apr. 1990.

[71] A. S. Debs and R. E. Larson, "A Dynamic Estimator for Tracking the State of a Power System," in the IEEE *Transactions on Power Apparatus and Systems*, vol. PAS-89, no. 7, pp. 1670-1678, Sept. 1970.

[72] W. Miller and J. Lewis, "Dynamic state estimation in power systems," in the IEEE Transactions on Automatic Control, vol. 16, no. 6, pp. 841-846, Dec 1971.

[73] M. F. Allam and M. A. Laughton, "Power-system dynamic-state estimation by optimal variable incremental displacements," in Electrical Engineers, Proceedings of the Institution of, vol. 123, no. 5, pp. 433-436, May 1976.

[74] M. F. Allam and M. A. Laughton, "Power-system dynamic-state estimation by optimal variable incremental displacements," in Electrical Engineers, Proceedings of the Institution of, vol. 123, no. 5, pp. 433-436, May 1976.

[75] K. Nishiya, J. Hasegawa and T. Koike, "Dynamic state estimation including anomaly detection and identification for power systems," in IEE Proceedings C - Generation, Transmission and Distribution, vol. 129, no. 5, pp. 192-198, September 1982.

[76] A. M. L. da Silva, M. B. D. C. Filho and J. M. C. Cantera, "An Efficient Dynamic State Estimation Algorithm Including Bad Data Processing," in the IEEE *Power Engineering Review*, vol. PER-7, no. 11, pp. 49-49, Nov. 1987.

[77] A. K. Sinha and J. K. Mondal, "Dynamic state estimator using ANN based bus load prediction," in the IEEE *Transactions on Power Systems*, vol. 14, no. 4, pp. 1219-1225, Nov 1999.

[78] F. Aminifar, M. Shahidehpour, M. Fotuhi-Firuzabad and S. Kamalinia, "Power System Dynamic State Estimation With Synchronised Phasor Measurements," in the IEEE *Transactions on Instrumentation and Measurement*, vol. 63, no. 2, pp. 352-363, Feb. 2014.

[79] L. Hu, Z. Wang and X. Liu, "Dynamic State Estimation of Power Systems With Quantization Effects: A Recursive Filter Approach," in the IEEE Transactions on Neural Networks and Learning Systems, vol. 27, no. 8, pp. 1604-1614, Aug. 2016.

[80] R. Huang, G. Cokkinides, C. Hedrington and S. A. P. Meliopoulos, "Distribution System Distributed Quasi-Dynamic State Estimator," in the IEEE *Transactions on Smart Grid*, vol. 7, no. 6, pp. 2761-2770, Nov. 2016.

[81] J. Zhao, M. Netto and L. Mili, "A Robust Iterated Extended Kalman Filter for Power System Dynamic State Estimation," in the IEEE Transactions on Power Systems, vol. 32, no. 4, pp. 3205-3216, July 2017.

[82] E. Ghahremani and I. Kamwa, "Local and Wide-Area PMU-Based Decentralized Dynamic State Estimation in Multi-Machine Power Systems," in the IEEE Transactions on Power Systems, vol. 31, no. 1, pp. 547-562, Jan. 2016.

[83] M. A. M. Ariff, B. C. Pal and A. K. Singh, "Estimating Dynamic Model Parameters for Adaptive Protection and Control in Power System," in the IEEE *Transactions on Power Systems*, vol. 30, no. 2, pp. 829-839, March 2015.

[84] N. Zhou, D. Meng, Z. Huang and G. Welch, "Dynamic State Estimation of a Synchronous Machine Using PMU Data: A Comparative Study," in the IEEE Transactions on Smart Grid, vol. 6, no. 1, pp. 450-460, Jan. 2015.

[85] S. A. A. Shahriari, M. Raoofat, M. Dehghani, M. Mohammadi and M. Saad, "Dynamic state estimation of a permanent magnet synchronous generator-based wind turbine," in IET Renewable Power Generation, vol. 10, no. 9, pp. 1278-1286, 10 2016.

[86] Y. Cui, R. G. Kavasseri and S. M. Brahma, "Dynamic State Estimation Assisted Out-of-Step Detection for Generators Using Angular Difference," in the IEEE Transactions on Power Delivery, vol. 32, no. 3, pp. 1441-1449, June 2017.

[87] N. Zhou, D. Meng and S. Lu, "Estimation of the Dynamic States of Synchronous Machines Using an Extended Particle Filter," in the IEEE Transactions on Power Systems, vol. 28, no. 4, pp. 4152-4161, Nov. 2013.

[88] G. Anagnostou; B. C. Pal, "Derivative-free Kalman filtering based Approaches to Dynamic State Estimation for Power Systems with Unknown Inputs," in the IEEE *Transactions on Power Systems* , vol.PP, no.99, pp.1-1

[89] E. Ghahremani and I. Kamwa, "Dynamic State Estimation in Power System by Applying the Extended Kalman Filter With Unknown Inputs to Phasor Measurements," in the IEEE Transactions on Power Systems, vol. 26, no. 4, pp. 2556-2566, Nov. 2011.

[90] A. Rouhani and A. Abur, "Observability Analysis for Dynamic State Estimation of Synchronous Machines," in the IEEE *Transactions on Power Systems*, vol. 32, no. 4, pp. 3168-3175, July 2017.

[91] J. Qi, K. Sun and W. Kang, "Optimal PMU Placement for Power System Dynamic State Estimation by Using Empirical Observability Gramian," in the IEEE *Transactions on Power Systems*, vol. 30, no. 4, pp. 2041-2054, July 2015.

[92] H. Chen, M. Liu and S. Zhang, "Event-triggered distributed dynamic state estimation with imperfect measurements over a finite horizon," in IET Control Theory & Applications, vol. 11, no. 15, pp. 2607-2622, 10 13 2017.

[93] H. Modir and R. A. Schlueter, "A Dynamic State Estimator for Dynamic Security Assessment," in the IEEE Transactions on Power Apparatus and Systems, vol. PAS-100, no. 11, pp. 4644-4652, Nov. 1981.

[94] Wikipedia, Available: https://en.wikipedia.org/wiki/Stochastic_process.

[95] Wikipedia, Available: https://en.wikipedia.org/wiki/Random_variable.

[96] G. C. Contaxis and G. N. Korres, "A reduced model for power system observability: analysis and restoration," IEEE Transactions on Power Systems, vol. 3, pp. 1411-1417, 1988.

[97] A. Chakrabortty, P. Khargoneka, "Introduction to wide-area control of power systems", Proc. Amer. Control Conf., pp. 6773-6785, 2013.

[98] J. Chen and A. Abur, "Placement of PMUs to Enable Bad Data Detection in State Estimation," in the IEEE *Transactions on Power Systems*, vol. 21, no. 4, pp. 1608-1615, Nov. 2006.

[99] N. G. Bretas and J. B. A. London, "Measurement placement design and reinforcement for state estimation purposes," *2001 IEEE Porto Power Tech Proceedings (Cat. No.01EX502)*, Porto, 2001, pp. 6 pp. vol.3-.

[100] E. Handschin, F.C. Schweppe, J. Kohlas, and A. Fiechter, "Bad data analysis for power system state estimation," IEEE Transactions on Power Apparatus and Systems, vol. 94, no. 2, pp. 329-337, May 1975.

[101] A. Monticelli, State Estimation in Electric Power Systems: A Generalized Approach. Massachusetts: Kluwer Academic Publishers, 1999.

[102] K. A. Clements and P. W. Davis, "Multiple Bad Data Detectability and Identifiability, A Geometric Approach," in the IEEE *Power Engineering Review*, vol. PER-6, no. 7, pp. 73-73, July 1986.

[103] M.C. de Almeida, E.N. Asada, A.V. Garcia, On the use of Gram matrix in observability analysis, IEEE Trans. Power Syst. 23 (2008) 249–251.

[104] M.C. de Almeida, E.N. Asada, A.V. Garcia, Power system observability analysis based on Gram matrix and minimum norm solution, IEEE Trans. Power Syst. 23 (2008) 1611–1618.

[105] G. N. Korres. A Gram matrix-based method for observability restoration," IEEE Transactions on Power Systems, vol. 26, no. 4, pp. 2569-2571, Nov. 2011.

[106] G. C. Contaxis, G. N. Korres, A reduced model for power system observability analysis and restoration, IEEE Trans. Power Syst. 3 (1988) 1411–1417.

[107] E. Castillo, A.J. Conejo, R.E. Pruneda, C. Solares, State estimation observability based on the null space of the measurement Jacobian matrix, IEEE Trans. Power Syst. 20 (2005) 1656–1658.

[108] E. Castillo, A.J. Conejo, R.E. Pruneda, C. Solares, Observability analysis in state estimation: a unified numerical approach, IEEE Trans. Power Syst. 21 (2006) 877–886.

[109] G. N. Korres. An integer-arithmetic algorithm for observability analysis of systems with SCADA and PMU measurements. Electric Power Systems Research, Vol. 81, pp. 1388-1402, March 2011.

[110] B. Gou, "Jacobian matrix-based observability analysis for state estimation," in the IEEE *Transactions on Power Systems*, vol. 21, no. 1, pp. 348-356, Feb. 2006.

[111] G. Strang, Linear Algebra and Its Applications, 3rd Edition ed.: Harcourt Brace Jovanovich, 1988.

[112] Z.Jin; P.Dattaray; P.Wall; J.Yu; V.Terzija, "A Screening Rule Based Iterative Numerical Method for Observability Analysis," in the IEEE *Transactions on Power Systems* , vol.PP, no.99, pp.1-1.

[113] Pserc.cornell.edu. (2017). Index for Directory matpower5.0. [online] Available at: http://www.pserc.cornell.edu/matpower/docs/ref/matpower5.0/menu5.0.html [Accessed 22 Nov. 2015].

[114] Manousakis, N.M.; Korres, G.N.; Georgilakis, P.S., "Taxonomy of PMU Placement Methodologies," in Power Systems, IEEE Transactions on Power Systems, vol.27, no.2, pp.1070-1077, May 2012.

[115] R. Sodhi, S. C. Srivastava, and S. N. Singh, "Optimal PMU placement to ensure system observability under contingencies," in *Proc. IEEE Power Eng. Soc. General Meeting*, 2009, pp. 1–6.

[116] F. Aminifar, A. Khodaei, M. Fotuhi-Firuzabad, and M. Shahidehpour, "Contingency-constrained PMU placement in power networks," *IEEE Trans. Power Syst.*, vol. 25, no. 1, pp. 516–523, Feb. 2010.

[117] D. Dua, S. Dambhare, R. K. Gajbhiye, and S. A. Soman, "Optimal multistage scheduling of PMU placement: An ILP approach," *IEEE Trans. Power Del.*, vol. 23, no. 4, pp. 1812–1820, Oct. 2008.

[118] R. Emami and A. Abur, "Robust measurement design by placing synchronised phasor measurements on network branches," *IEEE Trans. Power Syst.*, vol. 25, no. 1, pp. 38–43, Feb. 2010.

[119] S. Chakrabarti, D. Eliades, E. Kyriakides, and M. Albu, "Measurement uncertainty considerations in optimal sensor deployment for state estimation," in *Proc. IEEE Int. Symp. Intelligent Signal Processing*, 2007.

[120] S. Chakrabarti, E. Kyriakides, and D. G. Eliades, "Placement of synchronised measurements for power system observability," *IEEE Trans. Power Del.*, vol. 24, no. 1, pp. 12–19, Jan. 2009.

[121] B. Milosevic and M. Begovic, "Nondominated sorting genetic algorithm for optimal phasor measurement placement," in the IEEE Transactions on Power Systems, vol. 18, no. 1, pp. 69-75, Feb 2003.

[122] Mahdi Hajian, Ali Mohammad Ranjbar, Turaj Amraee, Babak Mozafari, Optimal placement of PMUs to maintain network observability using a modified BPSO algorithm, In International Journal of Electrical Power & Energy Systems, Volume 33, Issue 1, 2011, Pages 28-34, ISSN 0142-0615, https://doi.org/10.1016/j.ijepes.2010.08.007.

[123] I. Kamwa and R. Grondin, "PMU configuration for system dynamic performance measurement in large, multiarea power systems," in the IEEE Transactions on Power Systems, vol. 17, no. 2, pp. 385-394, May 2002.

[124] R. F. Nuqui, A. G. Phadke, R. P. Schulz and N. Bhatt, "Fast on-line voltage security monitoring using synchronised phasor measurements and decision trees," 2001 IEEE Power Engineering Society Winter Meeting. Conference Proceedings (Cat. No.01CH37194), Columbus, OH, 2001, pp. 1347-1352 vol.3.

[125] C. Rakpenthai, S. Premrudeepreechacharn, S. Uatrongjit and N. R. Watson, "An Optimal PMU Placement Method Against Measurement Loss and Branch Outage," in the IEEE Transactions on Power Delivery, vol. 22, no. 1, pp. 101-107, Jan. 2007.

[126] N. H. Abbasy and H. M. Ismail, "A unified approach for the optimal PMU location for power system state estimation," *IEEE Trans. Power Syst.*, vol. 24, no. 2, pp. 806–813, May 2009.

[127] G. B. Denegri, M. Invernizzi and F. Milano, "A security oriented approach to PMU positioning for advanced monitoring of a transmission grid," Proceedings. International Conference on Power System Technology, 2002, pp. 798-803 vol.2.

[128] M. Korkali and A. Abur, "Placement of PMUs with channel limits," in *Proc. IEEE Power Eng. Soc. General Meeting*, 2009.

[129] M. Korkali and A. Abur, "Impact of network sparsity on strategic placement of phasor measurement units with fixed channel capacity," in *Proc. IEEE Int. Symp. Circuits and Syst. (ISCAS)*, 2010, pp. 3445–3448.

[130] K.-S. Cho, J.-R. Shin, and S. H. Hyun, "Optimal placement of phasor measurement units with GPS receiver," *Proc. IEEE Power Eng. Soc. Winter Meeting*, pp. 258–262, 2001.

[131] H.-S. Zhao, Y. Li, Z.-Q. Mi, and L. Yu, "Sensitivity constrained PMU placement for complete observability of power systems," in *Proc. IEEE Power Eng. Soc. Transm. Distrib. Conf. Exhib.*, 2005.

[132] R. Kavasseri, S. K. Srinivasan, "Joint optimal placement of PMU and conventional measurements in power systems", Proc. IEEE Int. Symp. Circuits and Syst. (ISCAS), pp. 3449-3452, 2010.

[133] F. Aminifar, M. Fotuhi-Firuzabad, M. Shahidehpour, A. Khodaei, "Probabilistic multistage PMU placement in electric power systems", *IEEE Trans. Power Del.*, vol. 26, no. 2, pp. 841-849, Apr. 2011.

[134] S. Chakrabarti, E. Kyriakides, "Optimal placement of phasor measurement units for power system observability", IEEE Trans. Power Syst., vol. 23, no. 3, pp. 1433-1440, Aug. 2008.

[135] J. Peng, Y. Sun, H. F. Wang, "Optimal PMU placement for full network observability using Tabu search algorithm", Int. J. Elect. Power Energy Syst., vol. 28, no. 4, pp. 223-231, May 2006.

[136] K.-S. Cho, J.-R. Shin, S. H. Hyun, "Optimal placement of phasor measurement units with GPS receiver", Proc. IEEE Power Eng. Soc. Winter Meeting, pp. 258-262, 2001.

[137] H.-S. Zhao, Y. Li, Z.-Q. Mi, L. Yu, "Sensitivity constrained PMU placement for complete observability of power systems", Proc. IEEE Power Eng. Soc. Transm. Distrib. Conf. Exhib., 2005.

[138] C. Peng, H. Sun, J. Guoa, "Multi-objective optimal PMU placement using a non-dominated sorting differential evolution algorithm", Int. J. Elect. Power Energy Syst., vol. 32, no. 8, pp. 886-892, Oct. 2010.

[139] M. Hajian, A. M. Ranjbar, T. Amraee, B. Mozafari, "Optimal placement of PMUs to maintain network observability using a modified BPSO algorithm", Int. J. Elect. Power Energy Syst., vol. 33, no. 1, pp. 28-34, Jan. 2011.

[140] A. Ahmadi, Y. Alinejad-Beromi, M. Moradi, "Optimal PMU placement for power system observability using binary particle swarm optimisation and considering measurement redundancy", Expert Syst. Appl., vol. 38, pp. 7263-7269, 2011.

[141] F. Aminifar, C. Lucas, A. Khodaei, M. Fotuhi-Firuzabad, "Optimal placement of phasor measurement units using immunity genetic algorithm", IEEE Trans. Power Del., vol. 24, no. 3, pp. 1014-1020, Jul. 2009.

[142] M. Zhou, V. A. Centeno, A. G. Phadke, Y. Hu, D. Novosel, H. A. R. Volskis, "A preprocessing method for effective PMU placement studies", Proc. IEEE Int. Conf. Electric Utility Deregulation Restructuring Power Technologies, pp. 2862-2867, 2008.

[143] B. Gou, "Generalized integer linear programming formulation for optimal PMU placement," *IEEE Trans. Power Syst.*, vol. 23, no. 3, pp. 1099–1104, Aug. 2008.

[144] B. Gou, "Optimal placement of PMUs by integer linear programming," *IEEE Trans. Power Syst.*, vol. 23, no. 3, pp. 1525–1526, Aug. 2008.

[145] B. Xu and A. Abur, "Observability analysis and measurement placement for systems with PMUs," IEEE PES Power Systems Conference and Exposition, 2004., 2004, pp. 943-946 vol.2.

[146] Ranjana Sodhi, S.C. Srivastava, S.N. Singh, Optimal PMU placement method for complete topological and numerical observability of power system, In Electric Power Systems Research, Volume 80, Issue 9, 2010, Pages 1154-1159, ISSN 0378-7796, https://doi.org/10.1016/j.epsr.2010.03.005.

[147] J. Chen, A. Abur, "Improved bad data processing via strategic placement of PMUs", Proc. IEEE Power Eng. Soc. General Meeting, pp. 509-513, 2005.

[148] J. Chen, A. Abur, "Placement of PMUs to enable bad data detection in state estimation", IEEE Trans. Power Syst., vol. 21, no. 4, pp. 1608-1615, Nov. 2006.

[149] I. Kamwa, R. Grondin, "PMU configuration for system dynamic performance measurement in large multiarea power systems", IEEE Trans. Power Syst., vol. 17, no. 2, pp. 385-394, May 2002.

[150] W. Jiang, V. Vittal, G. T. Heydt, "A distributed state estimator utilizing synchronised phasor measurements", IEEE Trans. Power Syst., vol. 22, no. 2, pp. 1-6, May 2007.

[151] University of Washington. Power Systems Test Case Archive. Available: https://www.ee.washington.edu/research/pstca/, 2015

[152] A. G. Phadke, J. S. Thorp, R. F. Nuqui, and M. Zhou, "Recent developments in state estimation with phasor measurements," in Power Systems Conference and Exposition, 2009. PSCE '09. IEEE/PES, 2009, pp. 1-7.

[153] A. Gómez-Expósito, A. Abur, and P. Rousseaux, "On the use of PMUs in power system state estimation," presented at the Proc. Power Systems Computation Conf., Stockholm, Sweden, 2011.

[154] S. G. Ghiocel, J. H. Chow, G. Stefopoulos, B. Fardanesh, D. Maragal, B. Blanchard, M. Razanousky, and D. B. Bertagnolli, "Phasor-Measurement-Based State Estimation for Synchrophasor Data Quality Improvement and Power Transfer Interface Monitoring," Power Systems, IEEE Transactions on, vol. 29, pp. 881-888, 2014.

[155] L. Vanfretti, J. H. Chow, S. Sarawgi, and B. Fardanesh, "A Phasor-Data-Based State Estimator Incorporating Phase Bias Correction," Power Systems, IEEE Transactions on, vol. 26, pp. 111-119, 2011.

[156] S. Di, D. J. Tylavsky, and N. Logic, "An Adaptive Method for Detection and Correction of Errors in PMU Measurements," Smart Grid, IEEE Transactions on, vol. 3, pp. 1575-1583, 2012.

[157] Kirincic, V., Skok, S. & Frankovic, D. (2016). A Synchrophasor Assisted Hybrid State Estimator. Journal of Electrical Engineering, 67(2), pp. 103-110.

[158] A. Simões Costa, A. Albuquerque and D. Bez, "An estimation fusion method for including phasor measurements into power system real-time modeling," in the IEEE Transactions on Power Systems, vol. 28, no. 2, pp. 1910-1920, May 2013.

[159] J. Du, S. Ma, Y. C. Wu and H. V. Poor, "Distributed Hybrid Power State Estimation Under PMU Sampling Phase Errors," in the IEEE Transactions on Signal Processing, vol. 62, no. 16, pp. 4052-4063, Aug.15, 2014.

[160] A. G. Phadke and J. S. Thorp, Computer relaying for Power Systems: Research Sudies Press, Somerset, England, 1988.

[161] J. S. Thorp and A. G. Phadke, "Real-time voltage phasor measurements for static state estimation," IEEE Transactions on Power Apparatus and Systems, vol. Vol. 104, No. 11, November 1985, pp. 3098-3017, 1985.

[162] A. G. Phadke and J. S. Thorp, "State estimation with phasor measurements," IEEE Transactions on Power Apparatus and Systems, vol. Vol. 1, No.1, pp. 233-241, 1986.

[163] M. Göl and A. Abur, "Observability and Criticality Analyses for Power Systems Measured by Phasor Measurements," in the IEEE Transactions on Power Systems, vol. 28, no. 3, pp. 3319-3326, Aug. 2013.

[164] J. K. Mandal, A. K. Sinha and L. Roy, "Incorporating nonlinearities of measurement function in power system dynamic state estimation," in IEE Proceedings - Generation, Transmission and Distribution, vol. 142, no. 3, pp. 289-296, May 1995.

[165] G. Valverde and V. Terzija, "Unscented Kalman filter for power system dynamic state estimation," in IET Generation, Transmission & Distribution, vol. 5, no. 1, pp. 29-37, Jan. 2011.

[166] N.G. Bretas, An iterative dynamic state estimation and bad data processing, International Journal of Electrical Power & Energy Systems, Volume 11, Issue 1, 1989, Pages 70-74, ISSN 0142-0615, http://dx.doi.org/10.1016/0142-0615(89)90010-0.

[167] Gelb, A. (1974). Applied Optimal Estimation, MIT Press.

[168] P. Rousseaux, Th. Van Cutsem, T.E. Dy Liacco, Whither dynamic state estimation?, International Journal of Electrical Power & Energy Systems, Volume 12, Issue 2, 1990.

[169] A. K. Singh and B. C. Pal, "Decentralized dynamic state estimation in power systems using unscented transformation," 2014 IEEE PES General Meeting | Conference & Exposition, National Harbor, MD, 2014, pp. 1-1.

[170] A. Mam, B. Pal and A. Singh, "Estimating dynamic model parameters for adaptive protection and control in power system," 2015 IEEE Power & Energy Society General Meeting, Denver, CO, 2015, pp. 1-1.

[171] A. M. Leite da Silva, M. B. Do Coutto Filho, and J. F. de Queiroz, "State forecasting in electric power systems," *IEE Proceedings on Generation, Transmission and Distribution*, vol. 130, no. 5, pp. 237-244, Sept. 1983.

[172] I. Arasaratnam and S. Haykin, "Cubature Kalman Filters," in the IEEE Transactions on Automatic Control, vol. 54, no. 6, pp. 1254-1269, June 2009.

Appendices

Appendix A: The Chokesky Factorisation

Consider a positive definite symmetric matrix, **G**. The symmetry of the matrix allows it to be decomposed into a product of three matrices including a lower triangular matrix and its transposed matrix (A.1)-(A.2):

$$\begin{aligned}\mathbf{G} &= \begin{bmatrix} d_1 & \mathbf{l}_1^T \\ \mathbf{l}_1 & \mathbf{G}_1' \end{bmatrix} \\ &= \begin{bmatrix} 1 & \mathbf{0} \\ \mathbf{l}_1 & \mathbf{I}_{N-1} \end{bmatrix} \begin{bmatrix} d_1 & \mathbf{0} \\ \mathbf{0} & \mathbf{G}_1 \end{bmatrix} \begin{bmatrix} 1 & \mathbf{l}_1^T \\ \mathbf{0} & \mathbf{I}_{N-1} \end{bmatrix} \\ &= \mathbf{L}_1 \mathbf{D}_1 \mathbf{L}_1^T \end{aligned} \tag{A.1}$$

$$\mathbf{G}_1 = \mathbf{G}_1' - \frac{\mathbf{l}_1 \mathbf{l}_1^T}{d_1} \tag{A.2}$$

For the following steps, i=1…N, the factorisation process can be induced as follows:

$$\begin{aligned}\mathbf{D}_i &= \begin{bmatrix} d_1 & & & \\ & \ddots & & \\ & & d_i & \mathbf{l}_{i+1}^T \\ & & \mathbf{l}_{i+1} & \mathbf{G}_i' \end{bmatrix} \\ &= \begin{bmatrix} 1 & & & \\ & \ddots & & \\ & & 1 & \\ & & \mathbf{l}_{i+1} & \mathbf{I}_{N-i-1} \end{bmatrix} \begin{bmatrix} d_1 & & & \\ & \ddots & & \\ & & d_i & \mathbf{0} \\ & & \mathbf{0} & \mathbf{G}_i \end{bmatrix} \begin{bmatrix} 1 & & & \\ & \ddots & & \\ & & 1 & \mathbf{l}_{i+1}^T \\ & & & \mathbf{I}_{N-i-1} \end{bmatrix} \\ &= \mathbf{L}_{i+1} \mathbf{D}_{i+1} \mathbf{L}_{i+1}^T \end{aligned} \tag{A.3}$$

In the end, the symmetric matrix, **G**, can be factorised into a diagonal matrix left and right multiplied by a lower triangular matrix and its transposed matrix, respectively:

$$\mathbf{G} = \mathbf{L}_1 \mathbf{L}_2 \cdots \mathbf{L}_N \mathbf{D} \mathbf{L}_N^T \cdots \mathbf{L}_2^T \mathbf{L}_1^T = \mathbf{L} \mathbf{D} \mathbf{L}^T \tag{A.4}$$

Appendix B: Type 2 Pathological Case in the IEEE 118 Bus Test System

In this section, a Type 2 pathological case in the standard IEEE 118 Bus Test System that required multiple iterations is presented. The placement of the power injection measurements and the power flow measurements are given in Table A-1, while the results including the observable islands identified and the irrelevant injection measurements in the three iterations are presented in Table A-2. In the three iterations, the rank deficiency of the gain matrix, $R_d(\mathbf{G})$, is equal to 54, 56 and 77, and the corresponding calculated *PCIR*s are 1, 1 and 0, respectively.

Table A-1: Measurement Placement in the IEEE 118 Bus Test System

Power injection measurements at Bus #	5;8;11;12;16;17;18;19;25;26;27;30;31;32;34;43;44;45;49;65;66;68;77;80;81
Power flow measurements from at Branch #	5;7;11;13;14;15;16;18;19;25;26;35;40;41;43;49;50;54;62;65;66;69;70;71;75;76;97;98;99;100;103;107;118;119;120;122;123;124;149;151;152;153;179;182;183

Table A-2: Observable Islands and Irrelevant Injection Measurements Identified in the Three Iterations

Iteration 1 (55 observable islands that are expressed by {Bus #} and 2 irrelevant injection measurements at Bus#)	{1};{10};{21};{22};{24};{33};{35};{39};{40};{41};{52};{53};{55};{56;{57};{58};{59};{60};{61};{63};{70};{71};{72};{73};{74};{83};{84};{85};{86};{87};{88};{89};{90};{91};{92};{93};{94};{95};{100};{101};{102};{103};{104};{105};{106};{107};{108};{109};{110};{111};{112};{118};{2;3;4;5;6;7;8;9;11;12;13;14;15;16;17;18;19;20;23;25;26;27;28;29;30;31;32;34;36;37;38;42;43;44;45;46;47;48;49;50;51;54;62;64;65;66;67;68;69;75;76;77;80;81;97;98;99;113;114;115;116;117};{78;79};{82;96}
	77;80

Iteration 2 (76 observable islands that are expressed by {Bus #} and 21 irrelevant injection measurements at Bus#)	{1};{4};{10};{16};{17};{18};{21};{22};{24};{33};{35};{39};{40};{41};{43};{44};{52};{53};{55};{56};{57};{58};{59};{60};{61};{63};{70};{71};{72};{73};{74};{81};{83};{84};{85};{86};{87};{88};{89};{90};{91};{92};{93};{94};{95};{100};{101};{102};{103};{104};{105};{106};{107};{108};{109};{110};{111};{112};{117};{118};{2;3;5;6;7;11;12};{8;9};{13;14;15};{19;20};{23;25;26;27;30;32;38;113};{28;29;31};{34;36;37};{45;46};{42;47;48;49;50;51;54};{64;65};{62;66;67};{68;116};{69;75;76;77;80;97;98;99};{78;79};{82;96};{114;115}
	5;8;11;12;16;17;18;19;27;30;31;32;34;43;44;45;49;65;66;68;81
Iteration 3 (79 observable islands that are expressed by {Bus #} and 2 irrelevant injection measurements at Bus#)	{1};{4};{10};{16};{17};{18};{21};{22};{24};{25};{26};{33};{35};{39};{40};{41};{43};{44};{52};{53};{55};{56};{57};{58};{59};{60};{61};{63};{70};{71};{72};{73};{74};{81};{83};{84};{85};{86};{87};{88};{89};{90};{91};{92};{93};{94};{95};{100};{101};{102};{103};{104};{105};{106};{107};{108};{109};{110};{111};{112};{117};{118};{2;3;5;6;7;11;12};{8;9};{13;14;15};{19;20};{23;27;32;113};{28;29;31};{34;36;37};{30;38};{45;46};{42;47;48;49;50;51;54};{64;65};{62;66;67};{68;116};{69;75;76;77;80;97;98;99};{78;79};{82;96};{114;115}
	25;26

Appendix C: Data Sheets for IEEE Test Systems

Appendix C.1: Data Sheets for IEEE 14 Bus Test System

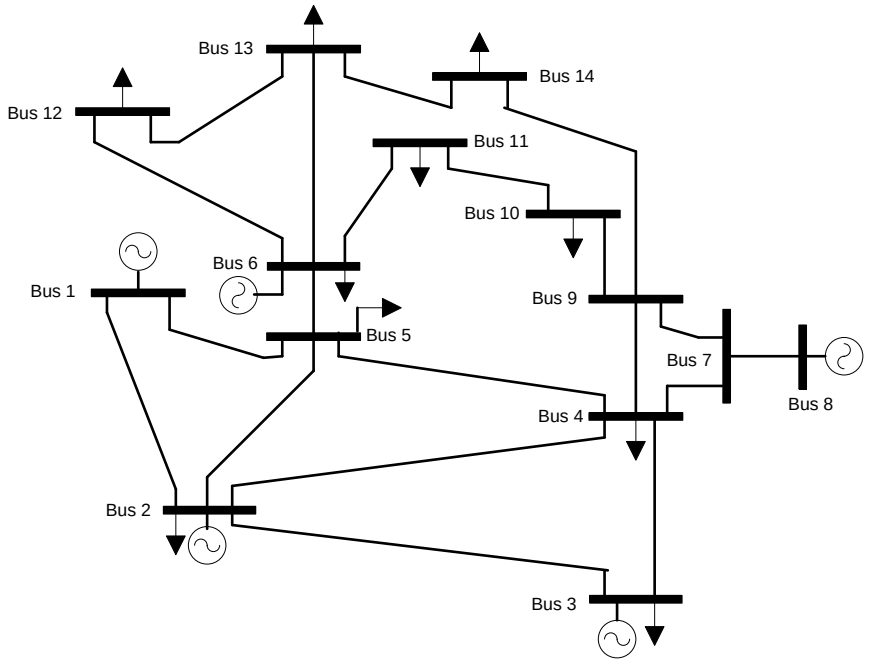

Figure A-1: Network Diagram for IEEE 14 Bus Test System

Table A-3: Bus Data for IEEE 14 Bus Test System

Bus	Voltage		Generation		Demand		Shunt Elements	
#	Mag(pu)	Ang(deg)	P (MW)	Q (MVAr)	P (MW)	Q (MVAr)	Gs (MW)	Bs (MVAr.)
1	1.060	0.000	232.39	-16.55	-	-	-	-
2	1.045	-4.983	40.00	43.56	21.70	12.70	-	-
3	1.010	-12.725	0.00	25.08	94.20	19.00	-	-
4	1.018	-10.313	-	-	47.80	-3.90	-	-
5	1.020	-8.774	-	-	7.60	1.60	-	-
6	1.070	-14.221	0.00	12.73	11.20	7.50	-	-
7	1.062	-13.360	-	-	-	-	-	-
8	1.090	-13.360	0.00	17.62	-	-	-	-
9	1.056	-14.939	-	-	29.50	16.60	-	-
10	1.051	-15.097	-	-	9.00	5.80	-	-
11	1.057	-14.791	-	-	3.50	1.80	-	-
12	1.055	-15.076	-	-	6.10	1.60	-	-

13	1.050	-15.156	-	-	13.50	5.80	-	-
14	1.036	-16.034	-	-	14.90	5.00	-	-

Table A-4: Branch Data for IEEE 14 Bus Test System

From Bus	To Bus	R p.u.	X p.u.	B p.u.	Tap p.u.
1	2	0.01938	0.05917	0.05280	1.0000
1	5	0.05403	0.22304	0.04920	1.0000
2	3	0.04699	0.19797	0.04380	1.0000
2	4	0.05811	0.17632	0.03400	1.0000
2	5	0.05695	0.17388	0.03460	1.0000
3	4	0.06701	0.17103	0.01280	1.0000
4	5	0.01335	0.04211	0.00000	1.0000
4	7	0.00000	0.20912	0.00000	0.9780
4	9	0.00000	0.55618	0.00000	0.9690
5	6	0.00000	0.25202	0.00000	0.9320
6	11	0.09498	0.19890	0.00000	1.0000
6	12	0.12291	0.25581	0.00000	1.0000
6	13	0.06615	0.13027	0.00000	1.0000
7	8	0.00000	0.17615	0.00000	1.0000
7	9	0.00000	0.11001	0.00000	1.0000
9	10	0.03181	0.08450	0.00000	1.0000
9	14	0.12711	0.27038	0.00000	1.0000
10	11	0.08205	0.19207	0.00000	1.0000
12	13	0.22092	0.19988	0.00000	1.0000
13	14	0.17093	0.34802	0.00000	1.0000

Appendix C.2: Data Sheets for IEEE 39 Bus Test System

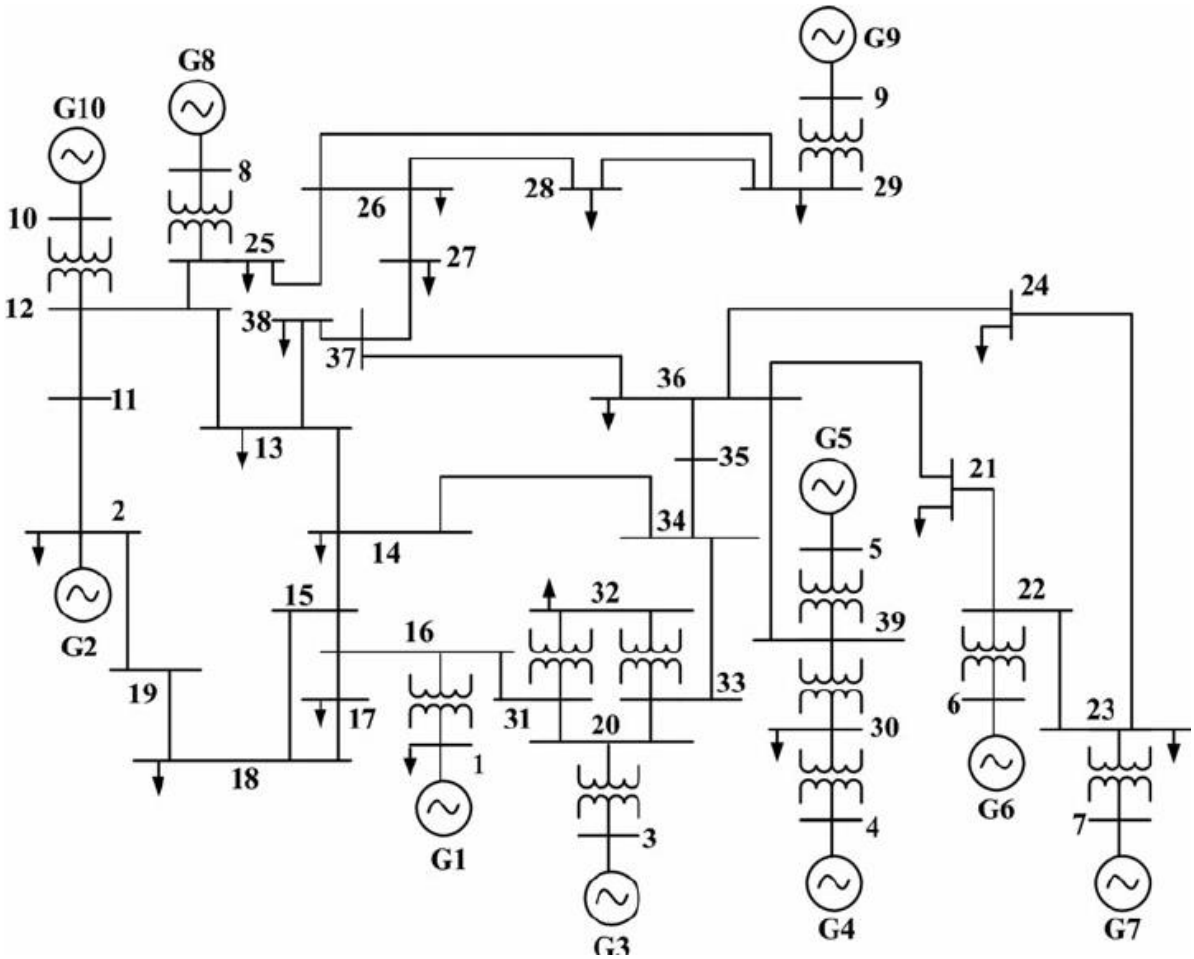

Figure A-2: Network Diagram for IEEE 39 Bus Test System

Table A-5: Bus Data for IEEE 39 Bus Test System

Bus	Voltage		Generation		Demand		Shunt Elements	
#	Mag(pu)	Ang(deg)	P (MW)	Q (MVAr)	P (MW)	Q (MVAr)	Gs (MW)	Bs (MVAr)
1	1	0	-	-	-	-	-	-
2	1	0	-	-	-	-	-	-
3	1	0	-	-	322	2.4	-	-
4	1	0	-	-	500	184	-	-
5	1	0	-	-	-	-	-	-
6	1	0	-	-	-	-	-	-
7	1	0	-	-	233.8	84	-	-

8	1	0	-	-	522	176.6	-	-
9	1	0	-	-	-	-	-	-
10	1	0	-	-	-	-	-	-
11	1	0	-	-	-	-	-	-
12	1	0	-	-	8.5	88	-	-
13	1	0	-	-	-	-	-	-
14	1	0	-	-	-	-	-	-
15	1	0	-	-	320	153	-	-
16	1	0	-	-	329.4	32.3	-	-
17	1	0	-	-	-	-	-	-
18	1	0	-	-	158	30	-	-
19	1	0	-	-	-	-	-	-
20	1	0	-	-	680	103	-	-
21	1	0	-	-	274	115	-	-
22	1	0	-	-	-	-	-	-
23	1	0	-	-	247.5	84.6	-	-
24	1	0	-	-	308.6	-92.2	-	-
25	1	0	-	-	224	47.2	-	-
26	1	0	-	-	139	17	-	-
27	1	0	-	-	281	75.5	-	-
28	1	0	-	-	206	27.6	-	-
29	1	0	-	-	283.5	26.9	-	-
30	1.0475	0	250	0	-	-	-	-
31	0.982	0	0	0	9.2	4.6	-	-
32	0.9831	0	650	0	-	-	-	-
33	0.9972	0	632	0	-	-	-	-
34	1.0123	0	508	0	-	-	-	-
35	1.0493	0	650	0	-	-	-	-
36	1.0635	0	560	0	-	-	-	-
37	1.0278	0	540	0	-	-	-	-
38	1.0265	0	830	0	-	-	-	-
39	1.03	0	1000	0	1104	250	-	-

Table A-6: Branch Data for IEEE 39 Bus Test System

From Bus	To Bus	R p.u.	X p.u.	B p.u.	Tap p.u.
1	2	0.0035	0.0411	0.6987	1
1	39	0.001	0.025	0.75	1

2	3	0.0013	0.0151	0.2572	1
2	25	0.007	0.0086	0.146	1
3	4	0.0013	0.0213	0.2214	1
3	18	0.0011	0.0133	0.2138	1
4	5	0.0008	0.0128	0.1342	1
4	14	0.0008	0.0129	0.1382	1
5	6	0.0002	0.0026	0.0434	1
5	8	0.0008	0.0112	0.1476	1
6	7	0.0006	0.0092	0.113	1
6	11	0.0007	0.0082	0.1389	1
7	8	0.0004	0.0046	0.078	1
8	9	0.0023	0.0363	0.3804	1
9	39	0.001	0.025	1.2	1
10	11	0.0004	0.0043	0.0729	1
10	13	0.0004	0.0043	0.0729	1
13	14	0.0009	0.0101	0.1723	1
14	15	0.0018	0.0217	0.366	1
15	16	0.0009	0.0094	0.171	1
16	17	0.0007	0.0089	0.1342	1
16	19	0.0016	0.0195	0.304	1
16	21	0.0008	0.0135	0.2548	1
16	24	0.0003	0.0059	0.068	1
17	18	0.0007	0.0082	0.1319	1
17	27	0.0013	0.0173	0.3216	1
21	22	0.0008	0.014	0.2565	1
22	23	0.0006	0.0096	0.1846	1
23	24	0.0022	0.035	0.361	1
25	26	0.0032	0.0323	0.513	1
26	27	0.0014	0.0147	0.2396	1
26	28	0.0043	0.0474	0.7802	1
26	29	0.0057	0.0625	1.029	1
28	29	0.0014	0.0151	0.249	1
2	30	0	0.0181	0	1.025
6	31	0	0.025	0	1.07
10	32	0	0.02	0	1.07
12	11	0.0016	0.0435	0	1.006
12	13	0.0016	0.0435	0	1.006
19	20	0.0007	0.0138	0	1.06
19	33	0.0007	0.0142	0	1.07
20	34	0.0009	0.018	0	1.009

22	35	0	0.0143	0	1.025
23	36	0.0005	0.0272	0	1
25	37	0.0006	0.0232	0	1.025
29	38	0.0008	0.0156	0	1.025

Appendix C.3: Data Sheets for IEEE 57 Bus Test System

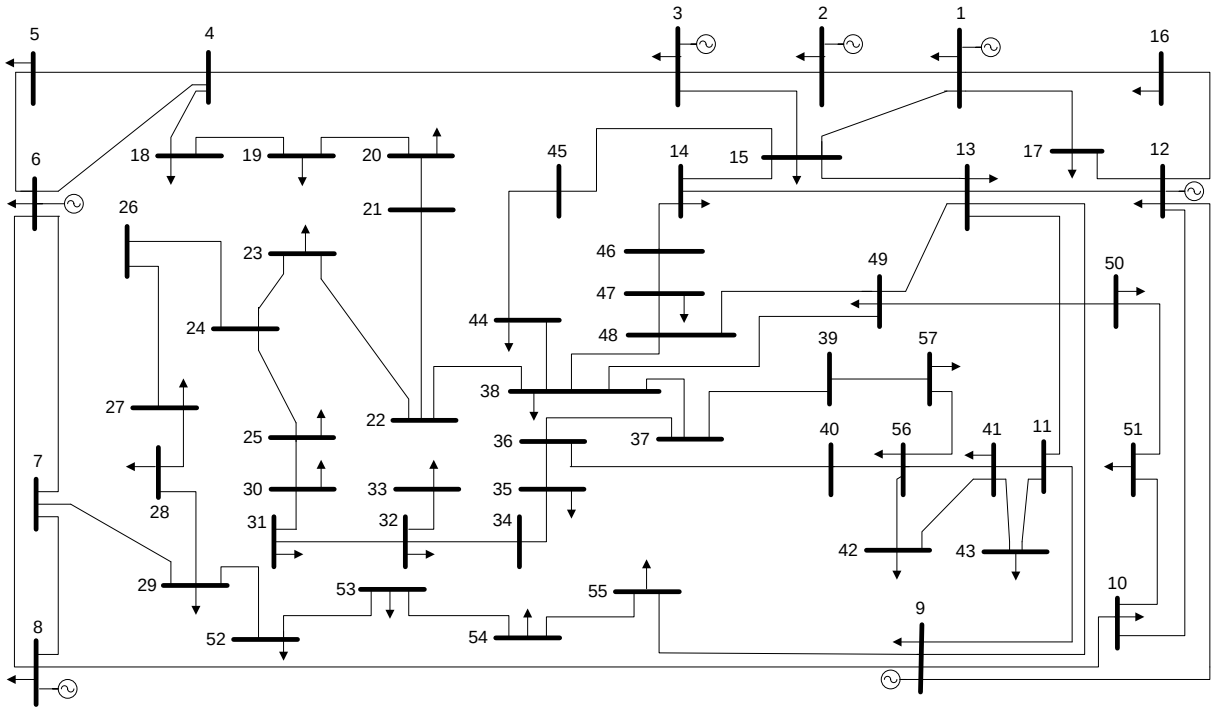

Figure A-3: Network Diagram for IEEE 57 Bus Test System

All data of the IEEE 57 Bus System can be found in [113].

Appendix C.4: Data Sheets for IEEE 118 Bus Test System

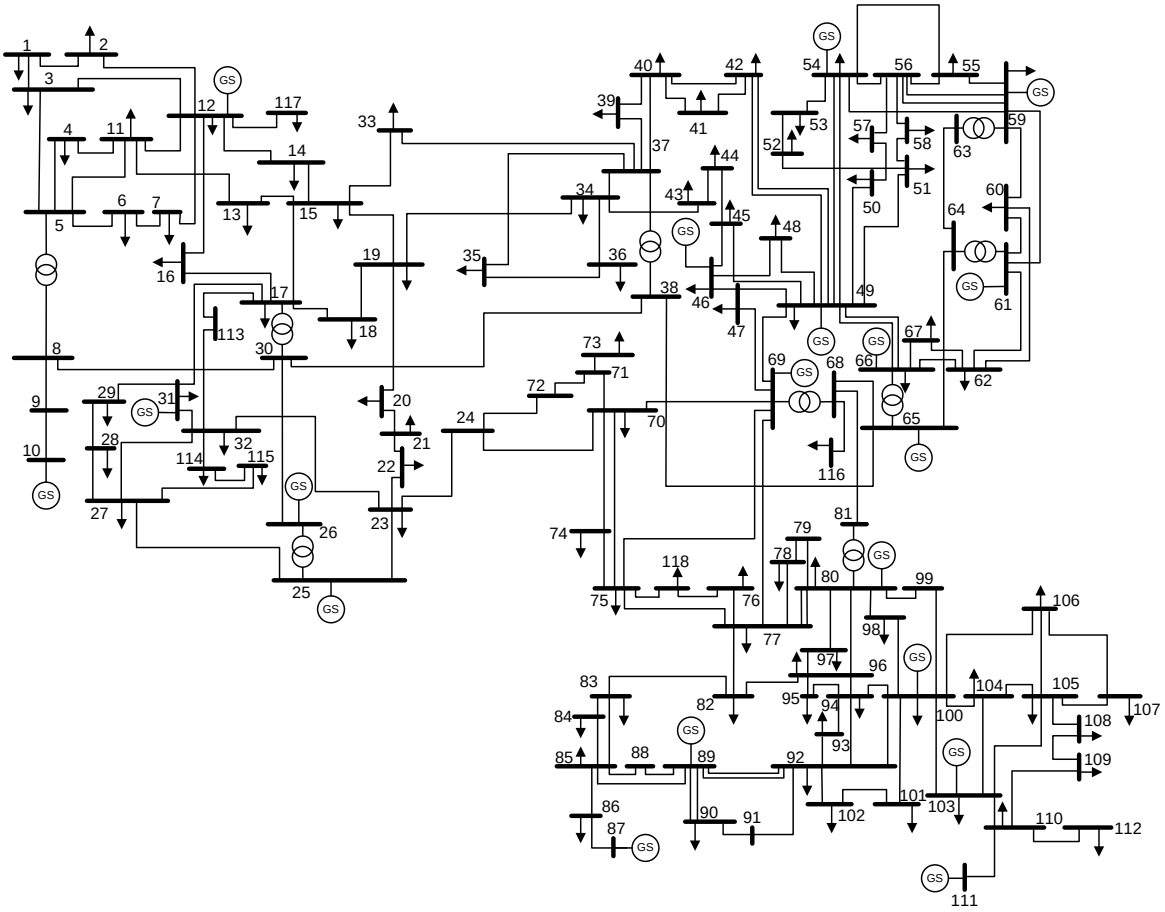

Figure A-4: Network Diagram for IEEE 118 Bus Test System

All data of the IEEE 118 Bus System can be found in [113].

Appendix D: Existing Algorithms for Optimal PMU Placement in the Presence of Conventional Measurements

Appendix D.1: Algorithm for the KCL Based Method

Step 1. Identify the power injection measurements, list the constrains imposed by each power injection measurement according to the KCL as given in (A.5).

Step 2. Identify the power flow measurements, list the constrains imposed by each power flow measurement as given in (A.6)

Step 3. These constrains can be written in a compact form as expressed by (A.7).

Step 4. Form the branch-bus admittance matrix, **A**, according to the topology of the network.

Step 5. Find the optimal placement by solving the optimisation problem defined in (A.8) and (A.9).

$$\sum_{i \in N_j} y_i \geq k_j - 1 \tag{A.5}$$

where y_i is the number of times of a bus observed by PMUs, N_j is a set including Bus j and the buses directly neighbouring to Bus j, and k_j is the number of elements of N_j.

$$y_l + y_m \geq 1 \tag{A.6}$$

where the subscript l and m represents the sending and receiving bus of the considered power flow measurement.

$$\mathbf{By} \geq \mathbf{b} \tag{A.7}$$

where **y** is the vector consisting of y_i's, **B** is the coefficient matrix, and **b** is the vector consisting of k_j's.

$$\min \mathbf{c}^T \mathbf{x} \tag{A.8}$$

$$s.t.\ \mathbf{ABx} \geq \mathbf{b} \tag{A.9}$$

where **c** is the cost coefficient vector, and **x** is the vector consisting of binary decision variables (A.10), which relates with **y** as shown in (A.11), and **b** is a vector whose elements are all 1's.

$$x_i = \begin{cases} 1 \text{ if PMU is placed at bus } i \\ 0 \text{ otherwise} \end{cases} \tag{A.10}$$

$$\mathbf{y} = \mathbf{A}\mathbf{x} \tag{A.11}$$

Appendix D.2: Algorithm for Observability Analysis Based Method

Step 1. Perform observability analysis and identify the observable islands.

Step 2. Identify the buses that are incident to multiple observable islands, group these buses in Set *M*.

Step 3. Form the partial branch-bus admittance matrix, $\mathbf{A}_M$, the branches considered are the unobservable branches and the buses considered are those from Set *M*.

Step 4. Find the optimal placement by solving the optimisation problem defined in (A.12) and (A.13).

$$\min \mathbf{c}_M{}^T \mathbf{x}_M \tag{A.12}$$

$$s.t.\ \mathbf{A}_M \mathbf{x}_M \geq \mathbf{b}_M \tag{A.13}$$

where $\mathbf{c}_M$ is the cost coefficient vector corresponding to Set *M*, and $\mathbf{x}_M$ is the vector consisting of binary decision variables corresponding to Set *M*, and $\mathbf{b}_M$ is a vector whose elements are all 1's.

Appendix E: List of Publications

Journal Publications

[A.1] Z. Jin, P. Dattaray, P. Wall, J. Yu and V. Terzija, "A Screening Rule-Based Iterative Numerical Method for Observability Analysis," in the IEEE *Transactions on Power Systems*, vol. 32, no. 6, pp. 4188-4198, Nov. 2017.

[A.2] P.Wall, P. Dattaray, Z.Jin, P. Mohapatra, J. Yu, D. Wilson, V. Terzija (2016). Deployment and demonstration of wide area monitoring system in power system of Great Britain. Journal of Modern Power Systems and Clean Energy, 4(3), 506-518. DOI: 10.1007/s40565-016-0218-3.

[A.3] Z. Jin; P. Wall; J. Yu; V. Terzija, "Optimal PMU Placement in the Presence of Conventional Measurements", submitted to *Electrical Engineering.*

[A.4] Z. Jin; P. Wall; J. Yu; S. Chakrabarti; V. Terzija, " Analysis of Hybrid State Estimators: The Effects of Estimator Formulations", *IEEE Transactions on Power Systems*. (under review)

[A.5] Z. Jin; V. Terzija, "Application of Cubature Kalman Filter in Dynamic State Estimation", *IET Generation, Transmission & Distribution*, under review.

Conference Publications

[A.6] Y. Cong, Zhaoyang Jin, P. Wall, V. Terzija and M. Osborne, "Economic optimisation of the actions of an enhanced Operational Tripping Scheme," 2016 Power Systems Computation Conference (PSCC), Genoa, 2016, pp. 1-7.

[A.7] Wall, Peter & Dattaray, Papiya & Jin, Zhaoyang & Mohapatra, Priyanka & Yu, J & Ashton, Phil & Osborne, Mark & Clark, S & Hay, K & Wilson, D & Terzija, V. (2016). Creating a WAMS for the GB power system and the lessons learned so far. 106 (8 .)-106 (8 .). 10.1049/cp.2016.1095